ACTA Technica CORVINIENSIS
BULLETIN OF ENGINEERING
fascicule 1
fascicule 2
ACTA Technica CORVINIENSIS
BULLETIN OF ENGINEERING

ACTA
TECHNICA
CORVINIENSIS
BULLETIN OF
ENGINEERING

fascicule 3
fascicule 4
ACTA Technica CORVINIENSIS
BULLETIN OF ENGINEERING

Universitatea
Politehnica
Timișoara

ACTA TECHNICA CORVINIENSIS — Bulletin of Engineering

Tome XII [2019]

Fascicule 3
[July – September]

EP
Editura POLITEHNICA

ASSOCIATE EDITORS and REGIONAL COLLABORATORS

The Editor and editorial board members do not receive any remuneration. These positions are voluntary. The members of the Editorial Board may serve as scientific reviewers.

We are very pleased to inform that our journal ACTA TECHNICA CORVINIENSIS – Bulletin of Engineering is going to complete its ten years of publication successfully. In a very short period it has acquired global presence and scholars from all over the world have taken it with great enthusiasm. We are extremely grateful and heartily acknowledge the kind of support and encouragement from you.

ACTA TECHNICA CORVINIENSIS – Bulletin of Engineering seeking qualified researchers as members of the editorial team. Like our other journals, ACTA TECHNICA CORVINIENSIS – Bulletin of Engineering will serve as a great resource for researchers and students across the globe. We ask you to support this initiative by joining our editorial team. If you are interested in serving as a member of the editorial team, kindly send us your resume to redactie@fih.upt.ro.

INTERNATIONAL SCIENTIFIC COMMITTEE MEMBERS and SCIENTIFIC REVIEWERS

BRAZIL   Alexandro Mendes ABRÃO, Universidade Federal de MINAS GERAIS – BELO HORIZONTE
Márcio Bacci da SILVA, Universidade Federal de UBERLÂNDIA – UBERLÂNDIA
Sergio Tonini BUTTON, Universidade Estadual de CAMPINAS – CAMPINAS
Leonardo Roberto da SILVA,Centro Federal de Educação Tecnológica – BELO HORIZONTE
Juan Campos RUBIO, Universidade Federal de MINAS GERAIS – BELO HORIZONTE
USA   David HUI, University of NEW ORLEANS – NEW ORLEANS

CHINA   Wenjing LI, Military Economic Academy – WUHAN
Zhonghou GUO, Military Economic Academy – WUHAN

The Scientific Committee members and Reviewers do not receive any remuneration. These positions are voluntary.

We are extremely grateful and heartily acknowledge the kind of support and encouragement from all contributors and all collaborators!

ACTA TECHNICA CORVINIENSIS – Bulletin of Engineering is dedicated to publishing material of the highest engineering interest, and to this end we have assembled a distinguished Editorial Board and Scientific Committee of academics, professors and researchers.

ACTA TECHNICA CORVINIENSIS – Bulletin of Engineering publishes invited review papers covering the full spectrum of engineering. The reviews, both experimental and theoretical, provide general background information as well as a critical assessment on topics in a state of flux. We are primarily interested in those contributions which bring new insights, and papers will be selected on the basis of the importance of the new knowledge they provide.

ACTA TECHNICA CORVINIENSIS – Bulletin of Engineering encourages the submission of comments on papers published particularly in our journal. The journal publishes articles focused on topics of current interest within the scope of the journal and coordinated by invited guest editors. Interested authors are invited to contact one of the Editors for further details.

ACTA TECHNICA CORVINIENSIS – Bulletin of Engineering accept for publication unpublished manuscripts on the understanding that the same manuscript is not under simultaneous consideration of other journals. Publication of a part of the data as the abstract of conference proceedings is exempted.

Manuscripts submitted (original articles, technical notes, brief communications and case studies) will be subject to peer review by the members of the Editorial Board or by qualified outside reviewers. Only papers of high scientific quality will be accepted for publication. Manuscripts are accepted for review only when they report unpublished work that is not being considered for publication elsewhere. The evaluated paper may be recommended for:

✓ **Acceptance without any changes** – in that case the authors will be asked to send the paper electronically in the required .doc format according to authors' instructions;

✓ **Acceptance with minor changes** – if the authors follow the conditions imposed by referees the paper will be sent in the required .doc format;

✓ **Acceptance with major changes** – if the authors follow completely the conditions imposed by referees the paper will be sent in the required .doc format;

✓ **Rejection** – in that case the reasons for rejection will be transmitted to authors along with some suggestions for future improvements (if that will be considered necessary).

The manuscript accepted for publication will be published in the next issue of ACTA TECHNICA CORVINIENSIS – Bulletin of Engineering after the acceptance date.

TABLE of CONTENTS

The **ACTA TECHNICA CORVINIENSIS – Bulletin of Engineering, Tome XII [2019], Fascicule 3 [July – September]**, includes scientific papers presented in the sections of:

— **ISB-INMA TEH' 2018 – International Symposium on Agricultural and Mechanical Engineering**, organized by University "POLITEHNICA" of Bucharest – Faculty of Biotechnical Systems Engineering and National Institute of Research-Development for Machines and Installations Designed to Agriculture and Food Industry – INMA Bucharest, in Bucharest, ROMANIA, in 01–03 November, 2018. The current identification number of the papers are the **#1, #7, #17–19** and **#23–24**, according to the present contents list.

— **ERIN 2018 – The 12th International Conference for Young Researchers and PhD Students**, organized by Brno University of Technology, CZECH REPUBLIC and Slovak University of Technology in Bratislava at Faculty of Mechanical Engineering, SLOVAKIA, in Častá-Papiernička, SLOVAKIA, in 02–04 May, 2018. The current identification number of the papers are the **#4, #9, #12** and **#20**, according to the present contents list.

Also, the **ACTA TECHNICA CORVINIENSIS – Bulletin of Engineering, Tome XII [2019], Fascicule 3 [July – September]** includes original papers submitted to the Editorial Board, directly by authors or by the regional collaborators of the Journal.

[1.]Mihaela Elena NAGY, [1.]Constantin COŢA, [1.]Zoltán GYÖRGY, [2.]Lucian Viorel FECHETE–TUTUNARU

RESEARCHES ON THE REALIZATION OF A TECHNOLOGY TO OBTAIN GRANULAR ORGANO–MINERAL FERTILIZERS BASED ON PEAT

[1.]INMA Bucharest, Branch Cluj–Napoca, Cluj Napoca, ROMANIA
[2.]Technical University of Cluj–Napoca, Faculty of Mechanics, Cluj–Napoca, ROMANIA

Abstract: Lately, researches in fertilizer fields focuses on reducing the negative impact of using them on the environment and consumers, and finding new, less costly fertilizer sources. The paper presents the results of the research regarding the realization of a technology for obtaining of peat based granular organo–mineral fertilizers. In order to improve the fertilizer role of the peat, the production formula used contains urea as a source of nitrogen, monoammonium phosphate (MAP) as a source of phosphorus and nitrogen, molasses from sugar beet as a source of organic nitrogen, potassium and vitamins, protein hydrolyzate, as a source of proteins, polypeptides and amino acids and other microelements
Keywords: peat, fertilizers, granule, organo–minerals

INTRODUCTION

Organic agriculture is practiced on approx. 1% of the global agricultural area, and its importance continues to grow, being perceived by many as having less negative environmental effects than conventional agriculture (K.Lorenz, R.L et al, 2016).

As a result, fertilizer research has recently focused on reducing the negative impact of its use on the environment and consumers and finding new, less costly fertilizer sources. It is aimed at making more concentrated organic fertilizers, easier to apply and more stable during plant growing periods.

Organic soil fertilization reduces or even eliminates the need for agrochemicals and mineral fertilizers, of which extensive use leads to economic and environmental imbalances. The combined application of organo–mineral fertilizers has proven to be a better approach to increase and sustain soil fertility and yields than applying only chemical or organic fertilizers (J. Aguilera, et al, 2012). The requirements introduced by the environmental protection legislation (Ministry of Environment and Water Management, 2005) and the provision of sustainable agriculture along with modern fertilization technologies have led to an increase in the diversity of organo–mineral fertilizers.

According to the European Parliament's regulation on fertilizer products bearing the CE marking, an organo–mineral fertilizer is composed of one or more inorganic fertilizers and a material containing organic carbon and nutrients of exclusively biological origin (CE nr. 1069/2009 şi CE nr. 1107/2009, Anexa 1, 2016).

Organo–mineral fertilizers are the result of an optimal blend of organic and mineral substances, depending on plant nutritional needs, which will lead to products that release nutrients (nitrogen, phosphorus, potassium, magnesium and other microelements) which, besides supplying deficient nutrients to plants, also have the qualities of improving soil attributes (Blaga, Gh. et al, 2008).

Due to its advantages, the use of peat, as the basis and source of organic matter for fertilizers, has gained increasing popularity lately. Organo–mineral fertilizers offer several advantages over organic or mineral ones taken separately, namely: they improve the plant–mineral interaction by reducing phosphorus absorption, increase the activity of rooting young plants, and influence the oxidation–reduction reaction in soil. (Parent. L., et al, 2003). At the same time, these products together with the methods of fertilization constitute and represent modern technologies with significant quantitative, qualitative effects, with positive economic and environmental impact.

Considering the importance and role of organo–mineral fertilizers for the growth and support of soil fertility and crop yields, this paper presents the results of the research on the development of a technology for obtaining peat–based granular organo–mineral fertilizers, which involves the combination of fertilizers (N, P, K) with biostimulators such as humic acids, fulvic acids, phytohormones, etc. to ensure both the efficiency of the use of macroelements and the quantitative and qualitative increase in agricultural production.

MATERIAL AND METHOD

In order for the product to meet the requirements of European regulations in the field (EC 1107/2009, Annex 1, 2016) and to carry out an efficient fertilization of the vegetable crops for which it is intended, it is proposed that the components added to the peat provide the following nutrients listed in Table 1.

Table 1. Value ranges of macroelements and microelements in organo–mineral fertilizer composition

	Fertilizing elements	Minimum values, %	Maximum values, %
Macronutrients	Nitrogen, N	14,0	18,0
	Phosphorus, in the form of phosphorus pentoxide, P_2O_5	22,0	26,0
	Magnesium, as Magnesium Oxide, MgO	1,0	3,0
	Sulfur, S	0,8	2,4
Micronutrients	Zinc, Zn	0,5	1,5
	Copper, Cu	0,4	1,2
	Iron, Fe	0,6	1,8
	Manganese, Mn	1,1	3,3
	Cobalt, Co	0,3	0,9

In order to improve the role of peat fertilizer, which is the basic raw material and supply with fertilizing macronutrients and micronutrients, the proposed formula will contain urea as a source of nitrogen, monoammonium phosphate (MAP) as a source of phosphorus and nitrogen, molasses sugar beet, as a source of

organic nitrogen, potassium and vitamins, proteic hydrolyzate, as a source of protein, cobalt sulfate, zinc sulfate, copper sulfate, iron sulphate and manganese sulphate.

Urea also contributes to the release of humic and fulvic acids from the peat and, together with molasses, serve as binders to ensure the cohesion of the recipe components.

To determine the proportion of ingredients that bring in the formula the nutrients within the mentioned limits proceeded as follows.

Since the Monoammonium phosphate (MAP) containe 62% phosphorus pentoxide, P_2O_5 and 12% nitrogen, N, therefore, to ensure the minimum and respectively maximum phosphorus demand, the following quantities of MAP are required:

$$MAP_{min}= 22/0,62 = 35,50 \text{ kg};$$
$$MAP_{max}= 26/0,62 = 41,94 \text{ kg};$$

Nitrogen results from MAP and Urea. Since MAP contains 12% nitrogen, it results that from the amount of MAP needed for P2O5 are obtained at minimum value: 35,5 x 0,12= 4,26 kg nitrogen and at maximum value: 41,94 x 0,12= 5,04 kg nitrogen

From urea, we have the difference in nitrogen needed. Since urea has 46% nitrogen, it results:

$$Urea_{min}= (14-4,26)/0,46=21,17 \text{ kg};$$
$$Urea_{max}= (18-5,04)/0,46=28,17 \text{ kg};$$

Magnesium sulphate contains 33.3% Magnesium oxide, MgO and 26.7% Sulfur, S. It follows that the following quantities of Magnesium Sulphate are required to ensure the required minimum and maximum Magnesium Oxide:

$$MgSO_{4min}= 1/0,333 = 3 \text{ kg};$$
$$MgSO_{4max} = 3/0,333 = 9 \text{ kg};$$

These amounts of magnesium sulphate, $MgSO_4$ provide a percentage of sulfur, S:

$$S_{min}= 3 \text{ x } 0,267 = 0,8 \text{ %};$$
$$S_{max}= 9 \text{ x } 0,267 = 2,4 \text{ %};$$

Zinc sulphate contains 40% Zinc, Zn. To ensure the minimum and maximum zinc requirements, the following quantities of zinc sulphate are required:

$$ZnSO4min= 0,5/0,4 = 1,25 \text{ kg};$$
$$ZnSO4max = 1,5/0,4 = 3,75 \text{ kg};$$

Similarly, depending on the percentage content of microelements in the sulphates, the minimum and maximum quantities of sulphates are set.

Copper sulphate

$$CuSO_{4min}= 0,4/0,4 = 1,0 \text{ kg};$$
$$CuSO_{4max} = 1,2/0,4 = 3,0 \text{ kg};$$

Iron sulphate

$$FeSO_{4min}= 0,6/0,37 = 1,62 \text{ kg};$$
$$FeSO_{4max} = 1,8/0,37 = 4,86 \text{ kg};$$

Manganese sulphate

$$MnSO_{4min}= 1,1/0,36 = 3,05 \text{ kg};$$
$$MnSO_{4max} = 3,3/0,36 = 9,15 \text{ kg};$$

Cobalt sulphate

$$CoSO_{4min}= 0,3/0,36 = 0,83 \text{ kg};$$
$$CoSO_{4max} = 0,9/0,36 = 2,50 \text{ kg};$$

It results the total mass of the components without peat:

$$M_{min}=67,95 \text{ kg}; M_{max}=102,37 \text{ kg};$$

Taking into account the composition of the formula and the mass of the other ingredients making up, for the use of a a percentage (25–30%) of dry peat results in a quantity of dry peat (MTU) of:

$$MTU_{min}=0,3/0,7 \text{ x } M_{min}= 29,12 \text{ kg};$$
$$MTU_{max}=0,30/0,7 \text{ x } M_{max}= 43,87 \text{ kg};$$

RESULTS

The calculations made with the purpose of providing fertilized macro and microelements have led to the establishment of the formula components underlying the development of the technology for obtaining peat–based granular organo–mineral fertilizers. Thus, the percentage of components is between the following limits:

(25–30)% peat with humidity of 30%,
(30–40)% monoammonium phosphate MAP,
(2.5–7.5)% Magnesium sulphate MgSO4,
(20–25)% Urea,
(2–10)% Molasses containing 0.5–2.1% nitrogen and 2–5% potassium,
(2–5)% Protein hydrolyzate containing 10–15% amino acids,
(1,2–3,6)% zinc sulphate ZnSO4,
(0.7–2.1)% CuSO4,
(1.5–4.5)% FeSO4,
(3–9)% manganese sulfate MnSO4,
(0.9–2)% cobalt sulfate CoSO4.

Figure 1 shows the diagram of technological process to obtain granular organo–mineral fertilizers based on peat.

The technological process comprises the following phases:

—— Preparation of raw materials

Preparation of raw materials consists of grouping and mixing them into categories:

mixture of solid components, consisting of dry peat at 30% moisture, monoammonium phosphate (MAP) and starch. The mixture thus formed was milled in the hammer mill, using a 3.5 mm sieve, at a rotor speed of 3000 rpm, thus rendering the texture and granulation corresponding to the feed of the extruder through the pulverulent dispenser.

mixture of liquid components consisting of the protein hydrolyzate in which urea, molasses and microelements in the form of sulphates are dissolved.

—— Supplying the extruder

Supplying the extruder with the two categories of mixtures is done through the two feed points, dosing the mixture of solid components in the extruder funnel with a two screw feeder and dosing the liquid mixture with a peristaltic pump.

The supplying is continuous, any supplying interruption resulting in variations in the flow and properties of the finished product.

Supplying rates are set so as to meet the proportions according to the formula that ensure the needed nutrient in the granules, to be possible to process the blends in the extruder and the product obtained has the characteristics necessary for it to be manipulated and applied in the field.

The ratio of the two feed rates determines among others the amount of binder in the final product, with great influence on its quality.
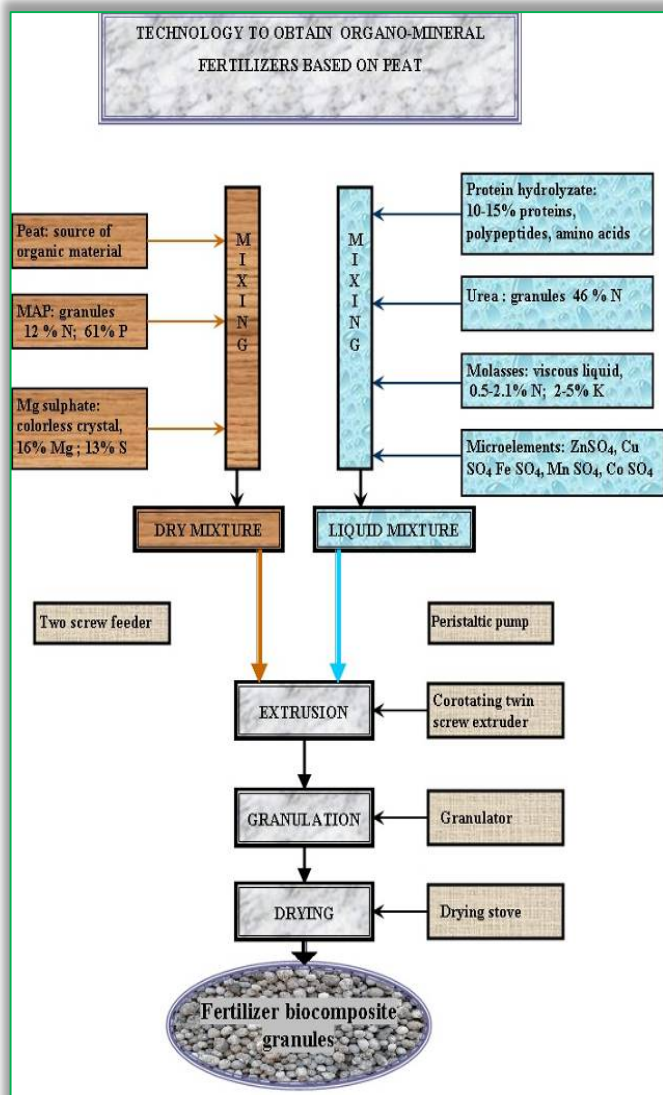
Figure1 – Diagram of technological process for obtaining granular organo–mineral fertilizers based on peat.

⎯ Extrusion

Mixtures dosed through the two feed points of the extruder, Figure 2, are taken up by the two co–rotative screws which homogenize and process them by shearing and heating while being moved to the die. On the other hand, due to the rotation of the screws, there is an increase in pressure to the die.

Figure 2 – Extrusion plant type „ZK 25", production Collin

The temperature of the cylinders is pressed and maintained at the values set by the cylinder heating and cooling system. The speed of the screws is adjustable, allowing the material to pass through the extruder.

When passing through the die, the material must have the temperature and pressure required to obtain a finished quality product.

In order to preserve the properties of the components in the formula, especially of the peat, the temperature and pressure regime in the extruder must be moderate.

Table 2. The parameters of the extrusion process

Parameter	units	Value					
Temperature in the area	^0C	Z1	Z2	Z3	Z4	Z5	Z6
		30	30	40	60	80	100
Flow rate of solid components	Kg/h	3,3					
Flow rate of liquid components	Kg/h	2,2					
Solid/liquid feed flow ratio	–	1,5					
Extrusion pressure	barr	60					

⎯ Granulation

Granulation has the purpose of ensuring the flow properties of the finished product and is carried out in a hammer mill whose 220 mm diameter rotor is driven at 1000 rpm with a single–phase electric motor having the power of 500 W.

⎯ Drying

Drying aims to reduce the humidity of the granules and improve their mechanical properties and is carried out in an air recirculation oven and placing the granules on a sieve in a single layer, with the possibility of bringing the hot air to the entire surface of the granules. The drying temperature is 40–60 °C.

CONCLUSIONS

The application of organo–mineral fertilizers is a better approach to sustain soil fertility and crop yield than applying only chemical or organic fertilizers. Due to the advantages it presents, peat is a basis and source of organic matter for fertilizing biocomposites.

The manufacturing formula that underpinned the development of the technology to obtain granular organo–mineral fertilizers based on peat aims to achieve an optimal blend of organic and mineral substances, depending on the nutrition needs of plants. It contains urea, as a source of nitrogen, monoammonium phosphate (MAP) as a source of phosphorus and nitrogen, sugar beet molasses as a source of organic nitrogen, potassium and vitamins, protein hydrolyzate as a source of protein, cobalt sulphate, zinc sulphate, copper sulphate, iron sulphate and manganese sulphate.

Obtaining the organo–mineral fertilizers according to the developed technology is achievable by thermo–plastic extrusion and granulation.

Acknowledgement

Note:

This paper is based on the paper presented at ISB-INMA TEH' 2018 International Symposium (Agricultural and Mechanical

Engineering), organized by Politehnica University of Bucharest – Faculty of Biotechnical Systems Engineering (ISB), National Institute of Research-Development for Machines and Installations Designed to Agriculture and Food Industry (INMA) Bucharest, The European Society of Agricultural Engineers (EurAgEng), Society of Agricultural Mechanical Engineers from Romania (SIMAR), National Research & Development Institute For Food Bioresources (IBA), University of Agronomic Sciences and Veterinary Medicine Of Bucharest (UASVMB), Research-Development Institute for Plant Protection (ICDPP), Hydraulics and Pneumatics Research Institute (INOE 2000 IHP), National Institute for Research and Development in Environmental Protection (INCDPM), in Bucharest, ROMANIA, between 01–03 November, 2018.

References

[1] Aguilera J et al., (2012), Initial and residual effects of organic and inorganic amendments on soil properties in a potato–based cropping system, American Journal of Experimental Agriculture, 2, 641–666,

[2] Blaga, Gh., et al, (2008), Pedology (Pedologie), Ed. Mega, Cluj–Napoca;

[3] Davidescu V., (2000), Pesticide agro–chemistry and chemistry (Agrochimia şi chimia pesticidelor), AMD Pub. House, USAMV, Bucharest;

[4] Ciuperca R., et al, (2015), Organic plant and animal waste management system, INMATEH – Agricultural Engineering, Vol. 46, No. 2 / 2015, pag.69–76, Bucharest – Romania;

[5] Lorenz K, R.L. et al, (2016), Environmental Impact of Organic Agriculture, Adv Agron, 139, 99 152;

[6] Saleh S. N., (2016), Reduction of fine particle emission from a prilling tower using CFD simulation, Chemical engineering research and design 109, 171–179;

[7] Sotropa A., et al, (2010), The quality of peat from Călăţele, Cluj County (Calitatea Turbei din Călăţele, Judetul Cluj), ProEnvironment 3, 594–597;

[8] Vreman et al, (2009), A basic population balance model for fluid bed spray granulation, Chemical Engineering Science 64, 4389 – 4398;

[9] *** Code of good agricultural practice for the protection of waters against nitrate pollution from agricultural sources / Codul de bune practici agricole pentru protecţia apelor împotriva poluării cu nitraţi din surse agricole, Annex to Order no. 1182 of 22 November 2005, Ministry of Environment and Water Management, Bucharest, 2005;

[10] *** Regulation of the European Parliament and of the Council laying down rules for the making available on the market of fertilizer products bearing the CE marking and amending Regulations / Regulament al Parlamentului European şi al Consiliului de stabilire a normelor privind punerea la dispoziţie pe piaţă a produselor fertilizante cu marcaj CE şi de modificare a Regulamentelor (CE) nr. 1069/2009 and (CE) nr. 1107/2009, Annex 1, 2016.

[1.]Oluwaseun Adedapo ADETAYO, [2.]Olugbenga Oludolapo AMU,
[3.]Tochukwu Obumneme ONUORAH, [4.]Elijah Abiodun ADETONA

MODIFICATION OF CEMENT STABILIZED STRUCTURAL LATERITIC WOOD ASH

[1-3.] Department of Civil Engineering, Federal University, Oye-Ekiti, NIGERIA
[4.] Department of Civil Engineering, Obafemi Awolowo University, Ile-Ife, NIGERIA

Abstract: This paper investigates cement stabilized structural soil samples modified with wood ash as complement for cement in structural works and hence reduced the cost of construction. Soil samples were collected from three different excavated foundations labelled sample A, B, and C. Preliminary tests were performed on the samples at their natural states and when stabilized at optimum cement. Engineering tests were also performed on samples at their natural states, when stabilized with optimum cement and when wood ash powder (WAP) was introduced at 2, 4, and 6%. Results of the engineering tests showed that WAP increased the maximum dry density (MDD) of all the samples. At 2% WAP content, and with the optimum cement content kept at 10% for samples A and B and 8% for sample C, the MDD values increased from 1587.99 to 1588.23kg/m^3, 1548.89 to 1604.08kg/m^3 and 1506.45 to 1529.42kg/m^3 in samples A, B and C respectively. The samples shear strengths also increased from its natural state, samples A, B and C increased from 100.26 to 112.66kN/m^2, 95.76 to 133.27kN/m^2 and 64.88 to 92.95kN/m^2 at 4% WAP contents respectively. It was therefore concluded that WAP is an effective additive on cement stabilized lateritic soil for foundation construction.
Keywords: wood ash powder, cement stabilization, lateritic soil, structural foundation

INTRODUCTION

Structural soil foundation improvement could either be by modification or stabilization or both. Soil modification is the addition of a modifier (cement, lime and others) to a soil to change its index properties, while soil stabilization is the treatment of soil to improve its strength and durability, such that it becomes totally suitable for construction beyond its original classification.

Over time, cement and lime are the two main materials used for stabilizing soils, though these materials have rapidly increased in price due to a sharp increase in the cost of energy since 1970s (Neville, 2000).

The over dependence on the utilization of industrially manufactured soil improving additives (cement, lime and others) have kept the cost of structural engineering projects very high. This hitherto has continued to deter the developing, underdeveloped and poor nations of the world from providing relatively standard structures to dwellers that constitute the higher percentage of their population (Alhassan and Mustapha, 2007). The quest to discover materials that can serve as a replacement for cement in soil foundation amount to a worthwhile effort.

Adequate strength and engineering properties of soil material are prerequisites for standard structural foundation, the treatment of the natural soil to improve its engineering properties is known as soil stabilization. Because of the sowing construction cost of cement stabilizers, waste product from wood known as wood ash is considered as a pozzolan. Wood ash is available everywhere on earth especially in domestic places. Wood ash is a waste product derived from burning of wood, discovered as a suitable pozzolan used for partial replacement of cement in stabilization of lateritic soil. According to Amu (2010), when the quality of the sub-grade material meets the requirements expected of a sub-base, then a sub-base is not necessary. But in cases where suitable sub-base materials are not readily available, the in-situ material can be treated to meet the required engineering properties. The materials can be stabilized using any of these stabilizing agents like Portland cement, asphalt and lime.

Lateritic Soils

Lateritic soils form a group comprising a wide variety of red, brown, and yellow fine-grained residual soils of light texture as well as nodular gravels and cemented soils (O'Flaherty, 2002). They may vary from a loose material to a massive rock. They are characterized by the presence of iron and aluminum oxides or hydroxides, particularly those of iron, which give the colours to the soils. For engineering purposes, the term laterite is confined to the coarse-grained vermicular concrete material, including massive laterite. O'Flaherty (2002) referred the term lateritic soils as materials with lower concentrations of oxides.

Laterization is the removal of silicon through hydrolysis and oxidation that results in the formation of laterites and lateritic soils (Okunade, 2007). The degree of laterization is estimated by the silica-sesquioxide (S-S) ratio [SiO2 / (Fe2O3 + Al2O3)]. Lateritic soils can be effectively stabilized to improve their properties for particular uses. However, because of the wide range of silica-sesquioxidein the lateritic soil characteristics, no one stabilizing agent has been found successful for all lateritic materials. Laboratory studies, or preferably field tests, must be performed to determine which stabilizing agent, in what quantity that will perform adequately on a particular soil (Army Study Guide, 2008). Some stabilizing agents that have been used successfully are cement, asphalt and lime.

In analyzing the engineering properties of soil, three basic parameters that are of keen interest to Engineers are permeability, shear strength and compressibility (Okunade, 2007). Permeability is the soil property that permits the passage of fluid by a flow process under the action of eternally applied forces (Okunade, 2007). For the material to be permeable, the void spaces within it must be

continuous. The rate at which the soil allows water to pass through would affect the behaviour of the soil especially due to seasonal variations. In places where frost action is critical, permeability of the soil is a very critical factor to consider in pavement design. The shear strength of a soil is defined as the maximum or limiting value of shear stress that may be induced within its mass before the soil yields (Whitlow, 1995). The order of shear resistance within the soil mass must be accurately understood before the computation of slope stability and lateral pressure on earth retaining structure can be successfully carried out. The purpose of shear strength testing is to establish empirical values for the shear strength parameters.

Compressibility is a change in the stress system acting on a soil mass that results in a change in the volume of mass. Such changes in volume have important influence on the engineering properties of the soil. The compressibility of a soil is determined experimentally by the triaxial compression, unconfined compression.

Soil-Cement Stabilization

Stabilization is the process of blending and mixing materials with a soil to improve certain properties of the soil (O'Flaherty, 2002).The process may include the blending of soils to achieve a desired gradation or the mixing of commercially available additives that may alter the gradation, texture or plasticity, or act as a binder for cementation of the soil (United State Army, 1994).According to O'Flaherty (2002), there are three types of soil-and-cement mixtures as follows; Plastic soil-cement is a hardened mixture of soil and cement that contains, at the time of placing, enough water to produce a consistency similar to plastering mortar. It is used to line or pave ditches, slopes, and other areas that are subject to erosion. Cement-modified soil is an unhardened or semi hardened mixture of soil and cement. When relatively small quantities of Portland cement are added to granular soil or silt-clay soil, the chemical and physical properties of that soil are changed. Cement reduces the plasticity and water-holding capacity of the soil and increases its bearing value. The degree of improvement depends upon the quantity of the cement used and the type of soil. In cement-modified soil, only enough cement is used to change the physical properties of the soil to the degree desired. Cement-modified soils may be used for structural foundation base, sub base, and as trench backfill material.

Compacted soil-cement, often referred to as simply soil-cement, is a mixture of pulverized soil and calculated amounts of Portland cement and water that is compacted to a high density. The result is a rigid slab having moderate compressive strength and resistance to the disintegrating effects of wetting and drying and freezing and thawing.

Availability of Fuel Wood and Charcoal

The predominantly rural population depends mainly on fuel wood to meet basic energy needs for cooking and heating. Recent studies revealed that Nigeria produces about 1 million tons of charcoal annually of which 80% is consumed in the cities (FDF, 1986). Fuel wood and charcoal account for about 50% of the national primary energy consumption. Fuel wood is demanded by both household and industrial sectors in all ecological zones of the country. It is estimated that about 90% of the rural households in Southern Nigeria and up-to 98% in the Northern Nigeria depend on fuel wood as their source of domestic energy. Industrial uses include those by institutions, food and craft industries. Fuel wood is very important in local restaurant, bakeries, local breweries, pottery, blacksmith and burnt brick factories. Institutions such as hospitals, prisons and schools also demand fuel wood for cooking. The per capita consumption of fuel wood in rural area is 393.43 kg/annum while the urban households consume 255.75 kg/ annum.

Pozzolan

Pozzolan can be defined as a siliceous and aluminous material, which in itself possesses little or no cementation value but will in a finely divided form, such as a powder or liquid and in the presence of moisture, chemically react with calcium hydroxide at ordinary room temperature to form permanent, insoluble compound possessing cementitious properties. Pozzolan is a fine powdered material which is added to non-hydraulic lime mortars to accelerate the set. The material possesses little or no cementitious value, but in a finely divided form, it will react with calcium hydroxide in the presence of moisture to provide a chemical set (Traditional lime, 2010). The first pozzolans were used by eruptions. One of the compelling reasons for incorporating pozzolans in concrete today is to improve quality and to extend service life by enhancing the durability of this ubiquitous construction material. To function properly, pozzolans must be amorphous or glassy and generally finer than 325 mesh in particle size. Finer particle sizes generally have greater reactivity helping in the early strength development (Vitrominerals, 2005). Pozzolans can continue to react in concrete for many years, further strengthening the concrete and making it harder and more durable during its service life. Pozzolans also serve to increase density and reduce the permeability of concrete, which helps to make it more resistant to deterioration and swelling associated with various exposure conditions.

The two major types of pozzolans are; natural and artificial pozzolans. The natural pozzolans are present on earth's surface such as diatomaceous earth, opaline shale, volcanic ash, tuff and pumiced. These materials require further accessing such as calcining, grinding, drying and so on. The Aegean island of Santorini has volcanic ash, volcanic tuffs, pumicites and opaline shale are found in the west of River Mississippi in Oklahoma, Nevada, Arizona and California. Fly ash is an example of artificial pozzolan produced when pulverized coal is burnt in electric power plants. The glassy spherical particulars are the active pozzolani portion of the fly ash. Fly ash is 66 - 68% glass. Class F fly ash readily reacts with lime (produced when Portland cement hydrates) and alkalis to form cementitious compounds. Class C fly ash also may exhibit hydraulic (self-cementing) properties.

Wood Ash

Wood ash is a by-product of combustion from wood-fired boilers, at a typical paper mills and other wood burning facilities (Abdullahi, 2006). Main producers of wood ash are wood industries and power plants. Since wood is a renewable source of energy and environmentally benign friendly material, there will be increased use of wood in energy production in the future. As a result, there will be increased amount of wood ash generation. Approximately three million tons of wood ash is produced annually. Approximately 70% of the wood ash is being land filled, around 20% is being used as soil supplement, and the remaining 10% is being used in miscellaneous applications. The cost of land filling is increasing due

to passes of strict environmental regulations and limited availability of landfill space (Naik, 2000).In the light of these, it has become essential to develop beneficial uses of wood ashes to solve the problems associated with their disposal.

The physical and chemical properties of wood ash vary significantly depending upon various factors such as type or species of trees/wood, method and manner of combustion, efficiency of the boiler, and other supplementary fuel used with wood (Naik and Kraus, 2003). Wood ash is composed of both inorganic and organic compounds. Typically between 0.43 and 1.82 percent of the mass of burned wood (dry basis) results in ash. Many types of ash are found near campsites Naik (2000). The composition of wood ash is influenced by the type of wood that has been burned. Also the conditions of the combustion affect the composition and amount of the residue ash, thus higher temperature will reduce ash yield. Wood ash contains calcium carbonate as its major component, representing 25 or even 45 percent. According to Naik and Kraus (2003), less than 10 percent is potash, and less than 1 percent phosphate; there are trace elements of iron, manganese, zinc, copper and some heavy metals. However these numbers vary as combustion temperature is an important variable in determining wood ash composition. Presence of heavy metals and/or high alkalinity in wood ash may limit its application on land under a stricter environmental regulation.

— Wood Ash as a Pozzolanic Material

Pozzolan can be defined as a siliceous and aluminous material, which in itself possesses little or no cementation value but will in a finely divided form, such as a powder or liquid and in the presence of moisture, chemically react with calcium hydroxide at ordinary room temperature to form permanent, insoluble compound possessing cementitious properties. Pozzolans are commonly used as an addition (the technical term is "cement extender") to Portland cement concrete mixtures to increase the long-term strength and other material properties of Portland cement concrete and in some cases reduce the material cost of concrete. Pozzolans are primarily vitreous siliceous materials which react with calcium hydroxide to form calcium silicates; other cementitious materials may also be formed depending on the constituents of the pozzolan (Abdullahi, 2006).

Misra et al. (1993) found the major elements in wood ash to be calcium, potassium and magnesium, while sulfur, phosphorus and manganese are present at around 1% and iron, aluminium, copper, zinc, sodium, silicon and boron are present in relatively smaller amounts. They found the chemical compositions of wood ash to be mainly carbonates and oxides of the alkali metals, namely $CaCO_3$, $K_2Ca(CO_3)_2$, $Ca(OH)_2$, MgO, CaO, $Ca_4Mn_3O_{10}$, K_2SO_4 and others. Naik et al. (2003) have tested many sources of wood ash from the USA and Canada and have found their specific gravity to be between 1.6 and 2.8 and unit weight between 365 and 980 kg/m3 (Naik and Kraus, 2003). They also found that the major elements in wood ash to be carbon, calcium, potassium, magnesium, phosphorus and sodium, all in various proportions. Abdullahi (2006) found the specific gravity of wood ash obtained from a bakery in Minna, Niger State, Nigeria to be 2.13 and the bulk density 760 kg/m3 and his analysis showed the chemical constituents as SiO_2, Al_2O_3, Fe_2O_3, CaO, MgO, TiO_2, K_2O, SO_3 and organic matter (loss on ignition LOI = 27%).

Because of its being usually rich in calcium carbonate, which is a good binding agent and its other chemical components, wood ash acts as a pozzolana with good stabilizing properties. Naik (2000) performed some investigations into the properties of wood ash from different sources and established their potential for being used in cement-based construction materials. Naik et al. (2003), in an investigation into the use of wood ash in cement-based materials, found that wood ash could be utilized in making self-compacting Controlled Low-Strength Materials (CLSM), air-entrained and non-air-entrained concretes and bricks / blocks / paving stones. Initial test results indicated that wood ash could be successfully used in making:

CLSM (with up to 90% of total materials);

air-entrained structural-grade concrete up to 28-day compressive strength of 50 MPa with wood or its blends (up to 40%) of wood ash and coal fly ash;

non-air-entrained structural-grade concrete (up to 60 MPa 28-day compressive strength) with wood ash or its blends with coal fly ash (up to 40%) as partial replacement of cement and,

good quality bricks/blocks/paving stones with wood ash or its blends with coal fly ash (up to 35%) as partial replacement of cement.

Employing the Pozzolanic property of sawdust ash, it has been used by Elinwa and Ejeh (2004) and with acceptable results as partial replacement for Portland cement in the production of cement mortar. Udoeyo and Dashibil (2002) utilized it as partial replacement for Portland cement in concrete. Though the compressive strength of specimens with sawdust ash was lower at the 28th day, it was observed to gain rapid strength at later ages, indicating a pozzolanic activity of the ash. Abdullahi (2006) successfully used a wood ash obtained from a bakery in Minna, Niger State, Nigeria as partial replacement for Portland cement in the production of concrete. With regards to the usage of wood ash for soil stabilization, according to Andres and Honkala (1978), wood ash is one of the oldest stabilizers known. It is a good water proofer and its binding properties are adequate for stabilizing traditional adobe. It provides strength to the block and prevents cracking because of its chemical composition especially the potassium components, which aid the bonding properties. Fajobi and Ogunbanjo (1994) have used wood ash to impart greater strength to traditional adobe bricks and have determined that the amount of wood ash to be added to soil for optimum compressive strength is about 10% by weight, while Amu et al. (2005) have used wood ash (sawdust) in the stabilization of lateritic soil.

MATERIALS AND METHODS

The materials used include lateritic soil samples, Portland cement, wood ash and water. The lateritic soil samples were collected from excavated foundations located in Ojo, Akinyele at Ibadan, Oyo State and Mokuro at Ile-Ife in Osun State Nigeria. These were designated as samples A, B, and C. The soil samples pre-treatment was ensured before the commencement of the study. For easy identification of the soil samples, tags were placed on them to describe their dates of excavation, depths of excavation from the source and locations.

The soil samples were spread on sacks in the laboratory to air-dry them for a minimum of two weeks. The sacks were frequently turned to prevent water contamination and direct contact with sunlight. The required quantity of ordinary Portland cement for the study was obtained locally. Wood ash was obtained from hardwood (Iroko tree/planks), bought from a sawmill in Ile-Ife area and burnt in an open drum to get the required wood ash that was sufficient for the study. Potable water was obtained from treated water available in the laboratory.

Preliminary tests such as the natural moisture content, specific gravity, particle size analysis and Atterberg's limits were carried out on three unstabilized soil samples to determine their index properties. The major stabilizing material, cement was thoroughly mixed with the soil samples in varying percentages of (2, 4, 6, 8, 10) % by weight of the soil samples, so as to determine the optimum requirement of cement in the different soil samples. This was done by determine PI from Atterberg's limit test. The point of lowest PI gives the optimum amount of cement required. Hence, engineering properties of cement stabilized soil was determined. These engineering properties are used as the control against which the engineering properties of cement stabilized lateritic soil modified with wood ash are compared. The main objective of the study is to determine the change in the engineering properties of the stabilized soil sample modified with wood ash.

Engineering tests such as compaction, California bearing ratio (CBR) and undrained traixial were also performed on them at their natural states, when stabilized with optimum cement and when wood ash powder (WAP) was introduced as pozollan to the samples. The various tests were carried out with standard procedures stipulated in BS 1377-1990:1-8.

RESULTS AND DISCUSSION
The results from the preliminary tests (grain size analysis, natural moisture contents, specific gravity, and Atterberg's limits test) as well as the engineering test (compaction test, California Bearing Ratio test and triaxial test) are presented and discussed below:

— Preliminary Test
The summary of the preliminary test results for soil samples A, B, C are shown in Table 1. The natural moisture content of the selected soil samples A, B and C are 20.19%, 17.72% and 2.39% respectively. The result showed that sample A has the highest natural moisture content and sample C the lowest. The specific gravity of samples A, B and C are 2.33, 2.33 and 2.77 respectively. Bwalya (1998) stated that the performance of lateritic soil may be influenced by the climate, the topography and hydrological regime of the area in which the structure is to be constructed which influences the strength of the soil. The results of the sieve analysis indicated that all the soil samples fall within the granular material group and ranged between A1 - A3 in the AASHTO classification system, suggesting that they are fairly good materials for construction, according to Fajobi (2008), soil is classified into seven major groups A-1 to A-7, soil classified under groups A-l, A-2, A-3 are granular materials while soil classified under groups A-4, A-5, A-6 and A-7 is mostly silt and clay-type materials. Bwalya (1998) in his studies on the relationship between the natural moisture content and the plastic limit indicated generally that soils with natural moisture contents lower than the plastic limits are normal lateritic soils, therefore samples A and B are normal lateritic soils.

Table 1: Summary of preliminary test for soil samples

Sample	Natural Moisture Content (%)	Specific Gravity	Liquid Limit (LL) (%)	Plastic Limit (PL) (%)	Plastic Index (PI) (%)
A	20.191	2.33	66.858	44.850	22.008
B	17.721	2.33	50.782	27.399	23.384
C	2.390	2.77	54.152	45.567	8.585

The variations in the Atterberg's limits tests for the samples at the natural state and when stabilized with 2-10% cement are shown in Figures 1-3, the liquid limits, plastic limits and the plastic index for the natural soil samples respectively for sample A are 66.86%, 44.85% and 22.01%, for sample B are 50.78%, 27.40% and 23.38% respectively, and 54.15%, 45.57% and 8.59% respectively for sample C. The addition of cement in percentages desired (2%, 4%, 6%, 8% and 10%) to the soil samples caused a change in the Atterberg's limits of all the soil samples. The optimum cement stabilized for samples A and B were obtained at 10% and at 8% for sample C.
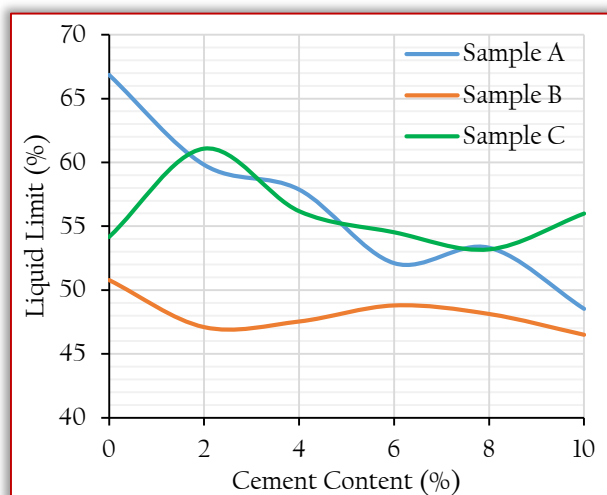
Figure 1: Variation in Liquid Limits for soil samples A, B and C with application of wood ash
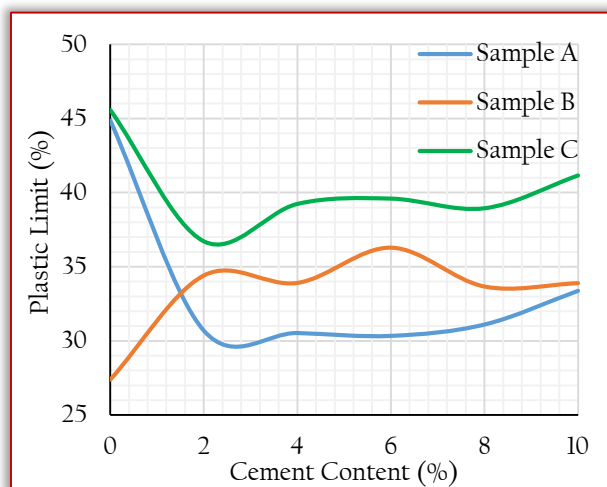
Figure 2: Variation in Plastic Limits for soil samples A, B and C with application of wood ash
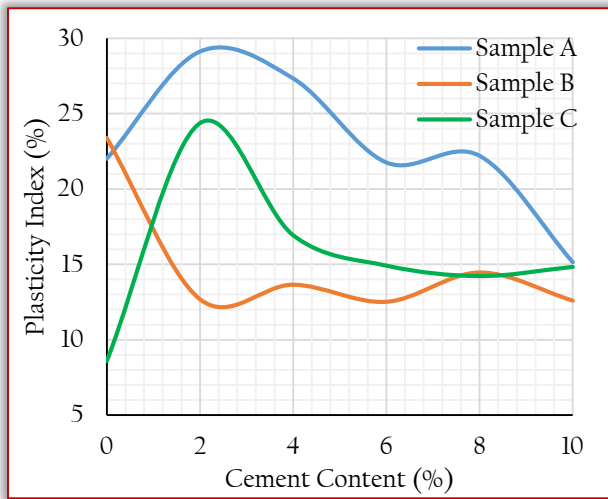
Figure 3: Variation in Plasticity Index for soil samples A, B and C
with application of wood ash

— Engineering Strength Tests
Table 2 shows the summary of the compaction test results at optimum cement stabilization. The Maximum Dry Densities (MDD) of all the samples attained maximum values at 2% wood ash stabilization before dropping. This indicates that the optimum MDD potential for the samples A and B is at 10% cement and 2% wood ash stabilization while that of sample C is at 8% cement and 2% wood ash stabilization.

Table 2: Summary of compaction test results for samples A, B and C at optimum cement

Sample	Percentage Stabilization Cement Wood-ash ratio (%)	Optimum Moisture Content (OMC) (%)	Maximum Dry Density (kg/m^3)
A	0	20.28	1587.99
	10 : 0	19.30	1588.76
	10 : 2	22.80	1588.23
	10 : 4	26.61	1483.78
	10 : 6	21.29	1462.64
B	0	24.19	1548.89
	10 : 0	20.96	1636.09
	10 : 2	22.27	1604.08
	10 : 4	24.61	1547.05
	10 : 6	21.16	1512.61
C	0	32.49	1506.45
	8 : 0	24.22	1555.67
	8 : 2	26.32	1529.42
	8 : 4	27.28	1524.51
	8 : 6	27.22	1523.62

The result of the CBR test on samples A, B and C at optimum cement is summarized in Table 3. The addition of wood ash lowered the unsoaked CBR of all the samples. The CBR value of sample A reduced from 11.00 to a minimum of 7.00 at both 2% and 4% wood ash stabilization, while those of samples B and C reduced from 17.00 and 5.00 to 6.00 and 2.00 at 6% and 2% respectively wood ash stabilization.
The summary of undrained triaxial shear strength tests results is presented in Table 4. The shear stresses of the samples increased when stabilized with wood ash at optimum cement contents.

Sample C with a natural shear stress value of 64.88 kN/m^2 increased to 141.14 kN/m^2 after stabilization with optimum 8% cement and 6% wood ash contents while those of samples A and B increased from 100.26 kN/m^2 and 95.76 kN/m^2 to 112.66 kN/m^2 and 133.27 kN/m^2 respectively after stabilization with optimum 10% cement and 4% wood ash contents.

Table 3: Summary of CBR test results

Sample	Percentage Stabilization Cement Wood-ash ratio (%)	CBR Value
A	0	2.00
	10 : 0	11.00
	10 : 2	7.00
	10 : 4	7.00
	10 : 6	8.00
B	0	4.00
	10 : 0	17.00
	10 : 2	9.00
	10 : 4	7.00
	10 : 6	6.00
C	0	2.00
	8 : 0	5.00
	8 : 2	2.00
	8 : 4	4.00
	8 : 6	4.00

Table 4: Summary of undrained triaxial test results

Sample	Cement, Wood-ash ratio (%)	Deviator stress (kN/m^2)	Cohesion (kN/m^2)	Angle of internal friction (Ø)	Shear stress (τ) (kN/m^2)
	0	160.63	35.56	21.94	100.26
	10 : 0	180.07	38.67	23.57	117.23
A	10 : 2	135.56	18.28	26.81	86.79
	10 : 4	156.39	19.47	30.79	112.66
	10 : 6	130.38	18.55	26.92	84.75
	0	175.83	72.70	7.47	95.76
	10 : 0	190.72	40.17	24.40	126.68
B	10 : 2	220.03	99.62	6.49	124.68
	10 : 4	221.75	125.37	2.04	133.27
	10 : 6	182.70	35.79	27.49	130.86
	0	116.67	28.96	17.11	64.88
	8 : 0	173.25	35.67	27.86	143.64
C	8 : 2	161.62	45.77	17.20	95.8
	8 : 4	151.28	32.81	21.68	92.95
	8 : 6	181.55	23.19	33.01	141.14

CONCLUSION
Stabilization of cement lateritic soil with wood ash improved the quality of soil by significantly reducing the plasticity index, plastic limit and liquid limit of the soil samples. Addition of cement with wood ash to subsoil samples increased their maximum dry densities by significant amount.
The CBR values for the unstabilized subsoil samples were also increased. The CBR values for the stabilized soil samples A and B, increased with the addition of 10% cement and up-to 6% wood ash. The CBR values for the stabilized soil sample C increased with the addition of 8% cement and 6% of Wood Ash.

It could also inferred from the shear stress test results that the addition of optimum cement content of 10% and 2% WAP content to sample A and B increased the shear stress of the soil samples while addition of optimum cement content at 8% and 2% WAP content increased the shear stress of the soil sample C.

It was therefore concluded that WAP is an effective additive on cement stabilized lateritic soil that improves the properties of the subsoil foundation and helps in forming colloidal particles and reduction in the tendency of the subsoil to swell when wet.

References

[1] Abdullahi, M., "Characteristics of wood ash/OPC concrete. Leonardo Electronic Journal of Practices and Technologies", Vol. 5: pp. 9-16, 2006.

[2] Alhassan, M., and Mustapha, M., "Effect of Rice Husk Ash on Cement Stabilized Laterite. Leonardo Electronic Journal of Practices and Technologies", Vol. 6, No.11: pp. 47- 58, 2007.

[3] Amu, O.O., "Lecture Note on Transportation Engineering II, Department of Civil Engineering, Obafemi Awolowo University, Ile-Ife", 2010.

[4] Amu, O.O., Adewumi, I.K., Ayodele, A.L., Mustapha, R.A., and Ola O.O., "Analysis of California bearing ratio values of lime and wood ash stabilized lateritic soil". Journal of Applied Science Vol. 5: pp. 1479-1483, 2005.

[5] Andres, C.K. and Honkala, T.I., "Masonry Materials, Design Construction". 1st Ed. Reston Publishing Company Inc., Virginia, 1978.

[6] Army study guide, (2008). Military Engineers Soil Mechanics. British Standards Institution, Methods of Testing for Soil for Civil Engineering Purpose, BS 1377, London.

[7] Bwalya, M., "Utilisation and improvement of lateritic gravels in road bases. International Institute for Aerospace Survey and Earth Sciences (ITC)", Section Engineering Geology, Kanaalweg 3, 2628 EB, Delft, Netherland, 1998.

[8] British Standard 1377-1990:1-8. "Soils for Civil Engineering purposes". British Standards Institution. ISBN 0580 17692 4

[9] Elinwa, A.U., and Ejeh, S.P., "Effects of the incorporation of sawdust waste incineration fly ash in cement pastes and mortars". Journal of Asian Architecture and Building Engineering Vol. 3: pp. 1-7, 2004.

[10] Fajobi, A.B., and Ogunbanjo, O.O., "Effect of moisture content and wood ash on the strength of adobe bricks. B.Sc. Thesis (unpublished)", Department of Civil Engineering, Obafemi Awolowo University, Ile-Ife, 1994.

[11] Federal Department of Forestry, "Nigerian Forestry Action Programme", Abuja, 1996.

[12] Misra, M.K., Ragland, K.W. and Baker, A.J., "Wood ash composition as a function of furnace temperature", Biomass Bioenergy Vol. 4: pp. 103-116, 1993.

[13] Naik, T.R., "Wood ash: As a new source of pozzolanic material". Center for By-Products Utilization (CBU) Report. University of Wisconsin, Milwaukee CBU-2000-02 (REP-371), 2000.

[14] Naik, T.R., Kraus, R.N., and Siddique, R., "Use of wood ash in cement-based materials". Center for By-Products Utilization (CBU) Report, University of Wisconsin, Milwaukee CBU-2003-19 (REP-513), 2003.

[15] Naik, T.R., and Kraus, R.N., "A new source of pozzolanic material. Concrete International", Farmington Hills, MI, USA: American Concrete Institute Vol. 25, No. 12: pp. 55-62. 2003.

[16] Neville, A.M., "Properties of Concrete, 4th ed.", Pearson Education Asia Ltd, Malaysia, 2000.

[17] O'Flaherty, C.A., "Soil-Stabilized Pavements. In: Highways: The Location, Design, Construction and Maintenance of Pavements". C. A. O'Flaherty, ed., Malta, Butterworth-Heinemann, 2002.

[18] Oguntona, O.T., "Geotechnical properties of lime stabilized lateritic soils modified with sawdust ash. B.Sc. Thesis (unpublished)", Department of Civil Engineering, Obafemi Awolowo University, Ile-Ife, 2008.

[19] Okunade, E.A., "Engineering properties of lateritic adobe bricks for local building construction and recommendations for practice". Journal of Engineering and Applied Science Vol. 2: pp. 1455-1459, 2007.

[20] Traditional lime, "Pozzolan <http://www.traditioallime.com/glossary/>", 2010

[21] Udoeyo, F.F., and Dashibil, P.U., "Sawdust ash as concrete material". Journal of Material and Civil Engineering Vol. 14: pp. 173-176, 2002.

[22] United State Army, "Soil Stabilization for Pavements. Technical Manual", NO.5-822-Air Force Manual NO. pp. 32-1019. 'Washington, DC, 1994.

[23] Vitromineral, "About pozzolan <http://www.vitrominerals.com/pozzlans, htm>", 2005.

[24] Whitlow, R., "Basic soil mechanics, 3rd Ed. John Wiley & Sons Inc.", New York, 1995.

[1.]Tamás MOLNÁR, [2.]Péter SZUCHY, [3.]Sándor CSIKÓS,
[4.]László GOGOLÁK, [5.]István BÍRÓ, [6.]József SÁROSI

INVESTIGATION OF MECHANICAL CHARACTERISTICS OF PLASTIC COMPOSITES

[1-6.]Department of Technology, Faculty of Engineering, University of Szeged, Szeged, HUNGARY

Abstract: This paper introduces the present state of plastic composite research on the Technical Faculty. The goal of our examination is to analyze the operational and economy efficiency anomalies with testing and analyzing the mechanical characteristics of the plastic composites used in the aircraft industry in order to make a proposal for such compounds that solve these problems. In the first period we made several tests of materials which were cut out of damaged airplanes. In the latest period of the research we analyzed different composite materials produced directly for our purpose. One part of the composites were produced by supplier, the other part were made by us. First we manufactured the specimens than we made tensile strength tests in order to get the basic mechanical parameters (upper and lower yield points, tensile strength, and elongation at rupture) of the composite materials. Here we introduce all the parameters of the tests. The following step is to test the composites for fatigue with our recently constructed folding machine.
Keywords: plastic composites, material test, mechanical strength characteristics

INTRODUCTION

Aircraft industry has a significant demand for light weight structural materials in order to reduce the costs of fuel, since the payload is only 20% of a presently used cargo aircraft's take-off weight, the circa half of the rest 80% is the empty weight. One of the most obvious ways to reduce weight of planes is using light structural materials with advanced parameters. The composite materials are one of the most promising potentials but their application in large quantities is still limited by their price and some disadvantageous attributions compared to some other structural material.

In this research project we previously purchased and calibrated the necessary instruments, we manufactured the standard test specimens from different damaged airplane wings received from the Airport of Szeged. The main goal was to analyse and compare such materials that are available from trade release. During the tests we analysed the upper and lower yield points, tensile strength, and elongation at rupture which features are essential from the point of view of their application.

The following step is presented by this paper, where the composite materials and specimens were produced directly for our demand. This was partly made by outer supplier but at the end we decided to produce the composites ourselves. This was a brand new production technology in the life of the Faculty, so we prepared it really carefully. After mapping the possibilities we decided which technic to choose, than purchased the necessary basic composite materials and the production tools were only hired. The first production was made together with outer experts, than we made the second production alone. Manufacturing and testing the specimens were done as before.

MATERIALS END METHODS

The cross-linked polymer matrix composites have usually low elongation at rupture and rigid breakage that means disadvantage for hitting or complex loads [Pukánszky, 2011]. At aircraft application there are many fatiguing or impulsive loads so it is an essential demand against the structural materials not to be rigid or break at small deformation. The fibre reinforced epoxy resin composites have long lifetime beside proper design and production technology. Due to their inhomogeneous structure the peak loads or long term alternating loads do not cause fatigue break [Czvikovszky, 2000]. The strength of composites decreases slightly but continuously in function of time and load because of the micro-cracks in bedding material and the insubstantial breaking of reinforcing fibres. There is a significant difference between the tensile strength and the compressive strength of composites which can be 15-30% in case of glass or carbon fibres, but it can reach even 50% at extreme high tensile strength carbon fibres. Composite materials with aramid fibres (Kevlar) can have 60% lower compressive than tensile strength so the structures loaded with alternate normal stress have to be sized for compressive strength [Vermes, 2015].

Stress causes deflection in materials, so on the basis of their tensile strength diagram we can distinguish rigid, tough or rubbery behaviour. The fibre reinforced systems are rather rigid generally [Koncz et al., 2000]. In case of polymers the reason of the local maximum can be the too fast mechanical impact (because of their time-dependent behaviour) that the material cannot follow up without detention by changing of its structure [Mészáros, 2009]. During the tests of composites the yield stress (σ_{Yield}) is defined as the stress value belonging to the intersection of the 10% parallel shifted line of the beginning modulus with the real stress-strain curve. The yield strain (ε_{Yield}) belongs to this point as well. The tough strain ($\varepsilon_{ductile}$) starts at this point and ends at the rupture stress [Vermes, 2015]. The typical tensile stress diagrams of polymers applied in the biggest amount nowadays are represented on Figure 1. The different polymer types show really variant behaviour. Some of them break rigidly and others can sustain even several 100% strain without breaking [Gunczer, 2009].

It is featuring the polymers that the circumstances of test influence significantly the mechanical properties of the material. The main influential parameters are the followings: speed of tear, test temperature, moisture. At higher speed of tear the materials with viscoelastic features (polymers) behave more rigidly, usually their

strength is higher. Only a few degree of test temperature difference can influence significantly the strength, the character of the tensile diagram. The polymers under their glass transition temperature (T_g) behave glassy, above it they behave rather tough [Sápi, 2015]. There are some polymers (e.g. polyamides, polyesters, natural polymers, some kind of fibre reinforced composites) which can absorb so many (1-4%) moisture that can influence their behavior. Moisture decreases the strength, the Young-modulus and increases the elongation break [Pék, 2000].

Figure 1. Tensile test diagrams of different polymers [Gunczer, 2009]

Figure 2. General plastic tensile strength diagram
with six stages [Pék, 2000]

As the result of the tensile test we get the load-elongation (F-Δl) curve (valid for the given circumstances) which can be transformed to stress-strain (σ-ε) curve (Figure 2.) This tensile strength diagram can be segmented to six stages:
— small loads, linear elastic deflection;
— as the load grows, the linear viscoelastic deformation starts (it deforms back by time);
— at higher loads nonlinear viscoelastic deformation comes;
— neck-formation stage, stress decreases, local arrangement of macro-molecules starts;
— spread of neck-formation, steady flow stage;
— because of the global arrangement the tensile strength increases (deformation hardening). In this stage the arranged fibres reach their ultimate tensile strength and break one after the other.

From the tensile strength diagram the following mechanical values can be determined [Sápi et al. 2015]: plastic, yield, maximum, break

values of strength and strain. Two kind of Young-modulus can be calculated:
— Chord modulus (E_{ch}): the chosen point of curve is connected with the origin and the gradient gives the modulus [Gáthi et. al., 2011].
— Tangent modulus (E_t): the tangent at the chosen point of curve gives the modulus.

As the tensile strength curve is non-linear, the tangent of it changes point by point as well. The tangent at the origin on the stress-strain curve is called initial Young modulus. In practice the Young modulus of the material is regarded as the gradient of the line going through the curve points belong to the 0,05% and 0,25% relative elongation values [Sápi et al. 2015].

RESULTS AND DISCUSSION

At choosing the right standard specimen shape for the test it was an essential consideration to be suitable for the Galdabini Quasar 100 tensile test machine (Figure 3.) available in the Technical Faculty, University of Szeged. The standard's smallest specimen was manufactured that could be tested by our tensile test machine adjusting with proper parameters. First we executed a probe test to control the accidentally emerging problems, this was the right calibration of the breaking elongation value. The specimen and its template was created by 3D solid body design software (Figure 3).

Figure 3. Tensile test machine, template of specimen,
material test labour

As it was mentioned before the first set of specimens were manufactured by outer supplier. The content of the specimens: Polymer, Polyethylene PE-TIP-7700M. Composite: Sulphur, argillaceous-mineral. The signature of the basic polymer PE-K001. The specimen samples are shown on Figure 4. It is visible that the elongation at neck-formation was really high.

There were several specimens prepared from the basic compound with different weight percent argillaceous-mineral and Sulphur. The signature of the samples: PE-K002: 0,5% mineral, PE-K003: 0,5% Sulphur. The result of tests are shown on Table 1.

Figure 4. The first set of specimen before and after the tensile tests

Table 1. Test results of specimens of the first set

Specimen code	Date of test	Thickness (a)	Width (b)	Elongation at break	F_t	F_m	R_m
		(mm)	(mm)	(mm)	(N)	(N)	(N/mm²)
PE-K001-1	18-02-2019	2,18	3,89	138,2	52,5	145,5	17,16
PE-K001-2	18-02-2019	2,14	3,89	122,3	58,5	131,0	15,74
PE-K001-3	18-02-2019	2,42	3,89	144,2	13,5	159,5	16,94
PE-K001-4	18-02-2019	2,09	4,00	63,2	21,5	117,0	14,00
PE-K001-5	18-02-2019	2,28	3,95	146,2	43,0	166,0	18,43
PE-K002-1	04-03-2019	2,11	3,85	25,34	63,5	123,5	15,28
PE-K002-2	04-03-2019	2,12	3,85	126,0	56,5	131,0	16,2
PE-K002-3	04-03-2019	2,11	3,85	164,6	12,5	169,5	20,96
PE-K002-4	04-03-2019	2,18	3,89	54,5	32,5	130,5	16,4
PE-K002-5	04-03-2019	2,14	3,85	26,22	52,5	139,0	17,19
PE-K003-1	04-03-2019	2,15	3,85	211,4	38,5	127,0	15,34
PE-K003-2	04-03-2019	2,15	3,85	13,28	67,5	121,0	14,62
PE-K003-3	04-03-2019	2,14	3,86	93,13	51,5	137,0	16,61
PE-K003-4	04-03-2019	2,16	3,85	93,22	49,0	139,0	16,79
PE-K003-5	04-03-2019	2,15	3,85	178,2	38,5	137,0	16,55

The tensile strength diagrams shows the different behaviors of the different specimens as it is indicated on Figure 5-7.

After the tests of the first set of specimen manufactured by outer supplier we decided to produce composites ourselves. With the help of some suppliers we chose the production technology: the vacuum-infusion procession with epoxy resin and carbon fibres.

The main advantage for us as selection criteria were the relative uniform quality and the environment-friendly technology. The first plates (with 4 and 6 reinforcing carbon-fibre fabric) were produced together with outer experts, than the second production (3 and 5 fabric) was executed without help. Only a few tensile tests were completed yet, Figure 8 shows only some introducing details of them. Number 1. specimen has 3 reinforcing layer, 2. specimen has 4 layer, 3. one has 6 fabric.

Figure 5. Tensile test result of PE-K001 (1-5) composites
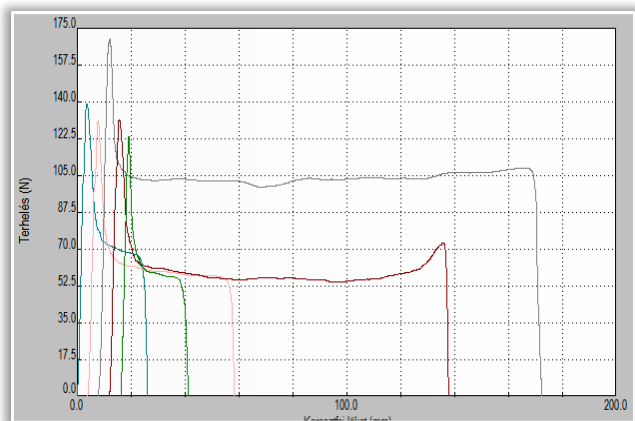
Figure 6. Tensile test result of PE-K002 (1-5) composites
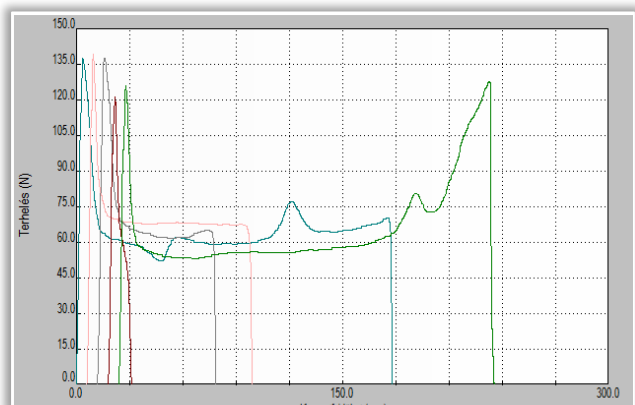
Figure 7. Tensile test result of PE-K003 (1-5) composites

We still have a lot of work on the production process and on the tensile test process to eliminate the visible problems, but the initial results are rather promising (Table 2). After the tensile tests we execute fatigue tests with our self-designed and constructed fatigue-test machine. We are searching the difference of tensile tests done before and after a 10 million fatiguing folding.
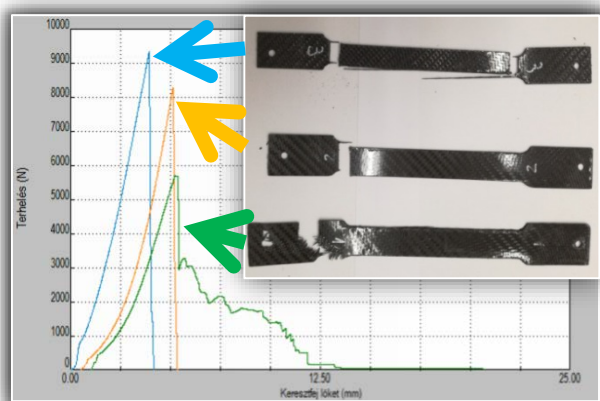
Figure 8. Tensile test results of self-made composites: **Preload:** 20mm/min, 100N; **Loading force:** 10mm/min up to break

Table 2. Test results of specimens of the self-produced second set

Specimen code	Date of test	Thickness (a) (mm)	Width (b) (mm)	Ft (N)	Fm (N)	Rm (N/mm2)
Composite 1	27-05-2019	0.75	21.00	41,5	5691,0	361,37
Composite 2	27-05-2019	1,15	21,00	40,0	8237,5	341,10
Composite 3	27-05-2019	1,9	21,00	75,5	9322,0	233,63

CONCLUSION

In the range of structural material the polymers and their composites applications are worldwide spread, because of their excellent mechanical, physical and chemical features. The small density and the light weight belongs to this with the high strength, the damping and insulating ability, the chemical and corrosion resistance, the designable anisotrophy, etc. make the synthetic polymers nowadays one of the most favourite structural material. With their application not only energy can be saved but this material group plays key role in the sustainable development as well. Nowadays the research of polymers trends towards developing such materials which are more environmentally friendly, reducing the energy supply, making our everyday life easier and comfortable.

Acknowledgements

REFERENCES

[1] Czvikovszky – Nagy – Gaál: A polimertechnika alapjai, Műegyetemi Kiadó, 2000
[2] Gáthi Balázs – Koncz Imre: Repülőgépek szerkezet, A II. Nemzeti Fejlesztési Terv Társadalmi Megújulás Operatív Program TÁMOP-4.1.2/A/2-10/1-2010-0018 azonosító számú programja keretében készült jegyzet. 2011.
[3] Gunczer L.(2009): Anyagismeret és Gyártástechnológia jegyzetmodulok.
[4] Gunczer L. (2009):, Anyagvizsgálatok. SZTE MK, Szeged 2009.
[5] Mészáros-Varnyú (2009): Műszaki anyagismeret (CooSpace elektronikus jegyzet).
[6] Gunczer L. (2009): Anyagszerkezettan és gyártástechnológia, Egyéb anyagok (kiegészítés). SZTE Univ Kiadó, Szeged 2009.
[7] Rácz, Elemér. Repülőgéptervezés. Budapest : Tankönyvkiadó, 1955.
[8] Lukács – Csomós – Gácsi - Karcagi – Magyar – Tomolya: Fáradásos repedésterjedés különböző típusú kompozitokban, Anyagvizsgálók Lapja, 2004/4
[9] Koncz – Magyarosi – Pusztai: Kompozitok és szendvicsszerkezetek - Repülőgép kompozit szerkezetjavító szakmai oktatási jegyzet, 2000
[10] Megson, T.H.G. Aircraft Structure for Engineering Students. Arnold, 1999. ISBN 0 340 70588 4.
[11] Pukánszky B., Móczó J.: Műanyagok. Typotex kft., Budapest, Magyarország (2011).
[12] Czél G., Jalalvand M., Wisnom M.R.: Demonstration of pseudo-ductility in unidirectional hybrid composites made of discontinuous carbon/epoxy and continuous glass/epoxy plies. Composites Part A: Applied Science and Manufacturing, 72, 75-84 (2015).
[13] Wisnom M.R., Czél G., Fuller J.D., Jalalvand M.: High performance pseudo-ductile composites. 20th International Conference on Composite Materials, Copenhagen, Denmark (2015).
[14] Czél G., Wisnom M.R.: Demonstration of pseudo-ductility in high performance glass/epoxy composites by hybridisation with thin-ply carbon prepreg. Composites Part A: Applied Science and Manufacturing, 52, 23-30 (2013).
[15] Sápi A. Nagy L. (2015): Segédanyag a Nanotechnológia és anyagvizsgáló laboratóriumi gyakorlathoz jegyzet, SZTE-TTIK, Anyagtudományi Intézet.
[16] Pék L. (2000): Anyagszerkezet és anyagismeret, Dinasztia Kiadó, Budapest, ISBN 9636573263
[17] Vermes B.(2015) BME-Gazdaságtudományi Egyetem Polimertechnika Tanszék, TDK: Megnövelt szívósságú, szénszál/epoxi kompozit főiránytól eltérő húzó tulajdonságainak meghatározása.

ISSN: 2067-3809

[1.]Maroš MARTINKOVIČ, [2.]Martin NECPAL

ESTIMATION AND UTILIZATION OF STRUCTURE ANISOTROPY IN TUBE DRAWING

[1–2.]Slovak University of Technology in Bratislava, Faculty of Materials Science and Technology in Trnava, SLOVAKIA

Abstract: Anisotropy of microstructure in case of forming of metal depends on technology parameters of processes. In case of deformation of metals grain boundaries orientation can be observed. In the polycrystalline material (metal, alloy) the main microstructural parameter is grain boundary – surface interface between individual grains. In case of isotropic non deformed structure the grains have isometric dimension mean grain size or specific surface area of grain boundaries can be measured. In case of anisotropic plastically deformed structure the grains have anisometric dimension, it is necessary to describe their anisotropy. Application of stereology methods to statistic reconstruction of three–dimensional plastic deformed material structure by bulk forming led to detail analysis of material structure changes. The microstructure of cold drawing tubes from STN 411353 steel was analysed. Grain boundaries orientation was measured on perpendicular and parallel section of tubes with different degree of deformation. The anisotropic microstructure was decomposed into isotropic, planar and/or linear oriented components – specific surface area of grain boundaries and these parameters were measured using stereology. Degree of grain boundary orientation is estimated as ratio of oriented specific surface area to total specific surface area. So the degree of grain boundary orientation depends on grain deformation, these results can be used for estimation of local plastic deformation in arbitrary places in volume of tube drawing which is not the same. This analysis can leads to optimization of technology parameters of the process.
Keywords: mechanical working, tube drawing, stereology, grain boundary, orientation, deformation

INTRODUCTION

Anisotropy of microstructure in case of forming of metal depends on technology parameters of processes. In case of deformation of metals grain boundaries orientation can be observed. In the polycrystalline material (metal, alloy) the main microstructural parameter is grain boundary – surface interface between individual grains. In case of isotropic non deformed structure the grains have isometric dimension mean grain size or specific surface area of grain boundaries can be measured.

In case of anisotropic plastically deformed structure the grains have anisometric dimension, it is necessary to describe their anisotropy [1]. The anisotropic microstructure is decomposed into isotropic, planar and/or linear oriented components – specific surface area of grain boundaries and these parameters are measured using stereology [2]. Degree of grain boundary orientation is estimated as ratio of oriented specific surface area to total specific surface area. These results can be used for estimation of local plastic deformation in arbitrary places in volume of forming pieces.

Real state of grain shape is quit impossible to describe, therefore model of conversion of degree of grain boundary orientation to deformation based on an idealized shape (tetrakaidecahedron) of grains has been proposed.

EXPERIMENTAL MATERIAL AND METHODS

— Material

The semi–product for cold drawing seamless tubes was hot rolled steel tubes from STN 411353 steel (recrystallization was passed, grain boundaries deformation was minimized) with the following dimensions: outside diameter 70mm, wall thickness 6,3 mm, length 4000 mm. These steel tubes were cold drawn in a one step with increasing of diameter reduction and simultaneous increasing of wall thickness reduction.

The tube dimensions after deformation were as follows: outside diameter 50mm, wall thickness 3,75mm, length 9255mm. True macroscopic deformation was calculated from these dimensions (see Table 1). The probe was cut from the tube. The section plains were oriented in three main directions of the tube deformation (see Figure 1) – parallel (perpendicular to φ_3), orthogonal (perpendicular to φ_1) and tangential (perpendicular to φ_2) in relation to the main tube's axes.

The cuts were metallographically prepared – mechanically grinded and polished, chemically etched in 3% HNO_3 alcohol solution. On these plains the structure of the steel material was observed with the proper magnification of a light microscope. An example of the steel structure in the initial state and in the state after deformation is shown in Figure 2.
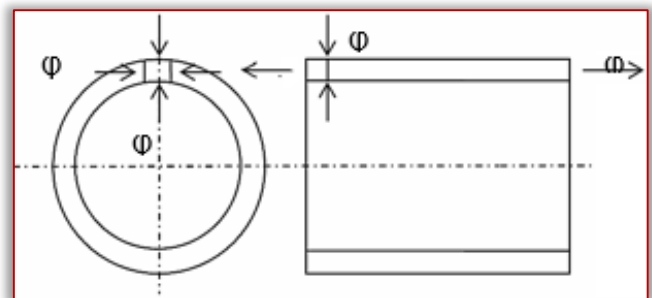
Figure 1: The scheme of tube deformation

— Orientation measurement

There are only three principal schemes of elementary bulk deformation, which allows very good evaluation of the strain analysed in place of the forming body. They are basic indicators for analysis and evaluation of the deformation state caused by external load. The scheme of deformation presented in Figure 3 relates to tube drawing, $\varphi_1 > 0$, φ_2, $\varphi_3 < 0$ and $\varphi_1 = -\varphi_2 - \varphi_3$. True (logarithmic) strain φ is defined from its dimension before deformation l_0 and after deformation l and from relative strain δ as:

$$\varphi = \int_{l_0}^{l} \tfrac{1}{l}dl \; ; \qquad \delta = \int_{l_0}^{l} \tfrac{1}{l_0}dl \; ; \qquad \varphi = \ln(1+\delta) \qquad (1)$$
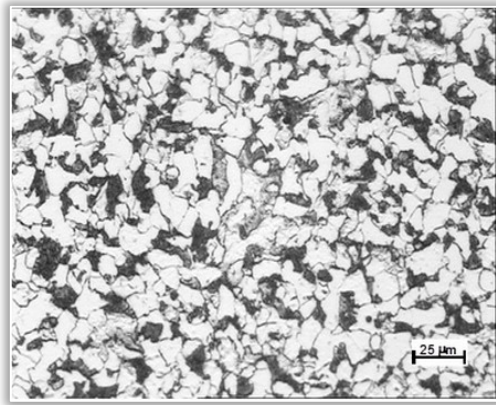
(a)
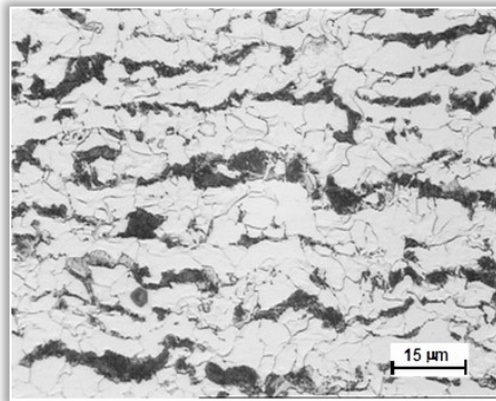
(b)
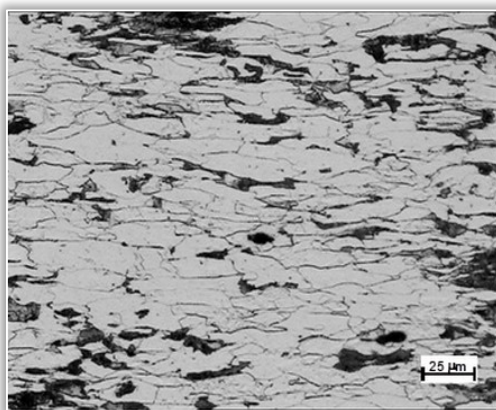
(c)
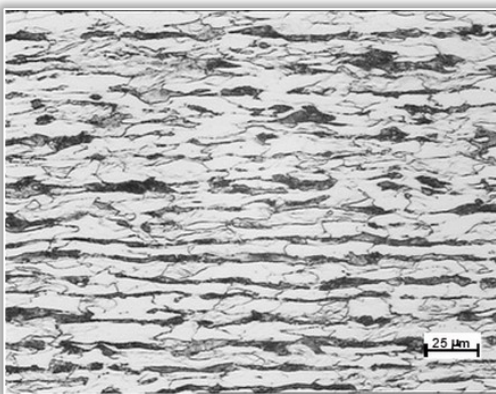
(d)

Figure 2: An example of structure in the middle of wall thickness: undeformed in the initial state a) and after deformation, b) in the orthogonal plane, c) in the tangential plane, d) in the parallel plane
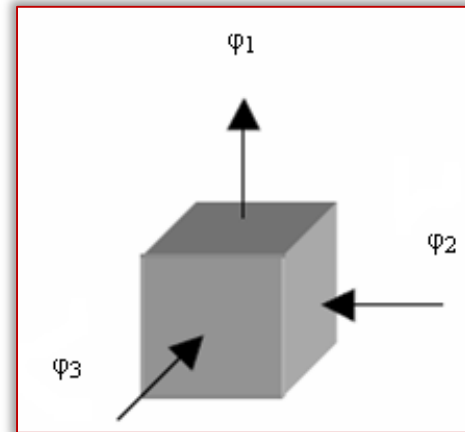
Figure 3: Principal schemes of elementary bulk deformation in case of tube drawing

Direction of the grain boundary's orientation is the same as the direction of deformation. If the deformation scheme is known, grain boundaries can be decomposed into isotropic, planar and linear oriented components. Saltykov stereology methods with oriented test lines were used [1].
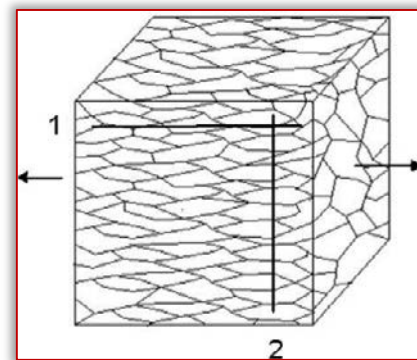
(a)
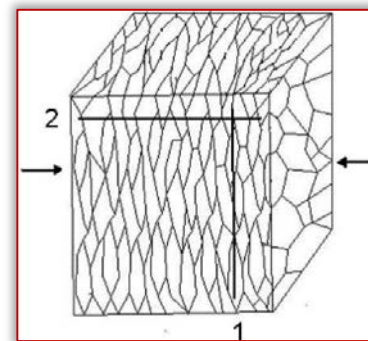
(b)

Figure 4: Anisotropic structure due to various types of deformation– linear a), planar b)

In the case of linear deformation (Figure 4a – direction of deformation is marked by arrows), grain boundary orientation can be observed in a plane parallel to drawing direction – linear orientation, in the case of planar deformation (Figure 4b) in a plane perpendicular to the deformation plane – planar orientation. On a metallographic cut, test lines are placed perpendicular and parallel to the grain boundary orientation direction affected by the straining.

From the specific number (number to unit of length) of parallel test lines (1 in Figure 4) intersections with grain boundaries $(P_L)_P$ and the

perpendicular lines (2 in Figure 4) $(P_L)_O$ was total specific surface area (area to unit test volume) $(S_V)_{TOT}$ of grains estimated – according to equation (2) in the case of planar orientation and according to equation (4) in the case of linear orientation.

The planar oriented part of the specific surface area $(S_V)_{OR}$ of grains was estimated according to equation (3), the linear oriented part according to equation (5). The physical dimension of all the values is mm^{-1}. Degree of grain boundaries orientation O was estimated as $(S_V)_{OR}$ to $(S_V)_{TOT}$ ratio.

$$(S_V)_{TOT} = (P_L)_O + (P_L)_P \qquad (2)$$

$$(S_V)_{OR} = (P_L)_O - (P_L)_P \qquad (3)$$

$$(S_V)_{TOT} = \frac{\pi}{2}(P_L)_O + \left(2 - \frac{\pi}{2}\right)(P_L)_P \qquad (4)$$

$$(S_V)_{OR} = \frac{\pi}{2}\left[(P_L)_O - (P_L)_P\right] \qquad (5)$$

—— Conversion of orientation to deformation
However grain boundaries orientation is proportional to deformation, it is not the same. Therefore a conversion of orientation to deformation must be developed. It is completely impossible to describe actual shape of the grain in material structure exactly. Therefore deformation of various idealized grain shapes can be investigated. For instance crystals can be modeled by regular polyhedron – tetrakaidecahedron [2].

One method is based on dependence of the ratio of relative surface area of grain boundaries in deformed state S_V and undeformed state S_{V0} to strain [3]. The method requires knowledge of the parameter of structure in case of zero value of initial deformation, which is unknown in most of cases and this parameter is not the same in the whole volume of pieces and it depends on grain size. Our conversion method is based on the analysis of orientation – deformation relationship of a grain. Dependence of true strain φ on the value of orientation O was derived from three basic equations – definition of deformation (1), definition of degree of orientation (2–5) and invariability of volume ($V_0 = V$ – initial volume is equal to volume after plastic deformation, $φ_1 + φ_2 + φ_3 = 0$).

The solution of the system includes one free parameter – grain size. Solution of the system of equations for used idealised grain shapes is independent of the initial dimension of the grain – strain depends only on the shape of grain and it does not depend on its dimension. As a result the method enables estimation of local plastic deformation from the estimation of microstructure anisotropy in an arbitrary place on the body with an arbitrary state of initial deformation. The solution and the result are relative complicated, so detailed description is in [4].

DISCUSION AND CONCLUSION

Degree of orientation of grain boundaries was measured in three places across the wall thickness – near the outside surface (Out), in the middle (Mid) and near the inside surface (In).

Test lines were placed perpendicular and parallel to the grain boundary's orientation direction which was affected by straining (see Figure 4). From the specific number (number to unit of length) of parallel test line intersections with grain boundaries $(P_L)_P$ and perpendicular ones $(P_L)_O$ the linear orientation O_L of grain boundaries affected by $φ_1$ (in the tangential plane) was calculated

from equations (4) and (5), planar orientation O_P of grain boundaries affected by $φ_2 - φ_3$ difference (in the orthogonal plane) was calculated from equations (2) and (3).

The relative measurement precision was always smaller than 10% with reliability 90%. True strain $φ_1$ and the difference between true strains $φ_2$ and $φ_3$ was determined using the procedure described in [4]. True strain $φ_2$ and true strain $φ_3$ were calculated from values of true strain $φ_1$, true strains $φ_2 - φ_3$ difference and invariability of volume ($φ_1 + φ_2 + φ_3 = 0$). The results of the measurement of grain boundaries orientation in different places of the steel specimens and the calculated true deformations are shown in Table 1.

Table 1: The measured of the grain boundary's orientation and the calculated deformation

Place	Deformed state						True macroscopic deformation		
	O_P	$φ_2 - φ_3$	O_L	$φ_1$	$φ_2$	$φ_3$	$φ_1$	$φ_2$	$φ_3$
Out	0,103	−0,166	0,645	0,867	−0,546	−0,351	–	–	−0,337
Mid	0,212	−0,329	0,694	0,975	−0,652	−0,323	0,839	−0,519	−0,320
In	0,238	−0,364	0,7	0,993	−0,678	−0,315	–	–	−0,301

We reported the problem of estimation and utilization of structure anisotropy in tube drawing. One can easily understand that there is a correlation between the change in the grain orientation and grain deformation and this correlation can be mathematically demonstrated [3, 4]. The analysis of local deformation could be performed experimentally on the basis of performed results.

One method [3] requires knowledge of the parameter of structure in case of zero value of initial deformation, which is in most of cases unknown. Our method can be used in case when knowledge of the parameter of structure in case of zero value of initial deformation is unknown.

The utilization of stereology metallography allow very simple and effective experimental estimation of plastic deformation degree by measurement of microstructure parameters of oriented grains caused by deformation in various places of bulk formed parts. Estimation of these parameters and consequential conversion of its values to true strain lead to determination of deformation in three main axes and an effective strain. Such results are very needful not only for effective technology application, but for instance for verification of bulk forming numerical model by comparing of these results with numerical simulated results of effective strain using finite elements method [5, 6].

Acknowledgment

Note:
This paper is based on the paper presented at ERIN 2018 – The 12th International Conference for Young Researchers and PhD Students,

organized by Brno University of Technology, CZECH REPUBLIC and Slovak University of Technology in Bratislava at Faculty of Mechanical Engineering, SLOVAKIA, in Častá-Papiernička, SLOVAKIA, between 02–04 May, 2018.

References

[1] S.A. Saltykov: Stereometričeskaja metallografia. (Stereometric metallography). Moskva: Metallurgia (1970).

[2] P.R .Rios, M.E. Glicksmanb: Modeling polycrystals with regular polyhedra. Materials Research 9 (2006), 231.

[3] Q. Zhu, M. C. Sellars, H. K. D. H. Bhadeshia: Quantitative metallography of deformed grains. Materials Science and Technology 23 (2007), 757.

[4] M. Martinkovic, S. Minarik: Short notes on the grains modification by plastic deformation, in: Hubbard D. (Ed.): Plastic Deformation. NOVA publishers (2016), 1.

[5] J. S. Chen, C. M. O. L. Roque, Ch. Pan, S. T. Button: Analysis of metal forming process based on meshless method. Journal of Materials Processing Technology 80–81 (1998), 642.

[6] S. Xiong, W. K. Liu, J. Cao, C. S. Li, J. M. C. Rodrigues, P.A.F. Martins: Simulation of bulk metal forming processes using the reproducing kernel particle method. Computers & Structures 83 (2005), 574.

[1.]Sridhar RAMASAMY, [2.]Rajenthirakumar DURAISAMY,
[3.]Karthick THANGAVEL, [4.]Srinivasan NAGARAJAN

EXPERIMENTAL EVALUATION OF SIZE EFFECTS IN MICRO DEEP DRAWING PROCESS OF THIN FOIL MATERIALS

[1-4.]Department of Mechanical Engineering, PSG College of Technology, INDIA

Abstract: Micro deep drawing of metallic cups is a cost effective technique if the parameters are suitably identified, but reducing dimensions increases the difficulties in manufacturing. In this work, formability study of pure copper foils and thickness distribution in micro deep drawing are carried out. The pure copper C1100 foil thickness of 100, 200 and 300 μm is selected and the limit drawing ratio is determined. In order to determine the forming depth in micro scale and force required in formed parts, a micro deep drawing tool assembly is developed. The results shows that 300 μm foil exhibits good formability in tensile test and Ericson cupping test. The excessive reduction in thickness specifically at the cup shoulder corner and the upper part of the side wall is located. The thinning is identified maximum at the side wall of the cup along the transverse direction. The results indicate that copper micro cups with high quality can be efficiently produced with appropriate forming parameters.

Keywords: Micro forming; cupping test; copper foils; formability; thickness distribution

INTRODUCTION

Microforming is an appropriate technology to manufacture very small metal parts, in particular for bulk production. Micro deep drawing process, which is a basic process of microforming to forming hollow, thin walled micro parts, is being one of the research focuses in microforming [1]. This process is prompted by the rapid development of micro electro mechanical systems, electronic industries and new energy and biomedical in recent years because of its high efficiency, high precision, mass production and low cost [2]. But better understanding of the process in relation to miniaturization is required to improve process stability, because several aspects of the process change when scaled down.

As a basic process of manufacturing, deep drawing provides a great application potential. But smaller the dimensions of part, the more difficult in manufacturing because of size effects. These size effects affect the tribology, which plays a great role in many forming technologies. This process involves forming products from metal foil of thickness ranging from 30 μm to 300 μm. In this work, a deep drawing process is carried out to produce micro cups using thin copper foils with a microforming die. The formability characteristics are studied for thin copper foils by using tensile tests and Erichsen cupping test. The forming force and thickness distribution is identified using microforming setup consists of a punch and die.

LITERATURE REVIEW

Micro deep drawing provides a great application potential to generate the mass production of micro-metallic cups of significantly lower overall cost and high quality [3]. Investigations in micro deep drawing are carried out and the limit drawing ratio was determined and the influences of friction coefficient at the flange and at the die radius are analyzed by vollersten et al. [4]. M.W. Fu et al. [5] conducted experiment of micro blanking and deep drawing using pure copper sheets with different grain sizes. The thinnest region appears at the bottom radius, while the bottom center region remains almost unchanged. Uneven thickness distribution along the cup axis is predicted in the surface and micro structural models are developed as a result of micro-friction and material heterogeneity [6]. Micro parts with two layers, copper and composite material annealed at 400 ºC is formed with micro deep drawing process. The formed cup shows no fracture and fewer wrinkles is reported by Fanghui et al. [7].

The pure copper C1100 conical cylindrical cups are successfully formed and thickness distribution is shown by Feng et al. [8]. Ihsan Irthiea et al. [9] recommended for the thin sheets to adopt relatively big initial gaps but not more than a particular limit. It may lead to excessive wrinkles at the shoulder corner and the flange region. It is proved that the stainless steel 304 cups with large aspect ratio can be produced by the micro deep drawing process by using flexible die. Polyethylene film is employed as lubricant in deep drawing of micro cups. The lubricant shows the significant decrease in forming load [10]. Liang Luo et al given that grain size affects micro deep drawing process and cup quality [11].

Chun-juwang noticed that there are many debris of copper sheet left on the contact surface of blank holder and female die after micro-deep drawing [12]. It is concluded from literature review that no sufficient research on parameter assessment for micro deep drawing operation. In this work, experimental investigations into micro deep drawing are carried out and the limit drawing ratio is determined.

EXPERIMENTS

To investigate the formability of material and thickness distribution, a robust die assembly is designed and micro deep drawing of pure copper C1100 of 100, 200 and 300 μm thickness have been conducted. The tensile test, Ericson cupping test performed in this work and die assembly are discussed in the subsequent sections.

⎯ Tensile test

The tensile tests have been carried out to examine the mechanical properties on micro tensile testing machine. The specimens used are shown in Figure 1.

Figure 1. Micro tensile test – copper C1100 foil

The sheets are cut into dog-bone shape for tensile test according to the ASTM standard specifications E8-04 [13].

── Erichsen cupping test

In Erichsen test, the punch is pressed into the sheet until fracture occurs. The depth of the bulge is noted at the fracture point. It is used to evaluate the formability of sheet metal based on the alloy and sheet thickness. In this experiment, nine samples (Figure 2.) of three different thickness of copper foil are taken and their responses are summarized in Table 1.

Table 1. Observations made during Erichsen cupping test of copper foil.

Thickness	Comments
100 µm	Uneven distribution of load and material tries to wrinkle while cupping
200 µm	Poor depth of deformation
300 µm	High depth of deformation and uniform thickness distribution

Figure 2. Erichsen cupping test – copper foil

── Experimental setup

Experimental set up developed to conduct micro deep drawing experiments, consists of three primary parts namely movable punch, blank holder and clamping plate. The copper C1100 circular blanks are made from 300 µm thickness by using the blanking punch and die sets shown in Figure 3.
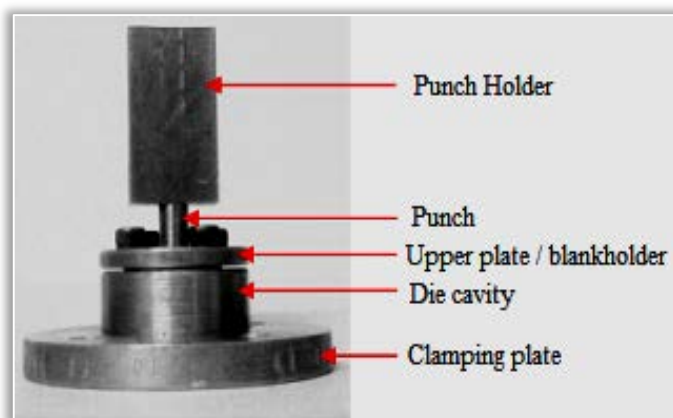
Figure 3. Micro deep drawing -Die assembly

The dimensions of the primary components in the die assembly are given in Table 2. In order to achieve the good shearing quality, clearance between the punch and die is to be 12-24 % of the initial foil thickness and it should be adopted for the punch-die set. The blanking tool setup is designed with about 45 µm clearance on its circumference.

Table 2. Geometrical parameters of micro-deep drawing die

Blank holder plate (mm)	Ø 50
Bottom plate (mm)	Ø 100
Punch (mm)	Ø 10

The experiments are conducted in zwick 10 kN capacity machine with punch velocity of 0.1 mm/s, punch load of 2373 N and blank holding force of 9.741 N. Figure.4. Shows the micro cups successfully produced under these forming conditions. In fact, the aspect ratios of the parts at different thickness are slightly various depending on how the sheet material sufficiently produces cups without any undesired tears.

Accordingly, results obtained that the final depths of the cups produced with different thick foils of 200 µm and 300 µm are 4.8 mm and 6.5 mm respectively. If it is formed beyond this limit, there will be the initiation of crack occurs at the interaction between wall and bottom of the cup near the shoulder (Figure 5) and it is propagated to the wall of the cup.

Figure 4. Cups formed with different initial thickness

Figure 5. Failure by crack propagation

RESULT AND DISCUSSIONS

The influence of the copper foil thickness, depth of formation, thickness distribution, failure mode, crack propagation and quality of the formed cups are investigated through these experiments. The results show that depth of deformation is 9, 5 and 4 mm for 300, 200 and 100 μm foil. It exhibits that the 300 μm has good formability in tensile test and Ericson cupping test.

⎯ Deep drawing force

The deep drawing force with deep drawing punch stroke for 300 μm thick copper foil is plotted. The peak indicates the maximum force required for deep drawing process and the slope after 4 mm depth shows possibility of crack propagation. The five trials have been conducted at room temperature of 29 °C with no lubrication condition. The various regions of deformations are shown in Figure 6 and the maximum failure load is 2400 N.
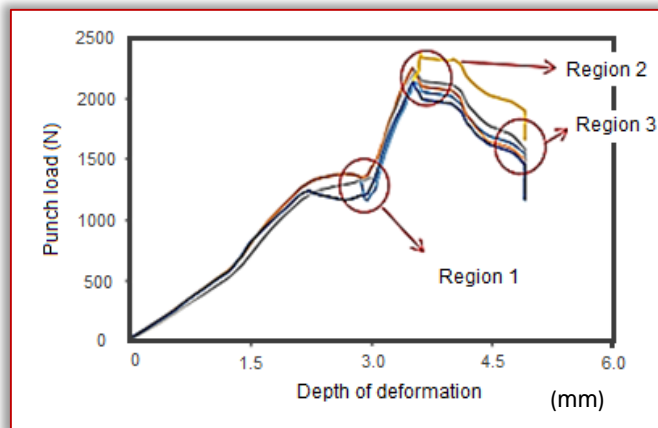
Figure. 6. Depth of deformation Vs Punch load on five trials

In region 1 is at which the depth of deformation crossed 3 mm material. In region 2, the blank is subjected to maximum force before attaining a cup height of 4 mm. During region 3, failure happened when depth of deformation approached around 4.8 mm. Hence it is clearly observed that drawing force decreases with the increase of grain size for each thickness size except the fracture case occurred in 300 μm, while under the particular grain size the load increases with the increase of thickness.

⎯ Thickness distribution

The thickness of the deep drawn cup is measured and the thickness distribution is obtained for the side wall and bottom of the cup.
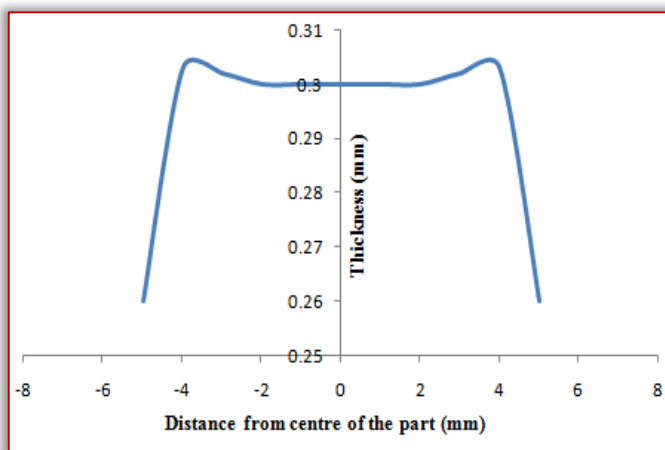
Figure. 7. Thickness distribution along circumference of cup

The thickness measurements are carried out at various points along the curvilinear path of the sectioned cup. The curves (Figure 7) relating to the thickness distributions along the transverse direction declare that the maximum thinning are observed in the side wall region of the cups and bottom of the cup shows no thickness variation.

CONCLUSIONS

Fundamental understanding of micro deep drawing technique is established by this work. Additionally, it has been found that the scaling effects not only appear within the process but also must be taken into account in all other areas of the forming process. Based on the micro drawing experiments with different thickness copper foils, the following conclusions are made:

⎯ It is found that 300 μm thick foils are very much suitable for Micro cylindrical cups forming.
⎯ The formability of 300 μm thick foils is found better than the 100 μm and 200 μm thick.
⎯ Excessive reductions in thickness are found at the cup shoulder corner and the upper part of the side wall.
⎯ Initial crack starts at the bottom corner radius of the cup and it propagates to the wall of the cup.
⎯ It is identified that the thinning is maximum at the side wall of the cup along the transverse direction.

FUTURE WORK

Incorporating the micro deep drawing technique proposed in this work on a most widely used industry need materials such as brass, aluminium, and even plastic materials for miniature parts. It is possible to study the effect of friction in micro deep drawing process and its reduction by using nano lubricants can be studied.

References

[1] Vollertsen, F. and Hu, Z. Analysis of punch velocity dependent process window in micro deep drawing, Production Engineering, Vol.4, pp.553–559, 2010.
[2] Zhang, K.F. and Kun, L.,'Classification of size effects and similarity evaluating method in micro forming', Journal of Materials Processing Technology, Vol 209, pp. 4949–4953, 2009.
[3] Irthiea, I.K. and Green,G.,' Evaluation of micro deep drawing technique using soft die-simulation and experiments', The International Journal of Advanced Manufacturing Technology, Vol 89 pp. 2363–2374, 2017.
[4] Vollertsen, F. Hu, Z. Niehoff, H.S. and Theiler C., 'State of the art in micro forming and investigations into micro deep drawing', Journal of Materials Processing Technology, Vol151, pp.70–79, 2004.
[5] Fu, M.W. Yang, B. Chan, W.L. ,'Experimental and simulation studies of micro blanking and deep drawing compound process using copper sheet', Journal of Materials Processing Technology, Vol. 213,pp.101–110,2013.
[6] Luo, L. Jiang, Z. and Wei, D,' Influences of micro-friction on surface finish in micro deep drawing of SUS304 cups', Wear, Vol.375, pp.36-45, 2017.
[7] Jia, F. Zhao, J. Luo, L. Xie, H. and Jiang Z.,' Experimental and numerical study on micro deep drawing with aluminium-copper composite material', Procedia Engineering, Vol. 207, pp.1051–1056,2017.
[8] Gong. F, Chen. Q, Yang . Z, Shu D, and Zhang S, 'Micro deep drawing of C1100 conical cylindrical cups, Procedia Engineering,

81, 1457–1462, 2014.

[9] Irthiea, I. Green, G. Hashim, S. and Kriama, A.,' Experimental and numerical investigation on micro deep drawing process of stainless steel 304 foil using flexible tools', International Journal of Machine Tools and Manufacture, Vol. 76,pp.21-33,2014.

[10] Gong, F. Guo, B. Wang, C.J. and Shan, D.B.,' Effects of lubrication conditions on micro deep drawing', Micro system Technologies, Vol. 16, pp.1741–1747, 2010.

[11] Luo, L. Jiang, Z. Wei, D. Manabe, K. and Sato H., 'Experimental and numerical study of micro deep drawing', MATEC Web of Conferences, Vol. 21, pp.1-6, 2015.

[12] Wang, C. Wang, C. Bin, G.U.O. and Shan, D. ,'Effects of tribological behaviour of DLC film on micro-deep drawing processes', Transactions of Nonferrous Metals Society of China, Vol 24,pp. 2877−2882,2014.

[13] ASTM Standard Specifications E8-04. Tension testing of metallic materials [metric]. West Conshohocken, PA: ASTM International, 1−24, 2004.

[1.]A. Mashood ALAO, [2.]A. HAMZA

ADSORPTION OF CHROMIUM (VI) ONTO ZnO: MODELLING, OPTIMIZATION AND ISOTHERM STUDIES

[1-2.]Department of Chemical Engineering, Ahmadu Bello University Zaria, NIGERIA

Abstract: The effects of pH, initial concentration of Cr(VI) and ZnO dosage on Cr(VI) adsorption onto ZnO were studied using the central composite design (CCD). A quadratic model equation was developed for the adsorption of Cr(VI) onto ZnO. The suitability of the model quadratic equation was ascertained using the analysis of variance (ANOVA). Perturbation and 3D response surface plots were used to explain the effects of the three studied parameters on the adsorption process. Adsorption of Cr(VI) onto ZnO is more sensitive to ZnO dosage followed by pH and then initial concentration of Cr(VI). pH and initial concentration of Cr(VI) have overall negative effect on the adsorption process. There is an optimum ZnO dosage, above which the percentage adsorption decreases. The optimization results predicted 45.91 % adsorption of Cr(VI) onto ZnO at a pH of 2.60, initial Cr(VI) concentration of 26.38 mg/L and ZnO dosage of 8.82 g/L. The model predicted maximum adsorption of Cr(VI) onto ZnO (45.91 %) was very close to the experimental value (42.40%). The adsorption equilibrium data was fitted to Langmuir, Freundlich and Dubinin-Radushkevich isotherms. The adsorption equilibrium was best described by the Freundlich isotherm model.
Keywords: Chromium (VI), Adsorption, ZnO, Optimization, Isotherm

INTRODUCTION

Occurrence of heavy metals in surface and underground waters is a serious public health problem in many parts of the world. Heavy metals are not biodegradable and toxic to human beings and animals (Gautam et al., 2014). Most of the heavy metals have an infinite lifetime; thus, they may accumulate in tissues of animals causing chronic health problems. Chromium is a heavy metal used in the production of ferrous and non-ferrous alloys, pigments, leather, catalysts etc (Dhal et al., 2013). Chromium mostly exists in the hexavalent chromium and trivalent chromium states in aqueous medium. Cr(VI) is much more mobile and toxic than Cr(III) (Bachate et al., 2013). The World Health Organization (WHO) limit of Cr(VI) in potable water is 0.05 mg/L (Mohod and Dhote, 2013).

Heavy metals can be removed from contaminated water via adsorption, ion-exchange, filtration, chemical precipitation, coagulation, flocculation, solvent extraction etc (Burakov et al., 2018, Fu and Wang, 2011). Compared to adsorption, some of the water treatment techniques are quite expensive because they require large amount of energy and chemicals. Adsorption has proven to be an attractive and economical method for the removal of various heavy metals from water (Uddin, 2017, Burakov et al., 2018). Indeed, adsorption process is characterized by low energy requirement and flexibility; hence, it can be used for various situations even with small equipment. Several adsorbents such as activated carbons, clays, ashes, crab shells, coconut shells, zeolites, metal oxides, rice husk, etc. have been applied for the removal of various heavy metals from water. However, most of the conventional adsorbents used in water treatment have certain problems such as high cost, slow rate of adsorption, etc (Afroze and Sen, 2018, Burakov et al., 2018).

Recently, there is a lot of research interest in developing metal oxide nanoparticles for water and wastewater treatment via adsorption. Metal oxide nanoparticles such as CeO_2 (Niu et al., 2018), ZnO (Olivera et al., 2018), Fe_3O_4 (Kumari et al., 2015), etc. usually have small particle size, large specific surface area, chemical and thermal stability, surface hydroxyl groups, ion exchange sites, high adsorption and regeneration efficiency for a wide variety of heavy metals in water (Kumari et al., 2015, Olivera et al., 2018, Niu et al., 2018). ZnO nanoparticles with varying shapes (nanoflowers, nanowires, nanorods, nanosheets. etc) can be readily prepared in large quantities using a wide variety of precursors (Lv et al., 2018, Kumar et al., 2013). ZnO nanoparticles are used in catalysis, gas sensing, solar cell technology, photocatalysis, antimicrobial formulations etc (Qi et al., 2017). ZnO nanoparticles are also used as adsorbents due to their favorable surface properties. Thus, ZnO nanoparticles have been applied for the adsorption of heavy metals in water (Sheela et al., 2012, Kumar et al., 2013). Kumar et. al. (2013) reported that the adsorption capacity of ZnO (9.38 mg/g) for Cr(VI) is three times higher than that of SnO_2 (3.09 mg/g) under similar experimental conditions even though the specific surface area of SnO_2 (24.48 m^2/g) is higher than that of ZnO (15.75 m_2/g).

In this paper, the effects of pH, initial concentration of Cr(VI) and adsorbent dosage on Cr(VI) adsorption have been studied using the response surface methodology (RSM) in order to develop model equation for the adsorption process and determine the optimum conditions for the adsorption of Cr(VI) onto ZnO. The adsorption were also studied under the optimum conditions of the process.

MATERIALS AND METHODS

The procedure for the synthesis of ZnO via thermal decomposition of $ZnCO_3$ has been described elsewhere (Alao, 2016, Shamsipur et al., 2013). The specific surface area and the average crystallite size pH at zero point charge of the ZnO are 55.0 m^2/g and 25 ± 5 nm, respectively.

— **Adsorption experiments**

Stock solution of Cr(VI) with a concentration of 1000 mg/L was prepared by dissolving $K_2Cr_2O_7$ in distilled water. The pH range of the Cr(VI) solutions was adjusted using either HCl or NaOH solution. The adsorption experiments were carried out in the dark in order to prevent photocatalytic reduction of Cr(VI) by ZnO. Adsorption experiments were performed by shaking 100 mL of Cr(VI) solution

of the desired concentration with the required amount of the adsorbent (ZnO). The flasks were continuously shaken for the desired contact time in a shaker. Thereafter, the adsorbent was separated. The concentration of the Cr(VI) in the filtrate was determined using an Atomic Absorption Spectrophotometer (AAS 500, England). Percentage adsorption of Cr(VI) and adsorption capacity (q_t) of ZnO for Cr(VI) were calculated using Eqs. 1 and 2, respectively.

$$\%\text{Adsorption} = \frac{C_o - C_t}{C_o} \times 100\% \qquad (1)$$

$$q_t = \frac{(C_o - C_t)V}{V} \times 100\% \qquad (2)$$

where C_o is the initial concentration (mg/L) of Cr(VI), C_t is the Cr(VI)concentration (mg/L) after a certain contact time, t, W and V are the weight of adsorbent and volume of the Cr(VI) solution, respectively.

— Design of adsorption experiments

The effects of three process parameters (pH, initial concentration of Cr(VI) and adsorbent dosage) on the adsorption of Cr(VI) onto ZnO were investigated using the central composite design as implemented in the Design Expert software version 6.0.6 (Stat-Ease Inc., Minneapolis, USA). The lowest and highest levels of each independent variable are given in Table 1. For the three variables, 20 experiments presented in Table 2 were designed conducted. In this work, the response is the percentage adsorption of Cr(VI) expressed by Eq. 1.

Table 1: Experimental ranges of the investigated independent variables

Independent variable	Code	Ranges	
		Low	High
pH	A	2	10
Initial concentration of Cr(VI) (mg/L)	B	25	100
Adsorbent dosage (g/L)	C	2	10

RESULTS AND DISCUSSION
— Adsorption of Cr(VI) onto ZnO

Figure 1 shows the effect of contact time on percentage adsorption of Cr(VI) onto ZnO; from where it can be seen that the percentage adsorption of Cr(VI) on ZnO increases with increase in contact time up to 120 minutes.
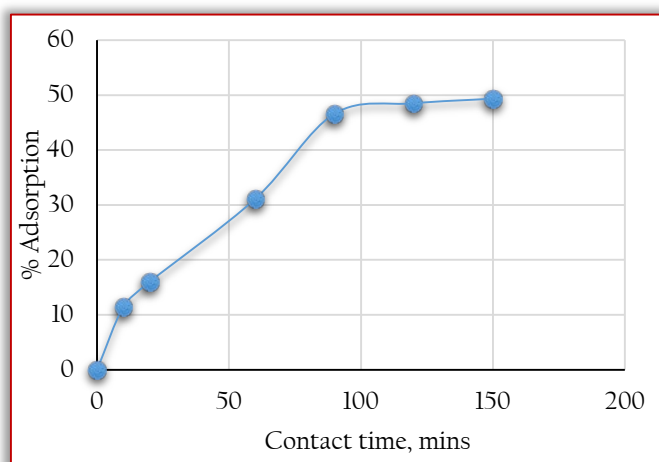
Figure 1: Effect of contact time on percentage adsorption of Cr(VI) onto ZnO

The adsorption is faster at shorter contact times due to the larger surface area of ZnO available at the beginning of the process. As the surface adsorption sites become saturated with increase in contact time, the adsorption is slowed down (Uddin, 2017). Thus, the adsorption-desorption equilibrium was achieved after contact time of 120 minutes. Therefore, all subsequent adsorption experiments aimed at studying the effects of the three process variables presented in Table 1 and adsorption isotherms (*vide infra*) were carried out for120 minutes.

— Modelling of Chromium (VI) Adsorption onto ZnO

The central composite design matrix and experimental responses are presented in Table 2. Based on experimental results obtained, an empirical relationship between the response and independent variables was fitted to second order polynomial using the Design Expert software. The experimental data was fitted to the model quadratic equation 3.

$$\%\text{Adsorption} = 37.52 - 3.01A - 6.12B + 5.24C - 1.01A^2$$
$$- 3.34B^2 - 6.40C^2 + 1.98AB - 0.20AC + 2.77BC \qquad (3)$$

Table 2: Central composite design matrix and experimental values of the response for Cr(VI) adsorption using ZnO

Run	Independent variables			Response
	A	B	C	% Adsorption
1	1.00	25.00	10.00	45.80
2	5.50	62.50	6.00	37.50
3	5.50	62.50	12.73	31.50
4	1.00	100.00	2.00	20.30
5	5.50	62.50	6.00	38.10
6	5.50	62.50	6.00	37.60
7	5.50	62.50	0.73	10.50
8	10.00	100.00	2.00	15.40
9	13.07	62.50	6.00	20.40
10	5.50	125.57	6.00	32.30
11	5.50	62.50	6.00	35.70
12	10.00	25.00	2.00	19.30
13	5.50	62.50	6.00	38.60
14	10.00	25.00	10.00	21.90
15	10.00	100.00	10.00	19.80
16	2.07	62.50	6.00	38.90
17	1.00	100.00	10.00	33.20
18	5.50	62.50	6.00	37.10
19	5.50	0.57	6.00	40.20
20	1.00	25.00	2.00	31.20

The suitability of the model quadratic equation was ascertained using the analysis of variance (ANOVA). The results of the ANOVA for the proposed model equation are presented in Table 3. Model parameters are significant if the probability value (p-value) is less than 0.05 at 95% confidence level (Montgomery et al., 2009). Thus, the model equation is significant. The insignificance of lack of fit with p–value of 0.192 showed that the developed model is valid. The good fitting of the experimental data to the model equation was also supported by the high values of the regression coefficients ($R^2 = 0.972$; $R^2_{adj} = 0.948$). The closeness in the values of R^2 and R^2_{adj} indicates good predictability of the model. The value of adequate precision ratio of 22.197 indicates an appropriate signal to noise ratio because the minimum desired ratio is 4.0; this indicates that the quadratic model can be used to find the optimum conditions of the adsorption process.

The plot of actual vs. predicted values presented in Figure 2a shows that the model equation adequately describes the experimental

ranges of the process variables investigated. As shown in Figure 2b, the residuals are scattered randomly in the range of -3.0 to +3; this reveals good fitting of the quadratic model equation with the experimental data (Sakkas et al., 2010, Montgomery et al., 2009).

Table 3: Results of ANOVA for Cr(VI) adsorption onto ZnO

Source	Sum of Squares	Degree of Freedom	Mean Squares	F - Value	p - value
Model	1799.48	9	199.94	39.15	<0.0001
A	123.61	1	123.61	24.20	0.0006
B	510.69	1	510.69	100.00	<0.0001
C	374.52	1	374.52	73.34	<0.0001
A^2	14.70	1	14.70	2.88	0.1206
B^2	161.09	1	161.09	31.54	0.0002
C^2	590.58	1	590.58	115.65	<0.0001
AB	31.20	1	31.20	6.11	0.0330
AC	0.32	1	0.32	0.063	0.8074
BC	61.60	1	61.60	12.06	0.0060
Lack of Fit	46.11	5	9.22	9.31	0.192

$R^2 = 0.972$; R^2 adj = 0.948; Adq. Prec. ratio = 22.197
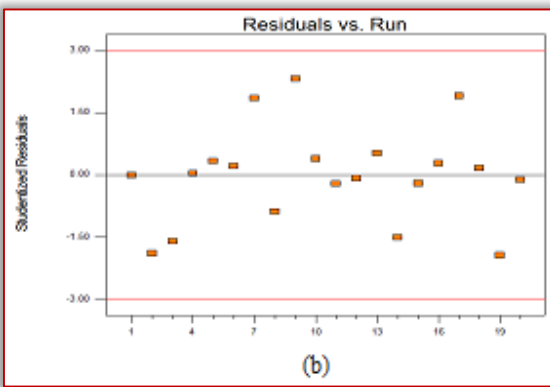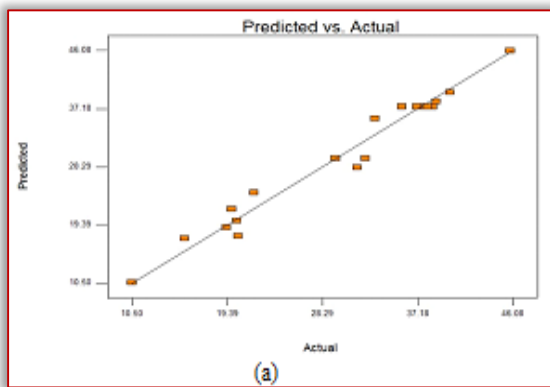
Figure 2: Plots of (a) the predicted against the actual experimental values and (b) the Studentized residuals against predicted values for Cr(VI) adsorption using ZnO

Perturbation is the deviation of the response (percentage adsorption) from the reference points (middle values of the independent variables). Herein, the reference points are: pH of 5, Cr(VI) concentration of 70.0 mg/l and adsorbent dosage of 5.0 g/l. The perturbation plots displayed in Figure 3 show the effect of each of the three studied independent variables on the response. Based on the slopes and curvature of the plots, it can be concluded that the percentage adsorption is more sensitive to adsorbent dosage (C) followed by pH (A) and then initial concentration of (B). The plots show that pH and initial concentration of Cr(VI) have overall

negative effect on the adsorption process. Hence, highest adsorption is achieved at the lowest pH and the lowest initial concentration of Cr(VI). On the other hand, the percentage adsorption increases with increase in the adsorbent dosage. However, there is an optimum adsorbent dosage, above which the percentage adsorption decreases. The negative coefficients of quadratic terms of the model equation (3) account for this observation.
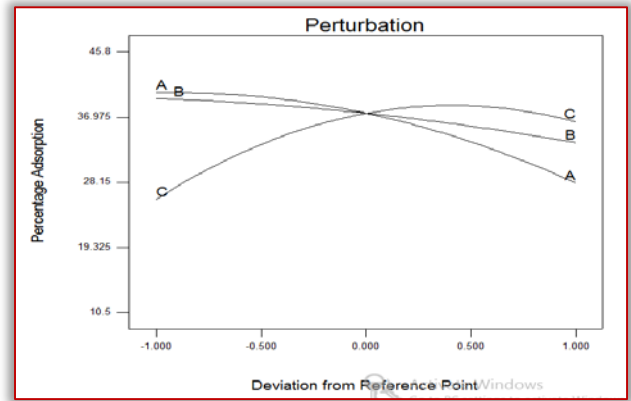
Figure 3: Perturbation plots for Cr(VI) adsorption onto ZnO
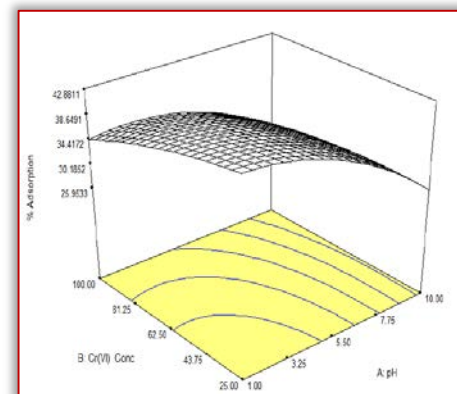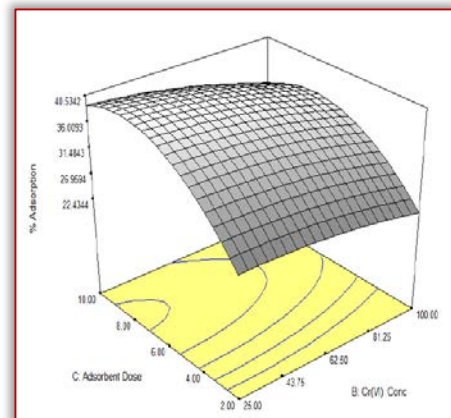
Figure 4: 3D response surface plots for Cr(VI) adsorption onto ZnO showing the simultaneous effects of (a) pH and initial concentration of Cr(VI), and (b) adsorbent dosage and initial concentration of Cr(VI)

So far, each of the three independent variables has been studied individually. As shown in Table 3, the interactions between pH and initial concentration of Cr(VI) as well as between initial concentration of Cr(VI) and adsorbent dosage are significant with p-values of 0.033 and 0.006, respectively. Whereas, the interactions between pH and adsorbent dosage are non-significant with p-

value of 0.8074. The interactions between the independent variables can be explained using the 3D response surface plots presented in Figures 4 and 5.

Figure 4a depicts the effects of pH and initial concentration of Cr(VI) on its adsorption. Cr(VI) adsorption onto ZnO decreases as the initial Cr(VI) concentration is increased. The decrease in Cr(VI) adsorption can be attributed to the fact that adsorbents have a limited number of active binding sites and at a certain concentration of an adsorbate the active sites become saturated (Khosravi et al., 2018, Bhatti et al., 2017). At low initial concentrations of Cr(VI), the available adsorption sites of ZnO were easily occupied by chromium ions resulting in higher percentage adsorption. However, as the initial concentration of Cr(VI) is increased, most of the available adsorption sites became occupied, leading to a decrease in the percentage adsorption (Mondal et al., 2018).

Depending on solution pH, Cr(VI) exists in various forms. The dominant specie is chromic acid (H_2CrO_4) at pH lower than 1.0 and $HCrO_4^-$ at pH between 1.0 and 6.5. At pH higher than 6.5, only CrO_4^{2-} is stable (Igberase et al., 2017). The pH of point zero charge of ZnO is around 9 (Omar et al., 2014) depending on the method of production. At a pH below the pH of point zero charge, the surface of ZnO is positively charged and above pH at point zero charge, the surface of the ZnO is negatively charged. The observed high adsorption of Cr(VI) at low pH can be attributed to availability of Cr(VI) in anionic forms ($HCrO_4^-$ and $Cr_2O_7^{2-}$) and the net positive charge of ZnO (Igberase et al., 2017). At low pH, the surface of ZnO is also protonated (Ballerini et al., 2007). This facilitates adsorption of Cr(VI) onto ZnO. As the pH is increased, the degree of protonation of the surface decreases leading to low adsorption of Cr(VI). Furthermore, at high pH, there is competition between OH^- and CrO_4^{2-} ions (Pradhan et al., 1999). The reduction in net positive charge of ZnO at high pH weakens the electrostatic forces between the ZnO and Cr(VI) and this leads to lower percentage adsorption.

Figure 4b shows that the number of surface sites for adsorption of Cr(VI) increases up to about 8 g/l. Thereafter, further increase in the adsorbent dosage lead to slight decrease in Cr(VI) adsorption. This observation can be attributed to overlap of surface active sites due to saturation of adsorbent particles and decrease in the charge of the dense outer layer of the cells, thereby blocking the active sites of ZnO from Cr(VI) (Igberase et al., 2017, Bhatti et al., 2017).

— Optimization of hexavalent chromium removal onto ZnO

The optimization was targeted at maximizing the percentage adsorption by setting the process variables (pH, initial concentration of Cr(VI) and adsorbent dosage) to be within the studied ranges presented in Table 1, whereas and the percentage adsorption was set to be maximum. The optimization results predicted 45.91 % adsorption of Cr(VI) onto ZnO at a pH of 2.60, initial concentration of Cr(VI) of 26.38 mg/L and adsorbent dosage of 8.82 g/L. In order to verify the optimization results, an experiment was performed under predicted optimum conditions. The experimental value obtained under the predicted optimum conditions was 42.40% which is very close to the predicted value of 45.91 %.

— Adsorption isotherms

Adsorption isotherm explains the interaction between the adsorbate and the adsorbent. In this work, Langmuir, Freundlich and Dubinin-Radushkevich isotherms were applied to investigate adsorption of Cr(VI) onto ZnO. The linearized forms of the Langmuir, Freundlich and Dubinin-Radushkevich isotherms are given by equations 4, 5 and 6, respectively (Kataria and Garg, 2018, Fida et al., 2015).

$$\frac{C_e}{q_e} = \frac{1}{q_{max}K_L} + \frac{C_e}{q_{max}} \tag{4}$$

$$\ln q_e = \ln K_F + \frac{1}{n}\ln C_e \tag{5}$$

$$\ln q_e = \ln Q_S - K_D \varepsilon^2 \tag{6}$$

where C_e is the equilibrium concentration of the Cr(VI) ions in solution, q_{max} is the Langmuir maximum adsorption capacity of mk, K_L is the Langmuir constant that is related to the energy of adsorption, respectively. K_F and n are the Freundlich adsorption isotherm constants which determine the extent of the adsorption process, and the degree of nonlinearity between solution concentration and adsorption, respectively. Q_s is the Dubinin-Radushkevich maximum adsorption capacity, K_D is the activity coefficient which indicates the mean adsorption energy (E). ε is the Polanyi potential which is calculated using Eq. 7.

$$\varepsilon = RT \ln(1 + 1/Ce) \tag{7}$$

The mean adsorption energy (E) is calculated using Eq. 8.

$$E = 1/\sqrt{2KD} \tag{8}$$

The linearized plots of the Langmuir, Freundlich and Dubinin-Radushkevich isotherms are shown in Figures 5, 6 and 7, respectively. The slopes and intercepts of the plots were used to derive isotherm parameters and correlation coefficients (R^2) that are reported in Table 4. Analysis of the values of regression coefficients (R^2) indicates that the Cr(VI) adsorption onto ZnO obeys Freundlich isotherm model due to highest R^2 value of 0.981. This indicates that the adsorption of Cr(VI) onto ZnO takes place on the heterogeneous surface sites of ZnO (Agarwal et al., 2006). Other researchers have also reported that adsorption of Cr(VI) is best described by the Freundlich isotherm model (Sarin and Pant, 2006, Agarwal et al., 2006). Moreover, the value of 1/n in the Freundlich model is 0.531, which further signifies favourability of the adsorption of Cr(VI) onto ZnO (Kataria and Garg, 2018).

Table 4 shows that the correlation coefficient (R^2) of the Langmuir isotherm model is lower than those of Freundlich and Dubinin-Radushkevich isotherm, indicating that Cr(VI) adsorption onto the developed adsorbents did not occur on homogeneous surface by monolayer adsorption. Based on the results obtained for Dubinin-Radushkevich isotherm, the mean free energy of the adsorption process is 5.47 kJ/mol as shown in Table 4.

Therefore, removal of Cr(VI) by ZnO is physical adsorption. This is because physical adsorption is characterized by a mean free energy in the range of 1 kJ/mol to 16 kJ/mol, while chemisorption prevails for mean free energy greater than 16 kJ/mol (Fida et al., 2015, Kataria and Garg, 2018).

Table: 4: Isotherm constants for Cr(VI) adsorption onto ZnO

Isotherm	Parameters	
Langmuir	q_{max} (mg/g)	9.49
	R^2	0.725
Frendliuch	K_F	0.119
	$1/n$	0.531
	R^2	0.981
Dubinin-Radushkevich	E (kJ/mol)	5.47
	Q_D (mg/g)	0.9011
	R^2	0.901
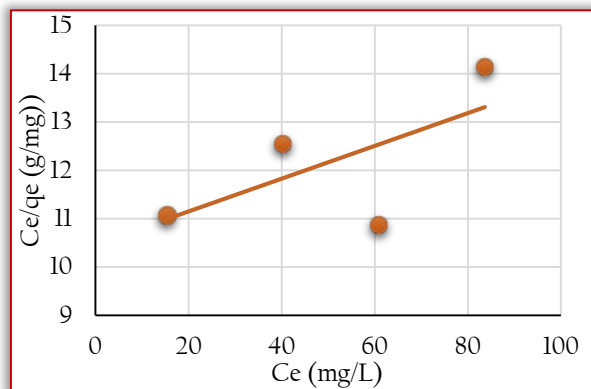
Figure 5: Langmuir isotherm plot for adsorption of Cr(VI) onto ZnO
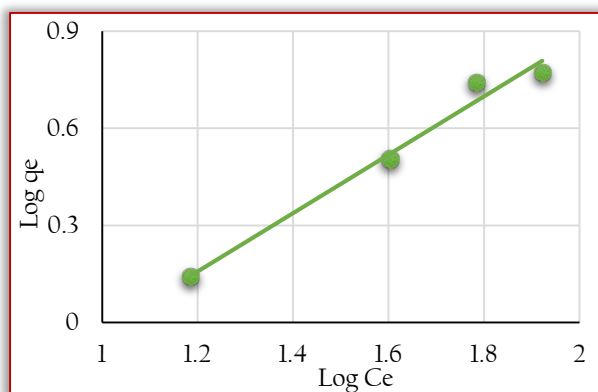
Figure 6: Freundlich isotherm plot for adsorption of Cr(VI) onto ZnO
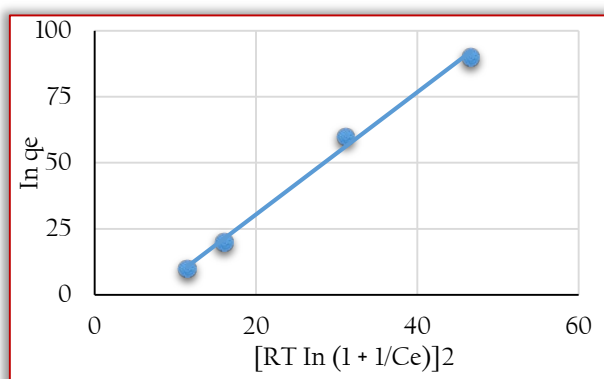
Figure 7: Dubinin–Radushkevich isotherm plot for adsorption of Cr(VI) onto ZnO

CONCLUSIONS

The adsorption-desorption equilibrium of Cr(VI) onto ZnO was achieved after a contact time of 120 minutes. A quadratic model equation was developed for the adsorption of Cr(VI) onto ZnO. Adsorption of Cr(VI) onto ZnO is more sensitive to adsorbent dosage followed by pH and then initial concentration of of Cr(VI).

pH and initial concentration of Cr(VI) have overall negative effect on the adsorption process. There is an optimum adsorbent dosage, above which the percentage adsorption decreases. The optimization results predicted 45.91 % adsorption of Cr(VI) onto ZnO at a pH of 2.60, initial concentration of Cr(VI) of 26.38 mg/L and adsorbent dosage of 8.82 g/L. The model predicted maximum adsorption of Cr(VI) onto ZnO (45.91 %) was very close to the experimental value (42.40%). The adsorption equilibrium was best described by the Freundlich isotherm model. Removal of Cr(VI) by ZnO is physical adsorption mean free energy of 5.47 kJ/mol.

References

[1] Afroze, S. and Sen, T. K.: A Review on Heavy Metal Ions and Dye Adsorption from Water by Agricultural Solid Waste Adsorbents. Water, Air, & Soil Pollution, vol. 229, pp. 225, 2018.

[2] Agarwal, G., Bhuptawat, H. K. and Chaudhari, S.: Biosorption of aqueous chromium (VI) by Tamarindus indica seeds. Bioresource technology, vol. 97, pp. 949-956, 2006.

[3] Alao, A. M.: Development of ZnO/metakaolin composite for the removal of hexavalent chromium ion from potable water. M.Sc dissertation, Department of Chemical Engineering, Ahmadu Bello University Zaria, Nigeria, vol., pp., 2016.

[4] Bachate, S. P., Nandre, V. S., Ghatpande, N. S. and Kodam, K. M.: Simultaneous reduction of Cr (VI) and oxidation of As (III) by Bacillus firmus TE7 isolated from tannery effluent. Chemosphere, vol. 90, pp. 2273-2278, 2013.

[5] Ballerini, G., Ogle, K. and Barthés-Labrousse, M.-G.: The acid–base properties of the surface of native zinc oxide layers: an XPS study of adsorption of 1, 2-diaminoethane. Applied surface science, vol. 253, pp. 6860-6867, 2007.

[6] Bhatti, I. A., Ahmad, N., Iqbal, N., Zahid, M. and Iqbal, M.: Chromium adsorption using waste tire and conditions optimization by response surface methodology. Journal of environmental chemical engineering, vol. 5, pp. 2740-2751, 2017.

[7] Burakov, A. E., Galunin, E. V., Burakova, I. V., Kucherova, A. E., Agarwal, S., Tkachev, A. G. and Gupta, V. K.: Adsorption of heavy metals on conventional and nanostructured materials for wastewater treatment purposes: A review. Ecotoxicology and environmental safety, vol. 148, pp. 702-712, 2018.

[8] Dhal, B., Thatoi, H., Das, N. and Pandey, B.: Chemical and microbial remediation of hexavalent chromium from contaminated soil and mining/metallurgical solid waste: a review. Journal of hazardous materials, vol. 250, pp. 272-291, 2013.

[9] Fida, H., Guo, S. and Zhang, G.: Preparation and characterization of bifunctional Ti–Fe kaolinite composite for Cr (VI) removal. Journal of colloid and interface science, vol. 442, pp. 30-38, 2015.

[10] Fu, F. and Wang, Q.: Removal of heavy metal ions from wastewaters: a review. Journal of environmental management, vol. 92, pp. 407-418, 2011.

[11] Gautam, R. K., Sharma, S. K., Mahiya, S. and Chattopadhyaya, M. C.: Contamination of heavy metals in aquatic media: transport, toxicity and technologies for remediation. Heavy metals in water: Presence, removal and safety, vol., pp. 1-24, 2014.

[12] Igberase, E., Osifo, P. and Ofomaja, A.: Chromium (VI) ion adsorption by grafted cross-linked chitosan beads in aqueous solution–a mathematical and statistical modeling study. Environmental technology, vol. 38, pp. 3156-3166, 2017.

[13] Kataria, N. and Garg, V.: Optimization of Pb (II) and Cd (II) adsorption onto ZnO nanoflowers using central composite design: isotherms and kinetics modelling. Journal of Molecular Liquids, vol. 271, pp. 228-239, 2018.

[14] Khosravi, R., Moussavi, G., Ghaneian, M. T., Ehrampoush, M. H., Barikbin, B., Ebrahimi, A. A. and Sharifzadeh, G.: Chromium adsorption from aqueous solution using novel green nanocomposite: Adsorbent characterization, isotherm, kinetic and thermodynamic investigation. Journal of Molecular Liquids, vol. 256, pp. 163-174, 2018.

[15] Kumar, K. Y., Muralidhara, H., Nayaka, Y. A., Balasubramanyam, J. and Hanumanthappa, H.: Low-cost synthesis of metal oxide nanoparticles and their application in adsorption of commercial dye and heavy metal ion in aqueous solution. Powder technology, vol. 246, pp. 125-136, 2013.

[16] Kumari, M., Pittman Jr, C. U. and Mohan, D.: Heavy metals [chromium (VI) and lead (II)] removal from water using mesoporous magnetite (Fe3O4) nanospheres. Journal of colloid and interface science, vol. 442, pp. 120-132, 2015.

[17] Lv, Y., Zhang, Z., Yan, J., Zhao, W. and Zhai, C.: Al doping influences on fabricating ZnO nanowire arrays: Enhanced field emission property. Ceramics International, vol. 44, pp. 7454-7460, 2018.

[18] Mohod, C. V. and Dhote, J.: Review of heavy metals in drinking water and their effect on human health. International Journal of Innovative Research in Science, Engineering and Technology, vol. 2, pp. 2992-2996, 2013.

[19] Mondal, N. K., Samanta, A., Chakraborty, S. and Shaikh, W. A.: Enhanced chromium (VI) removal using banana peel dust: isotherms, kinetics and thermodynamics study. Sustainable Water Resources Management, vol. 4, pp. 489-497, 2018.

[20] Montgomery, D. C., Runger, G. C. and Hubele, N. F. 2009. Engineering statistics, John Wiley & Sons.

[21] Niu, J., Jia, X., Zhao, Y., Liu, Y., Zhong, W., Zhai, Z. and Li, Z.: Adsorbing low concentrations of Cr (VI) onto CeO2@ ZSM-5 and the study of adsorption kinetics, isotherms and thermodynamics. Water Science and Technology, vol., pp. wst2018157, 2018.

[22] Olivera, S., Hu, C., Nagananda, G. S., Reddy, N., Venkatesh, K., Muralidhara, H. B. and Asiri, A. M.: The adsorptive removal of Cr (VI) ions and antibacterial activity studies on hydrothermally synthesized iron oxide and zinc oxide nanocomposite. Journal of the Taiwan Institute of Chemical Engineers, vol. 93, pp. 342-349, 2018.

[23] Omar, F. M., Aziz, H. A. and Stoll, S.: Aggregation and disaggregation of ZnO nanoparticles: influence of pH and adsorption of Suwannee River humic acid. Science of the total environment, vol. 468, pp. 195-201, 2014.

[24] Pradhan, J., Das, S. N. and Thakur, R. S.: Adsorption of hexavalent chromium from aqueous solution by using activated red mud. Journal of Colloid and Interface Science, vol. 217, pp. 137-141, 1999.

[25] Qi, K., Cheng, B., Yu, J. and Ho, W.: Review on the improvement of the photocatalytic and antibacterial activities of ZnO. Journal of Alloys and Compounds, vol. 727, pp. 792-820, 2017.

[26] Sakkas, V. A., Islam, M. A., Stalikas, C. and Albanis, T. A.: Photocatalytic degradation using design of experiments: A review and example of the Congo red degradation. Journal of Hazardous Materials, vol. 175, pp. 33-44, 2010.

[27] Sarin, V. and Pant, K. K.: Removal of chromium from industrial waste by using eucalyptus bark. Bioresource technology, vol. 97, pp. 15-20, 2006.

[28] Shamsipur, M., Pourmortazavi, S. M., Hajimirsadeghi, S. S., Zahedi, M. M. and Rahimi-Nasrabadi, M.: Facile synthesis of zinc carbonate and zinc oxide nanoparticles via direct carbonation and thermal decomposition. Ceramics International, vol. 39, pp. 819-827, 2013.

[29] Sheela, T., Nayaka, Y. A., Viswanatha, R., Basavanna, S. and Venkatesha, T.: Kinetics and thermodynamics studies on the adsorption of Zn (II), Cd (II) and Hg (II) from aqueous solution using zinc oxide nanoparticles. Powder Technology, vol. 217, pp. 163-170, 2012.

[30] Uddin, M. K.: A review on the adsorption of heavy metals by clay minerals, with special focus on the past decade. Chemical Engineering Journal, vol. 308, pp. 438-462, 2017.

[1.]Andreea–Cătălina CRISTESCU, [1.]Lucreţia POPA, [1.]Vasilica ŞTEFAN, [2.]Alexandra ROTARU,
[1.]Alexandra ANGHELEŢ, [1.]Ana ZAICA, [1.]Alexandru ZAICA, [1.]Iuliana GĂGEANU

STUDY ON NEW MECHANIZED HARVESTING TECHNOLOGIES IN VINEYARDS

[1.]National Institute of Research–Development for Machines and Installations for Agriculture & Food Industry – INMA Bucharest, ROMANIA
[2.]University Polytechnic Bucharest, Faculty of Biotechnical Systems Engineering, ROMANIA

Abstract: Based on the needs of a constantly growing industry, researchers have been working on the development of vineyard mechanization in order to maintain the fruit quality and a good efficiency in the aspect of time, economy and productivity in the vineyards. The present paper presents the latest technologies used in vineyard harvesting, aiming to emphasize good practices in order to promote crop quality, reducing environmental impact and raising yield productivity, but also allowing the delay of some procedures that must pe done in vineyards without consequences. Studies have shown that mechanization in vineyards can achieve benefits of cost savings from hand labor, but also time saving and healthy grapes.
Keywords: vineyard machinery, harvesting, new technologies, self–propelled, mechanized harvesting

INTRODUCTION

Traditionally, growers have used manpower in vineyards for many years. In time, after the increasing of labor expenses, the needs of an expanding business and lack of time, but also the increase of local or global competition, the commercial growers had to seek methods of mechanizing vineyards operations. Since 1960, when the first machine was used in vineyards, researchers had conducted their work in developing postharvest handling, adapting harvesters to different trellises, developing machines that mechanize canopy management practices such as dormant and summer pruning, leaf removal, shooting positioning, fruit thinning etc. The main goal is to develop systems that are able to reach every expectation of a complete mechanized process in vineyards without any loss in fruit quality and quantity. (Morris J.R., 2008)

Mechanical harvesters quickly gained popularity in vineyards for wine grapes, but also for juice grapes. During the time of a continuous growing interest, researchers investigated the post harvesting quality of mechanically harvested grapes. Based on the fact that grapes have a rapid fermentation rates with time, the industry have established a maximum six hours interval between mechanical harvesting and processing. (Morris J.R., 2008, Hays P, 2008)

In time, several new generations of harvesters have been developed. Currently there are two types which beat and shake de vine, either by means of staves beating foliage, or the impulse harvester which beats the trunk and cordon. Both aim to detach the berries. The berries are then collected on a conveyor which move past a blower that removes the leaves, where after they are dumped into a bin.

Mechanical harvesters are able to work against slopes and adjustments may be made without stopping. Three basic adjustments may be effective, namely the width between the two sets of staves (pitch), the extent of the beating action (amplitude) and the speed of the beating action (frequency). Different combinations of these three factors may be used for various vineyards. The success of mechanical harvesting is ascribed 35–40% to the harvester, 30% to the operator and 30% to the vineyard. If the canopy is not suited to mechanical harvesting, the process will not be successful. (Morris J.R., 2008, Hays P, 2008, Kaye O. 2008) https://www.wineland.co.za/mechanical–harvesting–of–grapes/)

New generation of harvester offer several new advantages such as: automatic sorting on the harvesters that presents berries without any material other than grapes, sorting of different colour berries, sorting of the grapes according to the condition of ripeness of the grapes, easy cleaning based on the fact that the success of the mechanical harvesting is largely influenced by the maintenance of the harvester. (https://www.mondomacchina.it/)

A great area of interest revolves around the mechanization of harvesting, as testified to by the continuous arrival of new features on the market. What is not new is the idea of the selective collection of the grapes on the basis of their quality, beginning with a specific map of the site. Currently, this is now possible and becoming more and more accessible thanks to the availability of optic sensors capable of detecting in real time the phenolic, or physiologically ripe grapes, that is according to the content of grapes' anthocyanins and flavonoid. The important arrival of sensors and systems for the approach of the machine to the vines is justified by the need for precision provided for work in vineyards in which driving is often made difficult by a number of factors, such as sloping terrain, narrow rows and the length of the worksite. For this reason, assisted driving has taken on more and more interest. Thanks to GNSS (Global Navigation Satellite Systems) with real time corrections (with RTK, Real Time Kinematic systems) the tractor and machine can be positioned with precision of up to a couple of centimeters. This is of importance not only for planting cuttings and setting posts but also for making and using the prescribed maps and assisting and facilitating the work of the driver, especially when driving is complicated by combined operations. In this area, an Enovitis in the Field Technological Innovation Award was given to Spektra–Agri which, in collaboration with Fendt, came up with an AutoCombiGuide drive system which automatically controls operational sequences in the field and provides the possibility of controlling the equipment while running. These features enable work to be performed for carrying out various combined operations to reduce time and labor and entries to the field to lower stress on the operator and the soil.

There are now so many technologies and solutions for improving the quality of operations. Though the spread of agricultural mechanization in the vineyard involves in various ways nearly 30% of these vineyards for grape harvesting alone, for a total of some 2,600 machines at work on nearly 15,000 hectares harvested, it is important for manufacturers' research to continue in this direction to provide increasingly competitive and convincing solutions for agriculture. (https://www.winesandvines.com/).

MATERIALS AND METHODS

Various machines are available and technology is advancing rapidly to speed up harvesting of the grapes in the case of almost all kinds of trellis systems, and to harvest more "softly" with less damage to the bunches. Bunches may already be harvested as low as 25 cm from the surface of the soil. Machines are being developed to harvest even bush vines. There are currently two types of harvesters available on the market, such as self–propelled harvesters (Figure1) and towed harvesters (Figure 2) (https://pellenc.com/).

Figure 1 – Self propelled harvester–PELLENC (https://pellenc.com/)

Figure2 – Towed harvester– PELLENC (https://pellenc.com/)

Many winemakers prefer grapes, especially white varieties such as Sauvignon blanc, to be harvested by hand. Much progress has been made, however, in handling berries with a softer touch. An example of this is the used of extended beaters by means of which berries are shaken off with the minimum of skin damage. Furthermore, it is a well–known fact that the quality of many white cultivars is better if the grapes are pressed cool. Therefore, night and early morning pressing by harvesting machines can even result in an improvement in wine quality.

In order to carry out the harvesting process, the vineyardists inspects the samples of grapes whit a refractometer to determinate if the grapes are ready to be picked. If the answer is positive, the process may begin.

For the best results, the harvester may be equipped with several features that ensure a good efficiency of the process, with minimal impact on the grapes.

One of the best features that such harvesters present, is the continuous harvest bin system, which allows a great working efficiency with continuous harvesting bin. The harvest can be redirected directly to gondolas, valley or macro bins by using the side discharge conveyor for long rows. (https://pellenc.com/).

Figure3 – Continuous harvest bin system (https://pellenc.com/)

The cab is equipped with a console that allows frequency, pinch, amplitude, destemming and other settings adjustment instantly and continuous, while working, without stopping. Also, self–propelled harvesters, are equipped with position sensors that automatically align the harvesting head in the row, while an active system optimises the efficiency of shaking, without damaging the trellising and plants. The movement of the harvesting head is proportional to the working speed.

(Figure 5) has an anti–jam feature with five long fingers, while the adjustable sorting rollers can adapt to all grape varieties.

The screen rollers (1) allow the sorted berries to pass through and remove petioles and green waste. The solid notched roller feeders (2) separate small waste and route petioles to the screen rollers (Figure 6).

Another optional sorter can be added to the mechanized harvester, that allows optimal sorting of berries, whole bunches and leaves at the conveyor output. The grid belt of the sorter catches the harvest at the output of the Flexible Sorter Conveyor. Juice and berries pass directly into the bins.
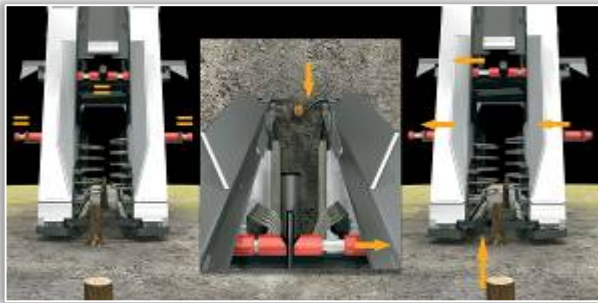
Figure 4 – Console and sensors systems (https://pellenc.com/)
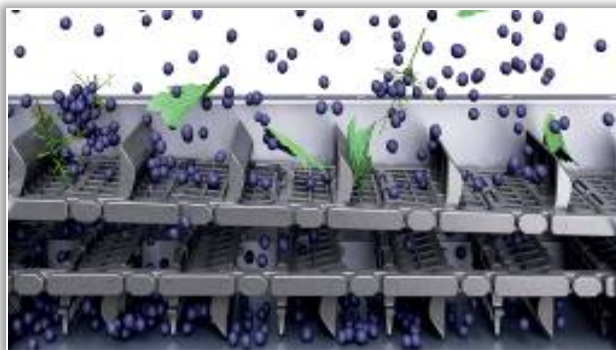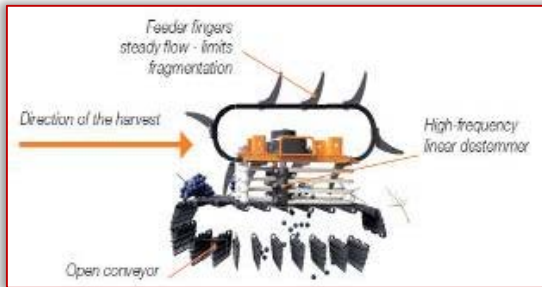
Figure 5 – Linear berry separator– Destemmer (https://pellenc.com/)

Figure 6 – Screen rollers (https://pellenc.com/)

Harvesters are equipped with selective destemming systems, with high–frequency linear berry separator, that gently removes the berries and the stems remain intact. The linear berry separator
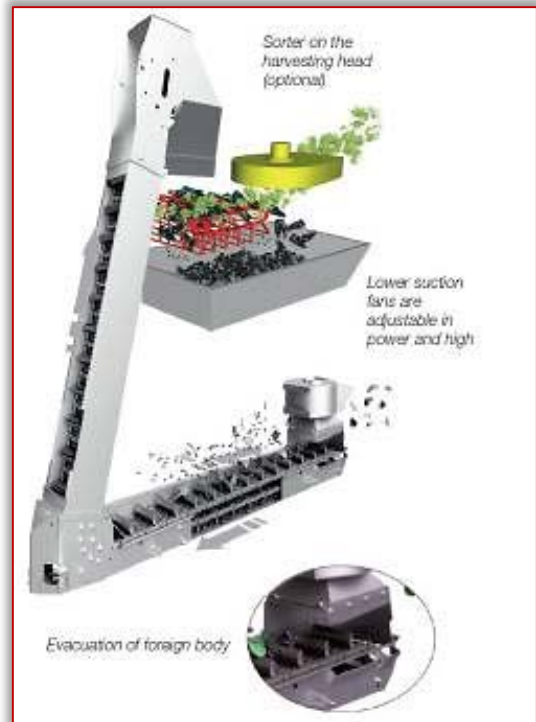
Figure 7 – Sorting and cleaning system (https://pellenc.com/)

RESULTS

Most of the harvesters, have a great efficiency, with 99.82% of cleanliness rate in the bin, and 82% of good berries, 100% of leaves are removed as well as 95% of whole stalks, the sorting table consists of a series of feeder rollers that distribute the berries on the sorting table, and aligns waste to evacuate it, thanks to the selective process. Only grape clusters and leaves pass under the lower suction fans, less than 30 % of the harvest. (https://pellenc.com/)

Figure 8 – Vineyard after harvesting (https://pellenc.com/)

CONCLUSIONS

With all the features available in the latest generations of mechanical harvesters, the whole system of harvesting and vinery crush pad, is basically operating on wheels. Most of the machines are equipped with on–board destemming and sorting. Some machines, are now standardized with destemmers and sorting systems, while others offer optional add–on equipment Harvesters can be towed by a tractor, or self–propelled. With an efficiency of 99.82%, the ability to pick any date for the harvesting process, but also with the advantage of working during night, the cost of the harvesters is worthy. Time saving, less human power, good efficiency represent the key factor in implementing mechanized equipment and good practices in vineyards, especially for mass production and large surfaces of vineyards.

Acknowledgement

Note:

References

[1] Hays P. (2008), Status and Future of Vineyards Mechanization in Australia and New Zealand, Justin R. Morris Vineyard Mechanization Symposium ~Proceedings~, Midwest Grape and Wine Conference, pp 31–33 Osage Beach, Missouri/USA;

[2] Intrieri C. (2008), Research and Innovation for Vineyard Mechanization in Italy, Justin R. Morris Vineyard Mechanization Symposium ~Proceedings~, Midwest Grape and Wine Conference, pp 33–52, Osage Beach, Missouri/USA;

[3] Kaye O. (2008), Advancements in Vineyard Assessment and Harvest Technology, Justin R. Morris Vineyard Mechanization Symposium ~Proceedings~, Midwest Grape and Wine Conference, pp 65–73, Osage Beach, Missouri/USA;

[4] Morris J.R., (2008), Commercialization of the Morris–Oldridge Vineyards Mechanization Systems, Justin R. Morris Vineyard Mechanization Symposium ~Proceedings~, Midwest Grape and Wine Conference, pp 9–30, Osage Beach, Missouri/USA;

[5] https://www.wineland.co.za/mechanical–harvesting–of–grapes/;

[6] https://www.mondomacchina.it/en/vineyard–mechanization–many–new–features–for–farmers–c844;

[7] https://pellenc.com/;

[8] https://www.winesandvines.com/features/article/183875/Mechanical–Grape–Harvesters.

[1.]Habib BENBOUHENNI

NEW ZERO VOLTAGE VECTORS IN DIRECT TORQUE CONTROL OF INDUCTION MOTOR DRIVE USING INTELLIGENT CONTROLLERS

[1.] Ecole Nationale Polytechnique d'Oran, ALGERIA

Abstract: Direct Torque Control (DTC) is known to produce the quick and robust response in AC drives. However, during steady state, torque, flux and current ripple occur. An improvement of the electric drive can be obtained using a new zero voltage vectors in DTC scheme based on the intelligent controllers. This paper discusses the application of fuzzy logic and neural network in a torque and flux control loops respectively. Torque output has good dynamical and stable response, and stable torque ripple of traditional DTC can be improved.
Keywords: Fuzzy logic, neural network, Induction motor, Zero voltage

INTRODUCTION

The New conception of electrical drives was influenced by the development of semiconductor components which enabled the development of modern frequency converters as the practical realization of modern control methods of A.C. drives including the vector control in the field coordinates of motor and direct torque control methods [1].

In 1970s, field oriented control (FOC) scheme proved success for torque and speed control of induction motor. Decoupling of two components of stator currents (flux and torque producing components) is achieved as DC machines to provide independent torque control. Hence the scheme proves itself superior to the DC machine. The problem faced by FOC scheme is complexity in its implementation due to the dependence of machine parameters, reference frame transformation. Later DTC was introduced. The method requires only the stator resistance to estimate the stator flux and torque [2].

The direct torque control (DTC) method was proposed in the middle of 1980 by I. Takahashi, this method has become one of the high performance control strategies for AC machine to provide a very fast torque and flux control. The name direct torque control is derived from the fact that, on the basis of the errors between the reference and the estimated values of torque and flux, it is possible to directly control the inverter states in order to reduce the torque and flux errors within the prefixed band limits [3].

DTC method is characterised by its simple implementation and a fast dynamic response. Furthermore, the inverter is directly controlled by the algorithm, i.e. a modulation technics for the inverter is not needed. The main advantages of DTC are the absence of coordinate transformation and current regulator, the absence of separate voltage modulation block.

Since DTC was first introduced, several variations to its original structure were proposed to overcome the inherent disadvantages in any hysteresis-based controller, such as variable switching frequency, high sampling requirement for digital implementation, and high torque ripple. To solve this problem, various techniques have been proposed. Including the use of variable hysteresis bands, predictive control schemes, space vector modulation techniques, and intelligent control methods [4].

This paper proposes a novel scheme and tables of DTC drive for an induction motor based neural and fuzzy logic controller hysteresis has been developed using Matlab Simulink. Stator current, rotor speed, electromagnetic torque and flux plot which show the performance of DTC with. Neural and fuzzy logic controller's hysteresis DTC has also tracked the required speed and torque successfully which represents the successful design of the DTC drive.

INDUCTION MOTOR MODEL

The dynamic model of an induction motor in the stationary reference frame can be written in d-q frame variables. Stator voltage vector Vs of the motor can be expressed as follows [5]:

$$Vds = \frac{d\Phi ds}{dt} + Rs.iqs \tag{1}$$

$$Vqs = \frac{d\Phi qs}{dt} + Rs.iqs \tag{2}$$

The stator flux vector $\overline{\Phi_s}$ and components can be written as

$$\Phi ds = Ls.ids + Lm.idr \tag{3}$$
$$\Phi qs = Ls.iqs + Lm.idr \tag{4}$$
$$\overline{\Phi s} = Ls.\overline{is} + Lm.\overline{ir} \tag{5}$$

The rotor flux vector $\overline{\Phi_r}$ and components in the stator reference frame are:

$$\Phi dr = Lr.idr + Lm.ids \tag{6}$$
$$\Phi qr = Lr.iqr + Lm.ids \tag{7}$$
$$\overline{\Phi r} = Lr.\overline{ir} + Lm.\overline{is} \tag{8}$$

where V_{ds} and V_{qs} are the stator voltages, i_{ds} and i_{qs} are the stator currents, i_{dr} and i_{qr} are the rotor currents, Φ_{ds} and Φ_{qs} are the stator fluxes, Φ_{dr} and Φ_{qr} are the rotor fluxes, i_s and i_r are the stator and rotor currents vectors, R_s is the stator windings resistance., and L_s, L_r, L_m are stator, rotor self-inductance and mutual inductance respectively. The electromagnetic torque T_e developed by the induction motor in terms of stator and rotor flux vectors can be expressed as

$$T_e = \frac{3}{2} p \frac{Lm}{\sigma.Ls.Lr} .|\overline{\Phi s}|.|\overline{\Phi r}|.\sin(\delta) \tag{9}$$

where $\delta = 1 - \frac{Lm^2}{Ls.Lr}$ is the leakage factor, p is the number of pole pairs. From the above equation, clearly, the electromagnetic torque

is cross vector product between the stator and rotor flux vectors. Therefore, generally torque control can be performed by controlling torque angle δ with constant amplitude of the stator and rotor fluxes [5].

TWO-LEVEL INVERTER

The voltage source inverter (VSI) is a static converter constituted by switching cells generally with transistors or IGBT for high powers (Figure 1). The operating principle can be expressed by imposing on the machine the voltages with variable amplitude and frequency starting from a standard network 791/1368v-60Hz. Voltages at load neutral point can be given by the following expression [3]:

$$\begin{bmatrix} v_A \\ v_B \\ v_C \end{bmatrix} = \frac{E}{6} \begin{bmatrix} 2 & -1 & -1 \\ -1 & 2 & -1 \\ -1 & -1 & 2 \end{bmatrix} \cdot \begin{bmatrix} v_{Ao} \\ v_{Bo} \\ v_{Co} \end{bmatrix} \quad (10)$$

This modeling for the two converters that feed the induction motor.
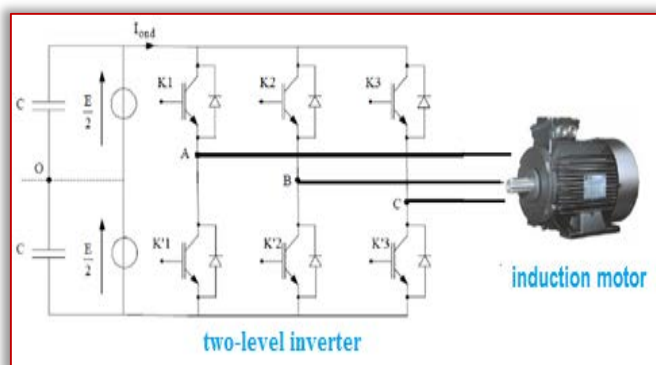
Figure 1. Voltage source inverter scheme

DIRECT TORQUE CONTROL WITH TWO-LEVEL INVERTER

The Direct Torque Control (DTC) method allows direct and independent electromagnetic torque and flux control, selecting an optimal switching vector [3]. The Figure 2 shows the schematic of the basic functional blocks used to implement the DTC of induction motor drive. A voltage source inverter (VSI) supplies the motor and it is possible to control directly the stator flux and the electromagnetic torque by the selection of optimum inverter switching modes [6].
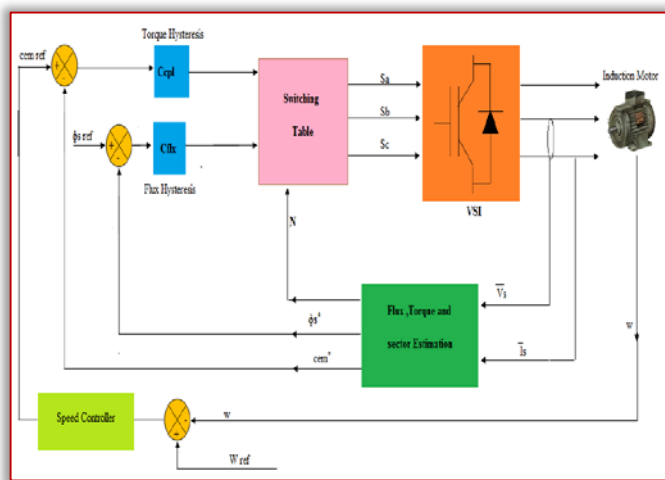
Figure 2 Basic direct torque control scheme for induction motor

— Vector model of inverter output voltage

In the PWM voltage source inverters, considering the combinations of the states of switching functions inverter switching state functions (C_1, C_2, and C_3) which can take either 1 or 0, the voltage vector becomes [7]:

$$v_s = U_0 \cdot \sqrt{\frac{2}{3}}(C_1 + C_2 e^{j\frac{2\Pi}{3}} + C_3 e^{j\frac{2\Pi}{3}}) \quad (11)$$

In the classical DTC method the plane is divided for the six sectors (Figure 3).
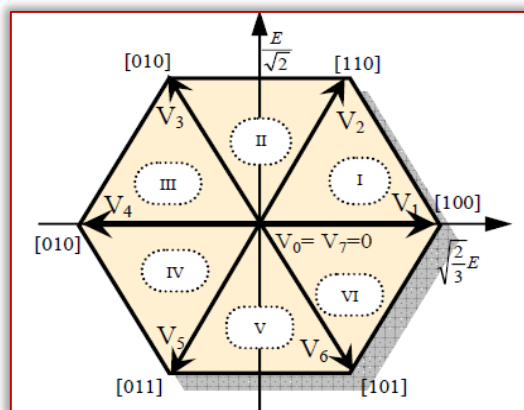
Figure 3. Partition of the αβ Plane into 6 Angular Sectors

— Stator flux and torque estimation

The components of the current ($I_{s\alpha}$, $I_{s\beta}$), and stator voltage ($V_{s\alpha}$, $V_{s\beta}$) are obtained by the application of the transformation given by (12) and (13) [7]:

$$\begin{cases} I_{s\alpha} = I_{sA} \sqrt{\frac{2}{3}} \\ I_{s\beta} = (I_{sB} - I_{sC}) \sqrt{\frac{2}{3}} \end{cases} \quad (12)$$

$$\begin{cases} v_{s\alpha} = U_0 \cdot [C_1 - \frac{1}{2}(C_1 + C_2) \cdot \sqrt{\frac{2}{3}} \\ v_{sB} = \frac{1}{\sqrt{2}} U_0 \cdot (C_2 - C_3) \end{cases} \quad (13)$$

The components of the stator flux ($\Phi_{s\alpha}$, $\Phi_{s\beta}$) given by (14):

$$\begin{cases} \overline{\Phi}_{s\alpha} = \int_0^t (\overline{v}_{s\alpha} - R_s \overline{I}_s) dt \\ \overline{\Phi}_{s\beta} = \int_0^t (\overline{v}_{s\beta} - R_s \overline{I}_s) dt \end{cases} \quad (14)$$

The stator flux linkage phase is given by (15).

$$\Phi_s = \sqrt{\Phi_{s\beta}^2 + \Phi_{s\alpha}^2} \quad (15)$$

The electromagnetic couple be obtained starting from the estimated sizes of flux $\Phi_{s\alpha}$, $\Phi_{s\beta}$ and calculated sizes of the current $I_{s\alpha}$, $I_{s\beta}$

$$c_{em} = \frac{3}{2} P[\Phi_{\alpha s} i_{\beta s} - \Phi_{\beta s} i_{\alpha s}] \quad (16)$$

The choice of one of the null vectors is performed having in mind the reduction of simultaneous commutations and consequently, the switching loses in the inverters legs. As the necessary further inverter's topology and therefore the voltage vector is determined at each sampling period, it is obviously that the last must be as small as possible in order to achieve a convenient switching frequency. In simulation it is possible to choose a fixed step size as small as we needed, but for the real time control, the limitations of the control system must be considered [8].

The switching Table allows to select the appropriate inverter switching state according to the state of hysteresis comparators of flux (Cflx) and torque (Ccpl) and the sector where is the stator vector flux (Φ_s) in the plan (α, β), in order to maintain the magnitude of stator flux and electromagnetic torque inside the hysteresis bands. The above consideration allows construction of the switching Table as presented in Table 1 [3].

Table 1 .Switching table for classical DTC

Cflx	N Ccpl	1	2	3	4	5	6
1	1	2	3	4	5	6	1
	0	7	0	7	0	7	0
	-1	6	1	2	3	4	5
0	1	3	4	5	6	7	8
	0	0	7	0	7	0	7
	-1	5	6	1	2	3	4

The voltage vector table receives the flux level, the torque level and the sector number and generates appropriate control for the inverter from a look-up table as in Table 1[9].

Tables 2 to 4 illustrates of modification tables of classical DTC with a voltages zeros.

Table 2. Switching table for strategy 1 of classical DTC

Cflx	N Ccpl	1	2	3	4	5	6
1	1	2	3	4	5	6	1
	0	2	3	4	5	6	1
	-1	7	0	7	0	7	0
0	1	3	4	5	6	1	2
	0	0	7	0	7	0	7
	-1	0	7	0	7	0	7

Table 3. Switching table for strategy 2 of classical DTC

Cflx	N Ccpl	1	2	3	4	5	6
1	1	2	3	4	5	6	1
	0	7	0	7	0	7	0
	-1	7	0	7	0	7	0
0	1	3	4	5	6	1	2
	0	3	4	5	6	1	2
	-1	0	7	0	7	0	7

Table 4. Switching table for strategy 3 of classical DTC

Cflx	N Ccpl	1	2	3	4	5	6
1	1	2	3	4	5	6	1
	0	1	2	3	4	5	6
	-1	7	0	7	0	7	0
0	1	3	4	5	6	1	2
	0	0	7	0	7	0	7
	-1	0	7	0	7	0	7

DIRECT TORQUE CONTROL USING REGULATORS HYSTERESIS BASED ON NEURAL AND FUZZY LOGIC

Since none of the inverter switching vectors is able to generate the exact stator voltage required to produce the desired changes in torque and flux, torque and flux ripples compose a real problem in DTC induction motor drive. Many solutions were proposed to improve performances [4].

According to the principle of operation of DTC, the torque presents a pulsation that is directly related to the amplitude of its hysteresis band. The torque pulsation is required to be as small as possible because of its causes vibration and acoustic noise.

A small flux hysteresis bands should be preferred when high switching speed semiconductor devices are utilized because their switching losses are usually negligible with respect to state losses. In this way, the output current harmonic can be strongly reduced.

In this paper, a neural and Mamdani-type FLC is developed to adapt the flux and torque hysteresis band in order to reduce the ripples in the motor developed torque.

The principle of fuzzy logic and neural direct torque control (DTC) is similar to traditional DTC. The difference is using a fuzzy logical controller to replace the torque hysteresis loop controller, and the neural controller to replace the flux hysteresis loop controller. As shown in Figure 4.
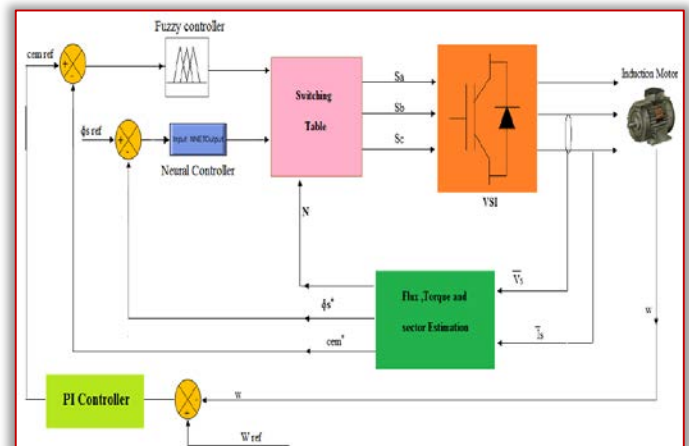
Figure 4. DTC with regulators hysteresis based
on neural and fuzzy logic

—— Design of neural for flux ripple

Artificial neural networks use a dense interconnection of computing nodes to approximate nonlinear functions. Each node constitutes a neurone and performs the multiplication of its input signals by constant weights, sums up the results and maps the sum to a nonlinear activation function g, the result is then transferred to its output.

A feed forward ANN is organized in layers: an input layer, one or more hidden layers and an output layer [7]. Multilayer Perceptron (MLP) is the most used neural network model. MLP utilizes a learning algorithm (back propagation) for training the network, MLP are capable to separate data that are not linearly separable. The MLP structure is shown in Figure 5 [10]. It includes a summer and a nonlinear activation function g [7].
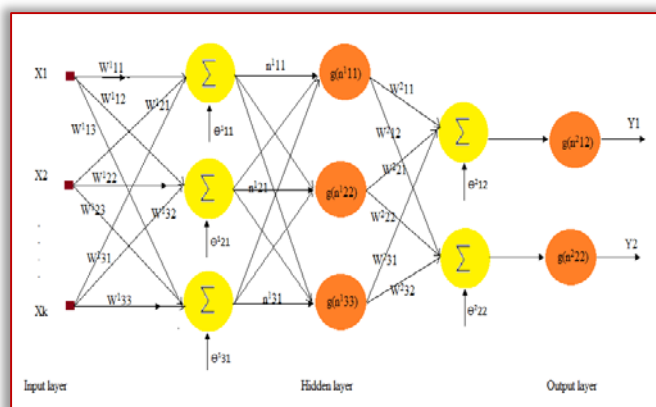
Figure 5. A Multilayer perceptron network with one hidden layer

The inputs xk, k = 1…K to the neuron are multiplied by weights wki and summed up together with the constant bias term θi. The resulting in is the input to the activation function g. The activation function was originally chosen to be a relay function, but for mathematical convenience a hyperbolic tangent (tanh) or a sigmoid function are most commonly used. The mathematical model of a neuron is given by (17) [7]:

$$y_i = g_i = g(\textstyle\sum w_{ji}\, x_j + \theta_i) \tag{17}$$

The ANN is trained by a learning algorithm which performs the adaption of weights of the network iteratively until the error between target vector and the output of ANN is less than an error goal. The most popular learning algorithm for complex networks the back propagation algorithm and its variants. The later is implemented by many ANN software packages such as neural network tool box from MATLAB [11, 12].

In this paper, neural is developed to adapt the flux hysteresis band in order to reduce the ripples in the motor. The neural controller design is based on intuition and simulation. Figure 6 shows the block neural network controller of flux hysteresis band.
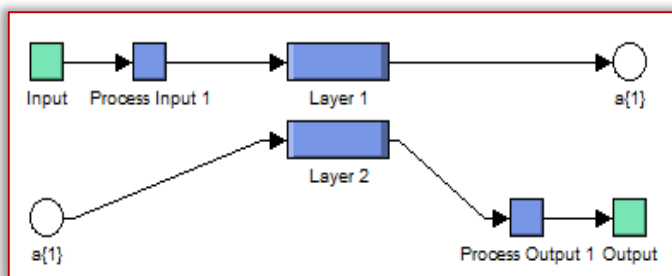
Figure 6. Block neural network controller of flux hysteresis band

— Design of FLC for torque ripple optimization

Fuzzy logic controller is online control. Recently, the fuzzy logic has been utilized for various control applications including motor speed control techniques. The fuzzy logic has made the control of complex nonlinear dynamic systems as simple as possible [13].

The principle of fuzzy logic direct torque control is similar to traditional DTC. The difference is using a fuzzy logical controller to replace the torque hysteresis loop controller. As shown in Figure 4. In this paper, an FLC is developed to adapt the torque hysteresis band in order to reduce the ripples in the motor developed torque. In conventional DTC technique, The amplitude of the torque hysteresis band is fixed. However, in this proposed scheme, the FLC

controls the upper and lower limits. The fuzzy systems are universal function approximators. The FLC is used as a nonlinear function approximator producing a suitable change in the bandwidth of the torque hysteresis controller in order to keep the torque ripples minimum.

The fuzzy controller design is based on intuition and simulation. For different values of motor speed and current, the values reducing torque and flux ripple were found. These values composed a training set which is used to extract the table rule U (Δe, e). The shapes of membership functions (Figure 7 and Figure 8) are refined trough simulation and testing.

Figure 7 and 8 show the membership functions of input and output variables respectively. The fuzzy control rules are illustrated in Table 5.

Table 5. Fuzzy rules of torque hysteresis controller

e Δe	NL	NM	NP	EZ	PS	PM	PL
NL	NL	NL	NL	NL	NM	NP	EZ
NM	NL	NL	NL	NM	NP	EZ	PS
NP	NL	NL	NM	NP	EZ	PS	PM
EZ	NL	NM	NP	EZ	PS	PM	PL
PS	NM	NP	EZ	PS	PM	PL	PL
PM	NP	EZ	PS	PM	PL	PL	PL
PL	EZ	PS	PM	PL	PL	PL	PL
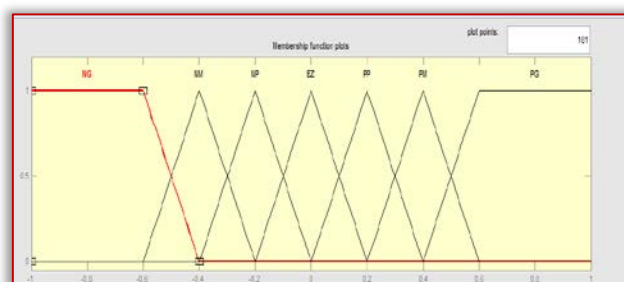
a)
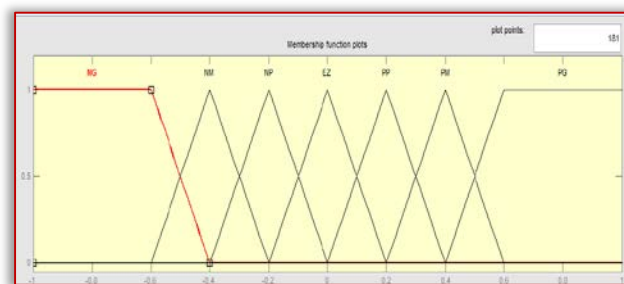
b)

Figure 7. Input variable membership functions
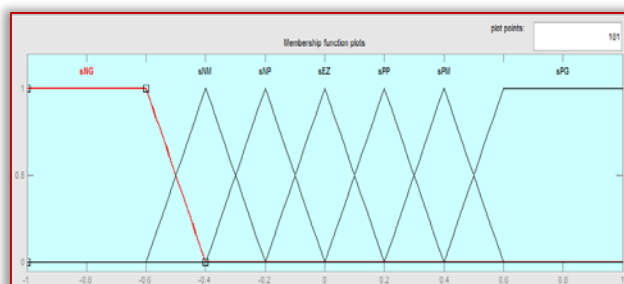
Figure 8. Output variable membership function

SIMULATION RESULTS

The motor parameters are Power = 1MW, Rated voltage = 791V, Poles = 3, Frequency=60Hz, Stator resistance = 0.228ohm, Rotor resistance = 0.332ohm, Stator inductance = 0.0084H, Rotor inductance = 0.0082H, Moment of inertia = 20 Kg.m2, Magnetizing inductance = 0.0078H.

Reference speed is chosen as 1000 r.p.m, and external load torques of 6500 N.m are applied at 0.8 sec with conventional DTC and DTC proposed.
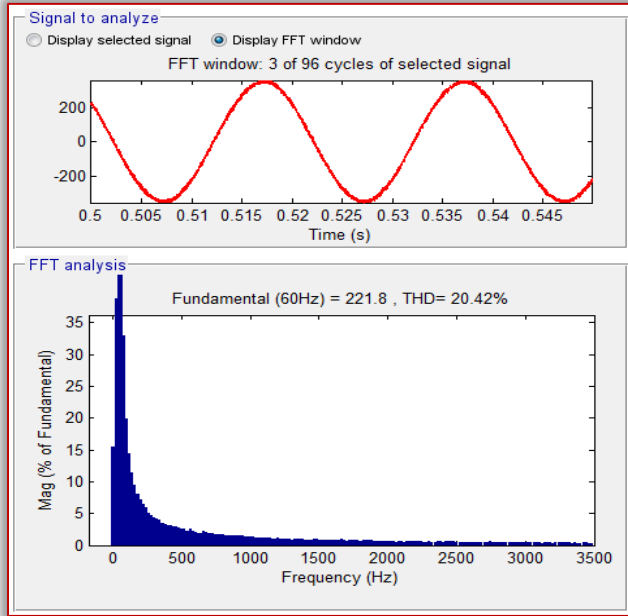
Figure 9. Performances of classical DTC
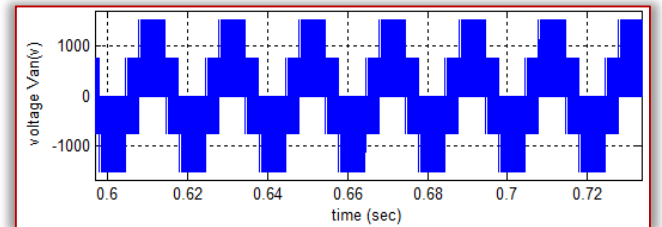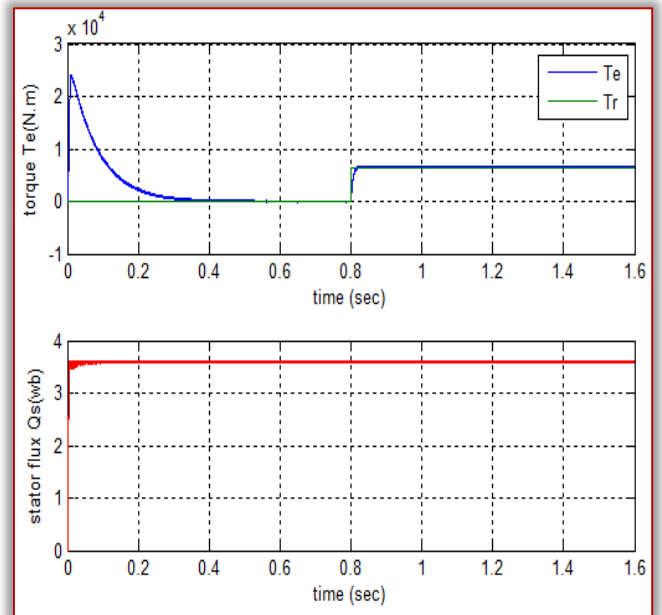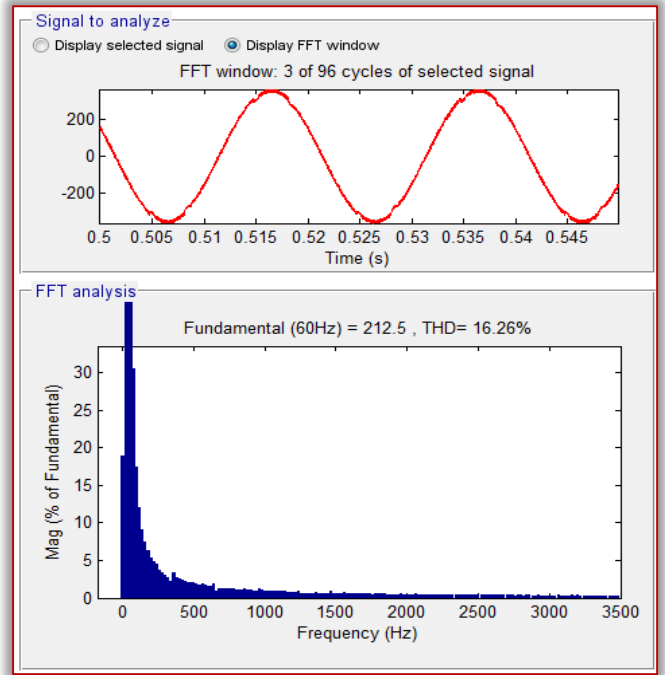
Figure 10. Performances of strategy 1 for classical DTC
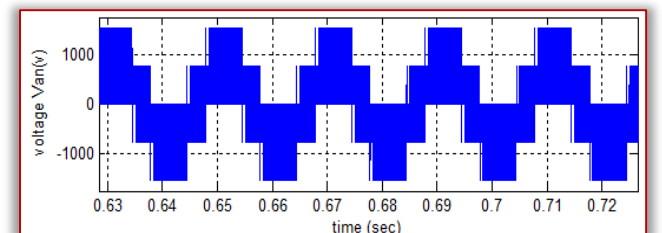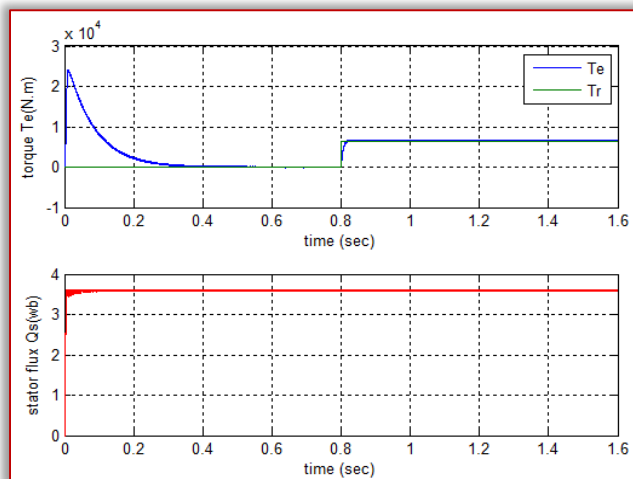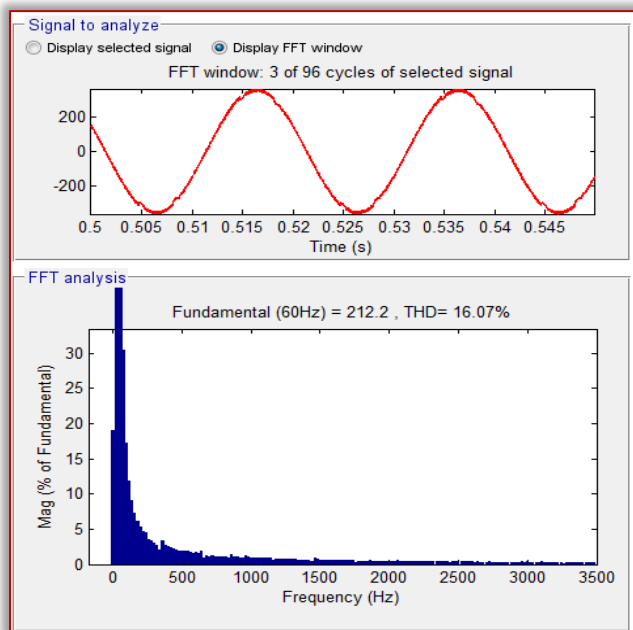
Figure 11. Performances of strategy 2 for classical DTC
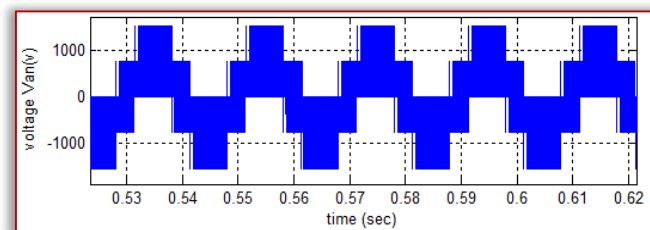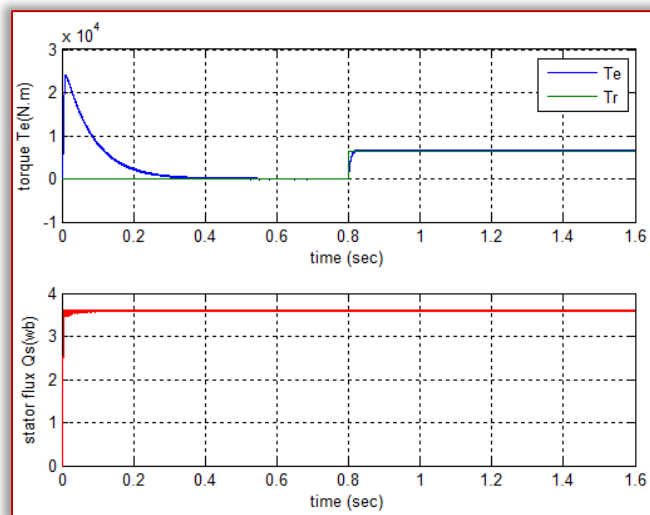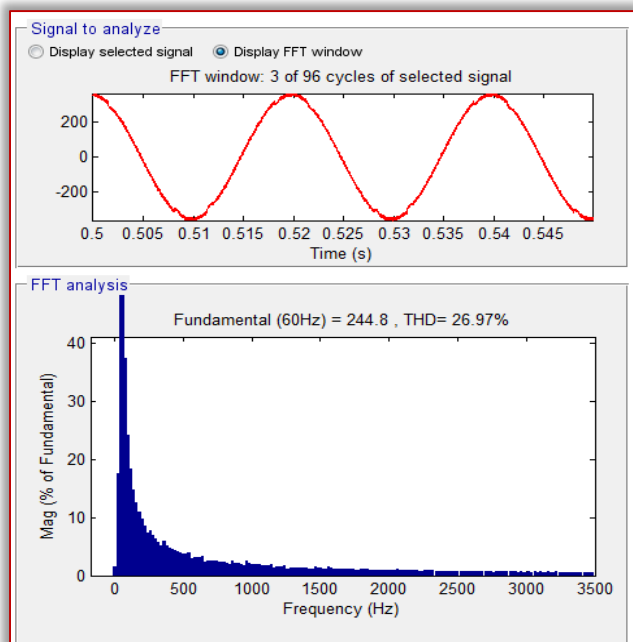
Figure 12. Performances of strategy 3 for classical DTC
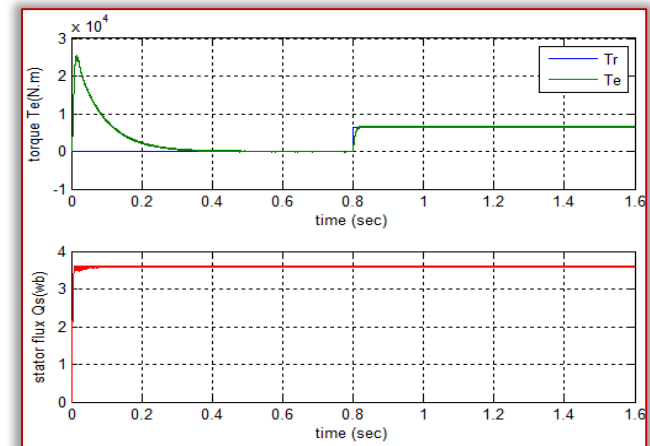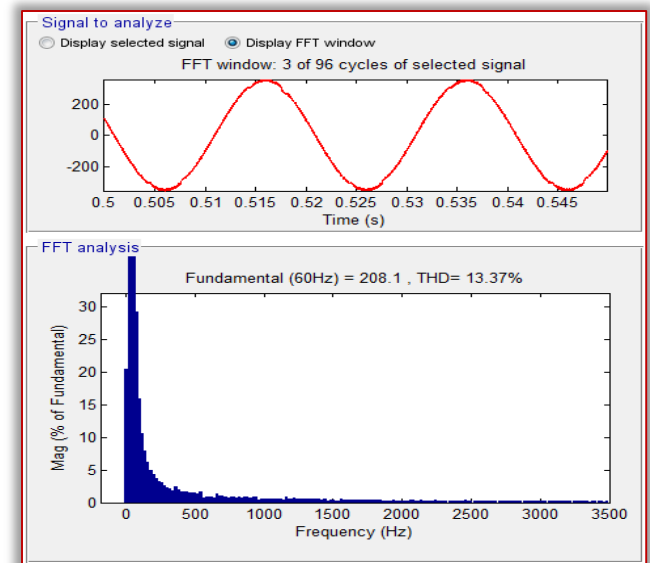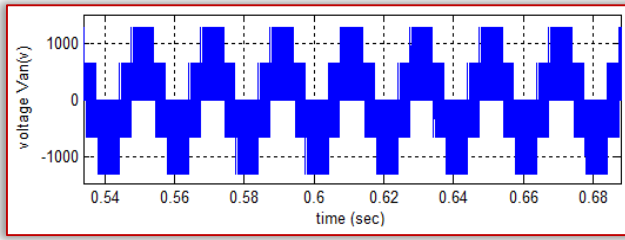
Figure 13. Performances of classical DTC with neural and fuzzy controllers
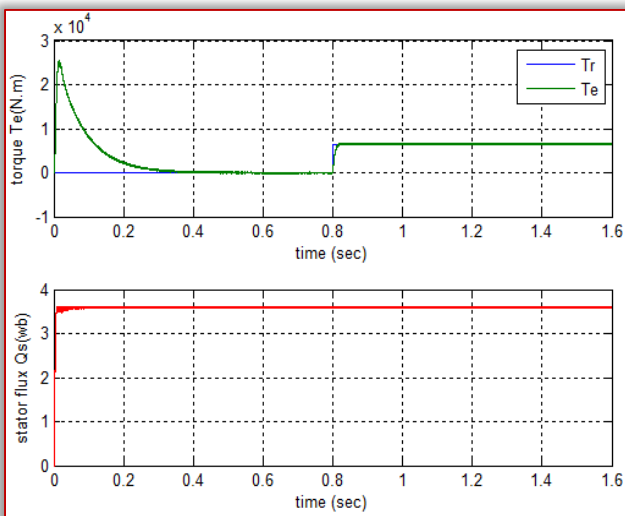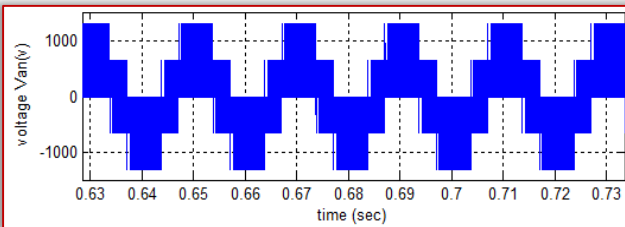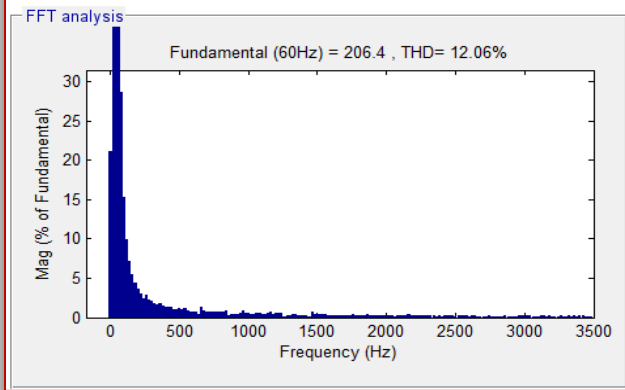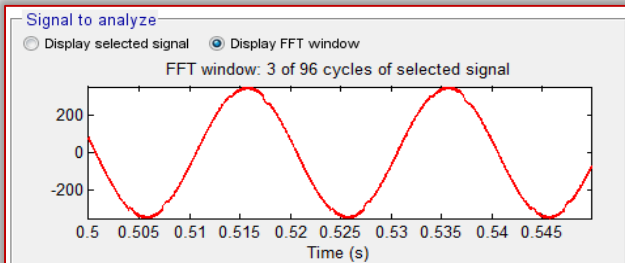
Figure 14. Performances of strategy 1 for classical DTC
with neural and fuzzy controllers
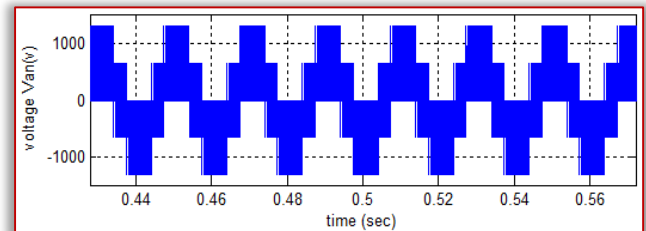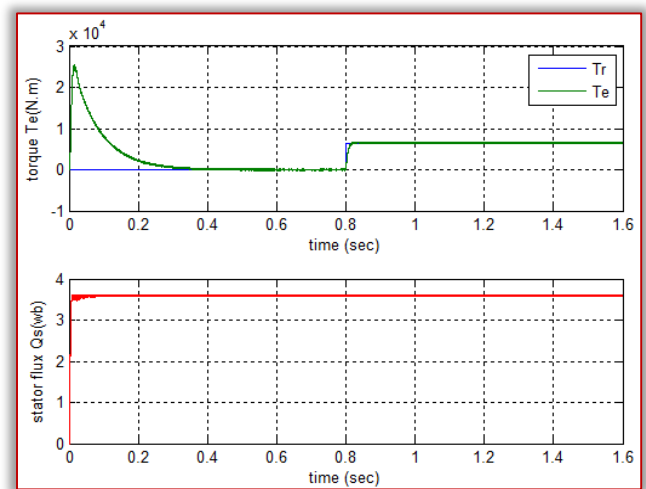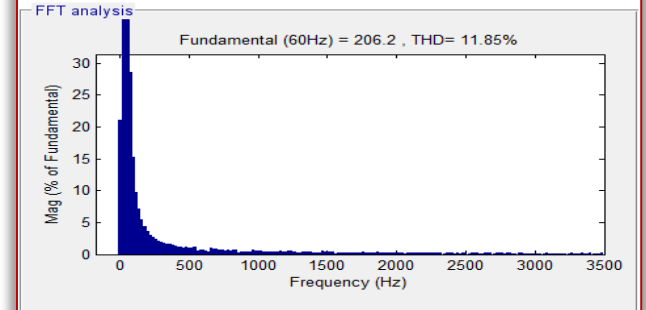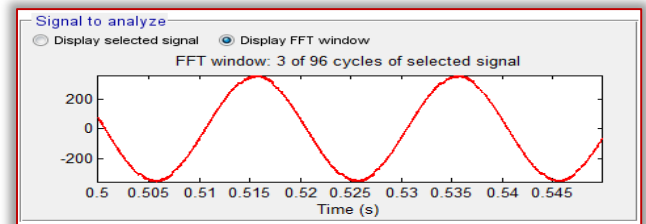
Figure 15. Performances of strategy 2 for classical DTC
with neural and fuzzy controllers
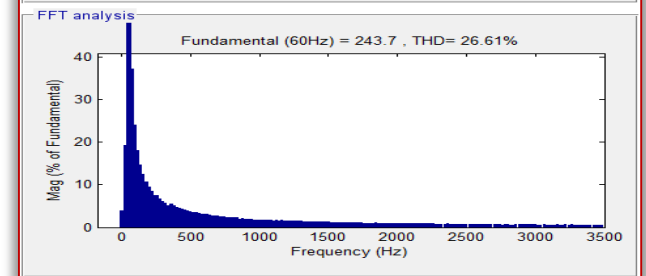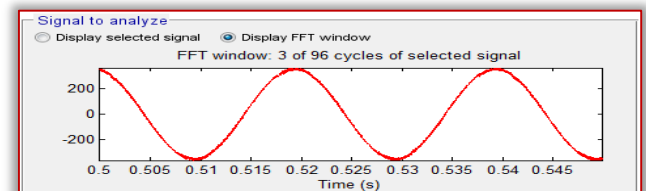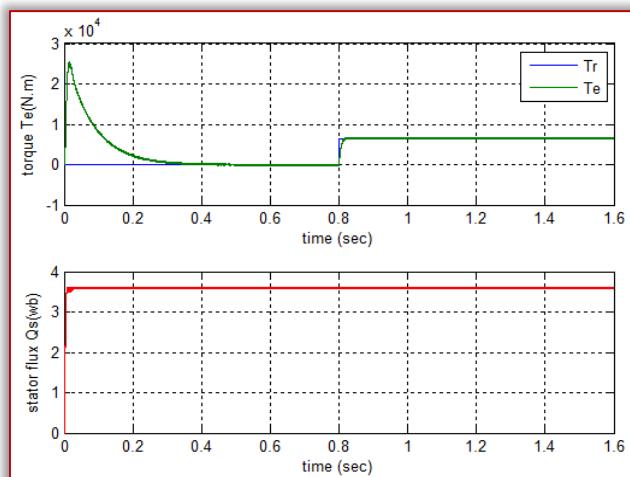
Figure 16. Performances of strategy 3 for classical DTC
with neural and fuzzy controllers

a) Classical DTC
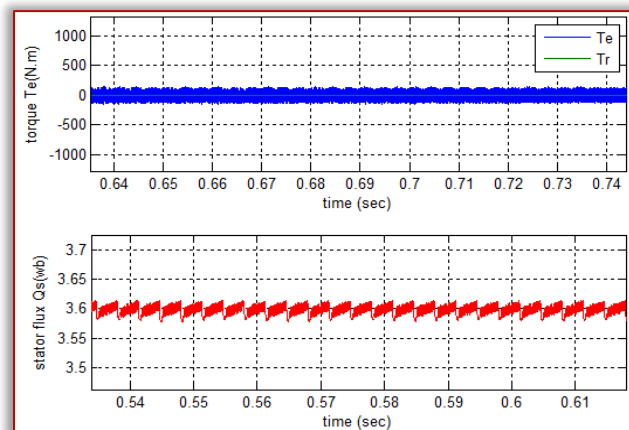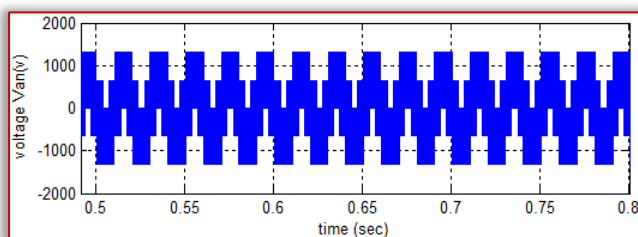
b) Strategy 1
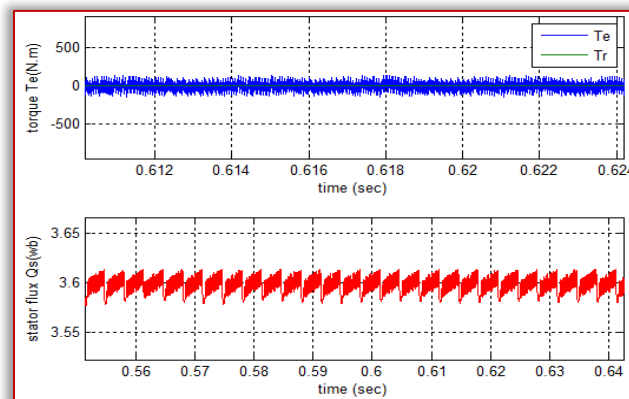
c) Strategy2

d) Strategy 3
Figure 17. Comparison between classical and proposed strategy of DTC
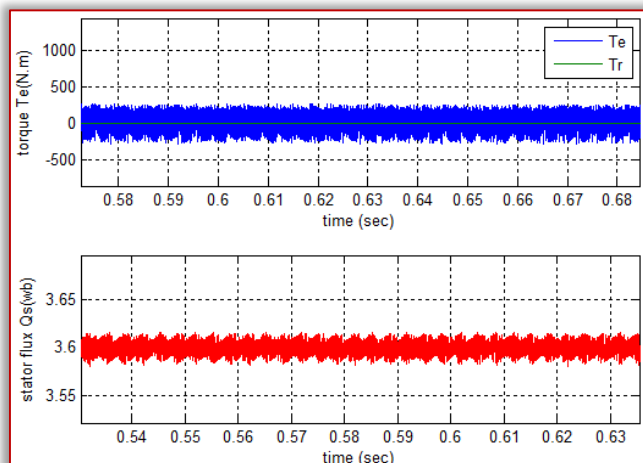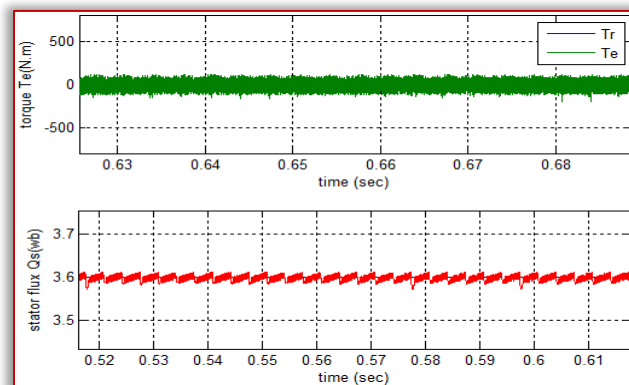
a) Classical DTC with neural and fuzzy controllers
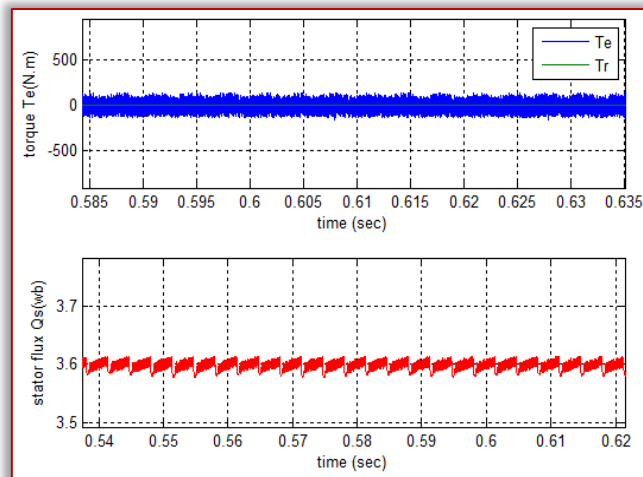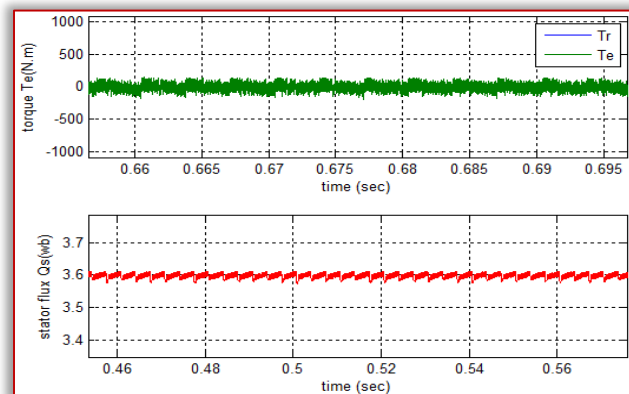
b) Strategy 1 with neural and fuzzy controllers of classical DTC
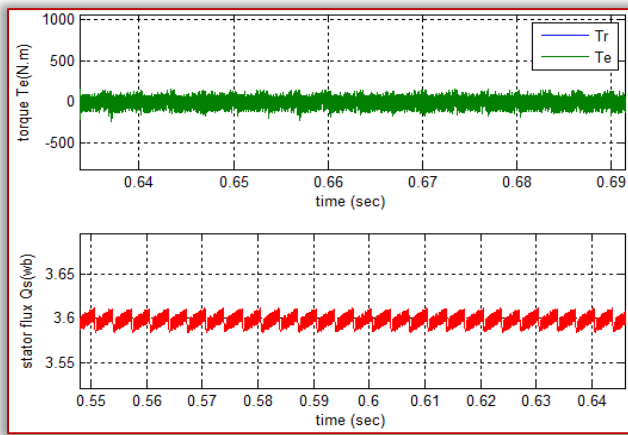
c) Strategy 2 with neural and fuzzy controllers of classical DTC
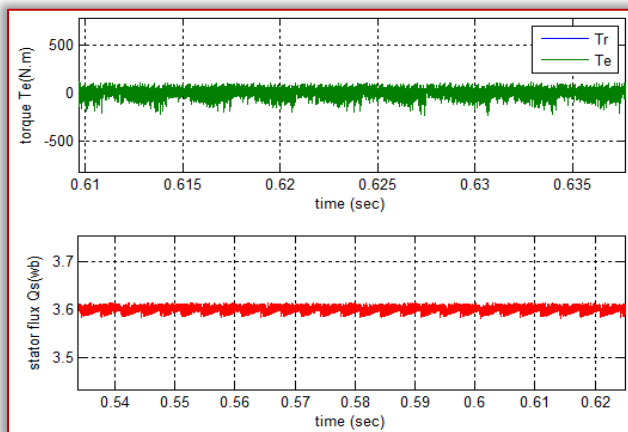
d) Strategy 3 with neural and fuzzy controllers of classical DTC

Figure 18. Comparison between the classical and proposed strategy of DTC with neural and fuzzy controllers

In Table 5, we summarize the simulation results obtained by conventional DTC and the proposed strategies.

Table 5. Comparison results

Strategy	I_{as} THD (%)
Classical DTC	20.42
Strategy 1	16.26
Strategy 2	16.07
Strategy 3	26.97
Classical DTC with neural and fuzzy controllers	13.37
Strategy 1 with neural and fuzzy controllers	12.06
Strategy 2 with neural and fuzzy controllers	11.85
Strategy 3 with neural and fuzzy controllers	26.61

To compare with classical DTC and DTC proposed a voltage zeros for induction motor using fuzzy logic and artificial neural networks controller's is simulated. See figures the torque ripple is significantly reduced when neural and fuzzy controllers are in use.

In Table 5 the value of THD for stator current is significantly reduced when DTC proposed. On the other hand, we note that the strategy 2 of the classical DTC given good result compared to the best strategy 1 and 3, and classical DTC.

The speed reaches its reference without overrunning at the empty start for all strategies. And the torque flows the load torque.

The dynamics of the components of the stator flux are not affected by the application of these load guidelines.

CONCLUSION

This paper proposes new tables and novel scheme to improve the drive performance. Fuzzy logic and neural networks controller's of direct torque control (DTC) is used to improve dynamic response performance and decrease the torque ripples. It can be seen from the simulation results above for the simulation model given and the parameters mentioned above that flux, torque and current ripples is reduced remarkably for the proposed method (strategy 2). The simulation results show that the torque has a very good dynamic response for the mentioned DTC methods. Applying ANN and Fuzzy to replace controller's result in reducing the over and under shoots and lead to swift speed response as shown in simulation results. Therefore using the proposed method results in improving the motor performance.

References

[1] P. Brandstetter, P. Chlebis, P. Palacky, "Direct torque control of induction motor with direct calculation of voltage vector," Advances in Electrical and Computer Engineering, Vol. 10, No. 4, 2010, pp: 17-22.

[2] A. Manuel, J. Francis, " Simulation of direct torque controlled induction motor drive by using space vector pulse Width modulation for torque ripple reduction, " International Journal of Advanced Research in Electrical, Electronics and Instrumentation Engineering, Vol. 2, No. 9, September 2013.

[3] R. Sadouni, A. Meroufel, "Performances comparative study of field oriented control (FOC) and direct torque control (DTC) of dual three phase induction motor (DTPIM)," International Journal of Circuits, Systems and Signal Processing, Vol. 6, No 2, 2012.

[4] A. Hassan Adel, S. Abo-zaid, A. Refky, "Improvement of direct torque control of induction motor drives using Neuro-Fuzzy controller," Journal of Multidisciplinary Engineering Science and Technology (JMEST), Vol. 2, No. 10, October 2015.

[5] M. K. Sahu, A. K. Panda, B. P. Panigrahi, "Direct torque control for three-level neural point clamped inverter-fed induction motor drive," Engineering Technology & Applied Science Research (ETASR), Vol. 2, No. 2, 2012, pp: 201-208.

[6] D. Kumar, I. Thakur, and K. Gupta, " Direct torque control for induction motor using intelligent artificial neural network technique," International Journal of Emerging Trends Technology in Computer Science (IJETTCS), Vol. 3, No. 4, July-August 2014.

[7] R. Toufouti S. Meziane, H. Benalla, "Direct torque control for induction motor using intelligent techniques," Journal of Theoretical and Applied Information Technology (JATIT), 2007.

[8] S. Ivanov, "Continuous DTC of the induction motor," Advances in Electrical and Computer Engineering, Vol. 10, No. 4, 2010, pp: 149-154.

[9] A. Idir, M. Kidouche, " Direct torque control of three phase induction motor drive using fuzzy logic controllers for low torque ripple," Journal of Proceeding Engineering & Technology, Vol. 2, pp.78-83, 2013.

[10] A. Mostefai, S. Benah, "Modeling and simulation of transistor MOSFET (HIGH-K) using neural network," Journal of Electrical Engineering (www.jee.ro).

[11] T. S. Murthy, T. V. Kiran, " Comparative Analysis of Fuzzy DTC and ANN DTC for Induction Motor," International Journal of Emerging Trends in Engineering and Development, Vol. 2, No. 3, March 2013.

[12] J. Jayachandran, R. M. Sachithanandam, "Performance Investigation of Unified Power Quality Conditioner Using Artificial Intelligent Controller," International Review on Modelling and Simulations (IREMOS), Vol. 8, No. 1, 2015.

[13] A. M. Youcef, F. K. Abo-Elyouser, "Fuzzy logic speed control for three-phase induction motor supplied by photovoltaic system with a robust MPPT," Journal of Electrical Engineering (www.jee.ro).

[1,2]Václav NOVOTNÝ, [1]Michal KOLOVRATNÍK

EXPANSION COOLING WITH POWER RECOVERY FOR DEWATERING OF CO_2 STREAMS FROM OXYFUEL CCS SYSTEMS

[1.] Faculty of Mechanical Engineering, Czech Technical University in Prague, Prague, CZECH REPUBLIC
[2.] University Centre for Energy Efficient Buildings, Czech Technical University in Prague, Bustehrad, CZECH REPUBLIC

Abstract: Carbon capture and storage (CCS) is one of the concepts some put hopes into for mitigation of climate change by separating CO_2 from power plant's flue gases and disposing (or utilizing) it. In the CCS systems with oxyfuel combustion the major advantage is considered to be fact, that the CO_2 stream contains only very few admixtures of other gases. This fluid however still contains significant amount of water which has its origin mainly in combustion of hydrogen content of fuels. This water needs to get separated from the mixture before CO_2 transport and storage. Typical concept for dewatering of the fluid is collection of the condensed liquid phase during cooling after each compression stage. The method for this collection is then use of flash tanks. Alternative method to obtain the liquid phase of the water so that it can be separated from the CO_2 stream is cooling, which can be well realized by the fluid expansion. This concept is still very new and hasn't been properly explored yet. In this work will be analysed one of possible configurations in which a stream CO_2-water mixture in vapour phase (simplified state of the oxyfuel flue gas) is expanded to a lower pressure, condensed phase is separated and CO_2 at higher purity is compressed back to previous near-ambient state. For this configuration there are presented results of separation effectiveness and power consumption as a function of inlet water fraction, expansion method (valve or expander with varying efficiency) and various methods for evaluation of the fluid properties. These results find its place in future and more rigorous analyses of these systems.
Keywords: CCS, two phase, expansion cooling, fluid property formulation

INTRODUCTION

The world is facing climate change in which the anthropogenic contribution has been linked primarily to CO_2 emissions as these can be easily quantified and tied with large producers as is a power production sector. Regardless the clear answer of the anthropogenic contribution in comparison to natural ones, large part of the world with many countries have signed the Paris agreement in hopes to fight the climate change and have committed to reduce greenhouse gas emissions. [1] Ultimate goal is to keep the average global temperature rise below 2°C when compared to the pre-industrial era [2].

Carbon capture and storage (CCS) is one of the concepts for decarbonisation. CCS technologies greatly reduce efficiency of power plants by consuming electricity in number of auxiliary systems and converting useful heat into a waste heat. [3] Regardless the fact that these systems actually use higher amounts of fuels, CCS systems enjoy large funding throughout the countries and many believe that it has a potential to play a significant role in the future of power generation in Europe, at least in a short to intermediate term. Reason is that it enables continuing of using mainly fossil fuels, which are to remain an important source for fuel and electricity production. In attempts to reduce amounts of CO_2 from the atmosphere there are also concepts of bio-CCS where biomass (relatively renewable) fuel is used and the CO_2 as a combustion product is captured and disposed underground so that it doesn't return into the atmosphere.

CCS systems are typically distinguished into three main principles of capture – precombustion (captures CO_2 before combustion via gasification and typically absorption), post-combustion (separates CO_2 from the flue gases) and oxyfuel combustion, which by combustion with pure oxygen the flue gas consists mostly of CO_2 with only very few admixtures of other gases. This fluid however still contains significant amount of water which has its origin mainly in combustion of hydrogen as a part of the fuel composition and especially in case of biomass. Extraction of water from the CO_2 stream is important not only to limit ballast carried in the stream for sequestration but also from more practical reasons. The most important aspect is that the water content causes serious corrosion of the transport and sequestration piping and equipment. Therefore, excluding water from the system is beneficial as soon as possible. [4]–[7]

Typically for the dewatering of the CO_2 are considered two methods. First one is collection of the condensed liquid phase during cooling after each compression stage. The method for this collection is using of flash tanks at the outlet of the cooling heat exchangers. Alternative method to obtain the liquid phase of the water so that it can be separated from the CO_2 stream is cooling. Refrigeration system is then a typical approach.

In this work will be explored and alternative method of CO_2 separation by cooling, where this cooling would be achieved by the fluid expansion. This concept is still very new and hasn't been properly explored yet. In this work will be analysed a configuration in which a stream CO_2-water mixture in vapour phase (simplified state of the oxyfuel flue gas) is expanded to a lower pressure, condensed phase is separated in a flash tank and CO_2 at higher purity is compressed back to previous near-ambient state. It needs to be noted that this is only a first analysis putting some first light into this concept and its results will be used in future analyses.

METHODS

The whole concept is depicted in Figure 1. The CO_2 rich fluid at approximately ambient pressure will most likely be in a state of saturation with water or in case of oversaturation the liquid phase

is assumed to be separated before inlet into the considered system. Therefore the inlet stream is considered to be in a saturation state and as so is routed into the expander. Expansion takes place to a pressure so that the temperature of the mixture is at 3℃ (not lower to limit possible freezing issues). By the temperature decrease the water condenses and is separated from the CO_2 in a subsequent flash drum. Separated liquid is pumped to a pressure required for its treatment. Finally the CO_2 is compressed, in this illustrational case back to ambient pressure in a single stage of compression.

Boundary conditions common to all explored configurations are inlet and outlet pressures (100 kPa), unit mass flow (1 kg/s) of the inlet flue gas and temperature after the expander of 3℃. Pressure drop across the flash drums is neglected. No dynamic effects are assumed the fluid in all processes is assumed to be in thermodynamic equilibrium.

The process was modelled in AspenPLUS software with isentropic efficiency specification for both, expander and the compressor. Baseline case assumes a 2% H_2O content in CO_2 (by mass) and at saturation state (35℃ flue gas temperature). Here the baseline concentration was chosen with respect to temperature around 35℃ to which the flue gas can be cooled without needs for refrigeration.

Further baseline parameters include 80% isentropic efficiency of both expander and the compressor and Peng-Robinson (PR) equation of state for determination of fluid properties. The other equations of state were chosen as potentially suitable for given system and these are Soave-Redlich-Kwong (SRK, note that here vapour-liquid-liquid equilibrium was necessary at turbine outlet for proper operation), non-random two-liquid model (NRTL), Peng-Robinson-Wong-Sandler (PRWS), Predictive Soave-Redlich-Kwong (PSRK) and Schwarzentruber and Renon (SR-POLAR).
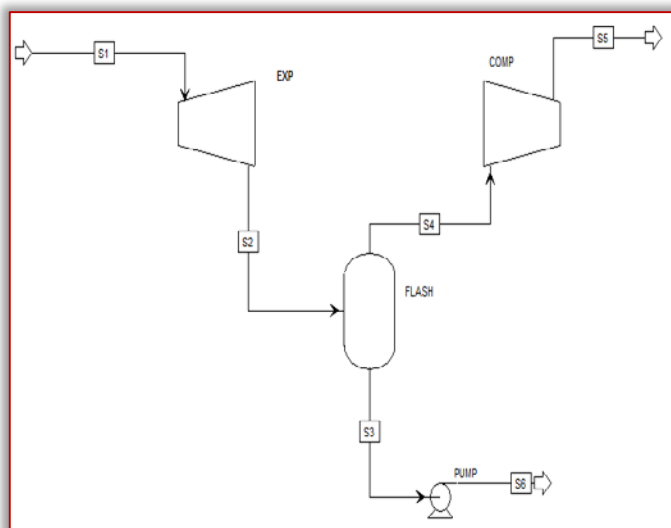
Figure 1: A process diagram of the proposed
dewatering concept for CCS systems

RESULTS AND DISCUSSION

Table 1 shows a whole set of explored varieties of the parameters. The m stands for mass fraction, x for quality, T for temperature, p for pressure, and W for work. The rate of power consumption increase can be observed from decreasing in isentropic efficiency of expander and compressor. More detailed design is necessary to validate actually achievable efficiency. Another issue that can be seen from the results is a discrepancy between various fluid property definitions while some are in decent agreement. This is a recognized issue in the CCS community where certain effort is being focused to specifications of CO_2 mixture properties which would provide required accuracy.

Graphically is in Figure 2 shown a dependency of outlet water fraction as a function of inlet water fraction from which is seen only slightly nonlinear dependency, where the decrease of water content is approximately to half in low H_2O contents but reaches almost 90% for the highest considered concentration.
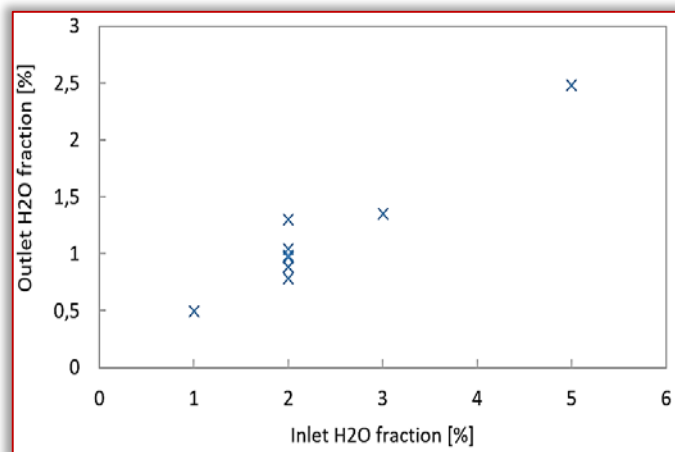
Figure 2: A dependency of outlet water fraction as a function of inlet
water fraction for all explored cases

The net power consumption to separated amount of water should be compared in future work to the results of conventional systems (in separation after each stage of compression and cooling then with the whole compression line) to assess actual feasibility of this system.

Alternatively this system could be inserted also into a later stage of the compression line or if combustion would take place at significantly elevated pressures with perspective of better dewatering. It could also be suitable to use multiple stages of compression with intercooling to limit compression work. Numbers of possible modifications are large (e.g. final cleaning after upstream systems, multiple stages or multiple numbers of these systems across the plant) and for a feasible application a much of work with a careful optimization seems to be necessary. One specific aspect is an actual temperature and water content of the inlet, which is yet to specified to provide best performance with combination of flue gas treatment and heat rejection methods.

This concept seems also very suitable for smaller units as will be exactly for biomass as it is widely accessible but quantity related to specific location is significantly smaller than in case of fossil fuels. Typical issue with CO_2 systems is small volumetric flow, which on the one hand causes devices to be small, on the other hand expanders and compressors suffer from tip, aspect ratio and similar losses. Expansion into vacuum might provide better compressor and expander efficiency than at higher pressures.

Table 1: Explored cases of expansion-compression dewatering

$m_{H2O\ in}$	T_{in}	η_{exp}	η_{comp}	Method
[%]	[°C]	[%]	[%]	[-]
5	51	80	80	PR
3	42	80	80	PR
2	35	80	80	PR
1	24	80	80	PR
2	35	65	80	PR
2	35	50	80	PR
2	35	80	65	PR
2	35	80	50	PR
2	36	80	80	SRK
2	32	80	80	NRTL
2	32	80	80	PRWS
2	32	80	80	PSRK
2	32	80	80	SR-POLAR

$P_{exp\ out}$	$X_{exp\ out}$	$m_{H2O\ out}$	W_{exp}	W_{comp}	W_{net}
[kPa]	[%]	[%]	[kW]	[kW]	[kW]
9,5	94	2,48	105	-208	-103
18	96	1,35	74	-140	-66
28	97	0,88	54	-99	-45
50	99	0,49	29	-50	-21
23	98	1,04	50	-117	-67
19	98	1,3	43	-136	-93
28	97	0,88	54	-122	-68
28	97	0,88	54	-158	-104
26	97	0,78	59	-105	-46
32	98	0,98	49	-88	-39
32	98	0,97	48	-87	-39
32	98	0,97	49	-87	-38
32	98	0,97	49	-87	-38

In specifically considered expander concepts, separation of liquid phase could already take place within the expander, thus flash tank separator would be substituted by integrated rotation (or generally centrifugal) one.

CONCLUSIONS

This paper gives first theoretical results for a novel approach for water separation from CO_2 streams in CCS systems. The system is based on expansion cooling of the fluid for decreasing the temperature and thus condensing the water. Water separation in operation under the assumed condition takes place but still there is non-negligible amount of water remaining in the CO_2 streams. Even though this concept might be interesting for CCS systems after a careful optimization and placement into a specific points within the process. Energy and economic comparison of this system with regular ones is a subject of future work. Another concept worth exploring is placing this system into the areas of higher pressures with potential to separate more water from the CO_2 stream.

Acknowledgment

Note:

References

[1] A. A. Akaev, "From Rio to Paris: Achievements, problems, and prospects in the struggle against climate change," Her. Russ. Acad. Sci., vol. 87, no. 4, pp. 299–309, Jul. 2017.

[2] UNFCCC, "Paris Agreement - Status of Ratification," Paris Agreement, 2016. .

[3] V. Novotny, M. Vitvarova, M. Kolovratnik, and Z. Hrdina, "Minimizing the Energy and Economic Penalty of CCS Power Plants Through Waste Heat Recovery Systems," Energy Procedia, vol. 108, pp. 10–17, Mar. 2017.

[4] I. S. Cole, P. Corrigan, S. Sim, and N. Birbilis, "Corrosion of pipelines used for CO2 transport in CCS: Is it a real problem?," Int. J. Greenh. Gas Control, vol. 5, no. 4, pp. 749–756, Jul. 2011.

[5] A. Dugstad, B. Morland, and S. Clausen, "Corrosion of transport pipelines for CO2–Effect of water ingress," Energy Procedia, vol. 4, pp. 3063–3070, Jan. 2011.

[6] M. B. Kermani and A. Morshed, "Carbon Dioxide Corrosion in Oil and Gas Production—A Compendium," CORROSION, vol. 59, no. 8, pp. 659–683, Aug. 2003.

[7] Y.-S. Choi, S. Nesic, and D. Young, "Effect of Impurities on the Corrosion Behavior of CO_2 Transmission Pipeline Steel in Supercritical CO_2–Water Environments," Environ. Sci. Technol., vol. 44, no. 23, pp. 9233–9238, Dec. 2010.

Fascicule 3

[April - June]

t o m e
[2019] XII

ACTA Technica CORVINIENSIS
BULLETIN OF ENGINEERING

[1.]Oluyemi O. DARAMOLA

FLEXURAL PROPERTIES AND WATER ABSORPTION CHARACTERISTICS OF HIGH DENSITY POLYETHYLENE-BASED SILICEOUS COMPOSITES

[1.] Department of Metallurgical and Materials Engineering, Federal University of Technology, Akure, Ondo State, NIGERIA

Abstract: The effect of silica particles on the flexural properties and water absorption behaviour of high density polyethylene matrix composites had been studied. Control sample and composites containing different weight fractions of submicron silica particles at a constant 0.3 wt. % titania particles loading and 5 wt.% maleic anhydride-grafted polyethylene (MAPE) compatibilizer were mixed with HDPE in a tumbler mixer and melt compounded with a laboratory single screw extruder. The extrudates were pelletized and moulded into flexural and water absorption tests specimens using carver laboratory press. It was observed that the flexural properties increased with an optimal value of 4 wt. % of silica particles in HDPE matrix. The water diffusion mechanism of the composites was also established and it was observed that the value of the diffusion exponent increases as the silica content in the polymer increases; less absorption took place in Silica/HDPE composite with 2 wt.% Silica weight fraction with an average value of 0.16%.
Keywords: silica particles, flexural properties, water absorption, high density polyethylene, diffusion mechanism

INTRODUCTION

Polymer composite materials occupy a significant position in the family of plastic materials; the inclusion of inorganic fillers can assist in modifying the physical, mechanical, thermal and electrical properties of polymeric matrices in relation to the application [1]. Generally, this class of material are used in several areas such as renewable energies, automobiles, medical, aerospace, sports and recreation [2].

Since the introduction of feasible pathways to harvest clean and renewable energy from the sun, polymers have become an integral part of developing reliable and durable clean energy systems [3]. Energy from the sun is converted to usable energy via Photovoltaic (PV) modules and this is a clear indication that total energy yield from the sun would be highly dependent on the efficiency of the PV module[4]. Recently, PV firms have identified the theatrical consequences of corrosion on module performance. Today, PV modules usually utilize a polymeric encapsulant material to protect the silicon parts from the pervasive potentially unpleasant situations initiated by diverse sources of water, comprising rain, snow and condensation. The protection initiated by the encapsulant shields the PV modules from corrosion and offers extra advatanges, comprising mechanical support, electrical insulation and defense from mechanical impairment [4].

Silicon-based material is the major material used by the PV industry for the manufacturing of the solar cell currently and as a result of the rapid evolution of PV firm, the request for solar grade silicon (SoG-Si)-based material has redoubled due to their exceptional properties and their prevailing and hypothetical applications in science and technology [5].

 At the commencement of PV-pursuits in 1980s, the very pure silicon scrap from the micro electronic industry was exploited by the PV-industry [6]. Conversely, unlimited demand that exceeded the partial supply of off-specification electronic grade silicon has initiated an impetus for developing a dedicated technology for the manufacture of cheap solar grade silicon.

The main fear for durability of PV module is corrosion of metallic parts within the module because it can decrease the power yield by intensifying resistance at the electrical interconnects. PV module durability studies have concentrated on the moisture absorptivity of encapsulation materials in as much as corrosion has been identified to be fast-tracked by the presence of water.

The diffusivity of different encapsulants can be assessed to establish how long it takes water to penetrate a module [7]. The extreme diffusivity of ethylene vinyl acetate (EVA) which is the existing encapsualant used today suggests that, even with the use of an water resistant back-sheet, moisture from the sides will spread all through the whole module. To drastically moderate moisture access necessitates a genuine airtight seal and the use of an encapsulant filled with dessicant. Establishing how long it takes water to penetrate a module necessitates knowledge of its diffusivity and solubility. This can be achieved by conducting water absorption test on the developed composites.

Silica, a silicon-based oxide, has a broad areas of application such as dessicant, as a preservative tool to control humidity, as an adsorbent, as a catalyst and as a catalyst support [8].

Some efforts have been made in this direction, using sol-gel technique to extract low cost high grade silica from rice husk ash and developed high density polyethylene matrix composites reinforced with the extracted rice husk silica (RHS) particles for solar encapsulant application; drastic enhancement in the mechanical properties (tensile, hardness and impact) of the composites were observed [9, 10].

The thermal, structural and morphological properties of high density polyethylene matrix composites reinforced with RHS particles had also been studied and there was significant improvement in the thermal properties of the composites [11].

The main objective of the present work is to study the flexural and water absorption behaviour of high density polyethylene matrix composites reinforced with rice husk silica particles.

MATERIALS AND METHOD
— Materials
Silica powder of 500 nm average particle size produced from rice husk ash by Daramola et al. [9] was used in this research; Submicron particles of titania powder supplied by Alfa Aesar High Purity Research chemicals, Vorna Valley, Republic of South Africa (RSA) was utilized as ultraviolet absorber. Maleic anhydride–grafted polyethylene (MAPE) supplied by Sasol Chemicals, Sasolburg, RSA was used as compatibilizer. High Density Polyethylene (HDPE) was supplied in Pellet form by DOW Chemicals, RSA; It has a melt flow index (MFI) of 8 g/10min (XZ 89712-00 RD, 10140182040), a molecular weight of 168,000g mol^{-1}, a melting point of 130 ^{o}C, and a density of 0.954gcm^{-3}. Ethylene-vinyl acetate (EVA), Elvax-220W, with a melt flow index of 150 g/10 min, vinyl acetate content of 30% and density of 0.951 g/cm^3, supplied by DuPont chemical company was used in this work.

— Methods
The composites were developed by compression moulding technique. Predetermined proportion of HDPE, silica powder, titania powder and maleic anhydride-grafted polyethylene (MAPE) were mixed together in a tumbler mixer for 20 minutes in other to obtain homogeneous mixture. Each mixed samples were melt-blended together using a Rapra single-screw extruder at a temperature of 200 - 230 ^{o}C and rotor speed of 40 rpm. The extrudates were pelletized with a laboratory plastic pelletizer. The pellets were thereafter poured into rectangular mould of dimension 150 x 100 x 4 mm. 60 g of the pellets was used for the rectangular mould. The filled mould was placed in between the lower and the upper plates of a carver laboratory press at a temperature of 230 ^{o}C for 10 minutes under applied pressure of 0.2 kPa. The materials were then water cooled at 20 ^{o}C min^{-1}. In this way, control sample and composite samples filled with various weight fractions of submicron silica particles (2, 4, 6, 8 and 10 wt. %) at constant 5 wt. % MAPE and 0.3 wt.% titania loading were prepared. EVA which is the conventional encapsulant was also moulded into various test specimens. Teflon sheet was used to cover the surface of the samples at the top and bottom part of the mould while silicone was sprayed at the inner edges of the mould for easy release after moulding. The moulded rectangular samples were cut into flexural and water absorption specimens of dimensions 150 mm x 50 mm x 4 mm and 15mm x 15mm x 4mm respectively.

— Flexural Test
Flexural test was carried out using Testometric Universal Testing Machine in accordance with ASTM D790 test standard [12]. The grip for the test was fixed on the machine and the flexural specimen was fixed on the machine and the test commenced. The plot and the data for the needed flexural properties were automatically generated.

— Water Absorption Test
Water absorption tests were carried out following the recommendations specified in ASTM D570-98 test standard [13]. Samples of each composite grade were oven dried before weighing. The weight recorded was reported as the initial weight

of the composites. The samples were then placed in rain water maintained at room temperature (25 ^{o}C) and at time intervals of 72 hours, the samples were removed from the water, cleaned using a dry cloth and weighed. The weight measurements were taken periodically for 504 hours which was after water saturation in all the composites had been noticed. The amount of water absorbed by the composites (in percentage) was calculated using equation 1

$$\% \, W = \frac{Wt - Wo}{Wo} X \, 100 \qquad (1)$$

where W is percent water absorption, Wo and Wt are the oven dry weight and the weight of the specimen after time t, respectively. Graphical plots of weight gained–immersion time and percent water absorption–immersion time for all the composites were produced and utilized to study the water absorption behaviour. The mechanism of water diffusion into the composites was studied by analysing the slope and intercepts of the water absorption graphs plotted by using the relations 2 and 3 as described by Sombastsompop and Chaochanchaikul [14]

$$\frac{M_T}{M_\propto} = KT^n \qquad (2)$$

$$\log \frac{M_T}{M_\infty} = \log T + n \log K \qquad (3)$$

where, M_T is water absorption at time T, M_∞ is water absorption at saturation point, K is a constant related to the polymernetwork structure, and n is the release exponent which determines the type of diffusion.

RESULTS AND DISCUSSION
— Flexural Properties
Flexural strength shows the aptitude of material to oppose the applied bending forces under three point loading conditions while flexural modulus is used as an indication of a material's stiffness when flexed. Figure 1 shows the variation of flexural strength at peak for HDPE/Silica composites. The flexural strength at peak for the HDPE and EVA are 21.3222 MPa and 21.523 MPa respectively. From the result, it was observed that, HDPE matrix composite with 4wt.% silica content have the best property with a value of 22.9134 MPa followed by 2 wt.% silica with a value of 22.7689 MPa.

Figure 1: Variation of Flexural Strength at Peak for HDPE, EVA and HDPE/Silica Composites

Although, the incorporation of submicron silica particles causes enhancement in flexural strength at peak of all the composites developed but it was discovered that the flexural strength increases with increase in silica content up-to 4wt.% and begin to decrease as from 6wt%. The increase in the flexural strength at lower silica particles reinforcement could be due to the less agglomeration of the silica particles at these weight fractions of silica (2 – 4 wt.%) as can be seen in the SEM images in Figure 9(b,c), the silica particles are better dispersed which resulted into good adhesion at the particle-matrix interface thereby enhancing the flexural properties of the composite. At higher silica particles reinforcement, there is migration of submicron silica particles into the particle-matrix interface which resulted into high particles agglomerations causing micro cracks at the interface as well as non-uniform stress transfer [15].

Figure 2 shows the variation of flexural strength at break for HDPE/silica composites. The neat HDPE have a value of 8.17375 MPa while EVA has a value of 10.1423 MPa. The optimum value was gotten at 4 wt.% silica reinforcement with a value of 18.81674 MPa followed by 2 wt.% silica reinforcement with a value 12.70363 MPa. It could be seen that the result followed the same trend with the result of flexural strength at peak.
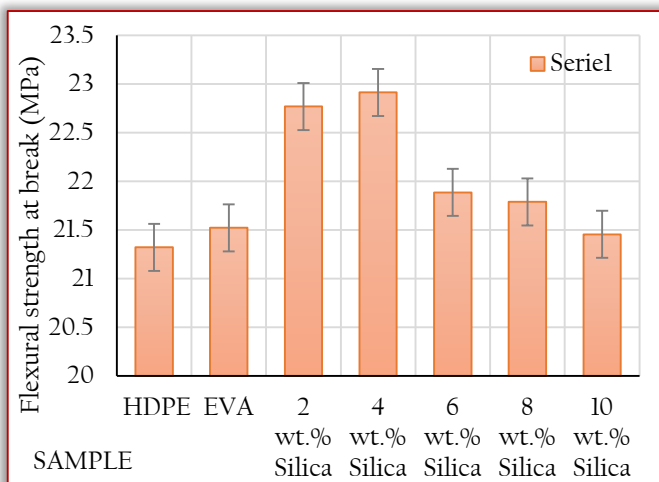
Figure 2: Variation of Flexural Strength at Break for HDPE, EVA and HDPE/Silica Composites
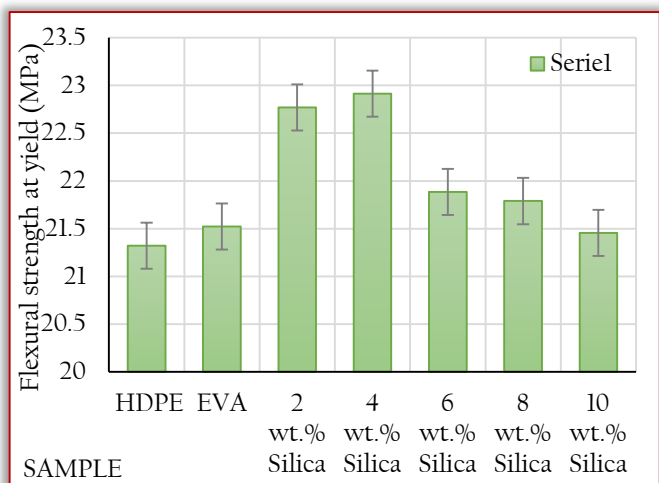
Figure 3: Variation of Flexural Strength at Yield for HDPE, EVA and HDPE/Silica Composites

Figure 3 shows the variation of the flexural strength at yield for HDPE/Silica composites. In this scenario, the flexural strength at yield of Neat HDPE and EVA are 21.10471 MPa and 21.234 MPa respectively. HDPE/Silica composite with 4 wt.% silica content have the highest flexural strength at yield with a value of 22.728 MPa followed by composite with 6wt.% silica content with a value of 21.688 MPa.
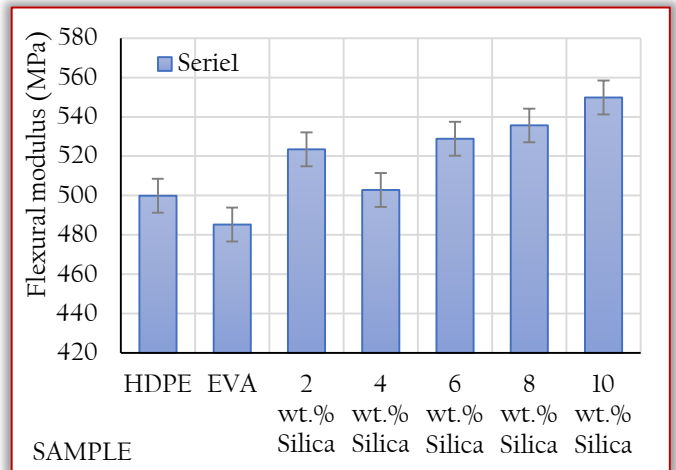
Figure 4: Variation of Flexural Modulus for HDPE, EVA and HDPE/Silica Composites

Figure 4 shows the variation of the flexural modulus of HDPE/silica composites. It is well known that the improvement in the modulus depends on the morphology of composites [16]. From the result, the addition of submicron silica particles significantly increases the flexural modulus of HDPE matrix. The flexural modulus of neat HDPE is 499.92 MPa while that of EVA is 485.2 MPa. As from 6 wt.% silica content, the flexural modulus of HDPE/silica composites increases linearly from 528.83 MPa to 549.9 MPa. The highest flexural modulus value is 549.9 MPa which is HDPE/silica composite with 10 wt.% silica content. The increase in the flexural modulus should be attributed to the rigid particles themselves.

── Water Absorption Behaviour

The water absorption plots of the composites with varied weight percent reinforcement are presented in Figures. 5-6. It was observed from Figure 5 that the water absorption by the composites increases with immersion time although the rate of absorption decreases with increased time. It is also observed that the water absorption attains equilibrium after 504 hour at which stage the composites have attained saturation point as far as water absorption is concerned. The amount of water absorbed by the composites, increase with the increase in the silica particles content. This may be due to the agglomeration of silica particles at higher particulate loading which led to cracks and formation of cavities at the matrix-particulate interface which allow transmission of water into the composite at higher particulate loading.

The percentage water absorption for Neat HDPE and EVA as shown in Figure 6 are 0.15% and 0.19% respectively; the results showed that less absorption took place in HDPE/silica composite with 2wt.% silica content with an average value of 0.16%

followed by composite with 4 wt.% silica content with a value of 0.17%.

Dhakal et al. [17] have reported that water absorption property of PMCs reinforced with natural fibres, particulate and their derivatives is dependent on the amount of the fibre/particulate, fibre orientation or degree of particles dispersion, immersion temperature, area of the exposed surface to water; also the permeability of fibres/particulate, void content, and hydrophilicity of the individual components (in this case silica and titania particles and HDPE matrix).

As a result of the re-known moisture resistance of silica, an improvement in the water absorption property of the composite developed was observed at lower particle loading (2-4 wt%), but as the particles weight fraction increases, the particles agglomerate, micro cracking of HDPE occurs particularly along the particle/matrix interface which gives room for further water penetration and swelling of the composite. Bismarck et al. [18] reported that the swelling stresses that develop under these circumstances can result in composite failure.
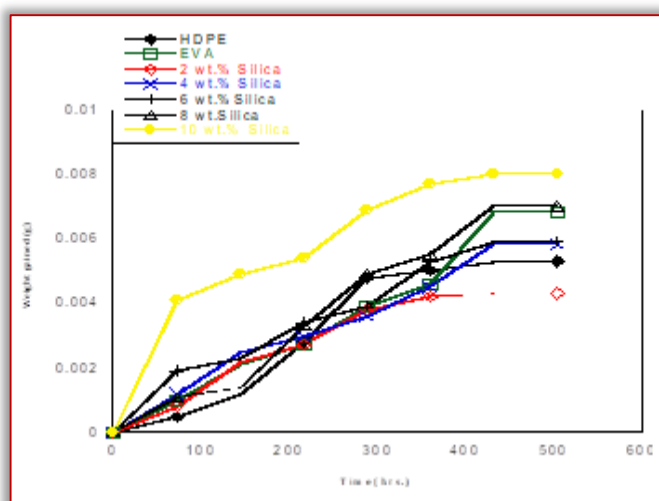
Figure 5: Water Absorption Curve for HDPE, EVA and HDPE/Silica Composites
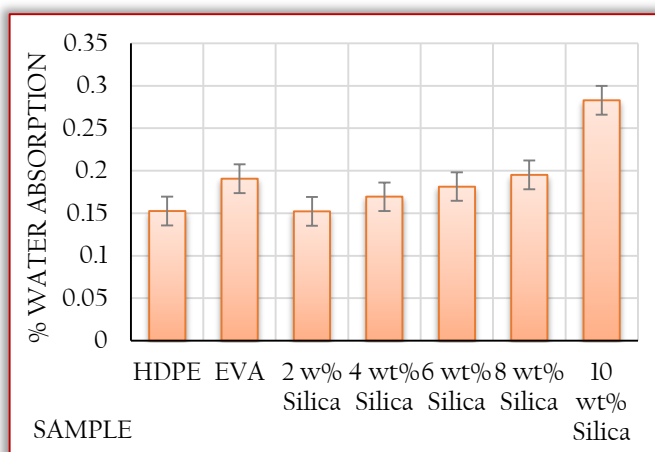
Figure 6: Variations of Percentage Water Absorption of HDPE, EVA and HDPE/Silica Composites

—— Water Diffusion Mechanism

The values of the slope n, from the plots of log (M_T/M_∞) versus log (T) presented in Figure 7 was used in establishing the water diffusion mechanism of the composites produced. The water diffusion behaviour of PMCs obeys Fick's diffusion theory and is reported to be dependent on the relative mobility of the penetrant (water molecules) and the polymer segment [17]. On the basis of the relative mobility of the penetrant and the polymer segments, three classes of diffusion can be distinguished. When the rate of diffusion of the penetrant (in this case water molecules) is much less than that of the polymer composite segment mobility, Fickian diffusion mechanism (Case I) is said to prevail. For this diffusion mechanism the value of n = 0.5 and independent of time, the equilibrium inside the polymer composite is rapidly reached and maintained [19]. For Case II, the value of n = 1.0 which indicates that the diffusion process is much faster than the relaxation process (Rdiff » Rrelax, system controlled by relaxation), this diffusion is characterized by the development of a boundary between the swollen outer part and the inner glassy core of the polymer. The boundary advances at a constant velocity, and the core diminishes in size until an equilibrium penetration concentration is reached in the whole polymer composite [20].

0.5<n<1.0 indicates non-Fickian (anomalous) diffusion mechanism, which describes those cases where the diffusion and relaxation rates are comparable (Rdiff ≈ Rrelax). In this case, an intermediate behavior between Fickian and non-Fickian diffusion will be observed [21].

Occasionally, values of n > 1 have been observed, which are regarded as Super Case II kinetics [22]. When the water penetration rate is much below the polymer chain relaxation rate, it is possible to record the n values below 0.5. This situation, which is classified also as Fickian diffusion, is called as 'Less Fickian' behavior [23]. These three cases of diffusion can be distinguished theoretically by the shape of the sorption curve [14] and on which basis the graph presented in Figure 7 was plotted. All types of water transport discussed above are presented in Table 1 for HDPE, EVA and HDPE/Silica composites with the coefficient, n and the intercept, k

Figure 7 shows the diffusion curve fittings of experimental data for 2 wt%, 4 wt%, 6 wt% , 8 wt% and 10 wt% silica reinforcements with constant 0.3 wt% titania for the developed composites. It was observed from Figure 7 that all the composites exhibited line graph shapes which are best fit by linear line graphs in agreement with equation 3. The values of the slope n and intercept k were calculated from the log plot, and presented in Table 1.

It can be clearly seen from Table 1 that the values of the diffusional exponent (n) range between 0.495 and 1.816. For the neat HDPE and EVA the diffusional coefficient (n) is greater than 1 (1.312 and 1.317) which indicates that the transport mechanism is Super Case II (relaxation controlled). Penetration of water molecules is much greater than the relaxation processes (the water penetration rate is much below the polymer chain relaxation rate).

The 'n' values for HDPE matrix composite with 2 wt.% silica reinforcement was found to be closed to 0.5(0.495), an indication that the rate of diffusion of the water molecules into the composites is much less than that of the polymer composite segment mobility. HDPE matrix composites with 4 wt. % silica particle reinforcement exhibited the intermediate behaviour

between Fickian and non-Fickian diffusion where the penetration mobility and the polymer segment relaxation are comparable. For other composites, the diffusion coefficients (n) are higher than 1.0 or approximately 1.0 which indicates that the transport mechanism is Super Case II or Case II (relaxation controlled). Penetration of water molecules is much greater than the relaxation processes. Generally, it is observed that the value of 'n' increases as the silica content of the polymer increases.
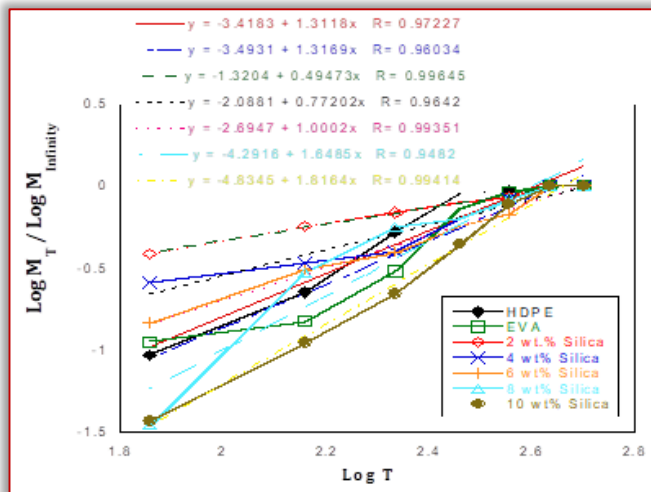
Figure 7: Diffusion Curve Fitting for Neat HDPE, EVA, and HDPE/Silica Composites

Table 1: Moisture Constants for the Composites

Sample designation	Slope (n)	Intercept (K)	R^2
Neat HDPE	1.312	3.418	0.972
EVA	1.317	3.493	0.960
2wt.% Silica	0.495	1.320	0.997
4wt.% Silica	0.772	2.088	0.964
6wt.% Silica	1.000	2.695	0.994
8wt.% Silica	1.649	4.292	0.948
10wt.% Silica	1.816	4.835	0.994

CONCLUSIONS

It has been found based on the studies carried out in this research that sub-micron silica particles could be successfully used as a reinforcing material in high density polyethylene-based composites.

The following conclusions are drawn from the present work:

— In the present study, it was observed that, HDPE matrix composite with 4 wt.% Silica content have the best fluxural strength with a value of 22.9134 MPa followed b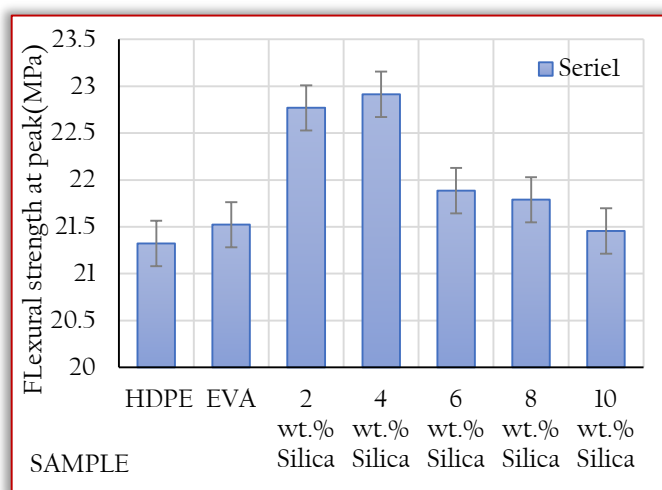y 2 wt.% Silica with a value of 22.7689 MPa. Although, the incorporation of submicron silica particles causes enhancement in flexural strength at peak of all the composites developed but it was discovered that the flexural strength increases with increase in silica content upto 4 wt.% and begin to decrease as from 6 wt%.

— The amount of water absorbed by the composites increases with the increase in the silica particles content. This is due to the agglomeration of silica particles at higher particulate loading which led to cracks and formation of cavities at the matrix-particulate interphase which allow transmission of water into the composite at higher particulate loading.

— The percentage water absorption for Neat HDPE and EVA are 0.15% and 0.19% respectively; the results showed that less absorption took place in HDPE matrix composite with 2 wt.% silica content with an average value of 0.16% followed by composite with 4 wt.% SiO_2 content with a value of 0.17%.

Acknowledgement

References

[1] Ahmed, S. and Jones, J.R., A Review of Particulate Reinforcement Theory for Polymer Composites, Journal of Materials Science, vol.25, pp.4933-4942, 1990.

[2] Zini, E. and Scandola, M., Green Composites: An Overview, Polymer Composite, vol. 32, pp.1905-1915, 2011.

[3] Ravichandran, R., Manoj, A.G., Liu, J., Manna, I. and Carrroll, D.L., A Novel Polymer Nanotube Composite for Photovoltaic Packaging Applications, Nanotechnology, vol. 19, pp. 1-5, 2008.

[4] Lee, B., Liu, J.U., Sun, B., Shen, C.Y. and Dai, G.C., Thermally Conductive and Electrically Insulating EVA Composite Encapsulants for Solar Photovoltaic (PV) Cell, Express Polymer Letters, vol. 2, no. 5, pp. 357-363, 2008.

[5] Prasad, R. and Pandey, M., Rice Husk Ash as a Renewable Source for the Production of Value Added Silica Gel and its Application: An Overview, Bulletin of Chemical Reaction Engineering and Catalysis, vol. 7, no. 1, pp. 1-25, 2012.

[6] Muller, A., Ghosa, M. Sonnenschein, R. and Woditsch, P., Silicon for Photovotaic Applications, Materials Science and Engineering, vol. 134, pp. 257-262, 2006.

[7] Kempe, M.D., Modelling of Rates of Moisture Ingress Into Photovoltaic Module, Solar Energy Materials and Solar Cells, vol. 90, pp. 2720-2738, 2006.

[8] Sarder, E.S., Production and Purification of Silicon by Magnesiothermic Reduction of Silica Fume, A Thesis Submitted in Conformity with the Requirements for the Degree of Master of Applied Science, Department of Materials Science and Engineering, University of Toronto, pp. 8-19, 2010.

[9] Daramola, O. O., Oladele I.O. and Adewuyi, B.O., Preparation of Submicron Silica Gel from Rice Husk Ash using Water Shaker Bath, Acta Technica Corvieniensis - Bulleting of Engineering, Tome Viii, Fascicule 3, pp. 61-64, 2015a.

[10] Daramola, O. O., Oladele I.O. and Adewuyi, B.O., Sadiku, R. and Agwuncha, S.C., Influence of Submicron Agro Waste Silica Particles and Vinyl Acetate on the Mechanical Properties of High Density Polyethylene Matrix Composites, The West Indian Journal of Engineering, vol. 38, no. 1, pp. 96-107, 2015b.

[11] Daramola, O. O., Oladele I.O. and Adewuyi, B.O., Sadiku, R. and Agwuncha, S.C., Structural and Morphological Properties of High Density Polyethylene Matrix Composites Reinforced With Submicron Agro Silica Particles and Titania Particles, Journal of Taibah University for Science, vol. 11, pp. 645-653, 2017.

[12] ASTM D790-15, Standard Test Methods for Flexural Properties of Unreinforced and Reinforced Plastics and Electrical Insulating Materials, ASTM International, West Conshohocken, PA, 2015.

[13] ASTM D570-10, Standard Test Method for Water Absorption of Plastics, ASTM International, West Conshohocken, PA, 2010.

[14] Sombastsompop, N. and Chaochanchaikul, K., Effect of Moisture Content on Mechanical Properties, Thermal and Structural Stability and Extruded Texture of Poly (vinyl chloride)/Wood Sawdust Composites, Polymer International, Issue 53, pp.1210 – 1218, 2004.

[15] Daramola, O.O., Akintayo, O.S., Adewole, T.A. and Talabi, H.K. Mechanical Properties and Water Absorption Behaviour of Polyester/Soil-Retted Banana Fibre(SBRF) Composites, International Journal of Engineering, Annals of Faculty of Engineering Hunedoara, Tome XV, Fascicule 1, pp.183-190, 2017.

[16] Jeziorska, R., Zielecka, M., Gutarowska, B. and Zakowska, Z., High-Density Polyethylene Composites Filled with Nanosilica Containing Immobilized Nanosilver or Nanocopper: Thermal, Mechanical, and Bactericidal Properties and Morphology and Interphase Characterization, International Journal of Polymer Science, Volume 2014, pp.1-13, 2014.

[17] Dhakal, H.N., Zhang Z.Y. and Richardson, M.O.W., Effect of Water Absorption on the Mechanical Properties of Hemp Fiber Reinforced Unsaturated Polyester Composites. Journal of Composite Science and Technology, issue 67, no. 7, pp. 1674 – 1683, 2007.

[18] Bismarck, A., Askargorta, I.A., Springer, J., Lampke, T., Wielage, B. and Stamboulis, A., Surface Characterization of Flax, Hemp and Cellulose Fibres; Surface Properties and the Water Uptake Behaviour, Polymer Composite, vol. 23, no. 5, pp. 872 – 894, 2002.

[19] Thwe, M. M. and Liao, K., Effects of Environmental Ageing on the Mechanical Properties of Bamboo-Glass Fiber Reinforced Polymer Matrix Hybrid Composites, Composites Part A, Issue 33, pp.43 – 52, 2002.

[20] Crank, J., The Mathematics of Diffusion, Clarendon Press, Oxford, 1975.

[21] Cárdenas, A., Argüelles Monal, W., Goycoolea, F.M., Higuera Ciapara, I. and Peniche, C., Diffusion Through Membranes of the Polyelectrolyte Complex of Chitosan and Alginate, Macromol Bioscience, Issue 3, pp. 535 – 539, 2003.

[22] Munday, D.L. and Cox, P.L., Compressed xanthan and karaya gum matrices: hydration, erosion and drug release mechanisms, International Journal of Pharmacy, Issue 203, pp. 179 – 192, 2002.

[23] Wang, J., Wu, W. and Lin, Z., Kinetics and thermodynamics of the water sorption of hydroxyethyl methacrylate/styrene copolymer hydrogels, Journal of Applied Polymer Science, Issue 109, pp. 3018 – 3023, 2008.

[1.]A.M. RAJESH, [2.]Mohamed KALEEMULLA, [3.]Saleemsab DODDAMANI, [4.]K.N. BHARATH

DEVELOPMENT AND CHARACTERIZATION OF HYBRID ALUMINUM METAL MATRIX COMPOSITES

[1.]Department of Mechanical Engineering, SJM Institute of Technology, Chitradurga, Karnataka, INDIA
[2.]Department of Studies in Mechanical Engineering, U B.D.T. College of Engineering, Karnataka, INDIA
[3.]Department of Mechanical Engineering, Jain Polytechnic, Davangere, Karnataka, INDIA
[4.]Department of Mechanical Engineering, GM Institute of Technology, Davangere, Karnataka, INDIA

Abstract: In the present investigations, the hardness test is conducted on Vickers' hardness tester at room temperature for both the age hardening and without age hardening conditions. Al7075 has chosen as the matrix material. HMMCs are produced utilizing stir casting route for enhancing the hardness number. The reinforcement used is silicon carbide with 5%,10%, &15% weight percentage and $Al2O_3$ as the another reinforcement in 5%,10%, &15% weight percentage. In the aluminum matrix microstructural characterization reveal the homogeneous mixing of reinforcements. The density of composite is incremented with the increase in weight fraction. The result reveals that the addition of silicon carbide and alumina particles in aluminum matrix improves the mechanical properties.
Keywords: Composites, SiC, Alumina, compression, Hardness with and without heat treatment

INTRODUCTION

MMCs comprise of an alloy or a metal as the matrix and a reinforcement such as the particles, short fibre or whisker and/or long fibre. MMCs were a group of material with perspective for a broad collection of applications in structural management. Their properties such as light in weight, superior strength and resistance to wear are the requirement for the aviation and automobile industries.

Most commonly used matrixes are magnesium, copper, titanium, and zinc. The most commonly used reinforcements are silicon carbide, alumina, boron, graphite and fly ash. The applications of these composites are primarily in aviation, vehicle engineering, marine and turbine compressor engineering. MMCs are also used for light weight as well as for high temperature applications. Discontinuously or particle reinforced MMCs have turned out to be extremely mainstream since they are more affordable than long fiber fortified composite and it has generally isotropic properties contrasted with fibre reinforced composite [1].

Discontinuously reinforced MMCs are much less expensive to fabricate than continuously reinforced composites. Consequently, performance enhancement of the matrix comes at lower additional costs with discontinuous reinforcements compared with aligned reinforcements. Particulate reinforced MMCs are not expensive to manufacture than reinforced composites. Accordingly, performance improvement of the matrix comes at lesser expenses with particulate reinforcements compared with fiber aligned reinforcements. In addition, particulate reinforced composites exhibit the isotropic properties [2], whereas the properties of composites with fiber aligned reinforcements are highly anisotropic. Thus, in applications requiring isotropic properties, less expensive, particulate reinforced composites can do better than fiber reinforced composites. Typically, ceramics and graphitic materials are used as reinforcement phases in particulate reinforced MMCs. Some common reinforcements for aluminium matrices are SiC, Al_2O_3, B_4C, and graphite [3].

Singla et al [4] developed aluminium alloy/ SiCp composites of varying weight fractions of silicon carbide (5–30%) by stir casting techniques using a two step–mixing method. Results showed that impact strength and hardness increased with an increment in weight percentage of silicon carbide.

G. B. V Kumar et.al [5] evaluated tensile strength, hardness and wear resistance characteristics of Al7075–Al_2O_3 and A6061–SiCp composite. The liquid metallurgy method has been utilized to fabricate the composites. The addition of reinforcements i.e. SiC and Al_2O_3, shows the improved mechanical properties such as resistance to wear, hardness and strength of the respective composites.

Komai et al [6] conducted the experimentation to determine the mechanical properties of Al7075–SiC composite. From the result, it is observed that the better mechanical properties of A7075–SiC whiskers composite have been obtained. Rupa Dasgupta et al [7] conducted experimentation to find the wear behavior and hardness of the A7075–SiC composite. From the outcomes, it is confirmed that the enhancement in hardness, wear resistance properties are obtained. This improvement in results is the contribution of heat treatment and formation of Al–Zn–Mg–Cu alloy composites by adding 15% by weight of SiC. Also, it has been revealed that improved properties are the results of the particle size of the Silicon Carbide (SiC) particles.

The enhanced hardness of the composite and base metal will be obtained through the heat treatment method which results in the reduction of wear rate [8]. On account of as–cast material, estimation of the constant of wear is larger than the heat treated material. The cracks will grow at the interface of the matrix and reinforcement, along with the wear process. Heat treated material demonstrate the resistance to wear [9]. Because of the higher ductility and strength of the aluminum matrix, the effectual stress connected on material surface along with the wear progression is less on account of the heat–treated alloys. This occurrence caused a reduction in the cracking propensity of the material surface when

contrasted with the as–cast alloy [8]. The heat treatment didn't drastically modify the morphology, but rather the matrix hardening by age hardening occurred, which prompted greater strength & hardness [9].

T6 thermal treatment condition was used to obtain the highest wear resistance. Studies indicate that the better hardening of the material was achieved when the composite was solutionized for 3 hours at 560℃, quenched at 0℃ in ice water and aged at 175℃ temperature for 07 hrs. Also it is reported that T6 heat–treatment for 07 hrs provides the great hardness to matrix and caused higher wear resistance in MMCs [10]. The yield strength and higher hardness of the material after this heat treatment condition may have the benefit of keeping generation of aluminium debris & reduction in its exchange to the steel surface [11]. After the aging at low temperature (b/n 50°–150℃), the resistance to wear of the materials is observed to be low. Peak aging conditions, at 2000C aging temperature, would increase the abrasion resistance of the composite and as well as the hardness.

In the background aluminium 7075 metal matrix hybrid composite composites have a wide range of scope for the research. Research has to be carried on the aluminium matrix composite reinforced with reinforced with silicon carbide and aluminum oxide in the area of wear in–order to enhance the strength and resistance to mechanical characteristics of the material.

MATERIALS AND PROCESSING

Al–7xxx alloys, for instance, 7075 are commonly used as a part of applications including transport, automobile, marine and also in aerospace, because of their high strength and low weight. The main constituents in the Al7075 are Si=0.4%, Zn = 6.1%, Mg=2.9%. The properties of the Al7075 are density = 2.85g/cc, ultimate strength = 480MPa, elastic modulus = 75GPa, Poissons' ratio = 0.33, melting point = 650^0C [12].

Silicon carbide is a ceramic material also known as carborundum, denoted as SiC. It is a blend of silicon and carbon. It is an outstanding abrasive material utilized to prepare grinding wheel and other abrasive parts. Now a day, the SiC material is formed into a technical grade better quality ceramic with excellent mechanical/physical properties. Some of the key properties of silicon carbide utilized here are Density – 3.1 g/cc, melting point – 2730^0c, molecular mass – 40.10 g/mol, grit size –16–100grit, Appearance –Black in color [13].

Aluminum oxide, commonly known as alumina (Al_2O_3) is corundum in its crystalline form is widely used in industry. The alumina (Al_2O_3) as a reinforcement [14] is steadier with aluminium and withstand higher temperatures. Some of the key properties of aluminum oxide utilized here are density=3.69g/cc, melting point – 2072^0C, mesh size=100–200 mesh, appearance – White in color.

Processing of Al7075–SiC/Al_2O_3 hybrid metal matrix composite is done by using stir casting technique. The procedure followed is displayed in Figure 1.

Density values of hybrid composites increases with increment in weight fractions of the reinforcement. The Density of both SiC and Al_2O_3 are higher than that of aluminum alloy therefore, an increment in the contents of reinforcements will increases the density of the composite. Similar results have been reported in the case of Al_2O_3 reinforced Aluminium composites, SiC reinforced Aluminium composites. Compared to the unreinforced alloy, SiCp and MoS2p contributed to a marginal increase (0.13– 2.7 %) in the density of hybrid composites by 36% and 64% respectively. The density of the Al7075–SiC/Al_2O_3 hybrid metal matrix composite is given in the table 1.
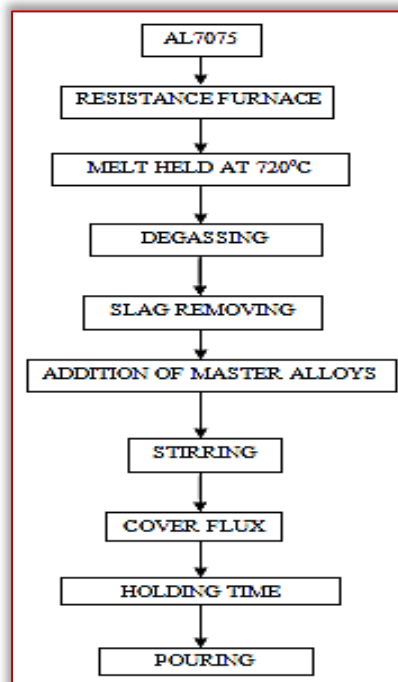
Figure 1: Activity chart of stir casting process

Table 1: Density test calculation

Material Composition	Mass gms	Volume cc	Density g/cc
R1–As cast (Al7075)	5.916	2.142	2.76
R2–Al7075+ 5%Al_2O_3+ 5% SiC	5.7255	2.091	2.73
R3–Al7075+ 10%Al_2O_3+ 10% SiC	6.213	2.256	2.754
R4–Al7075+ 15%Al_2O_3+ 15% SiC	5.9622	2.225	2.679

EXPERIMENTAL PROCEDURE

The Vickers' indentation hardness measurement technique comprises of diamond indenter used to indent the test specimen. The diamond indenters used is having square base with pyramid shape and a point of 136° in–between. Specimen material is subjected to applied load A by the indenter of somewhere in the range of 1gf to 100kgf. The load applied on the specimen through the indenter for 5 to 20 seconds. After removing the applied load, indentation applied on the specimen has been measured for both the diagonals on the surface utilizing a microscope and the average value has been considered. Diagonal area of slant surfaces is determined. The Vickers' hardness is the quotient gained by separating the kgf load by the square mm indentation area.

The term micro–hardness Vickers' indentation test generally uses Vickers diamond pyramid or the Knoop lengthened diamond pyramid to produce static indentations with the load not surpassing 1 kgf. The method for testing is fundamentally the same as that of the standard Vickers' hardness measurement, aside from that it is done on a microscopic scale with the high precision instrument. The surfaces to be indented usually required a metallographic machining. For lesser the load utilized, the higher the surface finish essentially.

SPECIMEN PREPARATIONS

Casting is done by varying the percentage reinforcement of alumina and silicon carbide that is 5, 10 and 15% with respect to the weight of Aluminium7075. The mould 1 size is 12mm in diameter and 100mm in length so as the casting that is taken out from the mould 1. Mould 2 is having 25mm in diameter and 100mm in length. The above said casting is machined to 10mm diameter and 35mm length for casting 1 and 25mm diameter and 1inch length for casting 2. These specimens are polished in a polishing machine for the greater surface finish. Figs 2 to 7 show the casting taken out from the mold and the machined specimens respectively.

Figure 2: Graphite Crucibles

Figure 3: Muffle furnace

Figure 4: Induction Furnace

Figure 5: Mould

Figure 6: Specimen

Figure 7: Specimen

The composite specimen is heat treated at a temperature of 465^0C for 02 hrs taken after by quickly quenched in cool water. After quenching the specimens, these are subjected to an age (precipitation hardening) by heat–treatment the specimens to 120^0C, maintaining this temperature for 05 hrs and after that taken after cooling in air to room temperature. Then follow the above procedure for hardness testing by using Vickers' hardness instrument.

EXPERIMENTAL RESULTS OF MICROHARDNESS

The below table shows the Vicker's hardness number for specimens of different percentages of reinforcements

Table 2: Vickers' hardness number for specimens

Specimen ID	Composition	Vickers Hardness Number
1	Al7075	106
2	Al7075 + 5%SiC + 5%Al$_2$O$_3$	114
3	Al7075 + 10%SiC + 10%Al$_2$O$_3$	116
4	Al7075 + 15%SiC + 15%Al$_2$O$_3$	109
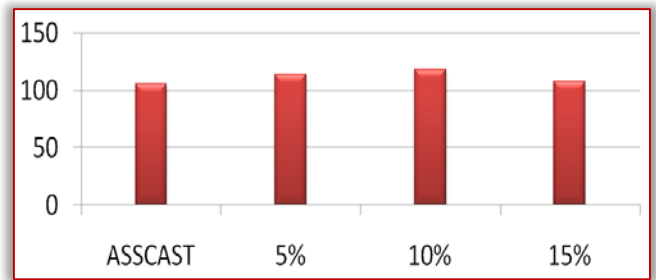
Figure 8: Graph plotted for Vicker's Hardness Number v/s Compositions of Specimens [without heat treatment]
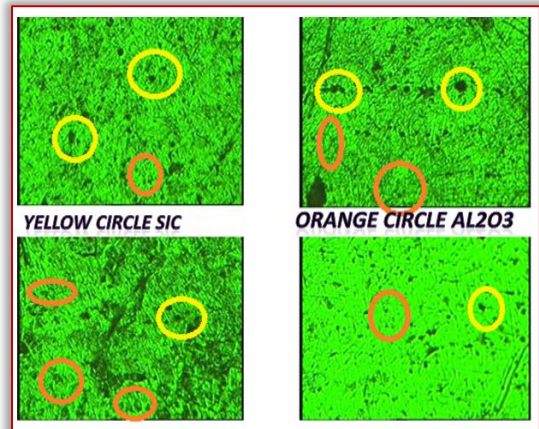
Figure 9: Vickers' Hardness test indentation photos
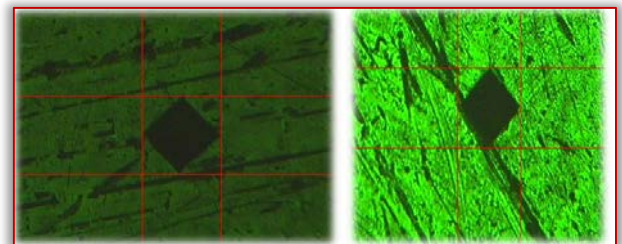
Figure 10: Vickers' Hardness test indentation photos [without heat treatment]

The below table shows the vickers' hardness number for specimens of different percentages of reinforcements on with heat treratment.
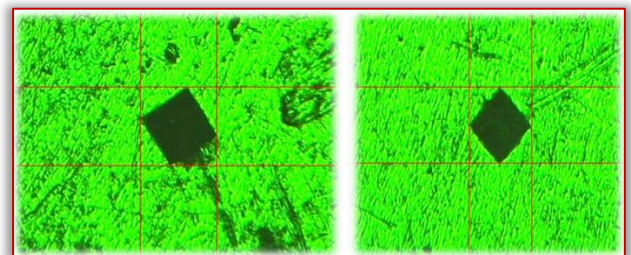
Figure 11: Vickers' Hardness test indentation photos [with heat treatment]

Table 3: Vickers' hardness number for specimens

Specimen ID	Composition	Vickers Hardness Number
1	Al7075	120
2	Al7075 + 5%SiC + 5%Al$_2$O$_3$	130
3	Al7075 + 10%SiC + 10%Al$_2$O$_3$	140
4	Al7075 + 15%SiC + 15%Al$_2$O$_3$	115
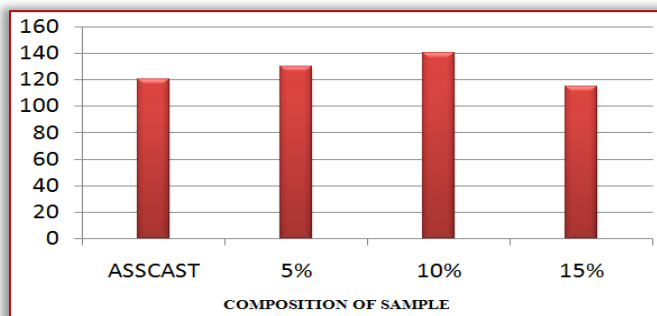
Figure 12: Graph plotted for Vicker's Hardness Number v/s Compositions of Specimens [with heat treatment]

The Fig 13 graph shows the effect of the addition of reinforcements on the composite hardness. The evidence is that as percentage of reinforcement is varied by weight, the hardness number of the composites increased monotonically and significantly from 106 to 116 VHN. It is also observed that the hybrid composite with 10% Sic 10% alumina shown good hardness property. It is reported that the addition of SiC+alumina to Aluminium7075 in metal–alloys lead to superior hardness number and strength.
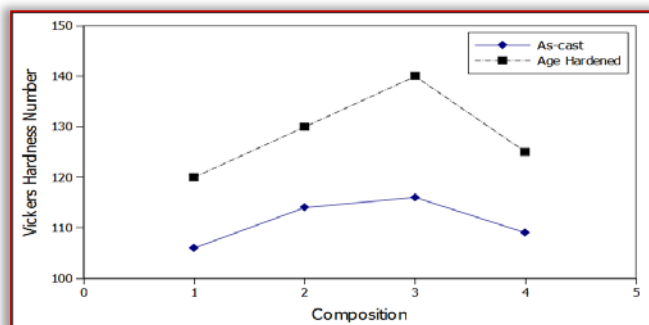
Figure 13: Graph plotted for Vicker's Hardness Number v/s Compositions of Specimens for as–cast and age hardened condition.

Micro–hardness of hybrid composites found incremented with raise in content of filler and enhance in hardness number of Al7075+Al$_2$O$_3$+Sic composites are in the range of 110–140VHN for with heat treatment.In T6 heat treated, aged HAMMCs the observed hardness was 120, 130, 140 AND 115 respectively for various wt% of Sic and alumina reinforcement in HAMMCs. It resulted in increase of 20 % of hardness in aged HAMMCs when compared with unaged heat treated HAMMCs. The highest hardness was noticed in composites for aged with 10%SiC+10%Al$_2$O$_3$ reinforcement. There is a gain in hardness of 20 % due to heat treatment in HAMMCs. In T6 heat treatment of HAMMCs, the thermal mismatching of matrix and reinforcement thermally promotes dislocation density improvement in dislocation densities outcome in advanced resistance to plastic deformation, led to better hardness.

CONCLUSION
From the experimental results, the following conclusions can be drawn. The incorporation of the SiC &Al$_2$O$_3$ constituents in the aluminum metal matrix as the reinforcement content increases the hardness of the material. For 10% reinforcement of SiC and Al$_2$O$_3$ to the Al7075 enhances the hardness for both without and with heat treatment. The percentage of enhancement of hardness is 22% with heat treatment compared to without heat treatment for 10% of addition of SiC and Al$_2$O$_3$ with Al7075.

References
[1] Jatitz, Whittenberger, J.D. 1990, in Solid State Powder Processing, ed. A.H.Clauer & J.J. deBarbadillo. The Minerals, Metals and Materials Society, Warrendale, PA, p.137.
[2] ASM Handbook, "Composites", ASM International, 21 (2001).
[3] D.M. Miller, Glass Fibers, Composites, Vol 1, 1987, Engineered Materials Handbook,ASM International, , p 45–48
[4] Singla, M, Dwivedi, DD, Singh, L, & Chawla, V. (2009). Development of aluminium based silicon carbide particulate metal matrix composite. Journal of Minerals & Materials Characterization & Engineering, 8(6), 455–467.
[5] Veeresh Kumar GB, Rao CSP, Selvaraj N, Bhagyashekar MS, "Studies on Al6061–SiC and Al7075–Al2O3 Metal Matrix Composites", J. Min. Mat. Char. & Eng. 2010, 9, 43 – 55.
[6] Komai K, Minoshima K, Ryoson H. Tensile and fatigue fracture behavior and water–environment effects in a SiC–whisker/7075–aluminum composite. Compos Sci Technol 1993; 46:59–66.
[7] Rupa Dasgupta and Humaira Meenai, "SiC particulate dispersed composites of an Al– Zn–Mg–Cu alloy: Property comparison with parent alloy", Materials Characterization, Volume 54, Issues 4–5, May 2005, Pages 438–445.
[8] S.Sawla, S Das "combined effect of reinforcement and heat treatment on the two body abrasive wear of aluminium alloy and aluminium particle composites",pp 555–561,2004.
[9] Vencl, A., Bobic, I., Arostegui, S., Bobicd, B., Marinkovic, A. and Babic, M. (2010) "Structural, mechanical and tribological properties of A356 aluminium alloy reinforced with Al2O3, SiC and SiC, graphite particles", Journal of Alloy and Compound, 506: 631–639.
[10] Gomes E.G. and Rossi, Sept 2001, Key Engg. Materials, Vol.189–191, pp. 496–502.
[11] N Singh, Shweta Goyal and Kishore Khanna, July 2010. "Effect of Thermal Ageing on Al Alloy Metal Matrix Composite", Department of Mechanical Engineering, M.E. Thesis, Thapar University, Patiala, India.
[12] Rajesh A M, Mohammed Kaleemulla, Experimental investigations on mechanical behavior of aluminium metal matrix composites, Materials Science and Engineering 149, 2016.
[13] Rajesh A M, Mohammed Kaleemulla, Experimental investigations on mechanical and wear behavior of hybrid aluminium alloy, IJERT, Volume: 05, Issue: 13, pp 128–131, Sep–2016.
[14] Rajesh A M, Mohammed Kaleemulla, Effect of heat treatment on hybrid aluminum metal matrix composites, International Journal of Emerging Research in Management &Technology, Volume–6, Issue–5, pp 548–551, 2017.

1.Nikola KANTOVÁ, 2.Michal HOLUBČÍK, 3.Alexander ČAJA, 4.Jozef JANDAČKA

OBSERVATION OF PARTICULATE MATTER VELOCITIES IN THE FLUE TRACT OF LOCAL HEAT SOURCE

1-4. University of Žilina, Faculty of Mechanical Engineering, Department of Power Engineering, Žilina, SLOVAKIA

Abstract: Presence of particulate matter (PM) in the atmosphere is a problem mainly in the winter time. PM are getting into atmosphere from combustion of solid fuels in heat sources. Their impact on people health is harmful, when we breathe them. Therefore, it is necessary for reduction these emissions in the atmosphere. This article investigates downfall velocities of particulate matter based on calculations and then it observes velocity simulation of particulate matter flowing through baffles placed in the flue tract of local heat source by using program Ansys. These baffles are usable for separation of particulate matter in the flue tract. When particles reach downfall velocity, forces which acting on them are in equilibrium and they would not get into atmosphere from the flue tract of heat source. CFD simulation in program Ansys allows us to observe velocity distribution in flue tract and compare it with calculated downfall velocity of these particles.
Keywords: particulate matter, local heat source, reduction emissions

INTRODUCTION

Residential combustion of solid fuels as well as biomass is considered to be a major source of particulate matter and hydrocarbons. Solid fuel contains more amount of inorganic ash forming elements. During combustion of wood, these inorganic elements such as alkali metals, chlorine, sulphur and some heavy metals are partly released to the gas phase, and they may cause deposition, high temperature corrosion, together with emission of harmful gases and particulate matter. Epidemiology studies have shown a clear correlation between the particle concentration in the air and severe health effects on human being [1]. Therefore, it is necessary for reduction these emissions in the atmosphere.

We can distinguish particulate matter into two main groups. PM10 is the coarse fraction, which contains the larger particles with a size ranging from 2.5 to 10 μm. PM2.5 is the fine fraction, which contains the smaller ones with a size up to 2.5 μm. The particles in the fine fraction which are smaller than 0.1 μm are called ultrafine particles. We also know particles with coarser fraction than PM10 [2].

This article as first investigates downfall velocities of particulate matter based on calculations. Downfall velocity is a velocity, when the forces acting on the particle are in equilibrium. These forces are gravitational, lift and resistance [3]. When particles reach downfall velocity, they would not get into atmosphere from the flue tract of heat source.

Then, it observes velocity simulation of particulate matter flowing through baffles placed in the flue tract of local heat source using by program Ansys. These baffles are usable for separation of particulate matter in the flue tract. CFD simulation in program Ansys allows us to observe velocity distribution in flue tract and compare it with calculated downfall velocity of these particles.

MATERIAL AND METHODS

For the calculation of particulate matter downfall velocity was considered shape of these particles as spherical. Equation for calculation of downfall velocity for laminar sedimentation area is:

$$u_P = \frac{d^2(\rho_\square - \rho)g}{18\mu} \qquad (1)$$

Equation for calculation of downfall velocity for turbulent sedimentation area is:

$$u_P = 1{,}74\sqrt{\frac{d(\rho_\square - \rho)g}{\rho}} \qquad (2)$$

For selection of sedimentation area, there is used equation:

$$C_D \, Re^2 = \frac{4}{3}\frac{d^3(\rho_\square - \rho)\rho g}{\mu^2} \qquad (3)$$

≡ for laminar sedimentation area: $C_D . Re^2 < 12 – 48$ with accuracy +/- 0.5 – 5 %

≡ for turbulent sedimentation area: $1.1 \cdot 10^5 < C_D . Re^2 > 4 \cdot 10^{10}$

There is possible to use iterative method for calculation of downfall velocity for transition sedimentation area [3, 4]. Based on the measurement of particle density, such as a ratio of their weight and volume, was considered density value of 2000 kg.m^{-3} during downfall velocity calculations.
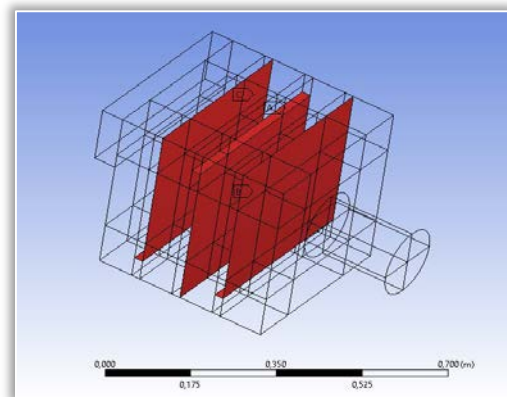
Figure 1: Used 3D model

For the observation of particulate matter velocities was used program Ansys. Particulate matter should be capturing on three baffles placed in the flue tract of local heat source. There was used 3D model with the same length of edge 400 mm, which is shown in the Figure 1. Escaped particles were getting into chimney with diameter 160 mm.

We created mesh with network of 194787 elements, which you can see in the Figure 2. All elements had aspect ratio lower than 10.
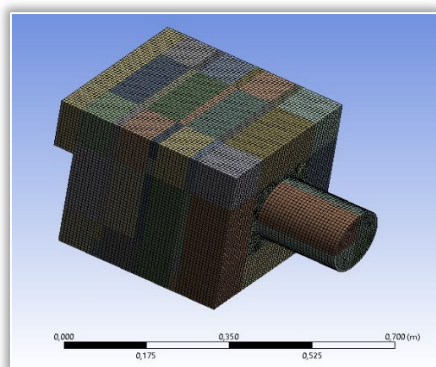
Figure 2: The mesh of 3D model

For the simulation was used k-ε model with standard wall function. The flowing of particles was realized using by a Lagrangian reference frame. Particles were considered spherical and also the influence of turbulence on particle motion. Flowing was time steady and a mass flow was 0.0168 kg.s^{-1} on an inlet place, without combustion with air density of 0.6 kg.m^3 and the influence of gravity was considered. There was used hybrid initialization and the calculation has converged.

RESULTS

Results of downfall velocity calculations are shown in the Table 1. It has been found that particles up to 50 μm settle in the laminar area. Particles in range from 50 to 950 μm settle in the transition area and particles over 950 μm settle in turbulent area. Downfall velocities during laminar sedimentation area have very small values, while velocities during turbulent sedimentation are significantly larger.

Table 1: Results of downfall velocity calculations

diameter [μm]	10	20	50	100	150
downfall velocity [m.s^{-1}]	0.007	0.029	0.181	0.487	0.939

Result of simulation of PM flowing through baffles is shown in the Figure 3. We can see velocity distribution in the 3D model and compare it with the downfall velocities. Maximum flow velocity in this model was 2.5 m.s^{-1}. This velocity is much higher than downfall velocities of particles.
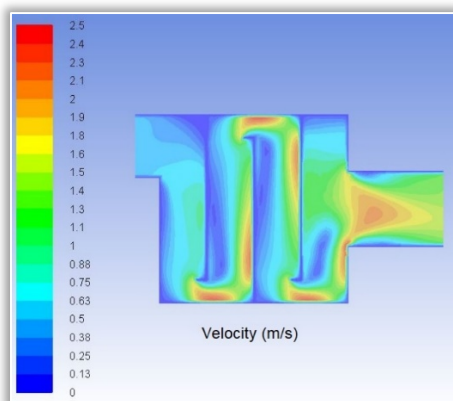
Figure 3: Velocity distribution in the 3D model

Particles achieve bigger velocities in a places of boundary walls after a transition of the baffle and also on the bottom parts of baffles. Smaller velocities are in a surrounding of first baffle place and on the upper parts of other baffles. It means that the smallest particles will escape in the flue gas stream and only larger particles will be capture.

CONCLUSION

Observation of particulate matter is important due their impact on our health. It is also important to try of reduction these emissions. This article investigates downfall velocities of particulate matter based on calculations and then it observes velocity simulation of particulate matter flowing through baffles placed in the flue tract of local heat source by using program Ansys. Calculated downfall velocities have very small values, while velocities in the 3D model are much higher. It means that the smallest particles will escape in the flue gas stream and only larger particles will be capture.

References

[1] K.G. NIGUSIE: Reduction of Fine Particle and Deposit Forming Alkali by Co-Combustion of Peat with Wood Pellets in 150 kWth Grate Firing Boiler Master´s thesis, online
[2] WHO: Health effects of particulate matter, Policy implications for countries in eastern Europe, Caucasus and central Asia. 2013
[3] GREEN, D. W., PERRY, R. H.: Perry's chemical engineers' handbook, 8th edition, United States of America, 2007
[4] KULKARI, P., BARON, P. A., WILLEKE, K.: Aerosol Measurement. Principles, Techniques and Applications, Third Edition, Printed in the United States of America, ISBN 987-0-470-38741-2, 2011

[1.]Mohamed Najeh LAKHOUA

METHODOLOGY OF ANALYSIS BASED ON A LEAN-MANAGEMENT

[1.] Research Unit Signals and Mechatronic Systems, National Engineering School of Carthage, ENICarthage, University of Carthage, TUNISIA

Abstract: In order to analysis the current state and to design a future state for the series of events that take a product or service from its beginning through to the customer with reduced lean wastes as compared to current map, we used a lean-management method. This project presents a work to eliminate waste in the production line in a pharmaceutical company. Then we used Value Stream Mapping (VSM) study followed by an analysis of causes and a plan of action carried out successfully enabled the company to optimize its production time.
Keywords: Value Stream Mapping, project management, improvement

INTRODUCTION

Pharmaceutical companies are facing competition. Indeed, the price differences between competing products can be such that it becomes difficult to compensate them by differences in value added. The conditions of competition are no longer homogeneous for the players involved. The price of a product is a given that puts a company and its customer face to face [1], [2].

However, price fixing obliges the company to consider internal factors relating to production costs and external factors such as customer attitudes, the existence of regulations and the structure of the market on which the firm evolved. In setting the selling price, the company must first take into account internal factors relating to its costs: costs of production fall into two categories, fixed costs and variable costs that depend on the quantities produced [3], [4].

The pharmaceutical company has decided to launch a new range "Brand Generics". One of the objectives of the launch of this range was the development of export and the presence of the pharmaceutical laboratory abroad. The problem inherent in this product range was the high cost of storage. This has led to an increase in delays and wastage of various resources such as working time and slower production rates. This provision increases handling costs and reduces labor productivity. These results in delayed orders that further disrupt the overall schedule. To overcome these limitations, it is necessary to identify bottlenecks at the workshop level (Figure1).
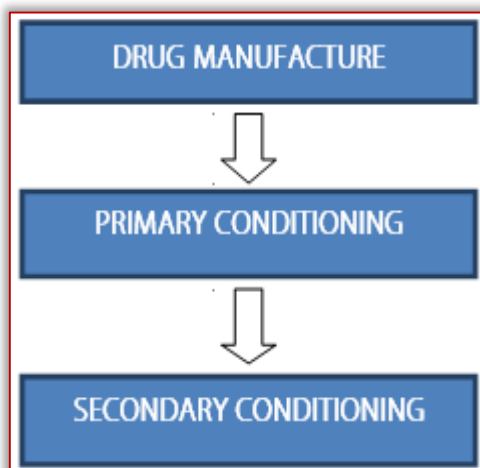
Figure 1- Flow diagram of the pharmaceutical company

The VSM tool is the ideal solution for this case of problem in order to locate the source of waste in the value stream by lean concepts and techniques to improve the performance of the current system. This paper presents the implementation of the Value Stream Mapping (VSM) project in a pharmaceutical company. It is structured as follows:

≡ determination of the family of products,
≡ drawing of the current state,
≡ drawing of the future state,
≡ action plan and implementation.

PRESENTITION OF THE VSM METHOD

Value Stream Mapping (VSM) is a lean-management method (Figure 2) for analyzing the current state and designing a future state for the series of events that take a product or service from its beginning through to the customer with reduced lean wastes as compared to current map. A value stream focuses on areas of a firm that add value to a product or service, whereas a value chain refers to all of the activities within a company [5].
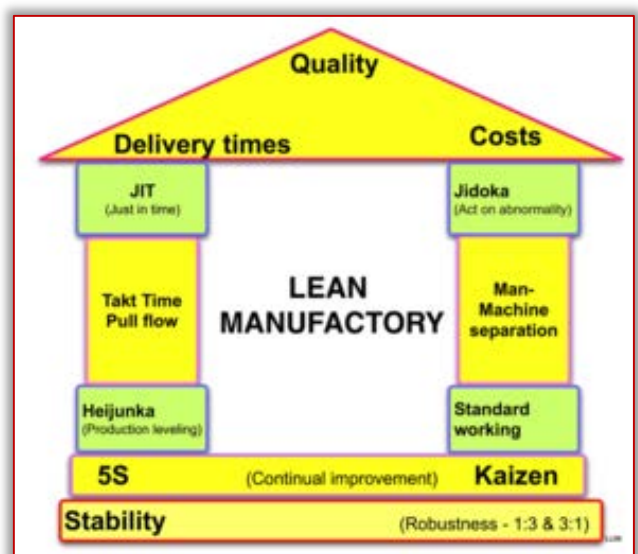
Figure 2- Modèle du système « Lean production » [6]

The purpose of value stream mapping is to identify and remove or reduce "waste" in value streams, thereby increasing the efficiency of a given value stream [6]. Waste removal is intended to increase productivity by creating leaner operations which in turn make waste and quality problems easier to identify.

Value Stream Maps are usually drawn using a set of standard symbols (Figure3) some of which can be seen here [7], [8].
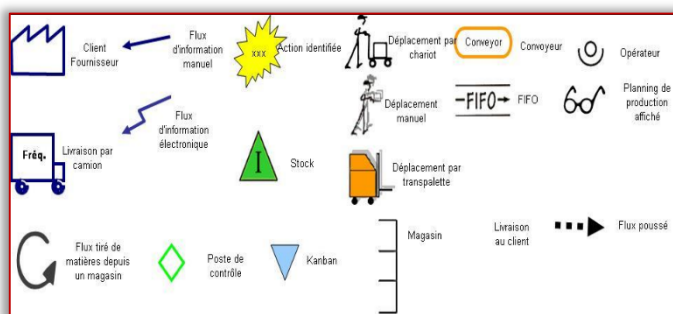
Figure 3- Symbols of the VSM method [6]

VSM has supporting methods that are often used in Lean environments to analyze and design flows at the system level (across multiple processes).

Although value-stream mapping is often associated with manufacturing, it is also used in logistics, supply chain, service related industries, healthcare, software development, product development, and administrative and office processes [9], [10]. VSM is a recognised method used as part of Six Sigma methodologies.

DETERMINATION OF THE PRODUCT FAMILY

For the case of this pharmaceutical company, the study will focus on a family of products that undergo the same treatments [11], [12], [13], [14], [15]. Then, we start this work in a one hand by a system analysis in order to describe the case study [16], [17], [18] and on the hand we develop any applications in this company [19], [20], [21].

— Application of ABC method

The ABC method proposes to distinguish three classes A, B and C which are distributed as follows:- (1) Class A: elements representing 80% of observed effect ; (2) Class B: items representing the following 15%; (3) Class C: the elements representing the remaining 5%.

In the case of researching the family of products to be studied, the observed effect will be sales and the items will be Products of the enterprise. Once the classification is established, the choice will be made among the products of Class A. If there are too many products in the A-Class, then a second selection may become necessary. To do this, it is advisable to draw up a table summarizing which equipment is used for the different products of class A. This amounts to creating a matrix products / equipments composed of "0" and "1".

This type of matrix sometimes reveals obviously the product families. It will be able to be reorganized thanks to a mathematical tool: the Analysis in Principal Components (PCA) in order to group the close products in terms of use of equipment.

— Application of PCA

The method Principal Component Analysis (PCA) is based on the calculation of the correlation coefficients between the series of values of two variables in order to determine whether they are dependent on each other. To do this, it is necessary to calculate the variance of each series (the value that characterizes the dispersion of a distribution) and the covariance between the two series (a value that characterizes the dispersion of one distribution over another).

— Drawing of the current state

In order to develop a reworked map of the value chain of a product or a family of products, one must first know the current situation. This part is devoted to the drawing of the VSM card in its current version.

First Phase of Design: The Customer

The VSM is part of a chain-of-value improvement approach. This implies a clear definition of the value of the product (s), in the eyes of the customer.

Second phase of the drawing: Manufacturing Processes

Then, the two icons used in the VSM are the manufacturing processes, also called Case Processes, and Stocks. Process boxes represent operations where the raw material is processed. In order to limit their number on the drawing, the connected steps or the workstations belonging to a single process are represented by a single icon. On the other hand, if an operation is cut off from the next (geographically or temporally) and intermediate stocks accumulate between the two or are moved in batches, then two process boxes are needed. This differentiation also depends on the purpose of the study, if the objective is to understand in detail an operation, then it will be necessary to use a process box for each of its steps. Placed end to end, the process boxes constitute the material flow, which is placed in the lower half of the design of the VSM, from left to right in the direction of the treatment of the materials and not according to the physical layout of the places.

Third phase of the drawing: Suppliers

After focusing on the customer and then on the manufacturing process, the third step concerns suppliers. The representation of the frequency and mode of delivery is the intermediary between the supplier (s) and the first step of the process, as well as between the last step and the customer(s). A wide arrow indicates a delivery between two factories, and a truck (or an aircraft, a boat...) which mode of delivery is used.

Fourth Drawing Phase: Information Flows

At this stage of construction of the VSM card, only material flows have been drawn. The fourth phase aims to represent information flows. To do this, we need to introduce new icons essential to the understanding of the drawing: a straight line represents a flow of physical information (on paper in general), while the lightning corresponds to an electronic information flow. A frame placed in the middle of an information flow is used to describe this flow (giving an exchange frequency for example). There is another type of connection that it is important to characterize: the movement of materials between the manufacturing processes.

MAPPING THE VALUE CHAIN

The mapping of the current state is now complete. This application, based on the example of a pharmaceutical company, has aroused a number of questions and observations concerning the areas of overproduction. The work carried out until now will have been in vain if the map of the current state is not analyzed and reworked, in order to construct the drawing of the future state.

The third part of the VSM approach is a transition stage: its purpose is to analyze the current state in order to reflect on the

future state. To do this, a new mode of operation of the production of products called production at the right.

This pharmaceutical company works with 2 teams that each work 8 hours a day (with 30 minutes of break). The customer request is 600 rings per day. The Takt Time of the production activity of this example is 90 seconds. This is tantamount to saying that if the company wants to respond to customer demand, hardware must exit its production line every 90 seconds.

This implies that the cycle times of each manufacturing process correspond to the Takt Time, or at least do not exceed it. This adaptation of production requires: 1) an effective response to functional problems leading to systematic delays; 2) the elimination of causes of unexpected stoppages (breakdowns, non-conformities, etc.); 3) redefining the manufacturing steps.

In the drawing of the future state, if a continuous flow is established between two processes, then their execution times will accumulate and the two process boxes will merge to form only one. But be careful, in accordance with Foundation # 1, the overall cycle time must be less than the Takt Time. The entire value chain must not necessarily be in continuous flow. When situations such as those described above arise, there are two alternatives: flow drawn with storage depots or the FIFO corridor. By definition, if a continuous flow is unthinkable, this implies that two discontinuous streams are kept at some point in the value chain. The link between these two processes can be managed through storage depots. In order to avoid recreating a situation of overproduction and product accumulation in stocks, it is preferable to control the process downstream rather than attempting to schedule production with estimates of customer needs.

The last part is devoted to the redesign of the VSM card. This phase of representing the future state of the value chain enters the Improve stage of the DMAIC process. The objective of Lean Manufacturing is to identify and eliminate sources of non-value added. Some waste is linked to the technology used, the plant layout in the plant, or the design of the products. These themes are not explored in the drawing of the future state, but they can be studied further by other tools than the VSM.

Staring from this analysis discussed in this paper, work is in progress to develop a novel strategy for system analysis for similar real cases [22], [23], [24], [25]

CONCLUSIONS

In this paper, we presented a work to eliminate waste in the production line in a pharmaceutical company. This work is based on a VSM study followed by an analysis of causes and a plan of action carried out successfully enabled the company to optimize its production time.

Thanks to the reorganizations carried out, Lead Time increased from 65.3 days to 12.2 days. The difference between the two comes from stocks that have been reduced or eliminated. The ratio of processing time on Lead Time was 1.5%, it was multiplied by more than five and is now 8.2%.

Then this work showed how the VSM tool is the ideal solution for this case of problem in order to locate the source of waste in the value stream by lean concepts and techniques to improve the performance of the current system.

References
[1] Kumar A. and Gureja L., Transformation of an Organisation into a Lean Organisation through Value Streem Mapping A case study, 2016.
[2] Hohmann C., Value Stream Mapping, Cartographie de la valeur, 1998.
[3] Rother M. and Shook J., Learning to See, value stream mapping to add value and eliminate muda, The Lean Enterprise Institute, 1998.
[4] Husson F., Lê S. and Pagès J., Analyse des données avec R, Presses Universitaires de Rennes, 2009.
[5] Drew J., McCallum B. and Roggenhofer S., Objectif Lean : réussir l'entreprise au plus juste, Eyrolles - Éditions d'Organisation, Paris, 2004.
[6] Benson B. and Hoshin K., The fundamental starting point for lean success. Cost Management, 2016.
[7] Mitchell A. and Millstein S., Takt Time Grouping: implementing kanban-flow manufacturing in an unbalanced, high variation cycle-time process with moving constraints, 2014.
[8] Bernier V. and Frein Y., Local scheduling problems submitted to global FIFO processing constraints, 2007.
[9] Zhen He, Xu-Tao Z. and Min Z., Reducing the voluntary turnover rate of dispatched employees by the DMAIC process, 2014.
[10] Hohmann C., Value Stream Mapping, Cartographie de la valeur, 1998
[11] Rother M. and Shook J., Learning to See, value stream mapping to add value and eliminate muda, The Lean Enterprise Institute, 1998.
[12] Holweg, M., The genealogy of lean production. Journal of Operations Management, 1990.
[13] Krafcik J. F., Triumph of the lean production system. Sloan Management Review. 1988.
[14] Ruffa S. A., Going Lean: How the Best Companies Apply Lean Manufacturing Principles to Shatter Uncertainty, Drive Innovation, and Maximize Profits, 2008.
[15] Lakhoua M.N., Systemic analysis of an industrial system: case study of a grain silo, Arabian Journal for Science and Engineering, Springer Publishing, 2013, Vol.38, pp.1243–1254.
[16] Lakhoua M.N., Investigation on the application of systemic analysis of the cereals stock mobility process, International Journal of Applied Systemic Studies, Inderscience, Vol.4, N°4, 2012, pp. 227-238.
[17] Lakhoua M.N., Systemic Analysis of a Wind Power Station in Tunisia, Journal of Electrical and Electronics Engineering, University of Oradea Publisher, vol.4, N°1, 2011.
[18] Beyaa R. and Majri H., Automatisation d'une ligne de production: étude de la situation existante, situation projetée, Master, ENICarthage, 2016.
[19] Meddeb D. and Achour M., Optimisation des temps d'occupation machine, Licence Appliquée, ENICarthage, 2014.
[20] Mokni A. and Matheli M., Amélioration de la capacité de d'une ligne de production, Licence Appliquée, ENICarthage, 2014.
[21] Lakhoua M.N. and Khanchel F., Overview of the methods of modeling and analyzing for the medical framework, Scientific Research and Essays, Academic Journals, ISSN: 1992-2248, Vol.

6(19), pp. 3942-3948, 2011.

[22] Lakhoua M.N, The need for systemic analysis and design methodology of the medical equipments, International Journal of Applied Systemic Studies, Inderscience, Vol.8, N°1, 2018.

[23] Lakhoua M.N., Jabri I, Battikh T, Maalej L and Mlouhi Y, Study on the use of Systemic Analysis and Image Processing Techniques in a Sports Meeting, European Journal of Scientific Research, 2015, Vol.132, N°1, 2015.

[24] Lakhoua M.N., Systemic analysis of a supervisory control and data acquisition system", Journal of Electrical Engineering, Politechnica Publishing House, vol.11, N°1, 2011.

[1.]Vasile ALEXA

TESTING OF AUTOMOTIVE INDUSTRY PRODUCTS USING MECHATRONIC SYSTEMS

[1.]University Politehnica Timisoara, Faculty of Engineering Hunedoara, Department of Engineering & Management, ROMANIA

Abstract: Higher quality requirements in the automotive industry, more and fiercer competition on the automotive market, and growing consumer demands, require the implementation of new testing and product quality testing methods. Another requirement is to increase working productivity by outsourcing to companies specialized in the automotive industry. Work productivity combined with increasing product quality is possible by automating assembly lines and implementing additional test and verification station. Automated testing and verification systems, being very complex, have combined mechatronic elements, enabling manufacturers to implement and adopt quality systems imposed by the beneficiaries. This paper describes a test algorithm on the assembly line of the car seat belt.
Keywords: mechatronic, pneumatic, seat belt, quality, FluidSim

INTRODUCTION

Under the conditions of increasing competition, the market has necessitated the development of systems that produce on the principle of production in flux, but in the conditions of serial production, i.e. of integrated systems of production organization. They meet under different names, such as [1]:

— linear programming;
— PERT method;
— CPM method (critical path method);
— "Just in Time" method (J.I.T.).

Pneumatic actuators are represented in the technical documentation by schemes. At the same time, the pneumatic actuators are made up of one or more pneumatic circuits, each of which fulfills a certain functional role in the scheme. The large number of possible functions distinguishes some elementary functions that are encountered in most of the current pneumatic drives used [2].

Mechatronics is the result of natural evolution in technological development. The scientific progress of electronics, informatics and mechanics and their synergistic and systematic combination led to the emergence of mechatronics.

Being a real-time combination of electronics, informatics and mechanics, it has quickly become applicable in real life, industry, and preponderantly in the Automotive industry, forcing major manufacturers to reorganize their technological flows. With the emergence of mechatronics there have also been developed programs for the design and simulation of technological flows.

PNEUMOTRONIC SYSTEM DESIGN AND SIMULATION, USING FLUIDSIM

In the present paper, the FluidSim program showed how to model and simulate a pneutronic verification system (quality and safety) of the belt head assembly.

In the technological belts testing process, the testing systems were reorganized using pneutronic systems. By introducing pneumatic systems, manufacturers have sought to reduce test times, costs, and ensure that headband belt assembly testing is functional and that only the functional parts leave the test area after the test process.

The figures below show the sketch of the experimental seat belt test stand as well as the functional diagram made in the FluidSim program [2].

FluidSim is a program for the design and simulation of pneutronic systems. This program can be used to perform experiments, produce real-time simulations and can be used as a virtual system control modulator.

As we can see in the figures below, everything started from a sketch showing the headband belt test. Pneutronic system must perform four basic operations, figure 1.
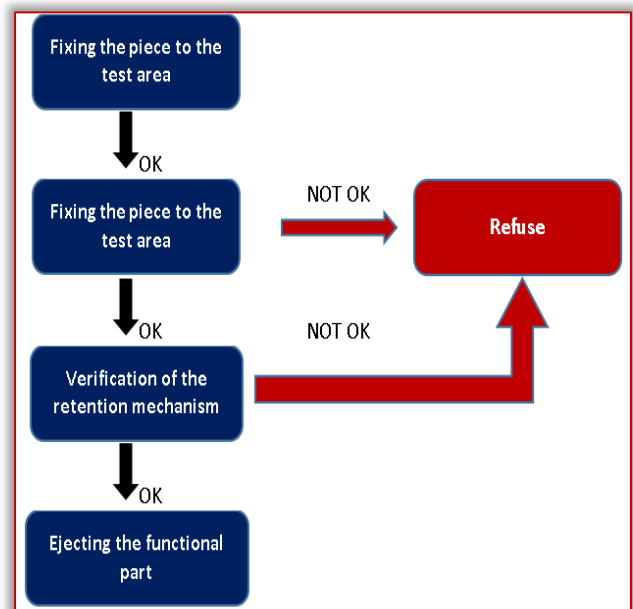
Figure 1. The operating algorithm of the mechatronic test system

In the first operation, the piece is fastened to the test area, followed by the belt release button check.

Testing the button is done to verify its functionality, being the first step in testing the mechanism. If the button is not working, the test process stops, and the piece has to be removed and taken to refuse. If the button is functional, continue the test process by testing the

belt tensioner mechanism. In this test phase, check the belt-to-belt retaining twice. If the mechanism is not functional then the piece is passed to the refuse, the piece remains in the test area and if the piece is functional, the process continues, this being the fourth operation, the piece is taken out of the test area.

We used four, 5/2 way valves, one 2/2 way valve, 3, pneumatic cylinders a one-way rod (button, tongue and release), and 1 pneumatic cylinder double-action and double-barrel, a grease filter, an air filter, two pressure gauges and a drosel, figure 2 [3,4].
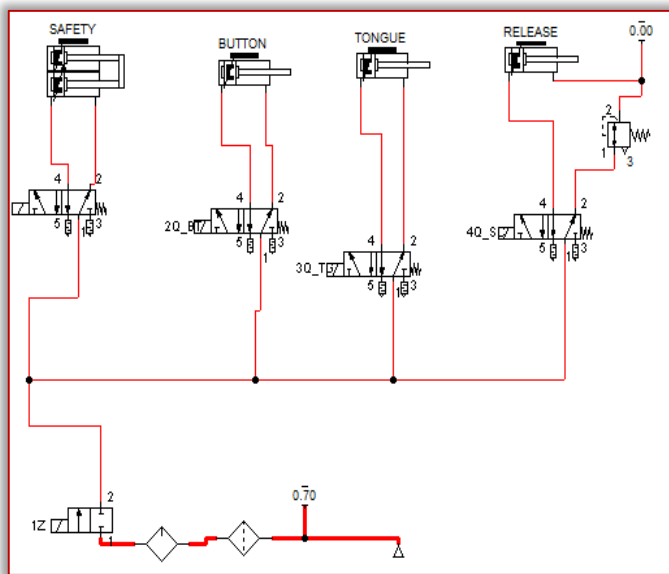
Figure 2. Pneumatic test bench system [4]

Simulation of the pneumatic system of Figure 2 was made using a logic element and coils connected to each other at 24V and 0V and actuated by a button as shown in Figure 3.
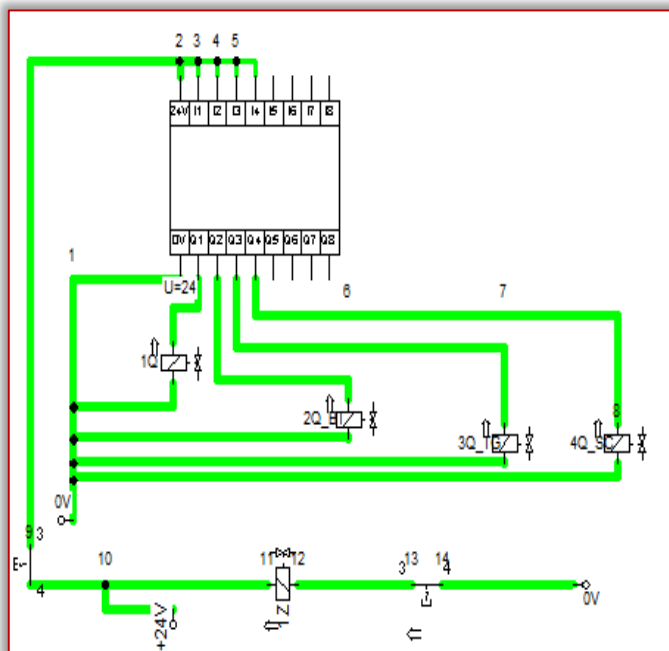
Figure 3. Electrical system of the test stands [4]

For the electrical system to work inside the logic element we used 4 pulse generators and 4 time delayers as in Figure 4.
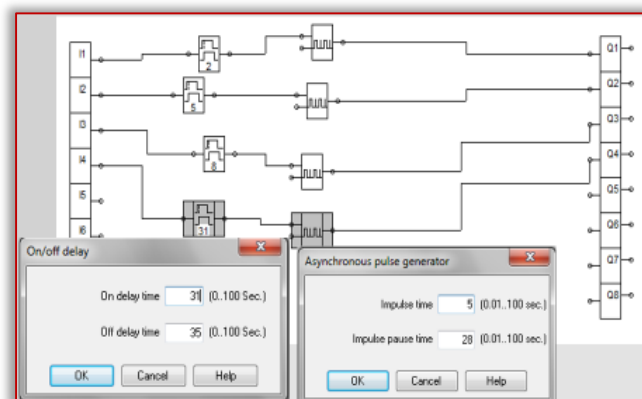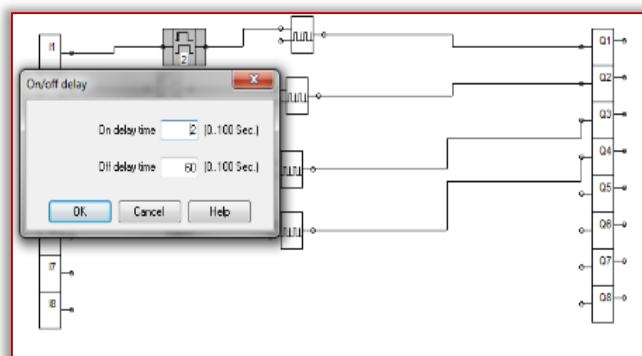
Figure 4. Impulse and time delay generators [4]
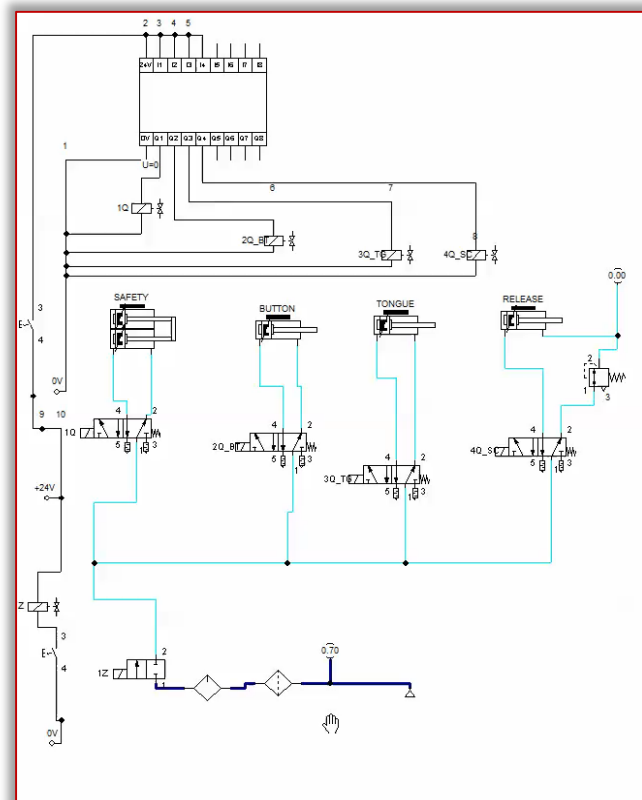
Figure 5. The mechatronic system for the test stands [4]

CONCLUDING REMARKS

For more than 20 years, FluidSIM® has been the world's leading circuit diagram design and simulation program for pneumatics, hydraulics, and now also for electrical engineering. Being able to freely design control systems is motivating, and promotes creativity and focus.

Whether in a training environment or in an engineering office, the simulation of control systems and processes has long been standard in industry, helping to minimize losses due to crashes and ensuring greater efficiency and improved quality. Pneumatics, hydraulics, electrical engineering: the libraries are available separately or together in the same program. The user decides which of the libraries to use in the program. All technologies interact optimally in a circuit diagram or project.

The simulation and design of the mechatronic system with the dedicated FluidSim software has a number of advantages, such as:

— less time and cost for simulation and design;
— real-time visualization of the order and action of the mechatronic system elements (figure 5);
— the possibility of changing the energetic and temporal parameters of the proposed mechatronic system;
— increasing labor productivity and product quality by eliminating the human factor.

References

[1]   Gania I.P., Stachowiak A., Oleśków-Szłapka J.(2017), Flexible manufacturing systems: Industry 4.0 solution, 24th International Conference on Production Research (ICPR 2017) ISBN: 978-1-60595-507-0, Poland
[2]   Alexa V, Raţiu SA, Birtok Băneasă C (2011) Logical pneumatics function simulated, using FluidSim penumatics software, a XI-a Conferinţă internaţională multidisciplinară, Profesorul Dorin Pavel, fondatorul hidroenergeticii româneşti, Sebeş, România
[3]   * * * www.festo.com
[4]   * * * Art System-Fluidsim 4 User Guide;
[5]   https://www.festo-didactic.com/

Fascicule 3
⸢ April - June ⸥
t o m e
⸢2019⸥ XII

ACTA Technica CORVINIENSIS
BULLETIN OF ENGINEERING

ACTA
TECHNICA
CORVINIENSIS
BULLETIN OF
ENGINEERING

ISSN: 2067-3809

[1.]Attila BARCZI, [1.]Dániel SZALAI, [2.]Valeria NAGY

THOUGHTS ON ENVIRONMENTAL MENTORING

[1.]Szent István University, Faculty of Agriculture and Environmental Sciences,
Department of Nature Conservation and Landscape Ecology, Gödöllő, HUNGARY
[2.]University of Szeged, Faculty of Engineering, Department of Technology, Szeged, HUNGARY

Abstract: This paper attempts to overview the possibilities of environmental mentoring. Nowadays, sustainability (or rather sustainable survival) has a decisive role. In essence, then, it is needed new knowledge and technologies. However, in addition to developing theoretical approaches, a full analysis of reality and practice is also challenge: it is necessary to think together about science and practice. There is no progress without it. It is also worth reflecting on how each discipline relates to all the others while discovering some complex problems. In the field of sustainability, with respect to (technological) innovation and environmental elements (and landscape issues), one of the key links is energetics, especially the challenges (environmental, technological and social) of renewable energy system. With a holistic view, but in a non-exhaustive may, we organized the relevant bits of thought on a "cognitive map" and designated the path to dynamic balance in the form of a few "actions", this way is pointing out the necessary symbiosis between humanity and nature. We have no absolute basis or an unquestioned principle, but we do have engineering work, saturated with the holistic approach mentioned above. Thus, this paper is primarily a thought-provoking, speculative writing, rather than an assertive one.
Keywords: sustainability, interdisciplinary, energy, innovation, environment, landscape, environmental mentoring

INTRODUCTION

We have chosen László Vekerdi's enduring words "Man is a thinking reed" to be the epitaph for this publication because it is man's marvelous ability – human thinking – that enables him to create (new) products, services and technologies which (may) facilitate so many people's everyday life in so many ways. In this manner of thinking, the role of universities as communities of teachers and disciples (or, to put it in a more "modern" way, places where the integration of RDIE (research-development-innovation-education) may occur), is indisputable. This also holds true for the role of engineers (especially those with a system- and process-oriented mindset), in as much they create balance between tradition and globalization.

The English word engineer is related to Latin ingenium, meaning "ability, inborn character", which suggests an innate ability for innovativeness. Just consider the Polish animated series Enchanted Pencil (Zaczarowany ołówek), the protagonist of which is a resourceful young boy, who solves every problem by using an enchanted pencil to draw objects which materialize in the episodes. It is his exceptional ability of thinking and observation that enables him to create new (technological) inventions, while it is his resourcefulness and creativity that allows proper utilization, hence amalgamating invention with innovation.

Doubtlessly, we now live in the era of Industry 4.0, but the philosophy of Industry 5.0 (the symbiosis of man and machine) is already around the corner, according to which a (more) efficient cooperation between humans and robots results in the culture of innovation. In other words, Industry 5.0 combines the benefits of human intelligence and cognitive IT to enhance efficiency (considering, of course, its impact on social aspects, as well (Davidson – Gross 2018)). Note here that social development is lagging (far) behind technological development, although, apart from system-oriented research, development and manufacturing, the support of society is also equally important as the 16th key task of sustainable development.

It is now also a fact that in addition to the communication differences between generations, the different values of the different generations are also more and more prominent, which manifests itself in different social expectations, created needs and accelerated lifestyles, requiring a constantly renewing, adaptive thinking, all of which directly or indirectly affect sustainability (including the measurable indicators of sustainability).

It would also have to manage demand to reasonable and sustainable levels, as has been extensively analysed and debated (Wynne 2011; Owen et al. 2013; Székács A. 2017). Therefore, this short publication attempts to demonstrate – enhancing the aspect the environment – the "actions and reactions" between energetics, the innovations of the energy industry and the surrounding environment on one hand, and the landscape on the other hand. The main roles of this paper are to help spreading the practice of environmental mentoring and to help softening energy transition challenges and worries, to shape the energy future, to raise creating action oriented innovative social, to promote common thinking. Because assessing past trends and future outlooks result responsible innovation.
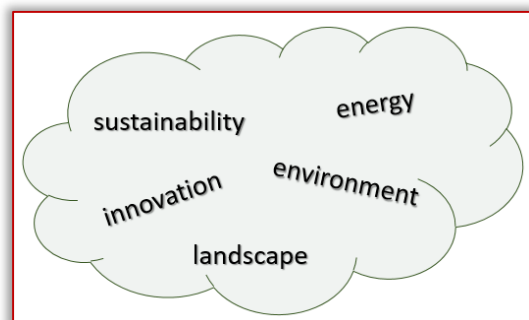
Figure 1: "Key words"

The Figure 1 presents the five most important words of this topic: sustainability, energy, innovation, environment, landscape. All five words can be found in 240,000 documents of Google Scholar system. This means that in an international context researchers/scientists (engineers, economists, managers, etc.) are dealing with social challenges extensively.

SUSTAINABILITY – THE CONCEPT OF HARMONY

The holistic approach of energetics and the multidimensional, interdisciplinary way of thinking has a great potential to promote sustainability in the symbiosis of human activity and nature. There is no absolute basis or principle, but there exists the aforementioned engineering activity inspired by the holistic approach, that is, the ability to explore and analyze "problems" that require a complex attitude (note here that this is a rather lengthy process).

A perfect example of this can be to solve a problem by generating another problem that (already) has a (technical) solution, or it is the indirect approach to the particular problem that may lead to a solution. Specifically, in the field of energetics, the reduction of the (economically exploitable) amount of carbon could be mentioned as an example, which can be partially eliminated by the direct burning of biomass, but this solution cannot be considered carbon neutral. However, by separating and utilizing the carbon dioxide content of the emitted flue gas, we may arrive at an innovative solution. Energy transfer depends on the acceleration of the technological development and open-minded and constructive social dialogue.

The above example well illustrates the importance of scientific creativity in the field of design, manufacturing, operation, use and application from the aspect of environmental sustainability. In this way technologies that are not mature enough or lack substantial social acceptance will never become long-term solutions and will function only temporarily.

In this context, the main goals and targets of sustainable development include:
— Ensure access to affordable, reliable, sustainable and modern energy for all (Goal 7)
— foster innovation (Goal 9), and
— sustainable use of terrestrial ecosystems (Goal 15),
— support inclusive societies as mentioned above (Goal 16) (Zlinszky – Balogh 2016).

Because natural resources are not replaceable key resources (in fact, they are ecological constraints in our lives), a complex analysis of a particular energetical (technical) innovation should be carried out to determine which of the pillars of sustainability (environmental, economic, social, "political") could temporarily be neglected or overlooked. However, it is unacceptable to contrast systems based on conventional and renewable energies.

In clarifying the direction of progress, as well as allocating and prioritizing resources, the introduction of indicators (may) help significantly (Gockler 2017; McBride et al. 2011).

Figure 2 illustrates a "cognitive map" of environmental mentoring (in terms of sustainability and energetical innovation). We have arranged bits of thoughts (facts, principles, theories and methods) concerning energetics (more precisely, technological innovation in the energy industry) and sustainability (impacts on the environment and landscape) on a "map", but we have also set up actions (if we create an inclusive environment for them), all of which is permeated by a holistic approach and interdisciplinarity.

Figure 2: Environmental mentoring (sustainability in relation to technological innovation (in energetics))

We have placed man at the center of sustainability, but we must constantly reassess and monitor the effects of human actions, and intervene at the appropriate level, if necessary. The cornerstone of harmony or the necessary symbiosis is constructive and cooperative action that must be coupled with self-discipline.

ADAPTIVE SYSTEMS

The basis for the environmental mentoring mentioned in the previous chapter relies on the "actions and reactions" between the system and its environment. A prerequisite for this is the ability to identify with the problems and challenges due to the internal value system. The technological challenges of a renewable energy system include redundancy, critical infrastructure (interconnection and interdependence of elements), and the impact of renewable energy systems (risk and opportunity analysis, or vulnerability) on environmental elements, and on the nature and quality of the landscape. Pasqualetti and Stremke wrote about energy landscape. The Collingridge dilemma also draws attention to the need for a comprehensive analysis of the effects of technology before a technical innovation (system) is introduced or embedded in order to obtain as much information as possible for its deployment, dissemination and long-term sustainability, as well as for working towards adaptability. There are open questions which still remain unanswered.

This interdisciplinarity, which is in the center of our study, allows for maximum scope for this "target research," since the most reliable determination of future effects can be made with a complex approach. Referring to some previous works (MacKay 2008; Liegey 2013; HTTP1; HTTP2; HTTP3), we can assume that the result is guaranteed by the linking and mutual thinking of several disciplines (risk management, environmental science, social sciences, etc.). Note here that the ever-increasing dissemination and use of computer programs in all areas of technology, as well as the constant growth of their worldwide distribution through the Internet, is a critical factor in technological innovation. It is also a fact that the problem-detecting and solving skills of society are

diminishing (too), owing to the excessive use of 'smart' electronic devices. A typical example of the external and/or internal dominance of motivation is the relationship between created needs and self-discipline.

Dynamic balance (i.e. the ability to adapt to a constantly changing environment) means that the change induced by the changing environment results in a rebalance. If engineering respects the character of the landscape, it will entail creativity and innovation, because the production and use of energy results in a more intensive use of the landscape that adapts to natural conditions. The energy landscape is changing, driven by the need to reduce emissions (Deane 2017). The character of a landscape is defined by a pattern or system of a combination of natural and anthropogenic landscape-forming factors that makes a particular landscape distinct from other parts of the land (Landscape Strategy of Hungary 2017-2026). In the development of energy model variants that respect all of this, priority is given to the fulfillment of the main goals of sustainable development mentioned above (Zlinszky – Balogh 2016).

For instance, point 7.a of the 169 subgoals calls for a more advanced and cleaner fossil fuel technology, investment in energy infrastructure and the launch of clean technologies, energy transition. Also, we should mention here subgoal 9.4 as a guiding principle, which is linked to the activities of technical engineers because of a more efficient use of resources, as well as the development and use of clean and environmentally friendly technologies and industrial processes. Suitable methods may include energy life cycle analysis or risk analysis: evaluation assessments with differentiated thinking make the production processes transparent and thus realize energy savings and impacts on a smaller environment. These will, then, be accepted and adopted by the members of society (in the form of a firm conviction, readiness to act, etc.), thus getting closer to sustainability.

SUMMARY, FINAL THOUGHTS

Our publication highlighted the complex relationship between sustainability and the (technical) innovations of the energy industry, where deeper analysis of relationships presupposes interdisciplinary thinking. In most other publications, the emphasis falls on "novelty" (a possible solution to a specific problem in a different way) in relation to a particular technical development, and only a very limited number of written texts contain an analysis of the full mechanism of the impact of technical or technological developments. Consequently, the introduction and application of technologies that are not yet mature will require future research that explores the potential for permanent, stable and reliable application of systems, and identifies the necessary (further) developments. Note here that the role of universities in the dissemination of scientific results is of paramount importance.

Certainly, switching to low-carbon systems is essential for the protection of our environment, but at the same time, the transformation of already existing systems into higher systems can be a solution, as redundancy shouldn't be neglected. One should also consider the types of investments entailed by the potential "new" solutions (greenfield/brownfield) and what impacts would they have on the character of the landscape, etc.

Environmental mentoring is a series of interdisciplinary activities to help avoid burdening, polluting and damaging the environment in an unreasonable way. With environmental mentoring, therefore, we can see the (possible) environmental changes brought about by the dampening (or, ultimately, solving) of a particular problem.

References

[1] Davidson D. J. – Gross M. (eds.) (2018): The Oxford Handbook of Energy and Society. Oxford Handbook Online

[2] Deane P. (2017): Chapter 13 - Conclusions and Outlook. In Europe's Energy Transition – Insights for Policy Making. Academic Press, pp. 89–90;

[3] Gockler L. (2017): A fenntartható fejlődés a gyakorlatban. In: Mezőgazdasági Technika, 58/4: 40–43

[4] Liegey V. et al. (2013): Un projet de Décroissance. Les Éditions

[5] MacKay D. J. C. (2008): Sustainable Energy - without the hot air. UIT Cambridge http://www.withouthotair.com/download.html

[6] McBride A. C. – Dale V. H. – Baskaran L. M. – Downing M. E. – Eaton L. M. – Efroymson R. A. (2011): Indicators to support environmental sustainability of bioenergy systems. In Ecological Indicators. 11(5), pp. 1277–1289

[7] Owen R. – Bessant J. – Heintz M. (eds.) (2013): Responsible innovation. Managing the responsible emergence of science and innovation in society. Chichester, UK, John Wiley & Sons. Ltd.

[8] Pasqualetti M – Stremke S. (in press): Energy landscapes in a crowded world: A first typology of origins and expressions. In: Energy Research & Social Sciences

[9] Stremke S. – Van den Dobbelsteen A. (eds.) (2013): Sustainable Energy Landscapes: Designing, Planning and Development, Boca Raton: CRC (Taylor & Francis Group)

[10] Székács A. (2017): Environmental and Ecological Aspects in the Overall Assessment of Bioeconomy. In: Journal of Agricultural and Environmental Ethics 30:153–170

[11] Wyne B. (2011): Lab work goes social, and vice versa: Strategising public engagement processes. Science and Engineering Ethics, 17(4), pp. 791–800

[12] Zlinszky J. – Balogh D. (eds.) (2016): Transforming our world: the 2030 Agenda for Sustainable Development, 2015, Resolution_General Assembly, Pázmány Press, Budapest, 130 p.

[13] National Landscape Strategy of Hungary (2017-2026), Ministry of Agriculture, Budapest 2016; https://www.kormany.hu/download/f/8f/11000/Hungarian%20National%20Landscape%20Strategy_2017-2026_webre.pdf

[14] HTTP1: https://m2.mtmt.hu/gui2/?type=authors&mode=browse&sel=10022554

[15] HTTP2: https://m2.mtmt.hu/gui2/?type=authors&mode=browse&sel=10001608

[16] HTTP3: Sustainable Energy News No. 82, April 2018 - INFORSE (International Network for Sustainable Energy); http://www.inforse.org/doc/SEN82.pdf

Fascicule 3
[April - June]
t o m e
[2019] XII

ACTA Technica CORVINIENSIS
BULLETIN OF ENGINEERING

ACTA
TECHNICA
CORVINIENSIS
BULLETIN OF
ENGINEERING

ISSN: 2067-3809

[1.]Olakunle F. ISAMOTU, [2.]Kabiru M. RAJI

PERFORMANCE EVALUATION OF DIFFERENT MATERIALS AS CHILLS IN SAND CASTING OF ALUMINUM ALLOY

[1-2]Dept.of Mechanical Engineering, Federal University of Technology, Minna, NIGERIA

Abstract: This study has evaluated the effectiveness of metallic materials as chill in sand casting of aluminum alloy. Four plates of dimension 165mm x 80mm x10mm were cast using sand mould. Steel, copper and brass chills in form of cylindrical bar of geometry 7mm in diameter and 50mm long were inserted, side by side at regular intervals of 30mm in each sand mould and the last sample was left unchilled. Experimentation involved testing of mechanical properties and metallographic analysis of cast samples. The results obtained revealed that the sample chilled with copper has the highest mechanical properties.
Keywords: casting; chills, aluminum alloy, impact strength test, mould

INTRODUCTION

Metal casting is a shape forming process whereby molten metal is poured into a prepared mould and allowed to solidify such that the shape of the solidified object is determined by the shape of the mould cavity. Sand casting is a metal casting process characterized by using sand as the mould material (Ibhadode, 2001). Casting can be broadly divided into two main categories as expendable and nonexpendable mould casting. It can also be classified according to the mould material used to cast the metal such as sand casting, ceramic casting or metal mould casting and depending on the pouring methods as gravity casting, low pressure die casting and high pressure die casting (Navaneeth, 2009).

Good mechanical properties are achieved in sand casting with the help of metallic insert in the mould known as chill (Mehr, 2012). Strong directional solidification is difficult to obtain in casting of intricate part made of aluminum alloys without the use of chills. The tendency for solidification to start throughout the metal makes proper feeding difficult. Chills must often be used to obtain satisfactory directional solidification (Chi-Yuan *et al.,* 2006). Chills are metallic inserts moulded into the sand surface to promote high solidification rate in metal casting. Normally the metal in the mould cools at a certain rate relative to thickness of the casting. When the geometry of the moulding cavity prevents directional solidification from occurring naturally, a chill can be strategically placed to help promote it to obtain good mechanical properties. Chills are of two types, internal and external chills. Chills are usually made from iron, aluminum or copper and can be machined or cast. The type of chill used depends on ease of manufacture and the desired thermal effects of the chill. Its effectiveness depends on size, conductivity, thermal capacity and the thermal transfer across the molten metal alloy/chill interface. Chilling has been found to improve the soundness of a casting when measured by standard non-destructive testing techniques like radiography or dye penetration inspection, but the influence of microstructure and mechanical properties can be significant (David, 2011).

This research purely emphasized on evaluation performance of different material as chill in sand casting to increase solidification rate and to improve the mechanical and microstructural properties.

MATERIALS AND METHODS

The materials used in this research work include;

Aluminium alloy scrap: Aluminium alloy scrap was obtained from pantaker (a spare part market) in Kaduna metropolis, Nigeria.

Chills: Mild steel, brass and copper chills were used in this research work.

Foundry sand: Foundry sand and other additives used in the present investigation were made available in metallurgical and Materials engineering foundry workshop of Ahmadu Bello University, Zaria.

— **Equipment**

Furnace: The melting of the alloy was carried out on charcoal fired furnace available in metallurgical and Materials engineering workshop.

Vicker Hardness Tester: Vicker Hardness machine of capacity 10 kg was used to carried out the hardness test of the samples.

Charpy Impact Tester: Impact test was carried out on a Charpy Impact Testing Machine of capacity 25J.

Optical Metallurgical Microscope: Microstructural examination was conducted on optical metallurgical microscope available at Metallurgical and Materials Engineering workshop.

Hounsfield Tensometer: Tensometer machine in Mechanical Engineering workshop was used to carry out tensile test for the samples.

Thermocouples: Thermocouples were employed in the measurement of temperature gradient of the solidifying metal during casting operation.

— **Experimental Procedures**

The experimental procedures of this study consist:

Casting of Alloys

Four samples of the aluminium silicon alloy were cast by melting the spare part scrap on charcoal fired furnace using four different sand moulds where three of the moulds were inserted with steel, brass and copper chills respectively and the fourth one without chill which serve as control. The castings were labeled as samples A, B, C and D accordingly. The sample geometry is 165mm x 80mm x

10mm and the chill is of cylindrical shape of diameter 7mm with length 50mm. There are 10 pieces of chills in each mould and the chills were arranged side by side at regular intervals of 30mm. The fluxing and degassing were done before the molten metal was poured into the moulds cavity. The rates of cooling (temperature gradient) were studied with the aid of thermocouples attached to the sand mould immediately before the pouring of the molten metal. The arrangement of the chills within the sand mould is shown in Figure 1 whereas sand mould without chill is shown in Figure 2. The chemical composition of the sample is presented in Table 1.

Figure 1: Sand mould with chills

Figure 2: Sand mould without chill

Table 1: chemical composition of the cast aluminium alloy

Al	Si	Mg	Fe
90.742	7.155	0.388	0.359
Cu	Mn	Zn	Ti
1.228	0.054	0.008	0.066

The chemical analysis of the cast samples was conducted in the Tower Aluminium Rolling Mills Industry, Ogun State using Optical Emission Spectrometer.

Tensile Strength Test

The tensile test specimens were machined from the cast samples. The test piece was locked securely within the grips of the Tensometer machine. The test piece was stretch with force generated from manually operating the screw attached to the Tensometer until the test piece broke apart. The load and extension data available from the graph sheet attached to the machine were converted to specific values of stress and strain. The geometry of the tensile test sample is shown in Figure 3.
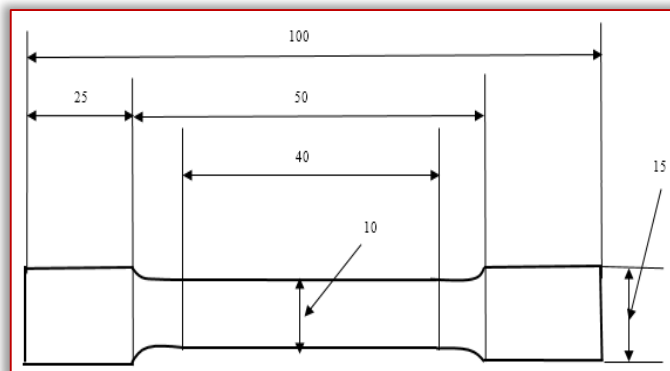
Figure 3: Dimension of the tensile test sample (mm)

Hardness Test

Hardness test was carried out on Vicker Hardness testing machine. An indentor was placed above the sample flat surface. A load of 50gm was applied on the indentor for about 10-seconds which then penetrates the surface of the sample and the hardness value is displayed on the machine. Three different indentations were made on a sample and the average is taken as the hardness value of the samples. This procedure was repeated for the remaining samples.

Impact Strength Test

Charpy Impact Testing machine was employed in conducting the impact test of the samples. A V-notch was machined into a 10mm wide and 100mm long test pieces with the notch depth of 4mm. The specimen was placed across parallel jaw of the testing machine and a heavy pendulum, released from a known height, struck and broke the test piece. This measured the energy necessary to fracture the standard notch test piece by an impact load and the dial pointer of the scale on the machine indicates the energy absorbed, in Joules, by the test piece from the impact. The value of the energy absorbed in breaking the test piece was recorded for the whole samples.

Metallographic Examination

Four specimens were prepared from the four aluminium alloy samples for metallographic examination. The procedure consists of cutting, successive grinding using silicon carbide grit paper of 240, 320, 400 and 600 microns. Polishing was carried out on a rotating cloth to ensure mirror-like surface. A solution containing 5ml nitric acid, 2ml hydrofluoric acid and 100ml of distilled water was used to etch the specimens for about 10 seconds. The specimens were observed under Digital Metallurgical Microscope where the micrographs of the specimens were recorded at a magnification of 100X.

The results of the tests carried out are shown in Table [2-3] below.

Table 2: Solidification rates of aluminium alloy

Time (min)	Sample A (J/min)	Sample B (J/min)	Sample C (J/min)	Sample D (J/min)
0	503.0	479.0	472.5	490.5
4	495.0	452.7	419.2	473.2
8	461.3	429.2	383.1	438.9
12	423.2	398.4	351.3	404.8
16	387.0	366.9	324.0	382.7
20	358.4	339.6	303.0	358.8
24	334.3	317.2	285.0	337.1
28	315.2	299.1	270.0	318.9
32	299.6	284.0	258.0	302.4
36	286.5	272.0	247.7	287.0
40	276.0	262.3	240.0	277.1
44	265.5	252.7	232.3	266.3
48	258.4	246.4	226.7	258.3
52	251.1	239.5	221.6	251.5
56	245.2	233.7	216.9	244.3
60	239.2	228.8	212.5	238.4

Samples: A- steel chill, B- brass chill, C- copper chill and D- no chill.

Table 3: Mechanical properties of aluminium alloy

Samples	Ultimate tensile strength (MPa)	Hardness (Hv)	Impact Strength (J)
A	101.33	5.40	22.7
B	115.83	5.73	22.4
C	126.13	6.87	23.5
D	70.67	4.2	22.5

RESULTS AND DISCUSSION
— Mechanical properties of aluminium alloy
The results of ultimate tensile strength, hardness values and impact strength of the samples are presented in Tables 3.
— Discussion of experimental results
Influence of chill materials on solidification of aluminium alloy
Cooling rate plays an important role in determining the microstructure of the casting. Higher cooling rate reduces solidification time and grain size of the casting. This may be attributed to the solidification process of aluminium alloy where a high percentage of solids are formed during the earlier stages of freezing and is followed by a pasty mode of solidification with non-equilibrium eutectic solidifying at the end.

Nucleation initiated at the mould wall, chill surface or at dispersoids and then spreads quickly into the interior of the liquid metal in the mould cavity and crystallization occurs at numerous centers in the liquid as presented by Joel, (2001). Hence, at this stage, a pasty mass of liquid and solid exists along with the fully solid and fully liquid zones containing intermetallic particles.

It is evident from Figure 4 that casting with copper chill solidified faster than any other one with other chills. This is followed by brass chill and casting with steel chill almost has the same solidification rate with that of no chill at the beginning but slightly higher than no chill casting towards the end of the solidification. The volumetric heat capacity and thermal conductivity of copper is higher than that of brass and steel which enable the copper chill to extract heat faster than any other chill materials from the melt. The brass is

higher than steel in terms of thermal conductivity and this also enhance its heat extraction rate from the melt faster than steel as a chill material. The steel chill shows little heat extraction rate when compared to the casting where chill material is not inserted in the mould. These observations of solidification gradient influence strongly the types of structure and the mechanical properties of the aluminum alloy formed.
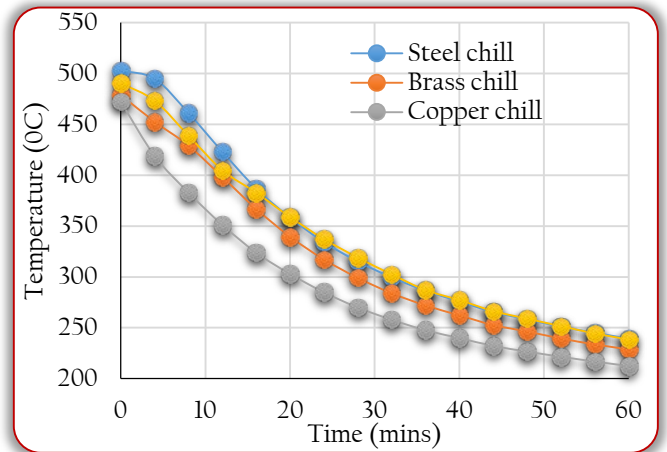
Figure 4: Cooling curves of aluminium alloy during solidification

Influence of chill materials on ultimate tensile strength of aluminium alloy
It is well known (Joel, 2001) that aluminium alloys that freeze over a wide range of temperature are difficult to feed during solidification. The dispersed porosity caused by the pasty mode of solidification can be effectively reduced by the use of chills as presented by Joel (2001). Chills extract heat at a faster rate and promote directional solidification. The casting with copper chill shows the highest ultimate tensile strength followed by the casting chilled with brass. This is as a result of high values of thermal conductivity displayed by the copper and brass materials. The casting with no chill material shows the least ultimate tensile strength when compared to the steel chilled casting indicating the essence of presence of chill materials in improving the soundness of the casting.
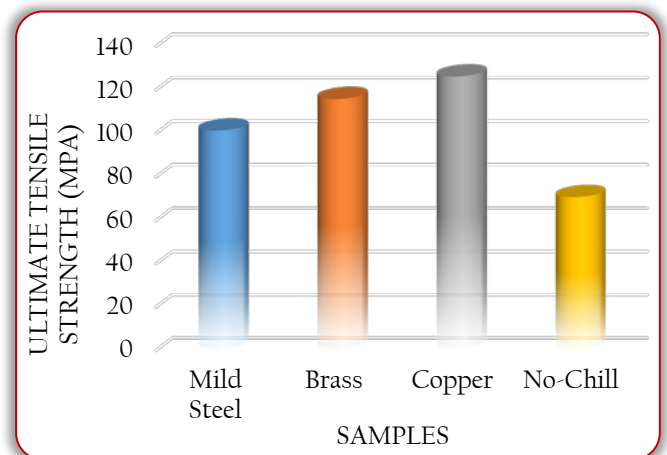
Figure 5: Chart of ultimate tensile strength of samples with different chill materials

The reason for these observations is attributed to the types of microstructures formed during solidification. A fine-grained material is harder and stronger than one that is of coarse grain

structure, since the former has a greater total boundary area to impede dislocation motion as observed by William (2009). The copper chilled sample are characterized with finer grains structure with uniformly distribution of intermetallic particles due to high heat extraction rate and when this sample was subjected to tensile experiment, the material shows a high ultimate tensile strength before fracture occurred. This trend was also observed in other samples chilled with brass and steel. The ultimate tensile strength of sample with no chill which are predominately characterized with coarse grains structure is very low due to slow cooling rate.

CONCLUSIONS

From the results and discussion of the study, the following conclusions can be drawn;

The cast aluminium alloy sample with copper chill displayed the highest mechanical properties (ultimate tensile strength of 126.13mPa, hardness value of $6.87Hv_{0.05}$ and impact strength of 23.5j respectively) and finer grains structure than any other samples under investigation. The cast sample inserted with brass chill also shows higher values in mechanical properties than sample with steel chill and unchilled sample. The cast sample inserted with copper chill solidified faster than any other cast sample with chill. The cast sample inserted with brass chill solidified faster than the cast sample with steel chill.

The coarseness of the grains in the microstructure of these samples also increased from samples chilled with brass, steel and no chill.

References

[1] Chi-Yuan, C., Jun-Yen, U. and Te-Chang, T. (2006). Effect of cooling rate on Mg17Al12 volume fraction and compositional inhomogeneity in a sand-cast AZ91D magnesium plate. Materials Transaction, Japan Institute of Metals, 47(8), pp 2060-2067. 2006.

[2] Ibhadode, A. O. A. Design and manufacture of a gas-fired furnace. Proceedings of the Third Uniben Conference on Engineering and Technological Development, Benin, pp 159-164. 1991.

[3] Ibhadode, A. O. A. Introduction to Manufacturing Technology. Ambik Press, 2nd Edition, Pp 212-272. 2001.

[4] Joel, H. Effect of chills on soundness and ultimate tensile strength (UTS) of aluminum alloy–corundum particulate composite. Journal of Materials and Design, 22, Published by Elsevier Science, pp 375-385. 2001.

[5] Mehr, F. F. Quantitative assessment of the effect of copper chills on casting/chill interface behavior and the microstructure of sand cast A319 alloy. Unpublished M.Sc Thesis, Department of Materials Engineering, University of British Colombia, Vancouver. 2012.

[6] Navaneeth, V. Developing an effective die cooling technique for casting solidification. Unpublished M.sc Thesis, School of Engineering, Auckland University of Technology. 2009.

[7] William, D. C. Material science and engineering. John Wiley and Sons, New Delhi, India, pp 361. 2009.

[1.]Remus Marius OPRESCU, [2.]Sorin Ştefan BIRIŞ, [1.]Iulian VOICEA, [1.]Valentin VLĂDUŢ

CONSIDERATIONS ON HEMP CULTIVATION TECHNOLOGY

[1.] National Institute of Research–Development for Machines & Installations for Agriculture & Food Industry – INMA, Bucharest, ROMANIA
[2.] University Politehnica Bucharest, Faculty of Biotechnical Systems Engineering, ROMANIA

Abstract: The paper presents some aspects regarding the technology of hemp cultivation (or *Canabis Sativa* as its specialty designation), this plant having the greatest capacity of industrialization among all the technical plants: nothing is thrown away, everything is capitalized and the products obtained are of an outstanding variety, starting from the ordinary rope until the medicinal or cosmetic substances, vehicles or construction materials.
Keywords: technology, hemp, fiber, seed

INTRODUCTION

Hemp (*Cannabis sativa*) is an annual herbaceous plant belonging to Cannabaceae family; it is of 2–3 m tall being able to reach up 5 m, exceptionally. Its stem is unbranched and it has long lanceolate leaves with toothed edges and dense, semi compact inflorescences. (Figure1).

Figure 1 – Hemp for spinning [5]

Hemp cultivation history is very old, being remembered since early neolithic (12,000 years ago) as a source of obtaining textile fibers, oil, food, but also as the environment where ancestral religious practices were developed or as medicinal herb. Each part of hemp has a different use and is processed according to it.

Term of cannabis, from which the Romanian word "cânepă" comes, has its origins in a Scythian or Thracian word. Greeks imported it first and afterwards Romanians and, thus it was known by Occidental civilizations. The word is very old having Indo–European roots. Ancient Oriental people (Acadiens, Babylonians and Assyrians) also knew the word as qunnabu. The original meaning was the smoky, demonstrating the ancestral habit of using the plant in recreational and practical goals.

Traditionally, the hemp was the raw material for obtaining oil, wax, resin, rope and cord, textile fibers for clothing and rough fibers for sacks and knitting, animal foddering and vegetal fuel (Figure 2). At those above, the industrial processing ads the cellulose, from which paper, chipboards for furniture industry, artificial silk, insulating down for plasterboards, can be obtained.

Figure 2 – Hemp traditional harvesting [6], [8]

Hemp is one of the oldest plants cultivated in Romania (over 2000 years), being mainly used for fibers designed to clothes. Hemp stems coming from local growing and wild hemp contain 10–12% fibers, and improved varieties– 26–32%. Fiber content within stems is influenced by each variety, technological and soil and climate conditions. Fibers have a series of valuable characteristics related to resistance (to traction, torsion, friction, rotting process), extension capacity (elastic and plastic), spining capacity, bigger length than fibers of sisal, jute, manila or cotton, that make them useful in various domains: textile industry, manufacturing industry, vehicle industry (Tabara, 2009).

MATERIAL AND METHOD

Hemp requires a gentle and humid climate (corn area). Seeds germinate at 2–3 °C, but a uniform springing is performed at over 8 °C. In optimum conditions, when soil temperature is of 8–10 °C, hemp germinates after 7–9 days, and at 20–24°C the germination takes place after 5–7 days, depending on soil humidity. A great attention should be given to groundwater depth, which must be at

least below 1m, because puddles can damage the crop. Excessive weeds in areas where hemp is cultivated can also risk to stifle the springing plants. That is why, the weeds should be destroyed by any means immediately after the harvest of plant, insisting on doing so up to the preparation of germinating bed. Weeds like creeping thistle (*Cirsium arvense*), couch grass (*Agropyron repens*), vilfa stellata (*Cynodon dactylon*) or Johnson grass (*Sorghum halepense*) and lamb's quarters (*Chenopodium album*), are difficult to control. The best precursor crops are vegetables and then, straw cereals. Hemp may be cultivated after beet or potato crops, but the fertilization doses will be increased by 15–25%, because the soil remains deprived of nutrients. At its turn, the hemp is a good precursor culture for most of crop plants, as it leaves the soil structured, deases and pests free. The growing rhythm of fiber hemp is rapid and it enables the weeds destroying, thus reducing the stock of weeds in the soil. The fiber hemp or seed hemp cultures are good precursors for autumn cereals and autumn fodder crops (alfalfa, rape, fodder, cereals) as they clear the field in August and early September and soil works can be appropriately performed. Furthermore, the hemp powerful swiveled root extends deeply into soil, mobilizing the nutritive elements and giving increased resistance to draught. Maize should not be used as precursor crop, as the same pests attack hemp, namely European corn borer (*Ostrinia nubilalis*), foddering plants after which the vegetal debris remain and the field is infested by wireworms (*Agriotes sp.*) , sunflower, that has commum deseases and pests as hemp, like white mold (*Sclerotinia sclerotiorum*) and broom–rape (*Orobanche sp.*). Although, in the opinion of certain authors, the hemp behaves very well as single crop and it is preferable not to be cultivated in the same field and neither in neighbouring ones for avoiding to be attacked by hemp moth (*Grapholitha delineana*), that produces important damages, in certain years up to 25–30%.

Hemp is a pretentious plant concerning the soil content in nutritive substances. The main fertilizer appropriate to ecological hemp is the manure. 30–40 t/ha of fermented manure will be applied in heavy and cold soils like black soil, excessive watering soil or brown soil. Better results are obtained when the manure is applied to precursor plants in a quantity of 40–50 t/ha. The manure should be combined with 40–60 kg/ha P2O5. Manure and phosphatic fertilizers will be performed in summer or autumn, along with the basic plower. Organic fertilizers should be compulsory applied in surfaces destined to ecological hemp cultivation. Phosphorus fertilizers applied to hemp for seed mostly compensate the unfavourable action of chemical fertilizers with nitrogen and potassium and positively influence the stem anatomical parts and seed formation, thus increasing the oil content and production. Phosphorus fertilizers are applied in quantities of 40–60 kg/ha s.a., during autumn or before preparing the germinating bed as complex fertilizers.

Generally, Romanian soils are well supplied with potassium. Potassium fertilizers applying is necessary to be done on soils having below 15 mg K2O/100 g , when it is compulsory to apply 40–60 kg/ha K2O. In the fields fertilized in previous years with organic fertilizers, the potassium fertilizers are not more necessary. Potassium is applied in autumn, before the basic plowing or in spring as complex fertilizers. Nitrogen fertilizers act on the general development of plants enabling the stems and seeds growing. The doses of nitrogen fertilizers applied are of 120–150 kg/ha s.a. depending on each zone, soil type and precursor plant. After vegetables, the nitrogen quantity should be reduced approximately by 20 kg/ha s.a., and in case of precursor plants with large consumption of nutritive substances (beet, corn, potato), the quantity is increased by 20 kg/ha s.a.

The nitrogen fertilizers are applied in spring, before preparing the germinating bed, but they can be also applied as little fractions, in a percentage of 15–20% out of total dose when the seed hemp mechanical hoeing is performed. When complex fertilizers (rich in nitrogen) were not applied in autumn, then complex fertilizers should be applied in spring when preparing the germinating bed. The nitrogen dose is completed by an additional share to the necessary one, previously planned. A great attention should be given to uniformity of fertilizers spreading, that, if it is not appropriate, can determine a non–uniformity of plants growing and development and, implicitly a worse quality and diminished production (Brian, Mahmoud, 2016; Tabara, 2005,2009).

RESULTS

⎯ Sowing

Hemp seed must have a minimum purity of 96 % (without broom–rape seeds) and minimum germinating capacity of 80 % (positive production increments are obtained when the germinating is over 90 %). The seed from previous year should be used. Seed material is treated with fungicides (Criptodin 3kg/t). Sowing is performed when at 5–6 cm soil depth, the temperature has stabilized at +8…+9℃ (practically before the corn sowing). In case of early sowing, the plants endure low temperatures, so their growing is slowed down and they do not reach the normal height and damages determined by fleas are bigger. When sowing is delayed, the moth can attack, the growing time is shortened and plants prematurely blossom. When the sowing period is failed, the stems and fiber production are diminished. The most appropriate distance between rows is of 12.5 cm. The sowing machine used is SUP–17. Sowing depth is 3–4 cm. In lighter soils or during draught spring, it can reach 5 – 6 cm. After sowing, the harrowing is performed for making rows less visible, thus limiting the damages produced by crows, pigeons, etc.

⎯ Crop preparation works

In medium well-structured soils and for an ideal preparation of soil (lack of weeds), hemp can be viable without any other preparation works. Though, there are cases when crops should undergo maintaining measures. If sowing is performed in loosen field or during draught spring, an immediate rolling should be performed after the sowing. When crust appears during the sowing till springing, then the harrows or ridged rollers should be used. After springing, the perennial weeds with vegetative multiplication (thistle, milk thistle, etc.) are controlled by weeding. Fleas control is performed during the springing time or by applying Lindatox. The hemp moth (*Grapholita delineana*), is controlled not only by rational crop rotation, but also by chemical treatments with Decis or Sumithion. One warning treatment and other two subsequent ones, at 12–15 days, are made, [2,3].

Like any other plant, hemp has the male and the female part. It is very important to determine in field which part is the male and which the

female in order to remove the male part from the crop, because pollination is not recommended. After being pollinated the plant has no more grains. A charge of maximum maxim 2% male per hectare is allowed. Male parts are manually removed. Differences between male and female parts:

\# male plant is higher;

\# has bigger inflorescence;

\# flowers are white;

\# flowers appear more rapidly at males than at females, [2, 3, 9].

Figure 3 – Hemp: 1,2–male hemp (of summer) ;
3,4–female hemp (of autumn) [2,3,9]

Hemp comprises three parts that can be used:

\# Seeds can be used to prepare different food, oils and medicinal products.

\# Fibers have all sorts of industrial uses (starting from clothing till vehicles) – they form the middle layer of the stem and are covered by a thin protective layer.

\# Woody core remained after extracting the fibers, represents the part (together with lime) used in constructions (although we have found information according to which it is possible to use the whole stem in buildings – meaning that fibers and woody core should not be separated).

── Harvesting

Harvesting is made during two phases both for fiber hemp and seed hemp. For fiber hemp, first, the plants are cut and left in field to dry and in the second phase the leaves are shaken and plants are tied up in bunches of 20–25 cm diameter, that are transported to retting processing plants. For seed hemp, the plants are cut and left to dry for 7–8 days. Threshing of inflorescences is performed with the cereal combine. Threshed seeds are immediately cleaned, conditioned and dried. [11]

Knitting hemp is harvested at the end of blossoming of male plants, when the pollen does not shaken any more. Premature harvesting diminishes the fiber productions as well as plant technological characteristics (mostly its resistance) that are lower. Harvesting delay is also very harmful. The most important losses are determined by stems damaging.

At the same time, fiber is less fine, becomes rough and breakable. In certain areas, hemp is manually harvested. Stems are cut at 4–6 cm height by sickle or special hooks, left on soil as bunches of 15–20 cm thickness, spread to dry.

When the upper part is getting yellow, the hemp bunches are reversed on their other part and dried for more 2–3 days (totally, drying lasts till 4–8 days). After that, the leaves are shaken (leaves should be removed, because chlorophyll depreciates the hemp fiber by staining during retting process and retting processing plants do not receive stems with leaves) and bunches are bound twice if they surpass 100 cm and once, if they are short. [7]

Figure 4 – Hemp harvesting machine, [14]

Mechanized harvesting is performed with special machines. The cut stems are left on soil as a thin layer (approximately perpendicular on machine forward direction). After having dried, the process is similar to manual harvesting, namely: leaves shaking and binding as bunches. Productivity of machines for this procedure without binding device is of 4–5 hectares/shift. In order to use special machines with binding device, the hemp leaves should be removed. Generally, there are recommended the treatments of 100–150 liters of solution per hectare, made by air means spraying. Treatments are performed in the morning up to 10 a.m. or in the evening after 5 p.m. The treatment is done when the leaves and male stems become green–yellowish (10–15 days since the beginning of pollen shaking, namely 10–12 days before harvesting or the blossoming period end). The moment is also chosen in accordance with weather report, as rains over 5 mm that appear in the first 4–6 hours after the treatment could impede the efficacity of products used. It is also to be noticed that the treatment delay till chrolophyll degradation does not ensure the defoliation.

Premature treatment, when male plant leaves are green, may depreciate the fiber, and production is reduced. When treatments are appropriately performed, the defoliation lasts 10–12 days, usually in a percentage of 90–100%. In some cases, magnesium chlorite may be also used for defoliation, 15–17 kg/ha in 200 de l of water, that produces drying and leaves removing within 5–6 days. After the defoliation, the machines directly harvest in bound bunches, that are put in hoods for being dried, and machine productivity in this case is of 1.5 Ha/shift.

Figure 5 – Combine of harvesting hemp seeds, stems and leaves [2,3]

HempFlax, a Dutch company established since 1994, is designing, developing and patententing equipment specialized in hemp cultivation, offering an innovating combine able to perform three different harvesting operations at the same time, namely hemp seeds, stems and leaves harvesting. [2,3]

CONCLUSIONS

Hemp is one of the oldest plants cultivated in our country (over 2000 years), being mainly used for fibers in clothing industry. Hemp stems coming from local growing and wild hemp contain 10–12% fibers, and improved varieties– 26–32%. Fiber content within stems is influenced by each variety, technological and soil and climate conditions. Fibers have a series of valuable characteristics related to resistance (to traction, torsion, friction, rotten process), extension capacity (elastic and plastic), spinning capacity, bigger length than fibers of sisal, jute, manila or cotton, that make them useful in various domains: textile industry, manufacturing industry, vehicle industry. [3].

Hemp is another agricultural plant that is cultivated either for fibers, or in mixed purposes, for fibers and seeds. Seed contains 32–35% oil. Hemp long fibers resistant to water action are used to manufacture strong and durable fabrics. The hemp oil is edible and is used in industry. The cakes resulted after extracting the oil, being rich in fats and proteic substances are used as concentrate products to farm animals foddering. The multiple materials resulted after the primary processing of stems are used for heating the plastic greenhouses.

The oldest proof attesting the hemp utilization is a piece of fabric discovered in Mesopotamia, 10,000 years ago. The oldest paper of hemp fiber registered comes from China, 2 millennia ago. The first Diesel engine has been designed to use vegetal oils mostly based on hemp. This is a non–toxic and bio–degradable bio–oil for Diesel engines. In 1930, Henry Ford has produced a car manufactured in a percentage of 70% from hemp (as raw material used). Great artists (Rembrandt, Van Gogh, Gainsborough) paintings have been made on hemp canvas, using water colours extracted also from hemp.

Until 1989, Romania owned the first place in Europe as regarding hemp crop–cultivating 56–70% out of total production and the fourth place in the world (45,000 ha), but in 1994 it reached only 800 ha. The hemp crop advantages and the outstanding characteristics of its fiber make necessary to revive this interesting domain.

Acknowledgement

References

[1] Brian F. T., Mahmoud A. E., 2016 – Book chapter 1: The botany of CANNABIS SATIVA L.
[2] Tabără V., 2005 – Phytotechny – Technical plants – Oleaginous and textile plants, VoL. I, Ed. Brumar, Timişoara.
[3] Tabără V., 2009 – Modern technologies of oleaginous species cultivation, Eurobit Publishing House – Timişoara.
[4] Van Der Werf B.W., Wijlhuizen M., De Schutter J. A. A., 1995 – Plant density and self–thinning affect yield and quality of fibre hemp (Cannabis Sativa L.), Field Crops Research, Vol 40, ISSUE 3, pp. 153–164.
[5] http://www.scda.ro/oferta/Tehnologie–canepa.pdf.
[6] https://ierburiuitate.wordpress.com/2013/08/14/canepa/.
[7] https://www.revista–ferma.ro/articole/tehnologii–agricole/canepa–cannabis–sativa–l.
[8] https://www.ziardecluj.ro/legalizati–canepa–romaneasca–un–student–de–la–cluj–lupta–cu–siste.
[9] http://www.biblioteca–digitala.ase.ro/biblioteca/pagina2.asp?id=cap8.
[10] http://agrointel.ro/31169/cum–se–cultiva–canepa–in–romania–tehnologie–cultura–canepa–pentru–boabe–profit/.
[11] http://www.usamvcluj.ro/files/teze/2015/dan.pdf.
[12] http://www.fortasigratie.ro/realitati–contemporane/canepa–canabis.htm
[13] https://www.gazetadeagricultura.info/plante/plante–tehnice/472–inul/12472–importanta–canepei–si–a–inului–pentru–economia–nationala.html
[14] http://verticalfinance.ro/canepa–cannabis–sativa–l–o–planta–minune–ignorata–de–agricultori–romani/.
[15] https://ciao.ro/romanii–recultiva–planta–canepa.

[1.]M. KHARYTONOV, [2.]N. MARTYNOVA, [1.]M. BABENKO, [1.]I. RULA,
[1.]S. SYTNYK, [1.]M. BAGORKA, [1.]O. GAVRYUSHENKO

BIOENERGETIC ASSESMENT OF SWEET SORGHUM GROWN ON RECLAIMED LANDS

[1.]Dnipro State Agrarian and Economic University, Dnipro, UKRAINE
[2.]Oles Honchar Dnipro National University, Dnipro, UKRAINE

Abstract: Sweet sorghum varieties of domestic breeding are the priority for studying their bioenergy potential, when they cultivated on reclaimed lands. Medove is a promising cultivar for growing on such sites in areas with insufficient water supply. The energetic characteristics of sorghum were studied on four types of mining substrates: loess-like loam (LLL), red-brown clay (RBC), green-grey clay (GGC), and piled up black soil mass (BS). Under such conditions, at the plots without fertilizer, Medove produced above-ground biomass from 38 to 82 ta ha^{-1}. The highest yield was recorded on loess-like loam. The sewage sludge application has promoted the increase of productivity by 4-44%. Although the sewage sludge introduction reduced the content of fermentable sugars in stem juice by 5.3-6.7% the theoretical ethanol yield was increased by 8-48%, except for the plot with loess-like loam. Thermal destruction of dry biomass proceeded in a similar way on all studied substrates. Nevertheless, it was revealed that the sewage sludge application shifts the process of thermolysis into the region of lower temperatures on BS and GGC, increases the stage of lignin decomposition on LLL, and affects the rates of the reactions, as well as slightly (LLL) and significantly (BS) augments the share of the incombustible residue.

Keywords: reclaimed lands, sweet sorghum, sewage sludge, biomass yield, conservative sugar yield, ethanol yield potential, kinetic characteristics of biomass

INTRODUCTION

Rapid depletion of natural resources and environmental degradation all over the world bring up the issue of creating environmentally friendly renewable energy sources. Biofuels are sustainable and renewable source of energy derived from organic matter in the form of biomass. In this connection, in recent decades, sorghum arouses particular interest as a multipurpose bioenergetic crop. The interest in sweet sorghum as an alternative energy crop is associated with the shortage and increase in the cost of non-renewable fossil energy products, and the use of ethanol as fuel (Rooney et al., 2007; Goff et al., 2010; Mathur et al., 2017).

Sweet sorghum belongs to the Sorghum bicolor (L.) Moench species, numerous cultivars and hybrids of which contain a large amount of fermentable sugars in stem juice. The ability of sweet sorghum to accumulate a lot of soluble sugars makes it a potential source of raw materials for the production of bioethanol. The biological features of this crop allow obtaining a good yield of green mass even on marginal lands and under insufficient water supply conditions. The most intense sugar in the stems accumulates after flowering. The maximum amount of sugars in plants is contained in the phase of wax and full ripeness of grain. The main components of extracted juice are sucrose, glucose, and fructose, which can be directly fermented into ethanol with efficiencies of more than 90% (Ratnavathi et al., 2010; Wu et al., 2010; Regassa & Wortmann, 2014). Lignocellulosic dry biomass can be used for the production of solid fuel (briquettes, granules) and for the making of biocomposite materials (Yu et al., 2012; Yin et al., 2013)

Due to its physiological traits and unique mechanism of moisture regulation, sorghum is highly resistant to soil and air drought, insects, diseases, salinity, and soil alkalinity (Reddy et al., 2007; Dalla Marta et al., 2014). In addition, this crop has one of the best rates of carbon assimilation (Prasad et al., 2007; Schmer et al., 2014).

Despite the unpretentiousness and resistance, if sorghum is grown on marginal lands, there is a risk of obtaining low yields due to the combined effect of multiple unfavorable factors. In this case it seems expedient to apply fertilizers. Given the current economic situation and the deficiency of mineral and organic fertilizers promising direction is the use composted sewage sludge in agriculture, fodder production, landscaping, for soil fertility restoration. Recently, the advantages and disadvantages of applying sewage sludge are widely discussed (Jamali et al., 2007; Wang et al., 2008; Singh & Agrawal, 2008; Hossain et al., 2010). Composted sewage sludge contains large amounts organic and inorganic elements essential to plants. Its effectiveness does not yielding to traditional organic and mineral fertilizers, but availability of potential toxic metals often restricts its uses. At the same time using sewage sludge which does not contain toxic impurities indicates a promising way of its use as a fertilizer.

MATERIAL AND METHOD

This study was carried out at Pokrov land reclamation station of Dnipro State Agrarian and Economic University which located in the Nikopol manganese ore deposit. The rocks of this ore basin are presented the holocene, postpliocene, neogen and paleogen deposits. These mining rocks are brought to the surface during process of manganese ore mining. The soil mass was taken off, piled up and heaped onto the land after the rock was replaced. Substrates formed in this way can be attributed to the category of Technosol which are soils strongly influenced by human activities, and as a result, their properties and pedogenesis are dominated by technical origin (De Kimpe & Morel, 2000).

Geographically, the land reclamation station is located in the Dnipropetrovsk region in the steppe zone of Ukraine with moderately continental climate: dry and hot summer and moderate winter. The average long-term air temperature is +8.5℃. The hottest month is July with the average temperature +22.0℃, the coldest is January with the average temperature -4.1℃. The site is located in the zone of unstable water supply with often prolonged droughts in the summer. The average hydrothermal coefficient is 0.9. In recent years, there has been a gradual increase in the average monthly air temperature with a simultaneous decrease in the

amount of precipitation during the vegetation period. Seasonal precipitation and mean temperatures are shown in Figure 1.
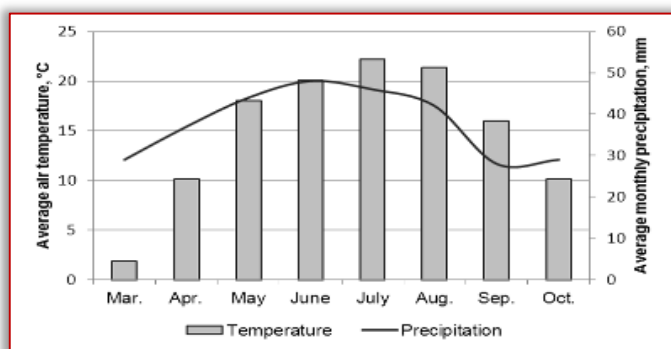
Figure1 - Average monthly temperature and precipitation amount at the reclamation station district (long-term data)

The sweet sorghum cultivar Medove was studied. This first generation hybrid was breeding at the Odessa Institute of genetics and breeding. This cultivar is mainly grown for silage and green mass, as well as for the sweet juice production and products of its processing (syrup, ethanol). Its potential productivity is 50-100 t ha^{-1}. The vegetative period before the milk-wax ripeness of grain is 90-100 days. The Medove is not affected by diseases and slightly damaged by aphids, resistant to lodging and is well suited for mechanized harvesting. Its main morphological characteristics are shown in Table 1.

Table 1. Morphological characteristics of sweet sorghum cultivar Medove

Height, cm	Number leaves per stem, pieces	Stem diameter, mm	Number stem per plant, pieces	Panicle form	Seed features
270-290	12-13	20-25	4-5	ellipsoid	brown, closed 3/4

The plants were sown on four types of mining substrates. Loess-like loam, (LLL), red-brown clay (RBC), and green-grey clay (GGC) were taken from the board of the quarry and exposed to long-term soil stabilization. Piled up black soil mass (BS) was taken in the soil stockpiling area. The humus content in these substrates is low (1.05- 1.25%), except black soil (3.29%). The ratio of humic and fulvic acids is 1.36 for BS and 0.62-0.69 for others substrates. The hygroscopic level varies from 7.6% (LLL) to 20.5% (GGC). To study the effect of sewage sludge, it was introduced into substrates in a dose of 30 ton ha^{-1}.

Biometric parameters, biomass productivity, brix, conservative sugar yield, theoretical ethanol yield, and dry biomass thermal characteristics were studied. The plant height was measured using a measuring line. To determine the yield of above-ground biomass, plants were harvested after the grain reached hard dough stage by cutting at the height of 10 cm from the ground level and weighed. After that, the biomass was dried to constant weight, and then weighed again. Brix was determined using a hand-held refractometer "RHBO–50ATC". Conservative sugar yield (t ha^{-1}) was calculated based on an approach assuming that the sugar concentration is 75% of Brix expressed in g kg^{-1} sugar juice (Wortmann et al., 2010; Ekefre et al., 2017).

Theoretical ethanol yield was calculated as sugar yield multiplied by a conversion factor: 0.58 L ethanol per kg of sugar (Rutto et al., 2013;

Ekefre et al., 2017). The thermal analysis of plant biomass was carried out using the derivatograph Q-1500D of the "F. Paulik-J. Paulik-L. Erdey" system. Differential mass loss and heating effects were recorded. The results of the measurements were processed with the software package supplied with the device. Samples of biomass were analyzed dynamically at a heating rate of 10°C/min in an air atmosphere. The mass of samples was 100 mg. The reference substance was aluminum oxide. To handling the results obtained, the statistical analysis was applied using the StatGraphics Plus5 software package at significance level of 0.95 % (P-value < 0.05).

RESULTS

Cultivar Medove grown on mining substrates mainly conformed to the varietal characteristics. However, the plants grown on red brown clay, green-grey clay, and black soil were slightly lower (Table 2). Fresh biomass yield on these substrates was also lower than on loess-like loam. Thus, the lowest yield was recorded on green-grey clay (38.05±0.13 t ha^{-1}), and highest on loess-like loam (82.5±0.36 t ha^{-1}). The sewage sludge application on loess-like loam had no effect on biometric parameters and biomass yield. At the same time, the positive effect was observed on others substrates (Figure 2). The growth and productivity indicators have increased by 4-16% and by 14.5-44.5% respectively.

Table 2. Effect of the sewage sludge application on the height of cultivar Medove

	Black Soil	Loess-like loam	Red brown clay	Grey-green clay
Without fertilizer	255.2±3.03	295.3±4.92	250.1±1.15	235.3±1.99
With the sludge application	295.3±2.31	300.0±2.70	260.2±1.66	250.4±1.65
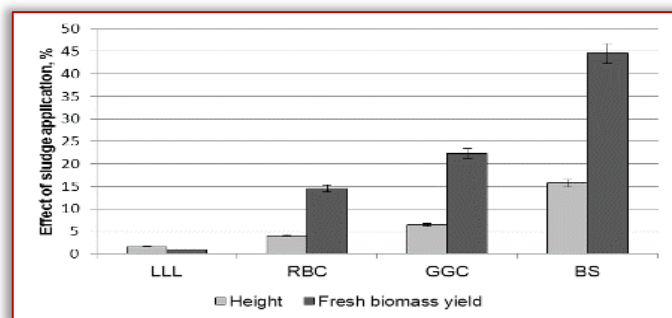
Figure 2 - Effect of sewage sludge application on growth and productivity of sorghum Medove grown on mining substrates

Due to the low biomass productivity on green-grey clay the conservative sugar yield was also small (2.75 t ha^{-1}). The highest yield was obtained on loess-like loam (5.91 t ha^{-1}). The same trend persisted in determining the theoretical ethanol yield, which was from 1611.4 L ha^{-1} to 3455.4 L ha^{-1}.

The sewage sludge introduction has reduced the content of fermentable sugars in stem juice by 5.3-6.7%, except plants grown on green-grey clay. Brix values on the plots without fertilizer varied between 19.0-19.3%, and on the plots with sludge application between 18.0-18.1%. Only on green-grey clay this index was 19.6%. Considering that in both variants on loess-like loam the amount of juice in the stems was practically the same, the yield of potential sugar and ethanol decreased by 4% in the version with the use of

sewage sludge. On the other experimental plots, an increase in the theoretical ethanol yield was observed, especially on green-grey clay (Figure 3).
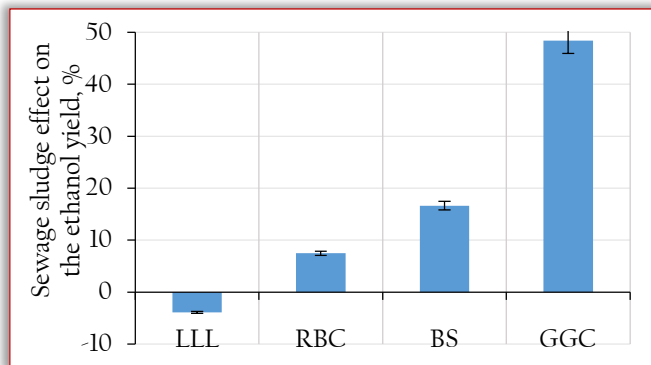
Figure 3 - Effect of sewage sludge application on theoretical ethanol yield of sorghum Medove grown on mining substrates

One of the most universal methods of treatment biomass for effective use as solid fuel is pyrolysis. Biomass is a highly reactive and thermally unstable raw material, so the low-temperature pyrolysis type is used for its processing (Fisher et al., 2002; Kumar et al., 2008). Conducted thermogravimetric analysis showed that thermolysis of Medove biomass passes in the temperature range from 30-40°C to 540-560°C. The water evaporation and the active removal of volatile components took place in the first stage within a temperature of 30-140°C (Table 3). The analysis of the rate of change in mass showed a single peak in this region. The mass loss was insignificant and varied within 5.2-8.6%.

In the second stage, the removal of volatile components was completed and the hemicellulose decomposition began. The mass loss was 13.6-14.2% (BS and LLL) and 17.4-19.6% (GGC and RBC). The highest rate of thermal reaction was observed at a temperature of 180-190°C. However, this rate was 14.0-14.4% / min for the samples taken on black soil and loess-like loam, and was almost twice as high on green-grey and red-brown clay (26.0%/min and 27.2%/min, respectively).

The main process of hemicellulose and cellulose decomposition was similar in all studied samples and took place in the temperature range 220-390°C (third stage). In this range, a small fraction of lignin decomposed as well. This phase was accompanied by the greatest mass loss (44.2-50.2%). The maximal rate of biomass destruction was 23.6-28.0%/min. During the last stage of thermolysis (390-560°C) thermal decomposition of cellulose and lignin was completed. In addition, the oxidation of formed at the previous stage char residue was occurred. At this stage, there were also no significant differences in the thermal behavior of biomass samples taken from different substrates. On the whole, the most complete combustion of biomass was observed on black soil.

The use of various amendments can affect the absorption of different elements from the soil and change the chemical composition of the biomass. This, in turn, can influence the process of thermal destruction. In our case, the sewage sludge application did not have any significant effect on the pyrolysis of sorghum biomass.

Nevertheless, some changes were noted in this process (Table 3, Figure 4). Thus, in the samples taken from black soil and green-grey

clay, the first three stages of thermolysis passed in zones of lower temperatures. On loess-like loam the last stage was longer. Also, there were small variations in the rates at different stages of the biomass destruction. Moreover, on black soil the share of residual mass was 78% bigger than on the plot without fertilizer.

Table 3. Data of Medove biomass thermal degradation on mining substrates

Stage of biomass destruction	Temperature interval, °C		Mass loss, %		The share of residual mass, %	
	without fertilizer	with sludge application	without fertilizer	with sludge application	without fertilizer	with sludge application
Black soil						
I	40–140	30–120	8.6	6.0		
II	140–220	120–180	13.6	9.6		
III	220–380	180–360	47.4	50.8		
IV	380–550	360–550	24.0	22.2	8.8	11.4
Loess-like loam						
I	30–130	40–130	6.4	4.2		
II	130–210	130–210	14.2	19.0		
III	210–390	210–380	50.2	44.0		
IV	390–540	380–570	20.4	22.4	6.4	10.4
Red-brown clay						
I	30–130	50–140	5.2	4.0		
II	130–220	140–220	19.6	16.0		
III	220–390	220–370	44.2	43.2		
IV	390–560	370–570	22.6	28.8	8.4	8.0
Green-grey clay						
I	30–140	30–130	6.6	7.6		
II	140–220	130–200	17.4	13.8		
III	220–390	200–370	44.2	43.0		
IV	390–540	370–550	22.2	26.0	9.6	9.6
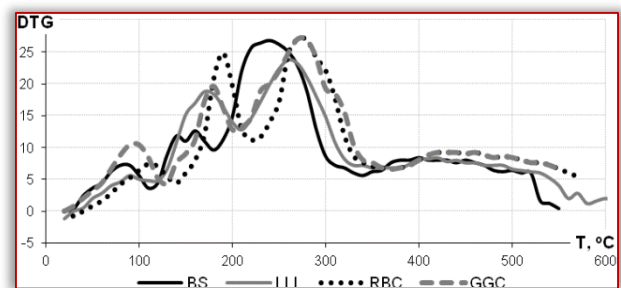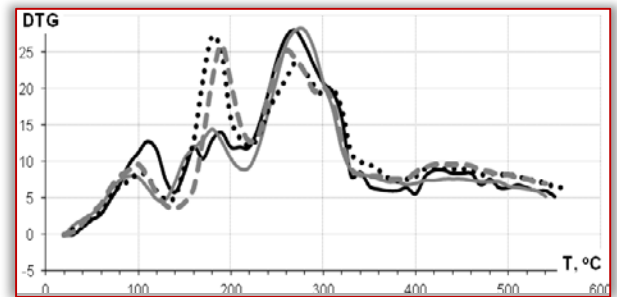
Figure 4 - DTG curves of biomass thermal destruction of sorghum cultivar Medove; variants without fertilizer (up) and with sewage sludge application (below).

CONCLUSIONS
Medove is a promising cultivar of sweet sorghum for growing on mining lands in areas of insufficient water supply. Under such

conditions it can produce above-ground biomass from 38 to 82 ta ha^{-1}. The sewage sludge application can promote increase of productivity by 4-44%. Although the sewage sludge introduction reduced the content of fermentable sugars in stem juice by 5.3-6.7% the theoretical ethanol yield was increased by 8-48%, except for the plot with loess-like loam.

Thermal destruction of dry biomass proceeded in a similar way on all studied substrates. It was revealed that the sewage sludge application shifts the process of thermolysis into the region of lower temperatures (for BS and GGC), increases the stage of lignin decomposition (for LLL), and affects the rates of the reactions, as well as slightly (LLL) and significantly (BS) augments the share of the incombustible residue.

Note:
This paper is based on the paper presented at ISB-INMA TEH' 2018 International Symposium (Agricultural and Mechanical Engineering), organized by Politehnica University of Bucharest – Faculty of Biotechnical Systems Engineering (ISB), National Institute of Research-Development for Machines and Installations Designed to Agriculture and Food Industry (INMA) Bucharest, The European Society of Agricultural Engineers (EurAgEng), Society of Agricultural Mechanical Engineers from Romania (SIMAR), National Research & Development Institute For Food Bioresources (IBA), University of Agronomic Sciences and Veterinary Medicine Of Bucharest (UASVMB), Research-Development Institute for Plant Protection (ICDPP), Hydraulics and Pneumatics Research Institute (INOE 2000 IHP), National Institute for Research and Development in Environmental Protection (INCDPM), in Bucharest, ROMANIA, between 01–03 November, 2018.

References
[1] Dalla Marta A., Mancini M., Orlando F., Natali F., Capecchi L., Orlandini S. (2014). Sweet sorghum for bioethanol production: Crop responses to different water stress levels. Biomass and Bioenergy, vol. 64, pp. 211-219
[2] De Kimpe C.R. & Morel J-L. (2000). Urban soil managment: a growing concern. Soil Science, vol.165(1), pp.31-40
[3] Ekefre D.E., Mahapatra A.K., LatimoreJr.M., Bellmer D.D., Jena U., Whitehead G.J., Williams A.L. (2017). Evaluation of three cultivars of sweet sorghum as feedstocks for ethanol production in the Southeast United States. Heliyon, vol. 3. e00490, pp. 1-18
[4] Fisher T., Hajaligol M., Waymack B., Kellogg D. (2002). Pyrolysis behavior and kinetics of biomass derived materials. Journal of Analytical and Applied Pyrolysis, vol. 62(2), pp.331-349
[5] Goff B.M, Moore K.J, Fales S.L, Heaton E.A (2010) Double-cropping sorghum for biomass. Agronomy Journal, vol. 102(6), pp 1586-1592
[6] Hossain M.K., Strezov V., Chan K.Y., Nelson P.F. (2010). Agronomic properties of wastewater sludge biochar and bioavailability of metals in production of cherry tomato (Lycopersicon esculentum). Chemosphere, vol. 78(9), pp.1167-1171
[7] Jamali M.K., Kazi T.G., Arain M.B., Afridi H.I., Jalbani N., Memon A.R., Shah A. (2007). Heavy metals from soil and domestic sewage sludge and their transfer to Sorghum plants. Environmental Chemistry Letters, vol. 5(4), pp.209-218
[8] Kumar A., Wang L., Dzenis Y.A., Jones D.D., Hanna M. (2008). Thermogravimetric characterization of corn stover as gasification and pyrolysis feedstock. Biomass and Bioenergy, vol.32(5), pp.460-467
[9] Mathur S., Umakanth A.V., Tonapi V.A., Sharma R., Sharma M.K. (2017). Sweet sorghum as biofuel feedstock: recent advances and available resources. Biotechnol Biofuels, vol. 10: 146, pp. 1-19
[10] Prasad S., Singh A., Jain N., Joshi H.C. (2007). Ethanol production from sweet sorghum syrup for utilization as automotive fuel in India. Energy & Fuels, vol. 21(4), pp. 2415-2420
[11] Ratnavathi C.V., Suresh K., Vijay Kumar B.S., Pallavi M., Komala V.V., Seetharama N. (2010). Study on genotypic variation for ethanol production from sweet sorghum juice Biomass and Bioenergy, vol. 34(7), pp.947-952
[12] Reddy, B V S and Kumar, A A and Ramesh, S (2007) Sweet sorghum: A Water Saving Bio-Energy Crop. In: International conference on Linkages between Energy and Water Management for Agriculture in Developing Countries, 2007, ICRISAT, Patancheru, India, pp.1-12
[13] Regassa T.H, Wortmann C.S. (2014). Sweet sorghum as a bioenergy crop: literature review. Biomass Bioenergy, vol.64, pp.348-355
[14] Rooney W.L, Blumenthal J, Bean B, Mullet J.E (2007) Designing sorghum as a dedicated bioenergy feedstock. Biofpr, vol.1(2)
[15] Rutto L.K, Xu Y., Brandt M., Ren Sh., Kering M.K. (2013). Juice, Ethanol, and Grain Yield Potential of Five Sweet Sorghum (Sorghum bicolor (L.) Moench) Cultivars. Journal of Sustainable Bioenergy Systems, vol.3, pp.113-118
[16] Schmer M.R, Vogel K.P, Varvel G.E, Follett R.F, Mitchell R.B, Jin V.L. (2014). Energy potential and greenhouse gas emissions from bioenergy cropping systems on marginally productive cropland. PLoS ONE, vol.9(3), pp. 1-8
[17] Singh R.P., Agrawal M. (2008). Potential benefits and risks of land application of sewage sludge. Waste Management, vol. 28(2), pp.347-358
[18] Wang X., Chen T., Ge Y., Jia Y. (2008). Studies on land application of sewage sludge and its limiting factors. Journal of Hazardous Materials, vol. 160(2-3), pp.554-558
[19] Wortmann C.S., Liska A. J., Ferguson R. B., Lyon D. J., Klein R. N., Dweikat I. (2010). Dryland Performance of Sweet Sorghum and Grain Crops for Biofuel in Nebraska. Agronomy Journal, vol. 102(1), pp. 319-326
[20] Wu, X., Staggenborg, S., Propheter, J.L., Rooney, W.L., Yu, J. & Wang, D. (2010). Features of sweet sorghum juice and their performance in ethanol fermentation, Industrial Crops and Products, vol. 31(1), pp. 164-170
[21] Yin R., Liu R., Mei Y., Fei W., Sun X. (2013). Characterization of bio-oil and bio-char obtained from sweet sorghum bagasse fast pyrolysis with fractional condensers. Fuel, vol. 112, pp.96-104
[22] Yu J.,Zhang T., Zhong J., Zhang X., Tan T. (2012). Biorefinery of sweet sorghum stem. Biotechnology Advances, vol. 30(4), pp.811-816

1.Alexandra Liana VIŞAN, 1.Dumitru MILEA, 1.Anişoara PĂUN,
1.Gabriel Constantin BOGDANOF, 2.Gheorghe STROESCU

A SURVEY REGARDING THE PERFORMING DRYERS USED IN MARC CAPITALIZATION TECHNOLOGIES

1. National Institute of Research - Development for Machines and Installations for Agriculture and Food Industry – INMA Bucharest, ROMANIA
2. Universities Polytechnic Bucharest, Faculty of Biotechnical Systems Engineering, ROMANIA

Abstract: In the current context of the waste capitalization technologies development designed for wine industry focus on the aspect of integration in industrial flows that respect the concept of circular economy and thus the economic process sustainability is justified on medium and long term. A representative part of the process waste of wine is grape marc (skins and seeds). The grape seeds have a particular importance because they are used to obtain nutritionally valuable oils, and the drying process can damage the final raw product quality, from this reason in this paper are presented some advanced equipment's
Keywords: dryers seeds, mark capitalization, seed qualities, mark technologies

INTRODUCTION

The marc capitalization technology used by the wine producers are mainly used to obtain bio-fuels but due to latest research in Phyto-pharmaceutic field revealed that the fresh mark can be used also as an important source of oxidants and valuable compounds for the human health, and in many other related fields (animal and fish feeding, soil bio-nutrients, etc.). Taking in to consideration that wine industry is present on all continents, the technical and environmental potential and impact has a great impact, for this reason the regenerative systems "is a must", because the resource input are the wine waste, emission, and energy leakage are minimized by slowing, closing, and narrowing energy and material loops.

The means to achieve circular economy, respectively "long-lasting design, maintenance, repair, reuse, remanufacturing, refurbishing, recycling, and upcycling" (Geissdoerfer, M, at all, 2017), is in contrast to linear economy which has a production model like 'take, make, dispose'. (Ellen MacArthur Foundation, 2012).

In favor of the circular economy approach is mentioned the next arguments: to achieve a sustainable world does not involve to change product quality and consumers purchasing power; doesn't require loss of revenues or extra costs for manufacturers and other economic agents. But the circular economy focuses on areas such as design thinking, systems thinking, product life extension, and recycling, in order to achieve models that are economically and environmentally sustainable, idea supported by most researchers and experts in the field of economy.

Based on the circular economy principles, the study of feedback-rich (non-linear) systems are similar to particularly living systems (Ellen MacArthur Foundation, 2012) and its practical applications to economic systems evolved incorporating different features and contributions from a variety of concepts sharing the idea of closed loops. Some of the relevant theoretical influences are cradle to cradle, laws of ecology, looped and performance economy, regenerative design, industrial ecology, biomimicry and blue economy. (Geissdoerfer, M, at all, 2017)

In 2017 in order to provide guidance to organizations that implement circular economy strategies, the British Standards Institution (BSI) developed and launched the first circular economy standard "BS 8001:2017 Framework for implementing the principles of the circular economy in organizations. Guide". BS 8001:2017 standard, intend to align the far-reaching ambitions of the CE with established business routines at the organizational level. It contains a comprehensive list of CE terms and definitions, describes the core CE principles, and presents a flexible management framework for implementing CE strategies in organizations. Circular economy monitoring and assessment is given, but it missing the consensus yet on a set of central circular economy performance indicators applicable to organizations and individual products.

This fact is generated maybe, because there are not yet implemented this system and the environmental polices strong enough to stimulate and reward the participants, or because the sanctions and fines have no impact on the phenomenon generators enough to stop and mitigate the contaminated sites.

Wine trade between the EU and third countries excels, with exports reaching the level of 6,7 billion euro, in 2010, almost a quarter of European exporters of agricultural products. Economically speaking, European production plays a strategic role, having in to consideration the fact that in 2016, the wine market turnover reached 377 million euro and it is estimated that in 2017 to be 385 million euro, reaching the highest level in recent years. The Romanian market place in the big wine producers in the world is placed on 13-th position, next to Portugal (6,6 mhl), Hungary (2,9 mhl) and Austria (2,4 mhl), and is among the few European countries that have registered an increase compared to 2016. According to KeysFin analyses, after more than 10 years of changes and reorganization, wine sector business has come close to maturity. (Chiriţă C., 2018)

In Romania from approximately 1 million tons of grapes used to processes wine, are obtained 120,000 tons of marc without bunch and 400,000 hectoliters of yeast. Usually from 1 tone of grapes it is made 1.2 [kg] of tartaric acid, 180 [kg] of marc and 4.5 [kg] of yeast, and by processing the marc and yeast is resulted 8.8 [l] alcohol, approximate 22 liters of yeast brandy of 40 % vol. (Pomohaci Nicolai, 2002).

If we apply the concept of circular economy in Romania, the innovative technology to capitalize marc is perfect integrable and can create a valuable chain reaction, see Figure 1, and in the main beneficiary is the human being for the food product (wine, grape seed flour and oil) and phyto-pharmaceutical.

Figure1 - An example of wine technological process combined with marc capitalization technology respecting the principle of circular economy (Milea, et all, 2018)

In some cases, the direct beneficiaries are the farm animals (bio concentrates with high nutritional intake in the form of pellets – as it is implemented in Nebraska Screw Press company) and the farmers because in the soil management process can be integrated the bio-fertilize technologies, namely bio-compost (fertilizers, if using the earth worm technology - one of the newest applications in the field) (Domínguez J., at all, 2016).

MATERIAL AND METHOD

Taking in to consideration the technological aspect of agro-ecosystem sustainability and ecological aspects of waste recycling, the INMA presents an innovative technology to recover the vineyard by-products, in accordance of newest trends in this field of activity, see Figure 2.

This technology its working upon a logical order to ensure the technological grape seed separation from skins, in accordance with specific processes of secondary material, which can be later capitalized in multiple ways and new products.

As it can be noticed, in this technology it is presented a primary segregation equipment that has a washing unit, this unit it is optionally, but it is necessary in case fresh marc separation followed by obtaining high quality grape seeds used for grape oil extraction. Furthermore, within the marc/grape seed technological flow is used drying equipment's, this operation is important because it influence the purity and quantity of grape seeds (Pomohaci Nicolai, 2002) and is stipulated that the maximum temperature to be 110ºC, in order to assure a humidity of 11÷12% during the conservation/deposition period and to provide sterile conditions to inhibit the growth of acetic bark and mildew lead to the degradation of extractives.

Usually in industrial technologies are used convective driers, typically the wet grape seeds come into contact with the drying agent, hot air or combustion gases, from which it receives by convective process the heat required by drying process; in most cases the drying agent is air.
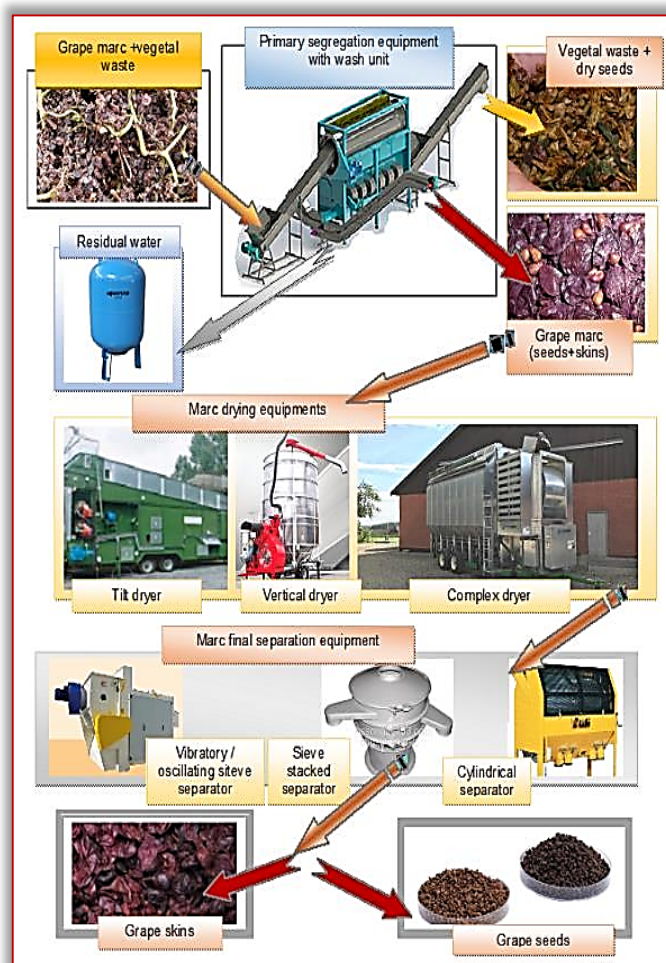
Figure 2 - Innovative technology to capitalize preclean grape marc (Milea, et all, 2018)

In the drying technique, outside of this type of dryer are also used: the intermediate heating dryer, the recirculation dryer, the recirculation and the intermediate heating dryer, and also the closed-circuit dryer. This large verity is influenced by the technologic flow placement, material low (in charge or in continuous flow), and the heating agent flow or with energy saving circuit. In the next paragraph will be presented several types of commercial driers.

RESULTS

Various stages of the technological process to capitalize the grape marc, are used for drying of, either whole material or its components, shells and seeds. In the following, some constructive variants will be briefly presented.

Intermediate heating dryer. From this category, on the market is the Alvan Blanch continuous double flow drier, is manufactured by UK and it is promoted also by Rusland company from Russian, because has in its construction a transport chain which takes the material on two ding levels: the upper level for hot-air drying and the lower level for cold air treatment to prevent hot spots when stored.

Also, this equipment is used on USA seed processing technologies to decrease from 25 % to 9 %, the temperatures that can be achieved are from 70 until 110 [⁰C]. An advantage is to remove particles of dust and chaff from the processing material, the light

part is discharged through the upper air vents into the collector box, and the heavier part is deposited at the base thereof. This system is necessary to reduce the risk of fire. The automatic control system ensures the flow control and the sensors placed on the power supply signal if there is no material, and there are also sensors for detecting possible blockages, overheating of the grain, overcharging of the motors and burner failure, as well as stopping the equipment in case of failure.
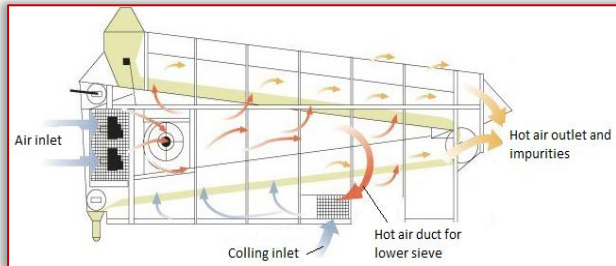
Figure 3 - The working principle of the continuous flow dryer [10]

Another constructive solution for chare flow dryer is the model presented in Figure 4, manufactured by PEDROTTI company from Italy, this model also can be found manufactured by the ex-communist states (like: Russia, Hungary, etc.). According to its spreading, it is noticed that this system is the favorite of seed/cereal processors and its technical advantages appreciated and used at large scale. This drying system is in line with technological developments and can be easily adapted to the processors needs.

Figure 4 - PEDROTTI trailed vertical dryer [11]
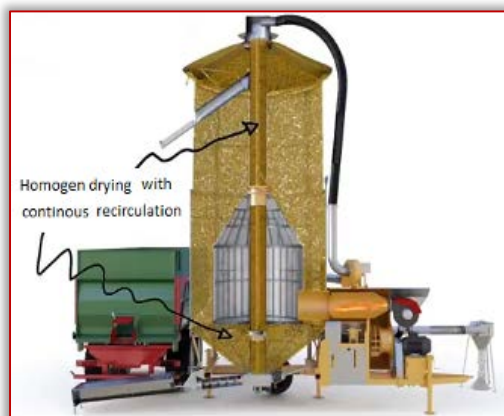
Figure 5 - Grain vertical dryer – FSN [12]

The Mecmar Company has the FSN model, see Figure 5, to dray cereals, sorghum, grape seeds, etc., in a closed loop circuit. This equipment was designed to make 5 operations: supplying, draying,

cooling, impurities selection and evacuation, and this working capacity can vary.

Recirculation dryers can be with different structures and gauges, apart from the model shown in Figure3 can be presented also the high humidity dryer manufactured by Stronga company. In Figure 6, is presented the working principle and the main components. The working draying principle is mainly the hot air diffusion in all processing material due to the belt transportation conveyor that generates also a waving motion.

a)
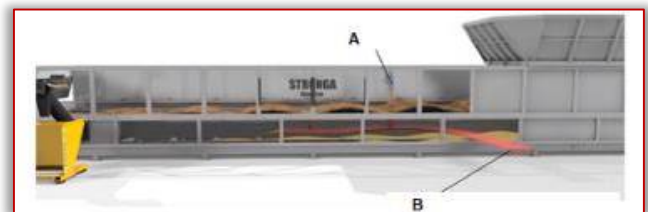
b)

Figure 6 - High humidity cereal and granular materials dryer [13]
1-supplay bunker; 2-programable control station; 3-pulsing draying belt;4 – go forth scraper transport system; 5- outlet opening; 6 -thermic isolation; 7 – transversal conveyor for small particles; A- diffusion hot air flow; B- hot air inlet provided by HEATEX.
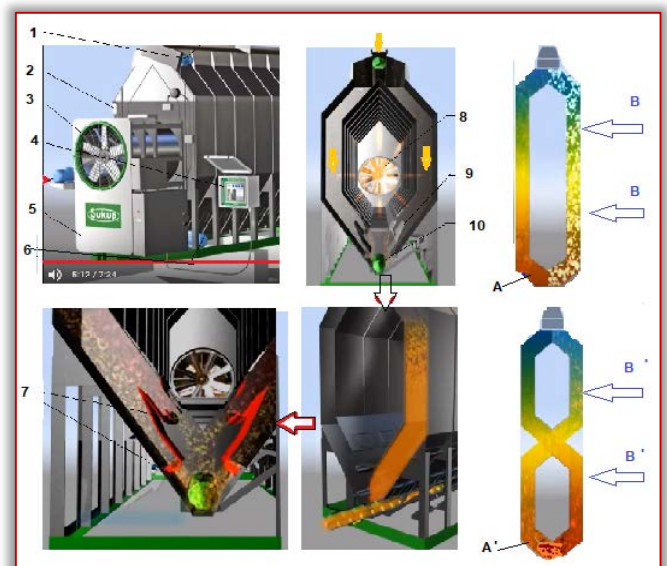
Figure 7 - FSN cereal/seed dryer working principle and patent drying solutions [14]
1-engine to supply conveyor; 2-process lighting boll; 3-ventilation system; 4- control and command panel; 5--heat generator; 6-seed outlet conveyor engine; 7-seed flow distributor 8-heating source; 9-distribution and weighting system; 10- outlet system with sensors; A and A'- drayed cereals; B and B'-cold air flow-wind.

SUKUP dryer, manufactured by DANCORN, has an interesting design and the drying process is fully automated and controlled, see Figure 7. Thus, model has a complex structure with modular construction and patented heating circuits with recirculation system in order to recover energy and optimize drying operation, constructing a closed-circuit dryer equipment. This model also is provided with innovative elements to assure maintenance and easy replacement of the moving parts.

Recirculation and the intermediate heating dryers, are used at large scale, such systems are rotative dryers, as develops the WESTPRO company, see Figure 8.

Figure 8 - Tubular rotative dryer [15]

These solutions are used mainly to industrial scale and have low maintenance, because: low cost of spare parts; low labour; are self-centring and do not have gears or chains which can easily be swallowed. Usually their dimension is external diameter of 0.6÷2.7 [m] and length of 0.4÷1.65 [m]. Depending on the processed material humidity, the rotary drum is provided with various ravaging systems, such as longitudinal and radial vanes (Figure9), wings (Figure9 b-f), helical profiles (Figure 9.g and j), dedicated profiles for different types of materials and their combinations (Figure9. k, m and n).
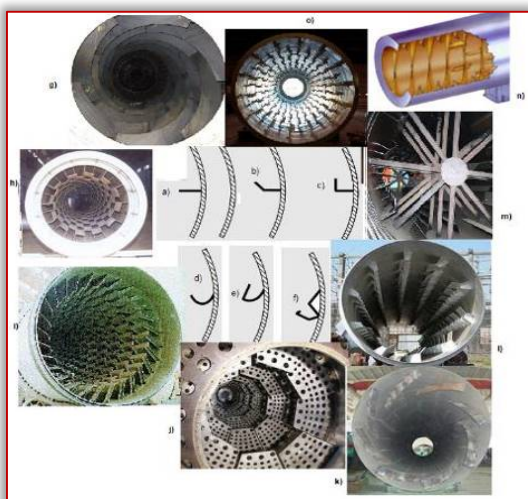
Figure 9 - Rotary drum is provided with various ravaging systems

In USA the company Economy Industrial have manufactured combined drying systems and separations of the solid granular materials with high humidity. The constructive solution is presented in Figure9.and presents 4 sectors: fan induction system; a rotary dryer; a rotating screen for separating the material and a heating system. For the maintenance of the separation element (sieve/sieves), a brush system parallel to the sieve axis is also provided to detach the wet material from the orifices of the rotary sites.
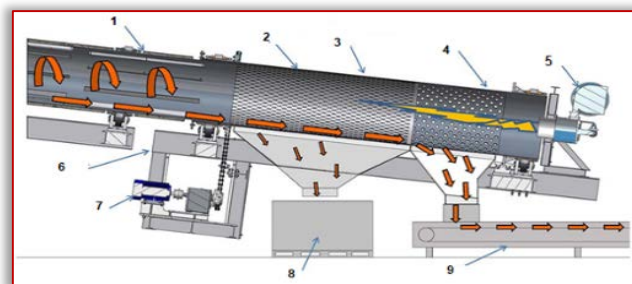
Figure 9 - Combined drying equipment to process granular material at industrial scale [16]

1-rotary dryer; 2-separation sieve (2 mm mesh); 3-rotary screen; 4-separation sieve (2-40 mm mesh); 5—heating chamber; 6-rotary screen support; 7-power engine of the rotary screen; 8- collector chamber; 9-Transport conveyor toward the packing and storage.

CONCLUSIONS

This survey has the purpose to present the technical state of seed dryers, that manly have the same working principle of the cereals ones, and their place in the marc capitalization technologies, a very appreciated by product in food and phytopharma industry due to their low harmful cholesterol, high content of mineral and antioxidants.

Here in presented technology has a modular structure and can integrate a large variety of performant equipment's, which can be harmonized and suited in an flexible technical processing flow that can be adjusted in accordance with seed (granular material) mechanical and physiologic characteristics, and also of mark state (humidity, seed concentration, marc components, etc.) that in many cases is processed in fresh state, right after it was exhausted from the grape pressing lines.

Another technical fact that can be observed, is the fact that drying equipment's have many constructive features that can be used in almost all processing conditions: on site, outdoors or on platforms, but also in the industrial halls. In almost all the cases presented on internet the marc processing lines are placed on open halls, especially when is processed the fresh marc, because the large marc quantity that the fermentation process is not finished and du this fact the working environment must be well ventilated.

Acknowledgement

Research and Development in Environmental Protection (INCDPM), in Bucharest, ROMANIA, between 01–03 November, 2018.

References

[1] Chiriţă C., (2018), Potentialul de specializare inteligenta in domeniul Vitivinicol in regiunea Sud-Est, Seria "Rapoarte privind ecosistemele de inovare" (Intelligent specialization potential in viti-viniculture field in Sud-Est region, Series "Reports on Innovation Ecosystems") Published by UEFISCDI;

[2] Domínguez J., Martínez H., Lores M., (2016) Earthworms and Grape Marc Simultaneous Production of a High-Quality Biofertilizer and Bioactive Rich Seeds; Grape and Wine Biotechnology, Chapter 8, Inteh Publisher, DOI: 10.5772/64751;

[3] Ellen MacArthur Foundation. (2012), Towards the Circular Economy: an economic and business rationale for an accelerated transition. "Developing BS 8001 - a world first". The British Standards Institution. Retrieved 29 December 2017;

[4] Geissdoerfer M.; Savaget P.; Bocken N. M. P.; Hultink E.J., (2017). "The Circular Economy – A new sustainability paradigm?". Journal of Cleaner Production. **143**: 757–768, doi:10.1016/j.jclepro.2016.12.048;

[5] Milea D., Vişan A.L., Păun A., Bogdanof C.G., Ciupercă R, (2018), Technological and ecological aspects of some wine waste recycling and their capitalization in food industry, Annals of the University of Craiova - Agriculture, Montanology, Cadastre Series, vol. XLVIII/2018;

[6] Ponohaci Nicolai, (2002) Tuica si rachiurile naturale, Editura Ceres, Bucuresti;

[7] Milea D., Visan A.L, Prospective study regarding actual technology to recovery the viticulture by-products and the capitalization oportininities (Studiu prospectiv privind tehnologiile actuale de recuperare a produselor secundare din viticultură şi modul lor de valorificare), phase 1 from project PN 18 30 02 01, made by INMA;

[8] https://www.westpromachinery.com/;

[9] http://economyindustrial.com/rotary-dryers.html.

Fascicule 3
⌈ April - June ⌉
t o m e
⌈2019⌉ XII

ACTA Technica CORVINIENSIS
BULLETIN OF ENGINEERING

[1.]Jozef POBIJAK, [1.]Andrej CZÁN, [1.]Michal ŠAJGALÍK, [1.]Tomáš PAVLUSÍK

DESIGN OF A MEASURING INSTRUMENT FOR A COMPONENT USED TO SYNCHRONIZE THE SPEED BETWEEN TRANSMISSIONS

[1.] Department of Machining and Manufacturing Technology, University of Žilina, Žilina, SLOVAKIA

Abstract: In today's modern times, it is necessary to simplify and speed up the work. Great advantage and help in this area, are auxiliary workshops, which we call briefly the preparations. These are used today in virtually every manufacturing process. This work deals with the design of the equipment, control auxiliary equipment. The work is deals with the issue of auxiliary workshops. In particular, a control device to be designed for components for synchronizing the speeds between gears in automobiles. The introduction is describe the need for such equipment in enterprises are of a technical and economic importance. In the core of the work is described and illustrated the device design itself, with a brief functional description and control procedure. Part of the work is to verify the facility's capability using the statistical method. Benefits and appraisal of work for a given area of application of the proposed equipment are presented at the end of this paper.
Keywords: device, equipment, control, design

INTRODUCTION

In today's modern era of fully modern and progressive technology is a very strong emphasis placed on the continuous acceleration of production and control processes in the field. In carrying out these processes is labor productivity significantly affected, and so on business creation. Productivity of work is possible improve then, that for example in company are improve manufacturing and control processes. [3] In the production process (especially mechanical), it acts on the manufactured component, respectively. to the produced component size, the entire chain of influences, and in fact it is not possible to produce a component with a perfectly precise dimension and the dimension produced must be checked. The question of control in engineering companies (especially automotive) is very important, but also financially demanding. [1,2] This fact, forces companies to get the equipment they can do use effective its function. One such device is an auxiliary workshop device. Their technical significance consists mainly of easier assurance of accuracy, reduction of non-production, reduction of physical effort but also reducing the requirements for qualified service. [1] The issue of auxiliary device will also be dealt with in this article. Specifically, the design of the device for a component witch to use on synchronizing speed between the gears in the car transmission. [2]

THE PART FOR THE DEVICE IS TO BE MADE

The requirements for the device design depend on the measured parameters on the component. It is a component that is mounted in a car transmission and its main task is to synchronize the speed between the gears. The design of the device will be designed to measure or control important parameters according to the manufacturing process. Due to the fact that the part has a conical shape, it is important to keep the cone 9 ° 40 '± 0 ° 5'. This cone angle on the component is controlled by another device before checking the other parameters. This means that the proposed device will control the parts that have passed the angle check. The device will control the depth or distance from the front of the ring 4,8 ± 0,07 mm. At this depth should be on the component kept

average Ø58,09 mm on the conical part as shown in Figure 1. The entire check should be performed at 100 N ± 10 N load according to the request. The device will record deviations from 4.8 ± 0.07 mm. This measurement has so far been carried out on three-axis measuring device. This has had disadvantages such as: long measuring sections, inability to measure the ring under load, the need for qualified service personnel to work with a three-axis measuring device.
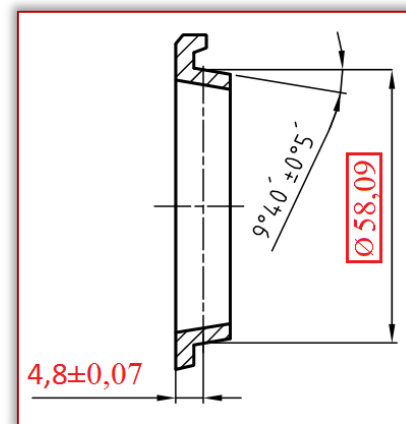
Figure 1: Measured component parameters for control

PRINCIPLE, SCHEMA AND DEVICE DESIGN

The device is designed to ensure fast, simple, and accurate component control. Controlled components will be placed on the motherboard and this motherboard must ensure exact horizontal position. As required, the ring must be under load 100N±10N, and under this load measured. The load to act on the component guarantees the weight of the designed top.

The upper part of the device is coupled with the produced "counterpart" of the synchronous ring (measuring cone) through the guide. The measuring cone is precisely manufactured so that at a certain point from its lower edge - specifically 1.1 mm - it has a value of the diameter of the inner conical part ø58,09 mm. A digital deviation is mounted on the top of the device and the measuring tip is in contact with this part and records the dimensional

deviations. For the proper operation of the device, it is necessary to produce an adjusting member. The adjusting member is made very precisely to the size of the ideal synchronous ring. Before the rings are checked, it is necessary to adjust the device using the adjusting member. The adjusting member is located on the base and the measure cone is pressed on it with power 100N. Since both pieces are made as counterparts with a value of average at a given location ø58,09 mm, these locations will overlap as shown in Figure 2. The diverter is reset by the operator and the device is set in this way. After setting up the device, check the synchronic rings. We will place the synchronic ring on the main board and push the cone through the line on a ring. Consequently, the digital deviation detects deviations from the required dimensions.
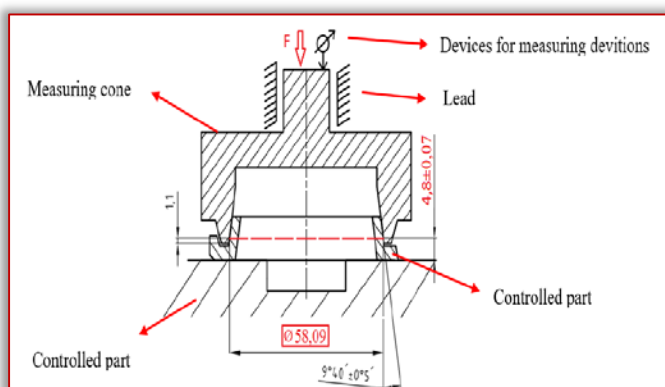
Figure 2: Schematic view of the proposed device
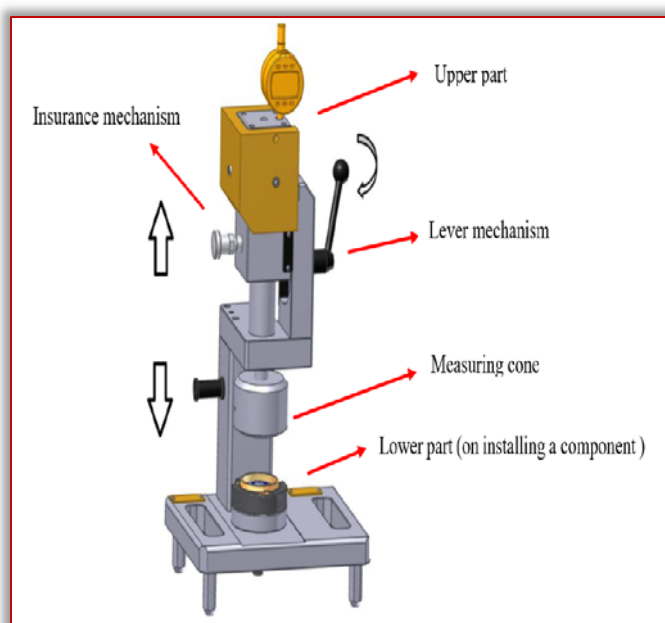
Figure 3: Device model

Figure 3 shows a model of a control device consisting of two main parts, the top and the bottom. The top part is equipped with a lever mechanism which, ensures its vertical movement. This part also includes components that ensure that a force of 100 N is applied to the measured synchronous ring, and also includes a meter with a mechanism that detects deviations from the nominal size on the controlled parts. This section also includes a functional part of the device, a measuring cone, which is in direct contact with the control ring and checks with a comparative measurement that the

parameter is in the tolerance field. The main function of the lower part of the device is location a controlled ring or adjusting member. Figure 3 shows the starting state of the device. The lever of the mechanism is in the upper location, which means that the movable part with the measuring cone is in the upper position.

The mechanism is designed so that the lever cannot be released automatically, thanks to the safety mechanism. Before starting the synchronous ring check itself, you need to set the device using the adjusting element that is part of the design.

So as possible to move the lever, the locking mechanism must be unlock. By moving the lever in the arrow direction in Figure 3, the measuring cone is pushed into the adjusting member until it stops. In the lower position overlaps the ø58,09 mm value on the measuring cone with the same value of the diameter of the adjusting member at a height of 4,8 ± 0,07 mm (according to the scheme in Figure 2).

The operator then sets the digital deviation. After setting, the measuring cone is pulled out of the adjusting member by means of the lever, so that insurance mechanism gets into starting place. Then the operator selects the adjusting member from the meter. At this stage, the device is ready for checking synchronous rings. The controlled ring is placed on the main washer. Again, the safety mechanism has to be unlocked and the measuring cone into the controlled ring is inserted by the lever. The operator then sees the deviation from the nominal size on the display.

VERIFY DEVICE PROPERTIES

Is possible use multiple authentication methods to check device accuracy. Device capability will confirm the functionality of the device and the data that will be measured will be trustworthy. The device was checked using statistical method where the functionality of the device is expressed using the Cgm and Cgmk indices. The facility's capability check is composed of repeated measurements at the place, where the gauge is uses.

The device performs 30 repetitive measurements and the resulting values are written into table, which is later the basis for the chart. Values that have been detected are put into relations for the mean value of the mean Xa, and the standard deviation Sw, and of them then calculate the Cgm and Cgmk eligibility indices.

Table 1: Values n, measured by the device in micrometers (μm)

-34	-33	-33	-34	-32	-32	-30	-32	-33	-33
-31	-31	-33	-32	-33	-31	-35	-31	-31	-32
-33	-33	-33	-32	-32	-33	-33	-33	-33	-33
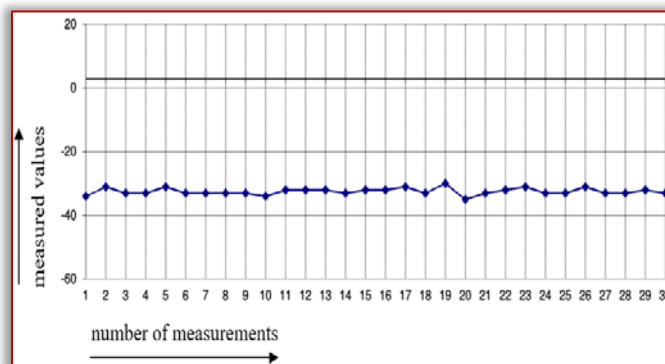
Figure 4: Dependence of the measured values on the number of measurements

Average value of the mean:

$$X_a = \frac{1}{n}\sum_{i=1}^{n} x_i = \frac{1}{30}\sum_{i=1}^{30} \text{-34; -31} \ldots = \text{-32,467 µm}$$

Standard deviation:

$$S_w = \sqrt{\frac{1}{n-1}\sum_{i=1}^{n}(X_i - X_a)^2} =$$

$$\sqrt{\frac{1}{30-1}\sum_{i=1}^{30}(\text{-34 - (-32,467)})^2} = 1,074\mu m$$

Process capability index:

$$C_{gm} = \frac{0,2T}{6.S_w} = \frac{0,2 .140}{6 .1,074} = 4,344$$

Top process capability index:

$$C_{gmKU} = \frac{(X_r + 0,1T) - X_a}{3.S_w} =$$
$$\frac{(-32+0,1 .140)-(-32,467)}{3 .1,074} = 4,488$$

lower process capability index:

$$C_{gmKL} = \frac{X_a-(X_r-0,1T)}{3.S_w} =$$
$$\frac{-32,467-(-32-0,1 .140)}{3 .1,074} = 4,199$$

The criterion for assessing the accuracy of the device is Cgm ≥1,34 and CgmKU, CgmKL ≥ 1,33. In the index CgmKU and CgmKL is the correct value that is less. It follows from that, that the device is correct.

CONCLUSION

The component for which the device was designed and constructed was at the factory first controlled by a three-axis measuring device. The main disadvantage of checking on a triangle measuring device and therefore the reason for solving this problem was: long control times, the need for an operator who can control the device software, training the operator, and the inability to control the component under load 100N.

The design itself was based on that the device was able to measure the relevant parameters on the synchrony ring under load, but in order to ensure simple operation of the equipment as well as fast and safe operation. The device is designed so that its movable part, ending with the measuring cone, which is pressed into the synchronous ring by a simple lever movement, proved load the ring and on display image the dimensional deviation from of nominal value.

Checking the rings is possible after setting the product with the adjusting member, which serves to preserve and reproduce the dimensional quantity. The main benefit of the designed product is to significantly reduce the time it takes to component check, simple operation and the possibility of checking the rings under the appropriate load.

In the measurements it was found that the measured values produced by new design device (synchronous ring measured under load) and three-axis measuring device, were different only minimal, in order of thousands of millimeters.

Note:

This paper is based on the paper presented at ERIN 2018 – The 12th International Conference for Young Researchers and PhD Students, organized by Brno University of Technology, CZECH REPUBLIC and Slovak University of Technology in Bratislava at Faculty of Mechanical Engineering, SLOVAKIA, in Častá-Papiernička, SLOVAKIA, between 02–04 May, 2018.

References

[1] M. Drbúl, A. Czán, M. Šajgalík, M. Piešová, K. Stepien: Influence of normal vectors on the accuracy of product´s geometrical specification in proceedia engineering, (2017).

[2] M. Drbúl, M. Šajgalík, J. Šemcer, T. Czánová, L. Petrkovská, L. Čepová: Metrology and quality of surfaces created by machining technologies, (2014).

[3] A. Czán, M. Šajgalík, J. Holubiak, M. Piešová, T. Czánová: Simulation of residual stresses in surface and subsurface layer after machining in communications, (2016).

Fascicule 3
[April - June]
t o m e
[2019] XII

ACTA Technica CORVINIENSIS
BULLETIN OF ENGINEERING

¹·Adeoye O. AKINOLA, ²·Akinlabi OYETUNJI

EFFECTS OF DIFFERENT ENVIRONMENTS ON THE CORROSION PROPERTIES OF WELDED MILD STEEL PLATE

¹·Department of Mechanical Engineering, The Federal University of Technology, Akure, NIGERIA
²·Department of Metallurgical and Materials Engineering, The Federal University of Technology, Akure, NIGERIA

Abstract: The study on the effects of diffent environment on the corrosion properties of welded mild steel was evaluated using the weight loss analysis method. Chemical analysis was done on the mild steel plate using ARX spectrometer. Three sets of samples were used; two samples were not subjected to any corrosive environment. Two other samples were immersed in 0.3 M NaCl and the last two samples were immersed in water. Results showed that the un-welded samples exhibited greater loss in weight compared to the welded samples; the rates of corrosion of welded samples were observed to be lower in comparison with their un-welded counterparts in their corresponding corrosive environment, and the maximum values of corrosion rates of the samples were obtained for un-welded steel sample immersed in 0.3 M NaCl (1.924344 mg/mm^2/yr.); welded steel sample immersed in 0.3 M NaCl (0.509108 mg/mm^2/yr.); un-welded steel sample immersed in water (0.001821018 mg/mm^2/yr.); and welded steel sample immersed in water (0.000780731 mg/mm^2/yr.).
Keywords: environments, corrosion, weight loss, welded and un-welded samples

INTRODUCTION

Mild steel is a type of steel alloy that contains a low amount of carbon as a major constituent. Its carbon content falls within the range 0.10 – 0.25% of low carbon steel. Mild steel is the most common form of steel and it is the major material used in construction industry due to its low cost. Mild steel have good strength, hard and can be bent, worked or can be welded into an endless variety of shapes for from vehicles to building materials. Its unique properties such as low cost, high strength, hardness and easy availability, made it to have wide range of applications in many areas such as vehicle parts, truck bed floors, automobile doors, domestic appliances, nut bolt, chains, hinges, knives, armour, pipes, magnets and military equipment (Kumar and Yadav, 2013; Talabi, *et al.*, 2014).

The interaction of these materials with their immediate environment results in the deterioration of the mechanical properties (such as hardness, toughness, ductility and strength) and physical properties of the materials. In metals, there is actual material loss either by dissolution or by the formation of non-metallic scale or film (Callister, 2007). This material loss is as a result of corrosion. Corrosion can therefore be regarded as the gradual degradation, destruction or deterioration of a material, usually metals, by chemical reaction with its environment. This is done as a result of the electrochemical oxidation of metals in reaction with an oxidant such as oxygen. A common example of electrochemical corrosion is rusting, which is the formation of iron oxides. This type of oxides typically provides oxide(s) or salt(s) of the original metal. All environments are practically corrosive to some degree. Some examples are air and moisture; fresh, distilled, salt, and other gases such as chlorine and ammonia (Fontana, 2007).

Corrosion is a multifaceted phenomenon that adversely affects and deteriorates metals through oxidation. Corrosion degrades the useful properties of materials and structures including strength, appearance, and permeability to liquid and gases. Katundi *et al.*, (2012) characterized the corrosion resistance in the steel sheets (Hot dip galvanizing of steel sheets) used in automotive industry. They carried out simulated corrosion tests, wet/humidity test and hot dust/dry cycle talk test in laboratory conditions. They tested dynamic behaviour of the corroded specimens dynamically to simulate under the crash test conditions. They exposed the samples to changing climatic conditions in terms of humidity. It was also observed that pitting corrosion damage and crack initiation sites were developed and propagated.

This research focuses on the evaluation of the effects of diffent environments on the corrosion properties of welded mild steel plate for automobile body service application using the weight loss analysis method.

MATERIALS AND METHOD

⸺ Materials and Equipment

The materials used for the experiment include: low carbon steel alloy of known chemical composition, emery paper of the following grades (60, 120, 180, 220, 320, 400, 600, 800, 1200 grits), tong, plastic containers, diamond paste, and zinc rod. The chemicals used for the experiment are sodium chloride (NaCl) and distilled water. The following equipment were used for the research: universal polishing machine; metallurgical microscope; mass spectrophotometric analyzer; universal hardness tester; cutting machine; grinding machine; digital multi-meter; pH meter; welding machine (electric-arc and oxy-acetylene); calibrated cylinder; digital vernier caliper and digital weighing balance.

⸺ Sample Preparation

The mild steel plate was sectioned into six samples each of equal sizes (20 mm length by 20 mm thickness). The first three samples were un-welded while the remaining three samples were further sectioned into two each and welded (using electric-arc welding). The six samples were then separated in pairs (each pair containing a welded sample and an un-welded sample) resulting into three pairs. The three pairs are M$_1$ and M$_2$ as un-corroded samples, S$_1$ and S$_2$ as samples immersed in the chloride environment and lastly W$_1$

and W_2 as samples immersed in water. Samples M_1 and M_2 were purposely set aside just to examine the pre-corrosion microstructure of the steel sample. The sample description is presented in Table 1.

Table 1: Sample Description

Sample	Description
M_1	Control sample for pre-corrosion microstructural analysis for un-welded samples
M_2	Control sample for pre-corrosion microstructural analysis for welded samples
S_1	Un-welded steel sample immersed in 0.3 M NaCl
S_2	Welded steel sample immersed in 0.3 M NaCl
W_1	Un-welded steel sample immersed in water
W_2	Welded steel sample immersed in water

—— Chemical Analysis

The chemical analysis was done on the mild steel plate using ARX spectrometer (Oyetunji, *et al.* 2013). Corrosion rate determination was done by weight loss method. In order to effectively calculate the corrosion rate of the samples, the initial weights of the samples were taken using the digital weighing balance. Two samples (M_1 and M_2) were not subjected to any corrosive environment for proper comparison. Two other samples (S_1 and S_2) were immersed in 0.3 M NaCl and the last two samples (W_1 and W_2) were immersed in sea water. The corrosion exercise lasted for 61 days and weighed at intervals of 4 days for the samples immersed in the chloride environment and samples immersed in sea water. The corrosion exercise was undertaken at room temperature, and the weight loss of each sample was obtained by calculating the difference between the initial weight and the obtained weight at each interval.

The corrosion rate of each sample is then calculated using equation 1 in accordance to (Fontana, 2007; Seifedine, 2008) and the results are presented in graphic form and depicted as Figures 1-4.

$$R = \frac{K\,W}{\rho\,A\,T} \qquad (1)$$

where: R, corrosion rate; K, a constant; W, the weight loss of the metal in gram; T, time of exposure (hours); A, the surface area of the metal exposed (cm^2); P, the density of the metal (kg/m^3).

RESULTS AND DISCUSSION

—— The chemical analysis result

The result of the chemical analysis of the as-received mild steel plate is as presented in Table 2.

Table 2: Elemental Composition (wt %) of the As-received Mild Steel Plate

Elemental composition	Weight percent (wt%)
C	0.133
Si	0.307
Mn	0.820
P	0.0061
S	0.0081
Cr	0.080
Ni	0.102
Mo	0.038
Al	0.0036
Cu	0.178
Co	0.0085
Ti	0.0003
Nb	0.0054
V	0.0016
W	<0.0001
Pb	<0.0001
B	0.0007
Sn	0.0063
Zn	0.0042
As	0.0005
Bi	0.0010
Ca	0.0010
Ce	0.0023
Zr	0.0006
La	<0.0001
Fe	98.300

Percentage of alloying elements = Mn 0.82 + Cr 0.080 + Ni 0.102 + Nb 0.0054 + W 0.0001 + Ti 0.0003 + V 0.0016 = 1.0094 %

From the above calculation, it can be deduced that the steel pipe is a plain carbon steel and definitely not an alloy steel because the percentage sum of all alloying elements is less than 2%. This implies that there is no inherent element to prevent or reduce the corrosion rate of the steel. The carbon content falls within the range 0.1 – 0.25%, therefore the steel is a low carbon steel (Degarmo, *et al*, 2003).

—— Effects of distilled water and chloride environment on the cumulative weight loss of low carbon steel samples

Samples S_1 and S_2 were immersed in a chloride environment and Figure 1 show the cumulative weight loss of both samples. Generally, cumulative weight losses of these two samples were said to increase with increasing exposure time. Sample S_1, being an un-welded sample, has a higher cumulative weight loss as the exposure time increases. This means that the weight lost by sample S_2 over the specified number of days were much lesser than the weight lost by sample S_1. It can be inferred from the graph that the welded sample (S_2) exhibits a better resistance to weight loss compared to un-welded sample (S_1), because the graph shows that the rate at which sample S_2 loses weight is not as high as the weight loss rate of sample S_1, (Chinwko, *et al.*, 2014).
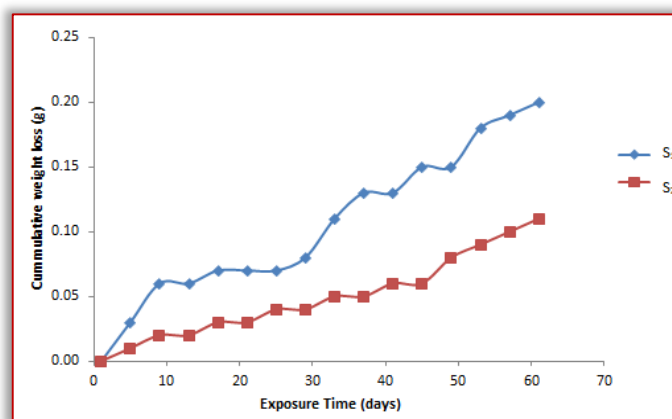
Figure 1: Variation of Cumulative Weight Loss with Exposure Time of Samples Immersed in 0.3 M NaCl

As shown in Figure 2, the cumulative weight loss of samples W_1 and W_2 with reference to the exposure time was analyzed with the two samples immersed in sea water. The cumulative weight losses of these two samples increased with increasing exposure time. Figure 2 shows that sample W_2 (welded) did not lose much weight as sample W_1 (un-welded). This implies that the overall cumulative

weight loss of sample W_1 is lower than that of sample W_2 which is an indication that the un-welded sample shows a better resistance to the loss of weight when immersed in water. The reason for this can be traced to the action and effect of welding on the steel sample, which had positively, affected the microstructural arrangement of the atoms (Oladele, *et al.*, 2014).
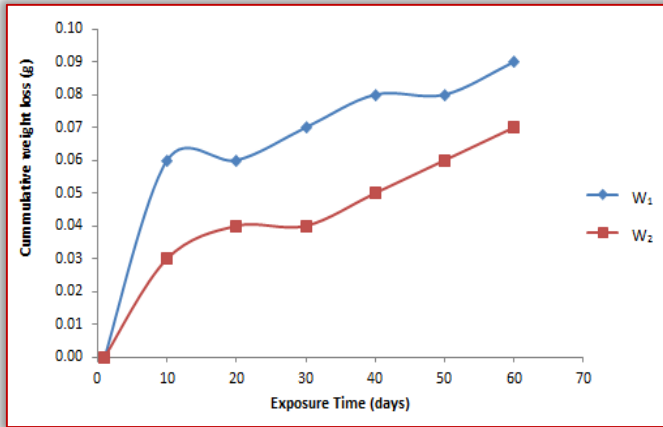
Figure 2: Variation of Cumulative Weight Loss with Exposure Time of Samples Immersed in Distilled Water

Figure 3 shows the comparison among the cumulative weight loss of all samples with distinctive difference between the cumulative weight loss of samples immersed in the chloride environment and samples immersed in distilled water, including welded and un-welded samples. Generally, the welded samples (S_2 and W_2) lost lesser weight compared to their un-welded counterparts (S_1 and W_1). However, samples S_1 and S_2 which were immersed in the chloride environment lost much weight compared to samples W_1 and W_2 which were immersed in water. This is due to the fact that the chloride environment is aggressive and more corrosive than the natural water environment. The corrosive nature of the chloride was majorly due to the actions of the chloride ions on the steel sample, but the available oxygen in the water formed a corrosion cell until passive films were formed, and the rate almost became constant (Chinwko, *et al.*, 2014).
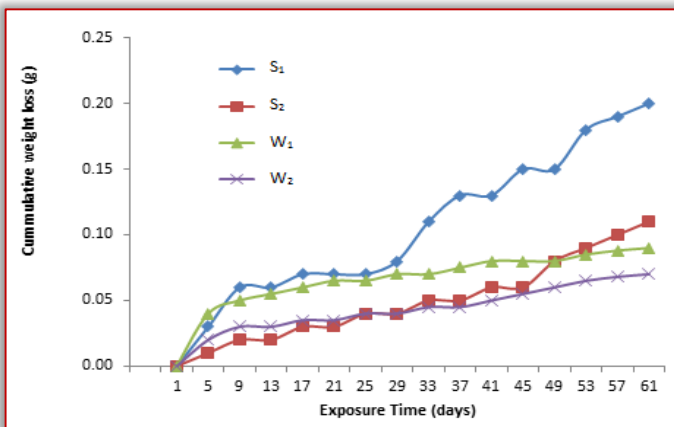
Figure 3: Variation of cumulative weight loss of all samples with the exposure time in days

— Effects of chloride environment on corrosion rate of low carbon steel plate samples

Figure 4 shows the relationship between the corrosion rates of the samples immersed in chloride environment. It can be seen from the figure that both samples S_1 and S_2 exhibited a higher corrosion rate within the first 10 days compared to the remaining days. This is usually expected holding to the fact that the chloride environment, in which the samples were subjected, tends to decrease in potency over time. However, the corrosion rate of sample S_1 was far higher than that of sample S_2 because the weldment of sample S_2 undoubtedly acted against the corrosion reaction of the sample compared to the other sample S_1 which had no weldment. In addition, sample S_2 was observed to exhibit a more uniform corrosion than sample S_1 with increase in exposure time.
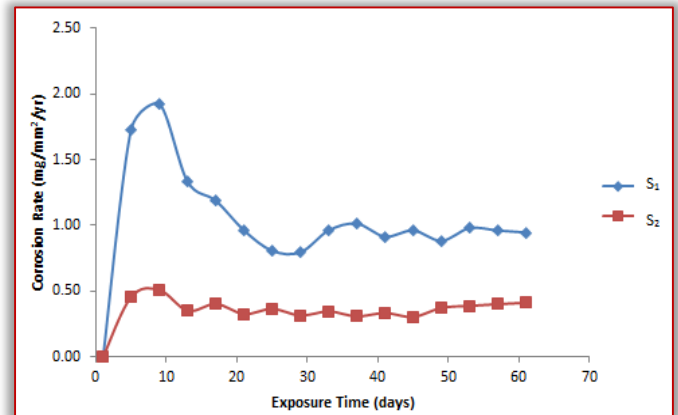
Figure 4: Variation of corrosion rate of samples S_1 and S_2 with the exposure time in days
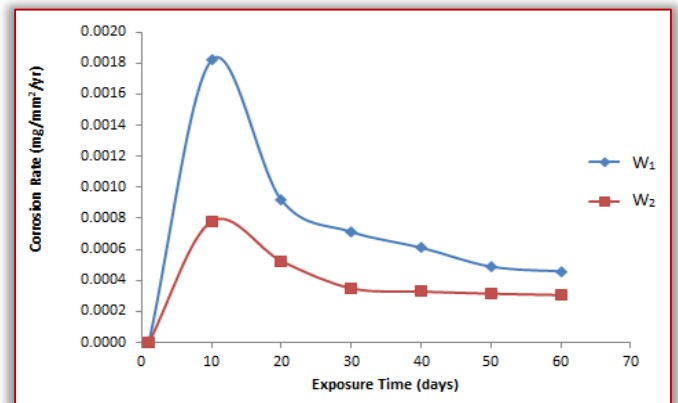
Figure 5: Variation of corrosion rate of samples W_1 and W_2 with the exposure time in days

The rate of corrosion of samples W_1 and W_2 in water can be seen on Figure 5. Sample W_1 (un-welded) exhibited a very low resistance to corrosion when compared to its counterpart (sample W_2 – welded). This is an indication of the fact that the welded sample exhibited a better corrosion resistance as a function of the action of the weldment with particular to the effect of the welding electrode. Although both samples shows a slightly noticeable uniform corrosion, however, their corrosion rate was very minimal and did not exceed 0.0018 mg/mm^2/yr. which implies that their rates of corrosion were within the passive extreme. To this end, the mechanical properties of the steels sample will only be slightly affected.

The corrosion rates of all samples were calculated and Figure 6 was plotted. Figure 6 therefore explains the corrosion relationship of all the samples immersed in different corrosive environments. Generally, the corrosion rates of the samples (S_1 and S_2) immersed

in the chloride environment were distinctively higher than those (W_1 and W_2) immersed in water. This was mainly due to the actions of chloride ion on steel samples, which is more corrosive than water. These chloride ions react with the Fe^{2+} in the steel sample and hence, form passive corrosive films on the steel samples and these makes the corrosion of mild steel faster in the chloride environment than in water. Moreover, the welded samples were observed to possess a lower corrosion rate when directly compared with their un-welded counterpart immersed in the same corrosive environment (Seidu and Kutelu, 2013).
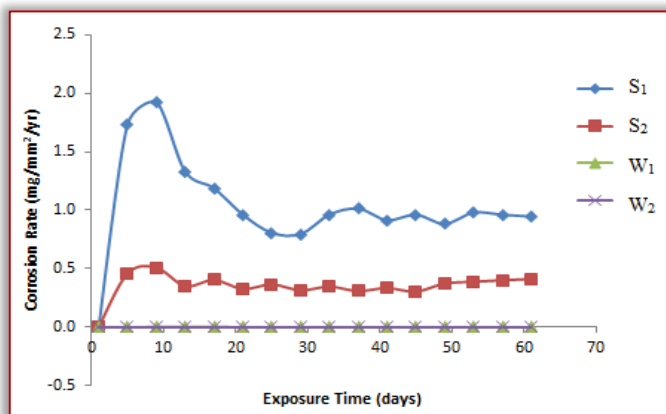
Figure 6: Variation of corrosion rate of all samples with the exposure time in days.

CONCLUSIONS

The effects of different environments on the corrosion properties of welded and un-welded mild steel were investigated, and the following conclusions were drawn:

— The un-welded samples exhibited greater loss in weight compared to the welded samples. This is due to the fact that the weldment of the welded samples reduced the rate of weight loss in the steel samples.

— The rates of corrosion of welded samples were observed to be lower in comparison with their un-welded counterparts in their corresponding corrosive environment.

— The maximum values of corrosion rates of the samples are S_1 (1.924344 mg/mm^2/yr.), S_2 (0.509108 mg/mm^2/yr.), W_1 (0.001821018 mg/mm^2/yr.), W_2 (0.000780731 mg/mm^2/yr.). This implies that samples (S_1 and S_2) immersed in the chloride environment exhibited the higher corrosion rate than samples (W_1 and W_2) immersed in distilled water. The factor responsible for this can be traced to the actions of chloride ions which tends to form passive films on the on the steel samples (S_1 and S_2) unlike the other samples (W_1 and W_2) that corrode uniformly under the influence of water.

— The corrosion behaviour of all the steel samples were within the passive region even-though there was a noticeable discrepancy between the corrosion behavior of samples immersed in the chloride environment and the distilled water environment. This implies that because all the values of corrosion rate fell within 0.00030583 mg/mm^2/yr. to 1.924344 mg/mm^2/yr. (i.e. they did not exceed 5 mg/mm^2/yr. because

active corrosion is known to be within the range of 10 mg/mm^2/yr. – 200 mg/mm^2/yr. or greater), the overall corrosion behaviour of the steel samples in the given corrosive environment can be regarded as being Passive.

References

[1] Callister, W. D. Jr. (2007). "Materials Science and Engineering: An Introduction", John Wiley and Sons, Inc., New York, Pp 349 – 351.

[2] Chinwko, E. C., Odio, B. O., Chukwuneke, J. L. and Sinebe, J. E. (2014): "Investigation of the Effect of Corrosion on Mild Steel in Five Different Environments". International Journal of Scientific and Technological Research, Vol. 3, Issue 7, Pp 306 – 310.

[3] DeGarmo, E. P., Black, J. T., and Kohser, R. A. (2003), "Materials and Processes in Manufacturing" (9th ed.), John Wiley and Sons, Inc., New York

[4] Fontana, M. G. (2007): "Corrosion Engineering", Tata McGraw-Hill Publishing Company Limited, New Delhi, P. 14.

[5] Katundi, D., Tosun-Bayraktar, A., Bayraktar, E., and Toueix, E. (2012). "Corrosion Behaviour of The Welded Steel Sheets Used In Automotive Industry". Journal Of Achievements In Materials And Manufacturing Engineering, 2012, 38(2), 146-153.

[6] Kumar, H. and Yadav, K. (2013) "Corrosion Characteristics of Mild Steel Under Different Atmospheric Conditions by Vapour Phase Corrosion Inhibitors". American Journal of Materials Science and Engineering, 2013, Vol. 1, No. 3, 34-39, Science and Education Publishing

[7] Oladele, I. O., Daramola, O. O. and Oyetunji, A. (2014): "Appropriate Technological Procedures for Fusion Welding of Low Alloy Carbon Steel". Journal of Engineering and Engineering Technology, Volume 8, No. 1, Pp 49 – 53.

[8] Oyetunji, A., Kutelu, B. J., and Akinola, A. O. (2013). Effects of Welding Speeds and Power Inputs on the Hardness Property of Type 304L Austenitic Stainless Steel Heat Affected Zone (HAZ). Journal of Metallurgical Engineering (ME), Volume 2, Issues 4. October 2013. Pp 124 -129.

[9] Seidu, S. O. and Kutelu, B. J. (2013): "Effect of Heat Treatments on Corrosion of Welded Low-Carbon Steel in Acid and Salt Environments". Journal of Minerals and Materials Characterization and Engineering, Pp.1, 95 – 100.

[10] Seifedine, K. (2008): "Corrosion Analysis of Stainless Steel". European Journal of Scientific Research, Vol 22, no 4, Pp 508 – 516.

[11] Talabi, S. I., Owolabi, O. B., Adebisi, J. A., and Yahaya, T. (2014). "Effect of Welding Variables on Mechanical Properties of Low Carbon Steel Welded Joint". Advances in Production Engineering & Management ISSN 1854-6250, Volume 9 | Number 4 | December 2014 | Pp. 181–186

[1.]Petr VONDROUS, [1.]Tomas VITEK, [1.]Lukas SYKORA, [2.]Michal VOJTISEK, [3.]Bohumil KOTLIK

THE PARTICLE EMISSION DURING ARC WELDING, COMPARISON OF WELDING METHODS

[1.] Department of Manufacturing Engineering, FME, CTU in Prague, CZECH REPUBLIC
[2.] Centre of vehicles for sustainable mobility, CTU in Prague, Roztoky, CZECH REPUBLIC
[3.] Unit for air pollution and wastes, National Institute of Public Health, Prague, CZECH REPUBLIC

Abstract: The research focuses on measurement of particle emissions during arc welding. The methodology of measurement follows the legal requirements of governmental regulation 361/2007 and relevant norms for welder exposure measurement, also approach used to evaluate outdoor air quality and automotive emissions were used. The exposure of students during welding classes never exceed the PEL limit. It was found out that legislation limit for welders, PEL, is rather high and can be easily met. In continuation, the particles size categorization done by cascade impactor and environmental dust monitor was done. We noticed many small particles and much less large particles, majority in sizes 0,1-1 μm, which can be easily breathed in and can enter blood stream.
Keywords: welding, fumes, airborne particles, emissions, occupational safety, 361/2007

INTRODUCTION

During arc welding there are many risks that should be understood, counteracted. These are EM radiation, electric shock, risk of fire, particle emissions, gases etc. The welders exposed to fumes for long hours, many years, can experience health problems.

The airborne particles, fumes, are created by physical, metallurgical, chemical processes, and size of particles widely varies, generally 0,01 – 10 μm and can be easily breathed in. Though many welders, employers consider fumes natural, and as such tend to neglect the related risk, the clean working environment increases safety and quality of work, so much research is done in area of fumes reduction. E.g. welding source manufacturer EWM recommends pulse compared to short arc transfer stating it can reduce fume generation from 2,3 mg/s to 0,7 mg/s. [1] The filler wire manufacturers can also reduce fumes. Eg. Lincoln Electric presented 24% reduction of fume emission rate with new metal cored wire Outershield MC710RF-H. [2]

In this paper we focus on measurement of welding particle emissions in realistic conditions of welding school, welders exposure and we try to relatively evaluate welding methods. Aims of the research are:

—— Measure level of student exposure to welding fumes during the class to assure safety.
—— Evaluate welder exposure to fume using different techniques, fillers and compare them.
—— Characterize welding emitted particles by size and weight for different methods.

METHODOLOGY

As the particles have influence on human health, the methods of measurement, legislative limits are given by occupational safety law and related standards. The Czech governmental regulation 361/2007 sets permissible exposure limit (PEL) of welders to particles, to certain gases etc. The PEL for welding dust in 8 hr shift is to be max 5 mg/m^3. For practical reasons, in this research the welding cycle was shorter, from 5-90 minutes.

—— Personal exposure measurement

To measure welder exposure according to law, norms, personal sampling unit on figure 1 was borrowed from Academy of Sciences. The unit composes of sampling head with filter, placed into the welding helmet close to the mouth, figure 2, and the pump with flow approx.. 2 l/min. After a specified time of welding, work, the filter is weighted and exposure evaluated.

Figure 1: Personal sampling unit with pump
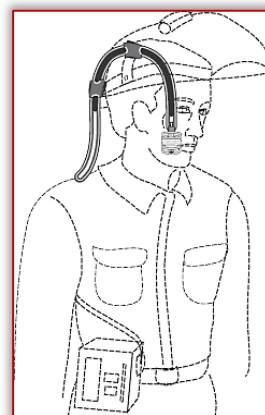
Figure 2: Placement of the sampling unit

⎯ Characterization of emitted particles

Two devices with different principle of work were used to characterize the welding particles size. In this research these measurements are used for relative comparison of methods in term of number and size of particles, parameters, influence of time on particle evolution etc. ELPI, figure 3, from Dekati is 14-stage cascade impactor to measure airborne particle mass size distribution based on electric charge of particles. Particle size distribution is measured in 14 fractions, range of 16 nm – 10 μm. Environmental dust monitor EDM from Grimm, figure 4, uses light absorption, diffraction to classify particles into 31 size classes, from 0.25 to 32 μm.

Figure 3: Dekati ELPI – cascade impactor

Figure 4: Environmental dust monitor Grimm 1.109

⎯ Welding methods, filler wires, parameters

Welding methods are SMAW (Shielded Metal Arc Welding), GMAW (Gas Metal Arc Welding), FCAW (Filler Cored Arc Welding). Filler material from Esab, Hyundai, Filarc and China OEM were used. Welding parameters were set according to recommendations of wire manufacturer and method as on the package. The parameters are not stated in detail in the research, because the high number of used wires and methods.

RESULTS

⎯ Exposure of students, SMAW welding class

The exposure of students to welding fumes during practical welding class was evaluated. The students were welding fillet welds with SMAW basic electrodes for 90 min (class duration). The measured weight concentration is at Figure 5. The PEL limit value 5 mg/m^3 (regulation 361/2007 Sb.) was not reached by any student. It can be noted, that 3 main groups of results exist.

The students 1-6 the students welded standing, students 7-11 welded sitting with fume extraction switched on, while measurement, 12-14 was done without fume extraction. Sitting students are closer to the fume generation place, so they have higher exposures. Standing students have lower exposure as their

head is further away from arc, source of fume. The exposition of students to fumes is highest in case without use of fume extraction. As SMAW has small productivity, especially in hands of students in the class, the exposure to welding fumes is low and even in the case without fume extraction. The safety and legal standards are met in the classes taught at CTU in Prague.
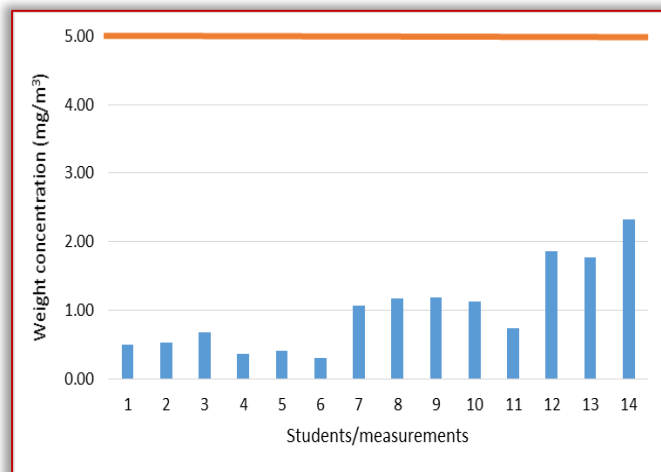
Figure 5: Results of measurement of personal exposure of 14 students during welding class

Note: The personal exposure limit (PEL) 5 mg/m^3 was not exceeded in any case. 1-6 – students welding standing with fume extraction on; 7-11 – students welding sitting with fume extraction on; 12-14 – students welding without fume extraction

⎯ Personal exposure, different welding methods

Short time gravimetric measurement using different welding methods was done with purpose to compare methods. From tab. 1 it is clear that particle emissions, i.e. welder exposure, are closely related to welding method, its productivity and most importantly the fume extraction.

Table 1: Exposure of welder using different welding methods (welding 5-15 min) [3]

Welding method (repetitions-with and without fume extractions)	Weight concetrations without fume extraction [mg m^{-3}]	Weight concetrations with fume extraction [mg m^{-3}]
GMAW-Cu uncoated wire (3)	10,0	-
GMAW-Cu coated wire (3, 1)	10,6	0,8
GMAW-stainless steel (2, 1)	6,2	0,4
FCAW – different cores (7)	27,2	-
SMAW – Rutile electrode (3, 1)	2,0	0,5
SMAW – Bazic electrode (5, 2)	1,1	0,5
Oxyfuel cutting	5,8	Outdoor rail cutting
Grinding	1,4	-
Casting – induction furnace	3,7	-

Note: The typical length of measurement was 5-15 min of straight welding, with just technological breaks if need, i.e. SMAW - electrode exchange, GMAW, FCAW – change of weld sample. In this measurement not the whole shift is considered.

The FCAW method, most productive, creates high amount of emissions, SMAW on the other hand the lowest. We can notice that all GMAW, FCAW methods would exceed 5 mg/m³ limit several times without fume extraction.

High exposure to welding fumes can be noted also for oxyfuel cutting, casting and grinding. In the right column, we can notice that fume extraction is very effective to reduce welder exposure and must be switched on every time.

─── Particle classification

The need of particle classification is related to discrepancy of personal exposure (particle weight) measurement and probable interaction of particles with human body. As is known the large diameter particles create the mass, while smaller particles (under 1 µm) can enter the blood stream and harm the body.

Example of results of ELPI particle classification of GMA welding is at figure 6. Manual GMA welding without fume extraction with solid wire G3Si1 Cu coated. Parameters are 19 V, wire feed 7 m/min (164 A). Visible is the fact that majority of emitted particles is of size 0,01-1 µm and as such can be breathed in. Small number of large particles, which cannot enter the alveoli and blood stream on the other hand creates weight, but actually are safer. To reflect this discrepancy certain change of welders exposure measurement should be done.
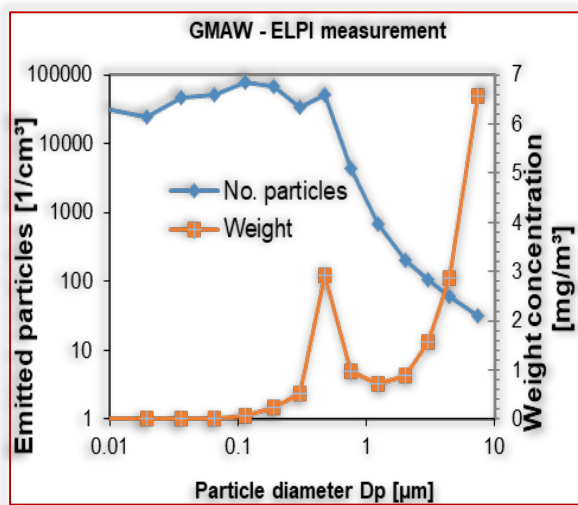
Figure 6: Result ELPI measurement – GMAW

─── Time evolution of the particle presence at the workplace

The fumes created by welding are not influencing the welder only, but everyone on the job floor as the particles are easily driven by air stream and are for long time suspended in the air even after welding is finished The results of measuring GMAW at time of welding and after the welding termination are at figure 7. Parameters: without fume extraction, solid wire G3Si1, Ø1 mm, 19 V, wire feed 7 m/min (164 A).

The principle of particle reduction in time are several:

- # dilution with surrounding air,
- # aggregation of small particles to larger clusters and
- # the particles settle down due to gravity force.

From the graph it can be noted, that all particles, especially those under 1 µm, tend to decrease their presence slowly, it takes up to 2 hours until the background environment has same conditions as before welding.
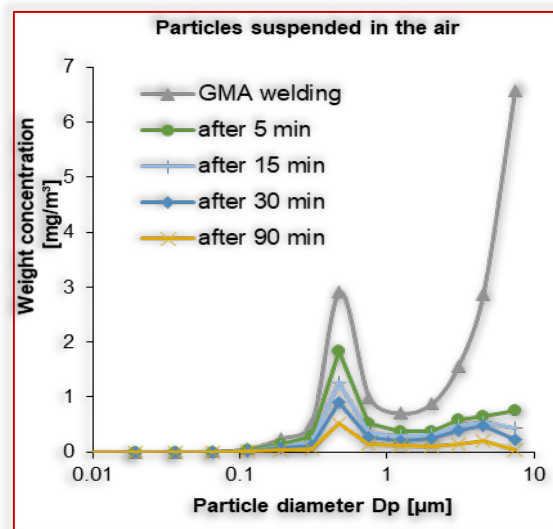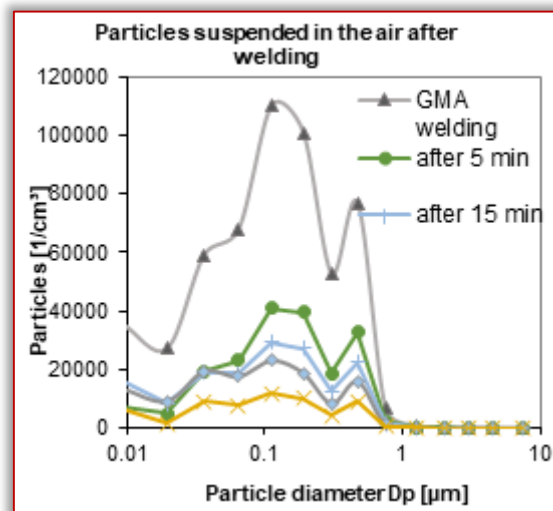
Figure 7: Result ELPI measurement – Particles in the air after finishing welding

─── Particle measurement according to position relatively to arc

The particles are emitted from the area of the arc and are driven by arc heated air upwards, where typically is the head of welder. By placing the inlet of ELPI machine to different positions, we mapped volume and size of particles. The positions of measurement and results are shown at Figure 8.

The graphs are using logarithmic scales. As can be seen on the logarithmic graphs, the measured curves can be divided into 2 groups with similar results:

- # central column, measurement above the arc (A1, A2, A3), number of particles 10E6-10E7 /cm³, total particle weight 500-600 mg/m³
- # the rest B1, B2, B3, REFERENCE – particles 10E4-10E5 /cm³, total weight up to 10 mg/m³
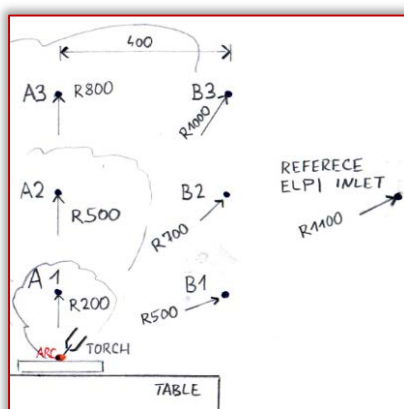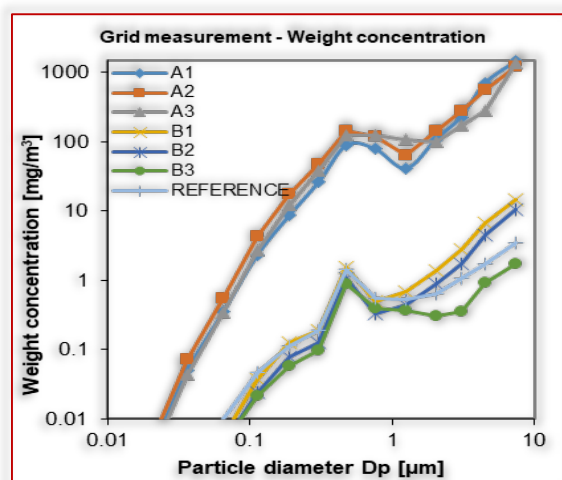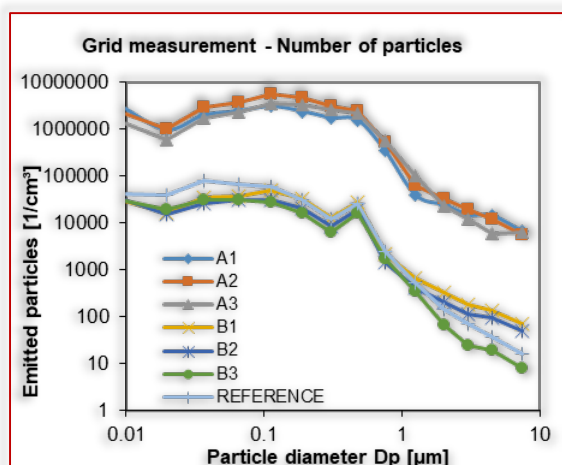
Figure 8. Result ELPI measurement – Particles no.,
weight measured in the grid, position

Particle emissions, i.e. welder exposure, are closely related to welding method, its productivity and work load of the welder. The higher the productivity of the method, the higher exposure of welder can be expected. The highest values were noted for metal cored wires FCAW. It was also noted that the fume extraction is extremely important and should be switched on. With fume extraction the 5 mg/m^3 limit was never exceeded.

— Aim 3. Characterize welding particles by size and weight for different methods.

In the welding fume the vast majority of particles are in the size range under 1 μm and as such can enter the blood stream and harm the body more than larger, heavy particles. Based on results the authors consider that legal welder exposure limit, or the method of measurement should be reconsidered based on size of created particles etc.

It must be stated that welding fumes increase the risk of lung cancer etc., so setting rather strict limits is in the interest of welders, their employers. During welding, also non-welding personnel is exposed to welding fumes. This exposure is of similar level as the welder in case the fume extraction is not used. Thus efficient air filtration or fume extraction is a must.

Acknowledgment

References
[1] EWM. Procedure variants reduce welding fume emissions. Company brochure. (2017)
[2] Sadurski K. Outershield® MC710RF-H, conference paper Zvaranie 45 (2017)
[3] Sýkora L. Měření prachových částic vznikajících pro svařování elektrickým obloukem. DP. ČVUT v Praze (2017)

CONCLUSIONS
— Aim 1. Level of student exposure to welding fumes during SMA welding class

It was proven that law exposure limit was not exceeded by any of the students. On the other hand, from this experiment it can be understood that the PEL limit is rather high, as even in the case of non-functioning fume extraction it was not exceeded.

— Aim 2. Evaluate welder exposure to fume using different welding techniques, fillers etc..

[1.]A.I. TSYLIURYK, [1.]S.M. SHEVCHENKO, [1.]N.V. GONCHAR, [1.]YA.V. OSTAPCHUK,
[2.]O.M. SHEVCHENKO, [2.]K.A. DEREVENETS–SHEVCHENKO

AGROPHYSICAL AND BIOTIC FACTORS OF REGULATION OF BIOLOGICAL ACTIVITY OF SOIL IN THE CROP ROTATION

[1.] Dnipro State Agrarian and Economic University, Dnipro, UKRAINE
[2.] State Institute of Grain Crops NAAS of Ukraine, Dnipro, UKRAINE

Abstract: In the field stationary experiment, the dynamics of the general biological activity of chernozem, depending on the biomass of plant residues, methods of the basic soil tillage under different hydrothermal conditions was studied. It was established, that the release of carbon dioxide by microorganisms from the soil more intensively occurred on the background of deep tillage, where the best conditions for aeration and distribution of plant residues in the profile of the arable layer were found. Minimization of soil tillage, in consequence of the compaction of the arable layer by more than 1.3 g / cm^3 limited the volume of active zone of biotic activity and growth processes of field crops in crop rotation while inhibiting the overall biological activity and reducing the amount of carbon dioxide released. However, small soil tillage contributed to the enhancement of the anti–erosion resistance of the chernozem surface from the shock energy of rain drops, and also provided more favorable conditions for the humification of organic residues instead of undesirable intensive mineralization, especially humus.
Keywords: crop rotation, soil tillage, biological activity, plant residues, soil hardness, volume mass, field crops

INTRODUCTION

The issue of arable layer differentiation at different methods of the basic soil tillage in the crop rotation on fertility and biological activity and dynamics of these parameters depending on the intensity of mechanical action on the soil and the cycle of organic matter is a very important aspect for the theoretical study of innovative soil protecting technologies of growing of field crops (Tsyliuryk et al. , 2015, 2017, 2018, Chumak et al., 2011; Tsyliuryk & Kozechko, 2017, Tsyliuryk & Sudak, 2014, 2016, Tsyliuiryk, Desyatnik, 2016, Tsyliuryk, Sudak, Shapka, 2015; Hadzalo, 2017).

By numerous investigations on the study of the nutrient regime of the soil during the transition to mouldboard–free methods of soil tillage in different zones has been established an actual increase of the concentration of basic nutrients (phosphorus and potassium) in the upper layer, decrease the biogenesity and effective fertility of the lower layers, with its long application (Tanchyk, 1999; Pabat, Shevchenko 2000; Tsyliuryk, 2017; Sayko, 2007). At the same time, in some cases, the localization of the elements of fertility is considered as a satisfactory fact, since near the weakly developed root system of plants in the beginning of the vegetation there is an increased content of elements of nutrition (Tsyliuryk & Shapka, 2016, 2017), in others – as negative, so long as in the conditions of drought, the elements of nutrition in the upper layer become positionally and physiologically unavailable to plants (Shevchenko & Rybka, 2002).

Mineralization and immobilization processes in the soil have a cyclic nature, reflecting the dynamic equilibrium between them at a certain point in time. The nitrogen of the soil substrate is constantly transformed from inorganic to organic form by means of assimilation processes, from organic to inorganic form – by decomposition and mineralization (Tsyliuryk, 2014, 2016; Lebid and Tsyliuryk, 2014). It is also established, that the increased amount of plant residues (mulch) leads to the decrease in the availability of nitrogen.

At the decomposition of plant residues, which have the broad correlation of carbon to nitrogen, there is a biological absorption of the latter by rapidly developing microorganisms for the synthesis of their own proteinic bodies (Desyatnik, 2017).

The intensification of mineralization processes to a certain level can be considered as positive phenomenon, because in parallel with such agrocenosis there is an increase in the productivity of field crops. Excessive activity of soil microorganisms can lead to rapid mineralization of humus and the growth of unproductive losses of gaseous nitrogen in the processes of denitrification and nitrification, accumulation of nitrates in the soil and further their washing with groundwater. At the same time, the coefficient of use of field crops of nitrogen from fertilizers is reduced whose content in the soil is not sufficiently high (Hordiyenko et al., 1991).

MATERIAL AND METHOD

The research was carried out at the State Enterprise "Experimental Farm of Dnipro" of the State Institution of the Institute of Grain Cultures of the National Academy of Sciences of Ukraine in the stationary field experiment of laboratory of the crop rotation and environmental protection systems of soil tillage in five–year crop rotation: peas – winter wheat – sunflower – barley spring – corn according to generally accepted techniques of experimental work (Yeshchenko, 2005), during 2010–2017.

The scheme of the experiment also consisted of three radically different systems of basic soil tillage, namely, moldboard soil tillage (for all crops of crop rotation, a moldboard soil tillage is executed), differentiated soil tillage (a combination of different methods of moldboard–free soil tillage (disking, subsurface cultivation, chiseling) and moldboard cultivation in the crop rotation), and zero cultivation (direct sowing). Soil cultivation was carried out by the following implements:

Moldboard soil tillage – by a plough PO–3–35 at a depth of 20–22 cm for spring barley and sunflower, 23–25 cm for corn, 25–27 cm for bare fallow (in autumn)

Chiseling – by Chisel Plow at the depth of 14–16 cm for sunflower and spring barley (in autumn);

Harrowing – by disc harrow BDVP (БДВП) – 6.3 at the depth of 10–12 cm for barley spring and bare fallow (in autumn);

Subsurface cultivation by subsurface cultivator – by means of combined unit KSHN (КШН)–5.6 "Resident" or KR (КР)–4.5 at the

depth 14–16 cm in corn and 12–14 cm in sunflower (in autumn) in the early fallow (in the spring).

As organic soil fertilizers were used the post–harvest residues of predecessors, which, after mineralization, are known, return to the soil epy significant part of previously alienated elements of plant nutrition (N–NO₃, P₂O₅, K₂O). In view of this, the experimental scheme included three fertilizer systems from the calculation per hectare of crop rotation:

without fertilizers + after harvest residues;
$N_{24}P_{18}K_{18}$ + after harvest residues;
$N_{48}P_{18}K_{18}$ + after harvest residues.

Mineral fertilizers were applied in the spring by means of broadcasting for pre–sowing cultivation.

The conventional generally accepted techniques of experimental work have been used in the process of carrying out of research by B.A. Dospekhov. As well as special methods of research have been used, in particular, the hardness of the soil was determined by the Revayakin hardness gauge, the density – by the cutting ring method, the surface coating of the plant residues and their mass by Shyiatyi, the biological activity of the soil by the method of Shtatnov, and others like that.

The soil of the experimental site is common chernozem heavy–clayey loam with content in the arable layer: humus – 4.2%, nitrate nitrogen–13.2 mg/kg, mobile phosphorus & potassium compounds (according Chirikov), respectively 145 and 115 mg/kg. Weather conditions during the research years were sufficiently favorable for the growth and development of field crops, except for the abnormally arid 2012, when the hydrothermal coefficient during the period of the largest water consumption of plants (May–July) was 0.6.

The hydrothermal coefficient less than 0.7 indicates the presence of soil drought and air drought, which have bad influence on the formation and swelling of grain and seeds. In all other years, the hydrothermal coefficient did not decrease below the indicated figure and was 0.8–0.9.

The purpose of the work is to establish the biological activity of the soil in accordance with volume of the release of CO2 in crop rotation, depending on the amount of plant residues left under the influence of soil tillage due to changes in agro–physical parameters and soil moisture.

RESULTS

According to the results of the research, the minimization of soil tillage causes the significant changes in the differentiation of the arable layer (0–30 cm) relative to the positional disposition of nutrients, the concentration of potential humus substances in the aerobic zone and the intensification of microbiological activity, as evidenced by the volumes of carbon dioxide releases.

The transformation of the mulch coverage of surface of the soil with plant residues was carried out under the influence of mechanical mixing with soil by means of soil tillage implements and decomposing by microorganisms (Table 1).

The largest organic mass in crop rotation naturally left itself corn, and the minimum – barley spring and sunflower. Substantial redistribution of the projective coverage of the surface of the field with plant residues and their mixing with the soil in the profile of the arable layer was carried out by various methods and systems

of basic soil tillage. For example, after harvesting of corn and carrying out of soil tillage on the surface of the field, the minimum number of plant residues remains for the moldboard soil tillage system – 0.61 t/ha. The intermediate position was occupied by the differentiated (discing) cultivation system – 3.12 t/ha, and the maximum amount of vegetative substrate was logically marked for zero soil tillage – 4.34 t/ha.

Table 1. Dynamics of biomass of mulching coverage of the field surface for different systems of basic soil tillage, on average for 2010–2017, t/ha

Cultures of crop rotation	Terms of definition	Soil tillage system		
		Mouldboard	differentiated	zero
Peas	in autumn	0.30	2.10	3.21
	in the spring	0.11	1.62	2.41
Winter wheat	in autumn	0.39	2.48	3.91
	in the spring	0.23	2.01	3.36
Sunflower	in autumn	0.28	1.87	2.24
	in the spring	0.21	1.42	2.03
Barley spring	in autumn	0.24	1.96	2.60
	in the spring	0.10	1.58	1.85
Corn	in autumn	0.61	3.12	4.34
	in the spring	0.35	2.88	4.05

According to the results of studies, soil tillage minimization contributes to the greater localization of plant residues in the upper layers of the arable layer (0–20 cm) and on its surface, while the application of moldboard soil tillage system leads to the wrapping of almost the entire biomass in the lower layers of the soil (20–27 cm).

As is known from literary sources (Hordiyenko et al., 1991), the degree of decomposition of plant residues largely depends on the microbiological activity of the rhizosphere zone, which in its turn is changed under the influence of agro–physical parameters (density and hardness of the soil) which are regulated by methods of basic soil tillage. The conducted agro–physical monitoring of soil condition showed that at growing of different crops in crop rotation, the arable layer was heterogeneous according to indicators of density and hardness in a vertical section.

In all fields of crop rotation in the spring, a clear pattern of differentiation of zone distribution have been appeared between the upper less hard pan of 10–15 kg / cm² and the deeper packed horizon with mechanical counteraction for plant roots at 25–30 kg / cm². That is, the depth of occurrence of a hard pan of soil significantly depends on the methods of basic soil tillage and biological peculiarities of crop rotation crops (Table 2).

During the vegetative period there was the gradual compaction of the arable layer, but the tendency continued to be characteristic for the spring determination. So and in the beginning of June, the deepest occurrence of the compacted layer was by the mouldboard system of soil tillage – 24 cm especially in the fields of sunflower and corn, while at the differentiated system of soil tillage (especially for discing – 8 cm) the compaction was detected at the depth of 8–16 cm in the sowings of peas, spring barley and winter wheat. For zero soil tillage system, there was no significant differentiation of the arable layer on density indicators, where it was maximum and was 1.35 g / cm³.

In general, the minimization of the soil tillage was accompanied by the compaction of the arable layer of soil (0–30 cm) deeper than 8–16 cm, while in the background of the mouldboard ploughing more

favorable conditions for growth and development of the root system up to 27 cm were noted.

Table 2. Depth of occurence of compacted layer of soil under different systems of basic soil tillage in crop rotation for 2010–2017

Field cultures of crop rotation	Phase of development of plants of field crops	Soil moisture in arable layer (0–30 cm) %	Soil tillage system		
			mouldboard	differentiated	zero
Peas	Formation and ripening of grain	15.3	$\frac{14}{66}$	$\frac{9}{60}$	$\frac{8}{55}$
Winter wheat	Formation and ripening of grain	13.4	$\frac{14}{94}$	$\frac{10}{90}$	$\frac{8}{87}$
Sunflower	4 pairs of leaves	19.4	$\frac{24}{42}$	$\frac{14}{38}$	$\frac{12}{32}$
Barley spring	Formation and ripening of grain	13.5	$\frac{14}{73}$	$\frac{10}{67}$	$\frac{8}{62}$
Corn	6–7 leaves	20.3	$\frac{24}{61}$	$\frac{12}{50}$	$\frac{9}{43}$

Note: Numerator – the depth of the compacted, hard pan of soil, see. Denominator – the height of plants of field crops, cm.

On zero backgrounds, as well as the decrease in the depth of the main soil tillage to 8–16 cm after the small soil tillage, with leaving the compacted layer in the lower horizons, all crops of crop rotation slowed the linear increase. In particular, for example, winter wheat plants had the lower height for zero soil cultivation, not exceeding 87 cm in comparison with the mouldboard soil tillage system, where the plant height was 94 cm. In the cotn sowings at the 6–7 leaf phase, the above indicators were 43 cm and 61 cm accordingly. One of the most powerful levelling factors for reduction of soil hardness is the level of soil and plant water supply. So, the hardness of the soil was in the inverse multiple correlation dependence with the soil moisture, that is, with increase of soil moisture the hardness decreased and the height of the plants of field crops increased. The correlation coefficient here was quite high and was 0.85.

After intensive heavy showers at the level of 45 mm of rainfall in the summer, at the time of harvesting of early cereal crops, as well as in the phase of milky–waxy ripeness of corn and flowering of sunflower, the most favorable layer of soil with respect to its hardness for plants significantly expanded to the depth of its aspiration. After heavy rains, the depth of the line of differentiation of the separation of the hard and loosening layers in the early cereal crops was deepened to 16–23 cm, and in fields of tilled crops (sunflower, corn) up to 21–27 cm, which was on 3–9 cm deeper, and then before rainfalls.

However, even in spite of the substantial moisture of the arable layer of soil, the advantage of the mouldboard soil tillage system over the differentiated and zero soil cultivation in terms of the ability to loosen the arable layer at the expense of a better soil digestion function was also manifested after the intense rainfall (Table 2). These processes are especially intensive in the autumn–winter period due to maximum moisture of the soil, as well as mutually opposite processes of its freezing and thawing, when the destruction of coarse fractions is > 10 mm to the most valuable aggregates of smaller sizes (from 0.25 to10.0 mm) .

The methods of basic soil tillage also had the significant influence on the indications of projective coverage of the soil surface with plant residues after each field crop in the crop rotation, which is of paramount importance in control of erosion processes (water and wind erosion) during the absence of vegetative cover.

The dynamics of the projective coverage of the surface of the field with plant residues showed that the methods of basic soil tillage differed significantly in the nature of anti–erosion efficiency and microbiological destruction of straw under the influence of moisture, temperature and mechanical action. At the same time, the methods of minimal soil cultivation contributed to the enhancement of the anti–erosion stability of the chernozem surface from the shock energy of rain drops, and also provided more favorable conditions for the humification of organic residues instead of undesirable intensive mineralization.

During the winter period, plant residues also undergone a slow stage of destruction and decomposition. In particular, for the differentiated system of cultivation on the background of small discing before the beginning of spring field operations, the reduction of biomass residues in different fields of crop rotation was within the range of 0.24–0.48 tons / ha, and in the case of zero cultivation and direct sowing 0.21–0.80 t / ha.

The intensity of the decomposition of organic matter in the soil is a heterogeneous process, which primarily depends on the determining factors – moisture, temperature and aeration level of the treated layer of chernozem. The intensity of the processes of breathing of soil microorganisms makes it possible to estimate the total biological activity of the soil, which is based on the amount of carbon dioxide released, depending on the different methods of soil tillage per unit area of the field surface (Table 3).

Table 3. Influence of crop rotation and soil tillage on the general biological activity, mg CO_2 / kg soil / day on average for 2010–2017

Field cultures of crop rotation	Terms of definition (number, month)	Soil tillage system		
		mouldboard	differentiated	zero
Peas	01.05 01.06	37.1 50.3	34.7 46.3	32.0 40.5
Winter wheat	01.05 01.06	31.7 40.9	30.2 38.0	28.9 35.1
Sunflower	01.05 01.06	35.0 49.2	34.7 43.9	29.5 42.0
Barley spring	01.05 01.06	32.8 43.3	31.3 39.7	29.6 36.0
Corn	01.05 01.06	33.1 47.5	31.4 45.8	28.2 41.1

As our studies have shown, the biological activity of the soil depended on the phases of development of plants of field crops and had a sufficiently wide amplitude of variation. Thus, as an example of the mouldboard plowing, it is evident that insufficient soil warming at normal humidification at the time of corn sowing has led to the decrease in biological activity to 33.1 mg CO_2 / kg of soil / day.

The maximum intensity of soil respiration (47.5 mg CO_2 / kg of soil / day) occurred at 30 days after corn sowing, when the optimal combination of temperature and humidity of the soil was noted. Similar regularities and tendencies in the release of CO_2 from the soil during certain phases of maize development are also noted for differentiated and zero cultivation systems, but with somewhat lower overall CO_2 release, respectively, by 1.7–5.3 mg CO_2 / kg ha / day (10–12%) and 5.8–9.8 mg CO_2 / kg ha / day (12–22%) compared to the mouldboard soil tillage system. Generally, this tendency took place both in the maximum and at the minimum

amplitude of the activity of respiration processes, that is, the indicators of the general biological activity of the soil were higher in the background of plowing and prevailed other systems of mechanical cultivation of chernozem (differentiated, zero system). One of the reasons for reduction the biological activity of the soil, depending on the methods of basic soil tillage, is the different profile dislocation of plant residues. That is why, the availability of oxygen, moisture, optimal agrophysical properties of the soil and the presence of a significant amount of plant residues in the profile of the arable layer over the mouldboard soil tillage system creates the most favorable medium for microorganisms. At the same time, when at zero soil cultivation, all plant residues are located on the soil surface and are isolated from the zone of vigorous activity of the soil biota.

CONCLUSIONS

Thus, the biological activity of the soil is the derived indicator, which depends on the features of the technology of growing of cultures in the crop rotations, the presence of organic matter of plant residues in the chernozem, the level of compaction of arable layer and the methods of basic soil tillage. The use of deep plowing due to the creation of favorable conditions for the expansion of the root system of crops with sufficient aeration and moisture absorbtion properties provides maximum biological activity under all crops of crop rotation, decomposition of residues and intensive mineralization processes. However, methods of unploughed treatment of the soil contributed to increasing the anti–erosion stability of the surface of chernozem from the shock energy of rain drops, as well as providing more favorable conditions for the humification of organic residues instead of undesirable intensive mineralization.

Note: This paper is based on the paper presented at ISB-INMA TEH' 2018 International Symposium (Agricultural and Mechanical Engineering), organized by Politehnica University of Bucharest – Faculty of Biotechnical Systems Engineering (ISB), National Institute of Research-Development for Machines and Installations Designed to Agriculture and Food Industry (INMA) Bucharest, in Bucharest, ROMANIA, between 01–03 November, 2018.

References

[1] Chumak V.S., Tsyliuryk A.I., Gorobets A.G., Gorbatenko A.I. (2011). Agroeconomic efficiency of different methods of basic cultivation of soil under sunflower in steppe. Bulletin of the Institute of Grain Farming, 40, 56–59, (in Ukrainian);
[2] Desyatnyk L.M. Integration of Classical and Organic Agriculture / Desyatnyk L.M.;
[3] Lorinets F.A., Shevchenko O.M., Shvets N.V. / The guidebook of Ukrainian grain growers. – 2017. – No 1. – P. 144–146;
[4] Gadzalo Ya.M., Zaryshniak A.S, Shevchenko M.S. [and others]. Actual crop rotations: a new look at the classics. Monograph. Dnipro: Royal Print Ltd, 2017.– 90 p;
[5] Gordienko V.P., O.M. Herkiial, V.P. Opryshko. Agriculture. K .: Higher School, 1991. –286 p;
[6] Lebid, E.M., Tsyliuiryk, A.I. (2014) Reproduction of chernozem fertility and productivity of short–term crop rotation of the steppe, depending on the system of multicultural soil cultivation. Bulletin of the Institute of Agriculture of the Steppe Zone, 6, 8–14 (in Russian);
[7] Pabat I. A., Shevchenko M.S. Problems of conservation of energy resources and soils in modern technologies of growing of agricultural crops. News UTIM. – Dnipropetrovsk. – 2000. – V. 2 – No 1, 2– P. 41–44.
[8] Saiko V.F. Soil tillage systems in Ukraine / V.F. Saiko, A.M. Malienko – K.: Publishing house VD "Ekmo" Ltd, 2007. – 42 p;
[9] Shevchenko M.S. Estimates of the possibilities of minimization of the soil tillage during growing corn in Steppe. Bulletin of Poltava SAA. No1.– 2002. – P. 19–20;
[10] Shevchenko M.S, Rybka V.S. Bioenergetic circulation and methods of its estimation for corn growing. Storage and processing of grain, 2003. – No 7. – P. 28–30;
[11] Tanchyk S.P. Effectiveness of the basic soil tillage in the weeds control at the growing of corn. Bulletin of Agrarian Science. 1999. – No 8 – P. 17–20;
[12] Tsyliuryk A.I., Shapka V.P. Minimization of soil tillage for spring barley in the Northern Steppe of Ukraine. Minimization of soil treatment for barley spring in the northern steppe of Ukraine. Stiinta agricola, 2017. – No 2 – P. 25–29;
[13] Tsyliuryk, A.I., Kozechko, V.I. (2017). The effect of mulching on tillage and fertilization on maize growth and development in the Ukrainian Steppe. Ukrainian Journal of Ecology, 7 (3), 50–55;
[14] Tsyliuryk, O.I., Shevchenko, S.M., Shevchenko, O.M., Shvec, N.V., Nikulin, V.O., Ostapchuk, Ya.V. (2017). Effect of soil cultivation and fertilization on the abundance and species diversity of weeds in corn farmed ecosystems. Ukrainian Journal of Ecology, 7 (3), 154–159;
[15] Tsyliuryk, A.I., Sudak V.N. (2014). Efficiency of flat–rope loosening cultivation of soil under sunflower in the northern steppe of Ukraine. Herald of the Lviv National Agrarian University. 18 (agronomy), pp. 161–167;
[16] Tsyliuryk A.I., Gorbatenko A.I., Shapka V.P. (2015). Influence of minimum tillage and fertilization on the yield and oil content of sunflower seeds in the conditions of the Northern Steppe. Bulletin of the Institute of Agriculture of the steppe zone, 9, 11–15, (in Ukrainian);
[17] Tsyliuryk A.I., Sudak V.M. (2016) Influence of minimal tillage of soil and fertilizer on the growth and development of sunflower plants in the conditions of the Northern Step. Bulletin of the Dnipropetrovsk State Agrarian and Economic University, 1 (32), 25–31, (In Ukrainian);
[18] Tsyliuiryk, A.I., Sudak, V.M., Shapka, V.P. (2015). Productivity of short crop rotation depending on the system of soil tillage on the background of continuous stubble mulching remains. Bulletin of the Institute of Agriculture of the Steppe Zone, 8, 66–72 (in Russian);
[19] Tsyliuryk, A.I. (2016) Efficiency of the minimum soil cultivation for corn under the conditions of the northern steppe of Ukraine. Herald of Dnepropetrovsk State Agrarian and Economic University, 2, 5–9;
[20] Tsyliuryk, A.I. Desyatnik, L.M. (2016). Minimal tillage of bread under conditions of the Northern Steppe of Ukraine. Far–Eastern agrarian bulletin, 3 (39), 38–44 (in Russian);
[21] Tsyliuryk, A.I. (2014). Scientific substantiation of the effectiveness of basic tillage systems in the short–rotation crop rotations of the Northern Steppe of Ukraine, Thesos of the Doctoral Dissertation. Dnipropetrovsk, 447 (in Ukrainian);
[22] Tsyliuryk, A.I. Shapka, V.P. (2016). Inflorescence of spring barley, depending on soil cultivation and fertilization in rotation crop rotations. Bulletin of the Institute of Agriculture of the steppe zone, 10, 25–31;
[23] Tsyliuryk, A.I., Tkalich, Yu.I., Masliiov, S.V., Kozechko, V.I. (2017). Impact of mulch tillage and fertilization on the growth and development of winter wheat plants in a cleanroom in Northern Steppe of Ukraine. Ukrainian Journal of Ecology, 7 (4), 511–516;
[24] Tsyliuryk, Al, Shevchenko, S.M., Ostapchuk, Ya.V., Shevchenko, A.M., Derevets–Shevchenko, E.A. (2018). Control of infestation and distribution of Broomrape in sunflower crops of the Ukrainian Steppe, 8 (1), 487–497.
[25] Yeshchenko V.O., P.G. Kopytko, V.P. Opryshko, P.V. Kostogryz (2005) Fundamentals of scientific research in agronomy / – K.: Publishing house Dia, – 285 p.

[1.]Remus Marius OPRESCU, [2.]Sorin Ştefan BIRIŞ, [1.]Iulian VOICEA,
[1.]Valentin VLĂDUŢ, [2.]Gigel PARASCHIV, [3.]A.M. MARINESCU

CONSIDERATIONS REGARDING THE CONSTRUCTION AND OPERATION OF AN EQUIPMENT DESIGNED TO MODEL THE SOIL IN COMPARTMENTED FURROWS IN VINEYARDS AND ORCHARDS

[1.]INMA Bucharest, ROMANIA
[2.]University "Politehnica "Bucharest, Faculty of Biotechnical Systems Engineering, ROMANIA
[3.]INOE 2000 IHP, ROMANIA

Abstract: Recently, the climate changes have more and more manifested by prolonged draught periods, while population number is continuously growing, therefore the agricultural production per surface unit should be increased, in order to cover the people food needs. View the reduce water resources, promoting new techniques and technologies able to efficiently valorize the water coming from different sources, with reduced energy consume, is very important. In vineyards and orchards, water is conducted along the row or is uniformly stocked by means of continuous or interrupted (compartmented) furrows. This paper aims at analyzing the construction and operating method of a soil modelling equipment in compartmented furrows, simultaneously in two furrows in a single interval, PCVM2,2+EMBC2–0, in tree and vine plantations.
Keywords: water, soil, interrupted furrows

INTRODUCTION

In order to supply additional water quantities (besides those naturally received through rains) to soil, quantities that were established according to soil, climate and plant requirements, and supplementary works are necessary. When establishing the water additional quantity, it should take into account that the soil layer where roots develop keeps an optimum humidity. Having in view the decrease of arable surface comparing to population increment, increasing the agricultural production per surface unit remains the main solution able to meet the many and high–quality food requirements.

In order to achieve high agricultural yields, it should take into consideration a lot of factors (mechanization, fertilization, weed and pest control, soil biological potential, seed quality), each having its importance, but the lack of water in soil, during periods that overlap the plant critical growing phases, diminishes the harvest and even destroys it because of draught.

In Romania, the surface with economic irrigating potential is estimated at 3 million ha, out of which 1.5 mill ha are highly efficient. In this context, irrigations will become the most important consumer of water in agriculture and one of the main national consumers, requiring approximately 35–45% out of Romania water resources. Romania water resources are rather reduced, of about 1660 m3/habitant, and in other European countries they are 2.5 times bigger. Thus, it is very important to promote techniques and technologies able to efficiently valorize water coming from different sources, with reduced energy consume. Water from soil and its circulation is mainly important, as approximately 41% out of Romania arable surface is affected by an excessive humidity in certain periods of the year and during the same year, short or long periods of draught are present; so, the irrigation with variable norms should be applied. At the same time, erosion phenomena are manifested on 35% out of the entire agricultural surface.

Water stock in Romania is rather modest comparing to other countries in Europe (the 11–th place for local resources and 21–st place for resources formed on its territory). [3] Gravity wetting is the oldest irrigation form. Surface drip consists in the fact that water is distributed on the field by free flowing in furrows or stripes concomitantly with water infiltration into soil. Method extended also to hoeing crops sown in stripes or at bigger distances between rows with a minimum slope necessary to free water drip into the furrow. [4]. The opening of interrupted furrows is necessary in the following situations:

\# In unevenness or sloped (that determine the water dripping and stagnation in micro–depressions) fields designed to be irrigated by fixed and mobile spraying installations;

\# In broken relief and little slope fields, non–arranged for irrigation and where the rain water drips rapidly downstream, not being used by plants and determining the erosion phenomenon.

Farmers are interested in preserving soil humidity and, therefore, they searched for appropriate methods to collect and stock a maximum quantity of water in soil, in order to meet the crops requirements. They recognize that during several years, crops yield was limited because of draught in majority of area in the country. Rains fall randomly, so the water quantity does not comply to plants requirements. Majority of rainfalls during the vegetation season happen during great intensity showers. Only a small part of rainfalls infiltrates into the soil, the rest of it provoking excessive drippings and erosion. Thus, a method of collecting rainfall water consists in culture practices, namely creating compartmented furrows. [8]. Little dams are performed by an agricultural machine endowed with working sections, each of them breaking the soil with a chisel, scraping it with a hoe and forming from place to place, at established distances, little dams that gather the rainfall water.. Machine is used in a reduced slope field, in arid or semi–arid areas, where is a shortage of water in crops.

MATERIAL AND METHOD

Irrigation represents an important technological phase in crop plants agro–technology, and also the most important technical mean of eliminating the soil water shortage, constituting the infrastructure of a sustainable development. Technologies of fighting against the climate change effects have importantly evolved through the reduction of water consume for plants (dripping, micro–spraying), high valorization of water by losses diminishing and performing agricultural works such as fertilization, herbicide applying, etc and utilization of other sources of water (wastewater coming from animals or rural, urban and industrial environment). Furrows used in agriculture are extremely important for agricultural production and represent a main component of agricultural ecosystem [5],[6],[7],[8]. It is estimated an increased agricultural production per hectare by 20% for agricultural crops, where interrupted furrows are performed. This is explained by a big quantity of water that infiltrates at plants roots and also by reducing soil erosion. [3].

When performing continuous or interrupted furrows, it is aimed to obtain large sections of furrow necessary to transport and respectively to accumulate a big volume of water. For low–drainage soils, farmers prefer to use alternative furrows.

Figure 1 – Continuous and compartmented furrows after rain

Figure 2 – Alternative furrows[1] [4]

The opening furrow work is named rarefying (soil modelling) and, at first was performed by little plows pulled by animals. Now, this is performed by the machine working in aggregate with a tractor; an equipment designed to perform continuous furrows or an equipment specialized in performing interrupted furrows being mounted on the machine.

The machine equipped to perform continuous furrows comprises small plows performing the furrow triangular section, and modelling devices performing parabolic section and furrow finishing; the machine designed to perform interrupted furrows comprises the main small plows, blade rotors and a mechanism that controls the rotors designed to interrupt the furrows and make small dams (stoppers),; both equipment is mounted on a frame with supporting wheels.

RESULTS

Equipment for soil modelling in compartmented furrows in vine and tree plantations, simultaneously in two furrows in the same space, PCVM2,2+EMBC2–0 (Figure 3) performs compartmented furrows at a distance of 20–40 cm in row, in order to accumulate rainfall water into the soil on which surface the drips fall, thus avoiding the water dripping outside the cultivated area or water accumulation in depressing areas, on sloped fields of up to 5 %, with light, medium or heavy texture soils, ploughed at minimum 250 mm depth, at a humidity close to minimum extreme limit.

Figure 3 – Equipment for soil modelling in compartmented furrows in vine and tree plantations, simultaneously in two furrows in the same space, PCVM2,2+EMBC2–0

Equipment designed to model the soil in compartmented furrows simultaneously in two furrows in vine and tree plantations, PCVM2,2+EMBC2–0 comprises the following sub–assemblies: a left plough body, a right plough body, a device for forming compartmented furrows endowed with control mechanism and optionally, two arrow knives, if concomitant hoeing is desired.

Plough bodies with left and right supports are mounted on plough frame in lateral parts corresponding to ploughing with furrow overthrow to the row inner side, having the distorted body supports to outer frame.

Device to perform compartmented furrows (Figure 4) is formed of following main parts: command mechanism, rotor support, blade rotor and blade pressing mechanism on soil. Adjustment of mechanism designed to compartmented furrows will allow to create soil stoppers along the furrow at distances of 1.5; 3 or 6 m.

Figure 4 – Device of forming compartmented furrows

Mechanism of command (Figure 5) comprises: spur wheel, a transmission system and a driving mechanism.

Figure 5 – Command mechanism

Spur wheeel is metallic and is endowed with steel spurs on the rim aimed at increasing the wheel adherence to soil, avoiding its skidding. The spur wheel should be mounted in a hinged manner at frame central part, being able to vertically oscillate around the spindle that drives the cams, in order to „copy" the field during the working process. For transport position, the spur wheel should be fixed in vertical position.

Transmission is of chain type and aims at transmitting the movement from the spur wheel to the cam wheel spindle. Transmission is made of: support, chain wheels, chain 10 A and protection device.

Driving mechanism (Figure. 6) aims at unlocking the blade rotor in order to form the soil cork on the furrow. Driving mechanism comprises:
- # support of cam spindle– 3 pieces (2 pieces for cams and one piece for spur wheel),
- # cam wheel,
- # lever/cable and locking bolt.

Figure 6 – Driving mechanism

The supports of cam spindle are mounted on rear bar of frame, behind the plough body, and the cam wheel and the lever are mounted on the support. Spur wheel support should be mounted on the bar behind the frame, in central position to the direction of spur wheel.

Cam wheel is made of one disk parallel with the disk with lever role, and cams (1, 2 or 3) are mounted on cam wheel disk, according to distance chosen for creating the soil corks for furrow compartments. Lever is hinged on the support on the direction of cams and has at one end one reel and at the other end one bolt fixing the steel cable. The cable transmits the movement from the lever driven by cam to the bolt locking the blade rotor. The ratchet is made of an axle with a welded plate at its end. Axle slides in two couples represented by two steel thimbles fixed on rotor support. On the axle is mounted a spring that compresses when driving the locking mechanism and helps to lock the blade when driving mechanism does not work. This mechanism has a secure operating without blocking.

Support of the rotor is mounted on the lateral bar of the frame, behind the body. It comprises: a vertical axle, a fork and a bar supporting the spring that presses the blade rotor on soil. The fork is hinged at vertical support and can freely oscillate in vertical plan and supports the blade rotor, the lower end of pressing spring of scraping blade in soil and thimbles guiding the locking ratchet axle. Rotor is made of 4 pentagonal–shaped blades fixed on an axle, the angle between two close blades being of 90^0. The blade has a vertical external side, position that enables the working section to

approach the plant row without harming the plants with the blades.

Pressing spring on soil of scraping blade is mounted by means of a steel rod between the fork supporting the rotor and the bar endowed on vertical support.

CONCLUSIONS

Compartmented furrows are the result of a mechanical work of soil that performs furrows interrupted by soil heaps, at adjustable distances, for forming small basins of accumulated water. During the rainfalls, the excessive water is gathered in these basins so that it could be slowly absorb by the soil, thus removing the dripping outside the cultivated area. This is very important, because during strong showers, the intensity of rainfalls often surpasses the water speed of infiltration.

Experience has demonstrated that wind erosion can be also reduced. In sloped fields, by practicing compartmented furrows, prevention and reduction of water stagnation in low areas of cultivated field, can be achieved. The basins limited by small dams aim at temporarily stock the water coming from rains, (which, otherwise would flow outside the cultivated surface) that will infiltrate into the soil, thus increasing the soil water stock and capitalizing the rainfall water. This practice has been largely adopted due to new irrigation technologies, as well as, to equipment designed to perform compartmented furrows. This equipment performs small dams at 1–2m distance in the furrow. Some cultivators do not open furrows on the path crushed by tractor wheels when applying herbicides or during other agricultural operations.

Note:

This paper is based on the paper presented at ISB-INMA TEH' 2018 International Symposium (Agricultural and Mechanical Engineering), organized by Politehnica University of Bucharest – Faculty of Biotechnical Systems Engineering (ISB), National Institute of Research-Development for Machines and Installations Designed to Agriculture and Food Industry (INMA) Bucharest, The European Society of Agricultural Engineers (EurAgEng), Society of Agricultural Mechanical Engineers from Romania (SIMAR), National Research & Development Institute For Food Bioresources (IBA), University of Agronomic Sciences and Veterinary Medicine Of Bucharest (UASVMB), Research-Development Institute for Plant Protection (ICDPP), Hydraulics and Pneumatics Research Institute (INOE 2000 IHP), National Institute for Research and Development in Environmental Protection (INCDPM), in Bucharest, ROMANIA, between 01–03 November, 2018.

References

[1] Edwin C. and Alexander U.U. (1986), Texas Agricultural Extension Service;** Texas Agricultural Experiment Station, 1986;

[2] AQUAPROIECT SA., Device of modelling the soil in compartmented furrows, in two constructive solutions. Financing Contract no.4639/2017;

[3] Biolan I., Serbu I., Mardare F., Biolan C., Modern irrigation techniques for agricultural crops, AGIR Publishing House, 2015;

[4] Biolan I., Serbu I., Tusa G.C., Mardare F., Irrigation of agricultural crops. Technologies, AGI Publishing House, 2016;

[5] Guo X.N., Hu T.S., Tan G.M., Farmland drainage standard based on multi–attribute analysis, Transactions of the Chinese Society of Agricultural Engineering, 25 pp. 64–70, 2009;

[6] He X.C., Shao D.G., Liu W.Y., Research progress and prospect of resource utilization of farmland drainage, Transactions of the Chinese Society of Agricultural Engineering, vol. 22 pp.176–179, 2006;

[7] Li Y.H., A review of environmental effect and ecosystem function of farmland drainage ditch. Heilongjiang Science and Technology Information, 2016;

[8] Song C.J., Li Q., Wang Y., Research overview of ecosystem effect of farmland drainage ditch, Modern Agricultural Sciences and Technology vol. 2 pp. 201–203, 2014.

[1.]Quazi Md. Zobaer SHAH, [2.]Md. Arefin KOWSER, [3.]Mohammad Asaduzzaman CHOWDHURY

INVESTIGATION ON THE FRETTING FATIGUE FAILURE MECHANISM OF HEAT TREATED Al 6061-T6

[1-3.] Dhaka University of Engineering & Technology, DUET, Gazipur-1707, Dhaka, BANGLADESH

Abstract: Being a prime constituent in various sophisticated applications like aerospace design, Aluminum alloy has ranked the apex point of interest for researchers in the field of fatigue. In this present study, effect of fretting fatigue on heat treated Al-Mg-Si alloy (Al 6061-T6) has been investigated. Experimental observation has been authenticated by developing a FEM model using simulation software ANSYS 14.5. It has been observed that, within lower stress range, fretting reduces the lifetime of Aluminum significantly than the normal fatigue. On the other hand, fretting effect almost vanishes at higher order loading as well as stress in comparison with normal fatigue. Nevertheless, crack initiation and catastrophic rupture follows the aspect of fretting loading parameter which shows that fretting affects not only in quantity but also in quality of the fatigue behavior of Al 6061-T6.
Keywords: fretting fatigue, ANSYS, Bending loading, crack propagation, rapid rupture

INTRODUCTION

Aluminum alloys have become essential parts in modern applications like aerospace, automotive industries and other light weight desirable sectors. Al6061-T6 is tempered heat treatable alloy that has good corrosion resistance, weld ability. Aluminum alloys does not show any distinguishable knee on life-stress diagram. Fatigue limit for giga (10^9 cycle) of Al 6061-T6 was investigated by Y. Takahashi et al [1]. Two types of specimen, one smoother and another one with small hole were used. Though smoother sample didn't show notable limit, however, holed sample exhibits distinct fatigue limit. J. Hao et al [2] showed weldable Al alloy 6061 fatigue life comparison in atmosphere and water. In water, significant decrease in life was noticed. Under giga cycle reversed (R = -1) loading, various Al alloys have been tested at 20 kHz by Q. Wang [3]. For giga cycle, tearing occurs instead of striation. Fatigue crack propagation was studied by H. Noguchi [4]. Rotating bending fatigue test of Al6061-T6 with pitting hole was shown by G. Almaraz [5]. He studied the fatigue characteristics of single or double pitting holes. H. Lin et al [6] showed the fatigue properties of Al6061-T6 welded butt joints. Recent advances on fatigue research of aluminum alloys can be found in [7-15]. Current authors have reviewed and carried out some researches on fatigue in [16-18].

MATERIAL PROPERTIES

In this present study, fretting fatigue of Al6061-T6 has been carried out through experimental & numerical approaches. General rotating bending fatigue setup has been used with screwed ring type fretting setup. Analytical results along with graphical & fracture surface has been monitored to conclude the consequence of fretting on fatigue life.

a

b

Figure 1: Designed specimen (dimensions are in mm) (a), prepared Specimens (b)

EXPERIMENTAL SETUP

Jockey loaded rotating bending machine is used here. Fretting loading is supplied by rotatable circular ring. Details of similar experimental procedure with calibration can be found in [14, 15, and 18]. To avail fretting fatigue, a ring system with screwed bolts inserted inside is provided as shown in figure 1(b). By adjusting bolts, fretting pressure can be applied manually.

Table 1: Chemical properties of Al 6061-T6

Mg	Al	Si	Cr	Mn	Fe
1.75	94.42	0.79	0.20	0.32	0.47

Table 2: Mechanical properties of Al 6061-T6:

Density	UTS	YTS	Young's Modulus	Poison's ratio	Elastic limit
2.7 g/cc	310 MPa	276 MPa	68.9 MPa	0.33	96.5 MPa

Figure 2: Experimental setup for fatigue test

Figure 3: Fretting arrangement

NUMERICAL SIMULATION

For FEM analysis, ANSYS 14.5 was used here. CONTA 174 and TARGE170 has been used as contact and target element. Refinement for meshing has been adopted for result convergence. Co-efficient of 0.2 has been taken between contacts. Fretting force of 1000 N has been taken as constant loading on pads.
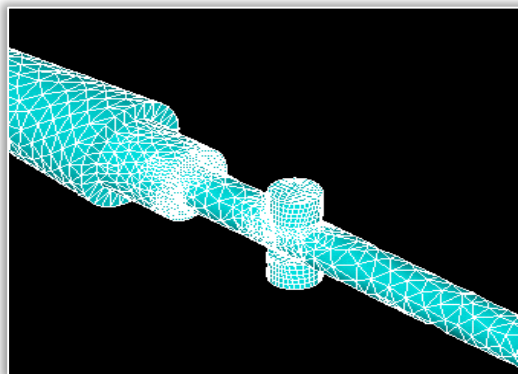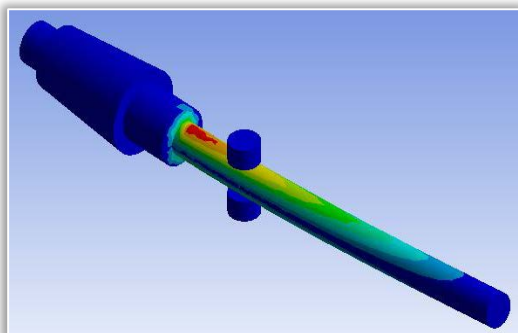

Figure 4: Geometry & Mesh convergence

Figure 5: FEM analysis for life under applied loading

Figure 6 shows the cracked surfaces of specimens used under different loading conditions. Most outer part of the periphery of circular shape observes the crack initiation by gradual but steady loading. Ratchet marks characterizes itself by continuous development of cracks. Each point of ending root of ratchet is introduced by crack initiation point. The middle zone, known as propagation period is characterized by striation and sometimes benchmarks like oval or circular shape that speaks about the sudden up gradation of stress to tear off the limited stressed circumference. The most inner differentiable circular zone is comparatively rough than other zones, marked as catastrophic failure zone. It happens because of sudden implied load upon which the specimen cannot withstand anymore.

FRACTURE FAILURE MECHANISM

At higher stress level along bending side, the nucleus zone slides away from the center due to both greater loading & higher rpm as well as low load impact period with higher stress (figure 6 a1, a2). For lower level of applied bending loading, gradual crack formation is observed that causes dartboard shaped classified zones for crack initiation, propagation & fracture as shown in figure 6(b1, b2). Because of dual action of tensile stress and bending stress in fretting fatigue, sample cracks at the collar/smaller neck area of the specimen that covers larger area for catastrophic failure zone as a result of extreme applied stress. Unlike the horizon cracked surfaces of previous cases (figures 6a, 6b), It cracks deeper to exert tensile stress into the head of specimen (figure 6 c1, c2).
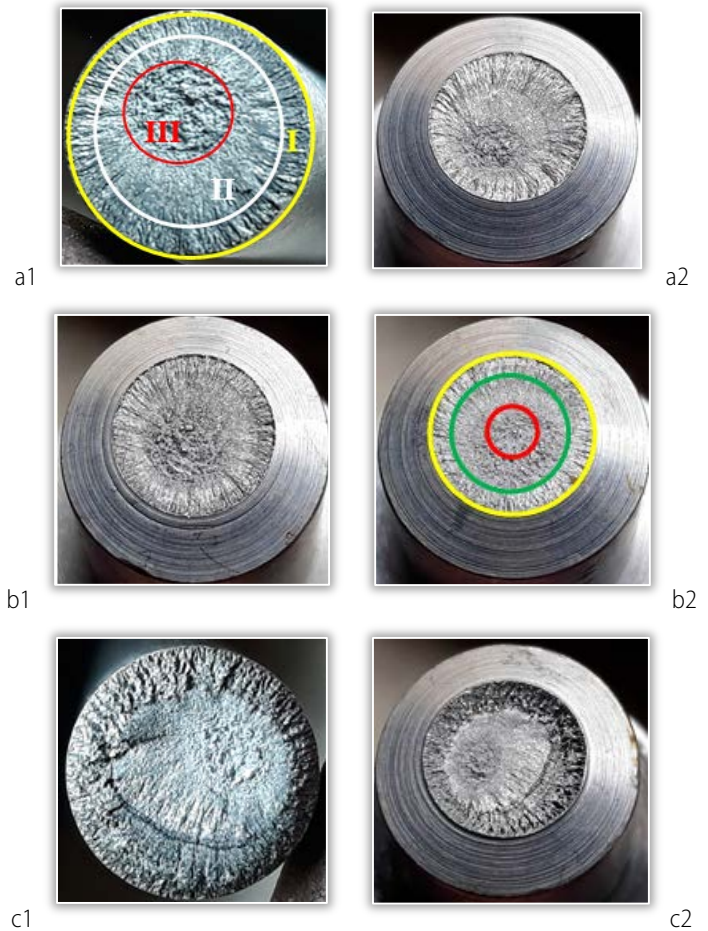

a1 a2 b1 b2 c1 c2
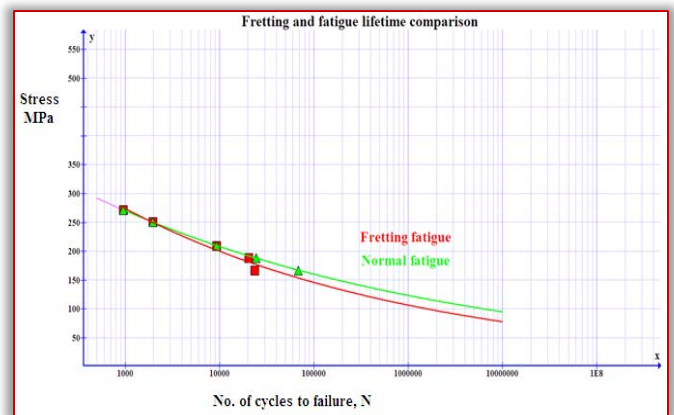Figure 6: fractured surfaces

Figure 7: Comparison of fretting fatigue lifetime with normal fatigue

RESULTS AND DISCUSSION

From S-N diagrams, it is obvious that, fretting reduces fatigue life considerably. For higher order loading it coincides with general fatigue life but as load level decreases for 1000 N fretting load life cycles decreases abruptly. In other words, it can be said that effect of notch and edge corner has much more impact on specimen than fretting load of even 1000 N at high bending loading. Fretting effect becomes obvious for low order loadings.

From Basquin equation, we know that

$$S = AN^B$$

Solving the above equation by taking log both sides yields the values of A and B from which we can get the value of endurance limit. Figure 7 shows that, for higher order bending stresses fretting doesn't affect the fatigue lifetime significantly whereas it shows noticeable reduction in lifetime for low order bending stresses. It is clear that, for high value bending loading under constant 1000N fretting loading, lifetime cycles remain the same which implies that for high order bending loading, fretting effects are not so obvious as those in low order bending loadings. So, corner edged and notched portions are as dangerous as fretting fatigue loads. Endurance limit is 94 MPa at 10^7 cycles for normal fatigue whereas for fretting fatigue, it becomes 77 MPa at 10^7 cycles. Endurance limit has been reduced of about 22% due to fretting of 1000 N while fatigue life time reduces 30-33% for low order loading.

CONCLUSION

On the basis of above discussed results, it can be said that fatigue associated with fretting affects the lifetime of Al 6061-T6 badly than the normal one significantly at lower order loading. However, at the peak value bending loading with greater stress it is difficult to differentiate individual effect of sharp corner and fretting effect, respectively. Here, preference of fillet edged corner over sharp edged object subjected to cyclic loading comes afore. Fretting effect is pre dominant for lower valued bending stresses by reducing the fatigue limit. Nevertheless, crack initiation & propagation as well as final rupture nucleus core direction is proved as an indicator of loading and rpm where fretting implies tensile effect in addition to bending fatigue.

References:

[1] Takahashi, Y., Yoshitake, H., Nakamichi, R., Wada, T., Takuma, M., Shikama, T., & Noguchi, H. (2014). Fatigue limit investigation of 6061-T6 aluminum alloy in giga-cycle regime. Materials Science and Engineering: A, 614, 243-249.

[2] Hao, J., Chengyu, Z., & Shengru, Q. (2015). Fatigue Life of 6061 Aluminium Alloy Welding Samples both in Atmosphere and Water. Rare metal materials and engineering, 44(5), 1116-1118.

[3] Wang, Q. Y., Lib, T., & Zenga, X. G. (2010). Gigacycle fatigue behavior of high strength aluminum alloys. Procedia Engineering, 2(1), 65-70.

[4] Shikama, T., Takahashi, Y., Zeng, L., Yoshihara, S., Aiura, T., Higashida, K., & Noguchi, H. (2012). Distinct fatigue crack propagation limit of new precipitation-hardened aluminium alloy. Scripta Materialia, 67(1), 49-52.

[5] Almaraz, G. M. D., Lemus, V. H. M., & Lopez, J. J. V. (2010). Rotating bending fatigue tests for aluminum alloy 6061-T6, close to elastic limit and with artificial pitting holes. Procedia Engineering, 2(1), 805-813.

[6] Lin, H., Hwang, J. R., & Fung, C. P. (2016). Fatigue properties of 6061-T6 aluminum alloy butt joints processed by vacuum brazing and tungsten inert gas welding. Advances in Mechanical Engineering, 8(4), 1687814016643454.

[7] Gong, B. S., Liu, Z. J., Wang, Y. L., Zhang, Z. J., Zhang, P., Jiang, H. C., ... & Zhang, Z. F. (2019). Improving the fatigue strength of A7N01 aluminum alloy by adjusting Si content. Materials Science and Engineering: A, 742, 15-22.

[8] Guo, S., Shah, L., Ranjan, R., Walbridge, S., & Gerlich, A. (2019). Effect of quality control parameter variations on the fatigue performance of aluminum friction stir welded joints. International Journal of Fatigue, 118, 150-161.

[9] Zhao, Y., Peng, Y., Fan, T., Kai, X., Chen, G., & Wang, W. (2019). U.S. Patent Application No. 15/771,432.

[10] Nelaturu, P., Jana, S., Mishra, R. S., Grant, G., & Carlson, B. E. (2018). Influence of friction stir processing on the room temperature fatigue cracking mechanisms of A356 aluminum alloy. Materials Science and Engineering: A, 716, 165-178.

[11] Sun, N., Jones, W. J., & Apelian, D. (2018). Friction Stir Processing of Aluminum Alloy A206: Part II—Tensile and Fatigue Properties. International Journal of Metalcasting, 1-11.

[12] Nambu, K., & Okumiya, M. (2018, July). Influence of Soft Particle Peening Treatment on Fatigue Strength of Aluminum Alloy A5052. In Fracture, Fatigue and Wear (pp. 390-400). Springer, Singapore.

[13] Nadot, Y., Houria, M. I., Fathalah, R., & Maijer, D. (2018). Through Process Modelling applied to the fatigue resistance of cast Aluminum. Procedia engineering, 213, 296-302.

[14] Zalnezhad, E., Sarhan, A.A.D. & Jahanshahi, P. Int J Adv Manuf Technol (2014) 70: 2211

[15] Zalnezhad, E., Sarhan, A.A.D. & Hamdi, M. Int J Adv Manuf Technol (2013) 69: 1153

[16] Chowdhury, M. A., Kowser, M. A., Zobaer Shah, Q. M., & Das, S. (2018). Characteristics and damage mechanisms of bending fretting fatigue of materials. International Journal of Damage Mechanics, 27(4), 453-487.

[17] M.A Kowser, M. A. Chowdhury, Q M Zobaer Shah, Effect of loading parameter on fretting fatigue. AIP Conference Proceedings **1851**, 020095 (2017)

[18] Zobaer Shah, Q.M., Asaduzzaman Chowdhury, M. & Arefin Kowser, M. J Fail. Anal. and Preven. (2019)

Fascicule 3

[April - June]

t o m e [2019] XII

ACTA Technica CORVINIENSIS
BULLETIN OF ENGINEERING

ISSN: 2067-3809

MANUSCRIPT PREPARATION – GENERAL GUIDELINES

Manuscripts submitted for consideration to **ACTA TECHNICA CORVINIENSIS – Bulletin of Engineering** must conform to the following requirements that will facilitate preparation of the article for publication. These instructions are written in a form that satisfies all of the formatting requirements for the author manuscript. Please use them as a template in preparing your manuscript. Authors must take special care to follow these instructions concerning margins.

INVITATION

We are looking forward to a fruitful collaboration and we welcome you to publish in our **ACTA TECHNICA CORVINIENSIS – Bulletin of Engineering**. You are invited to contribute review or research papers as well as opinion in the fields of science and technology including engineering. We accept contributions (full papers) in the fields of applied sciences and technology including all branches of engineering and management.

ACTA TECHNICA CORVINIENSIS – Bulletin of Engineering publishes invited review papers covering the full spectrum of engineering and management. The reviews, both experimental and theoretical, provide general background information as well as a critical assessment on topics in a state of flux. We are primarily interested in those contributions which bring new insights, and papers will be selected on the basis of the importance of the new knowledge they provide.

Submission of a paper implies that the work described has not been published previously (except in the form of an abstract or as part of a published lecture or academic thesis) that it is not under consideration for publication elsewhere. It is not accepted to submit materials which in any way violate copyrights of third persons or law rights. An author is fully responsible ethically and legally for breaking given conditions or misleading the Editor or the Publisher.

ACTA TECHNICA CORVINIENSIS – Bulletin of Engineering is an international and interdisciplinary journal which reports on scientific and technical contributions. Every year, in four online issues (**fascicules 1–4**), **ACTA TECHNICA CORVINIENSIS – Bulletin of Engineering [e-ISSN: 2067-3809]** publishes a series of reviews covering the most exciting and developing areas of engineering. Each issue contains papers reviewed by international researchers who are experts in their fields. The result is a journal that gives the scientists and engineers the opportunity to keep informed of all the current developments in their own, and related, areas of research, ensuring the new ideas across an increasingly the interdisciplinary field. Topical reviews in materials science and engineering, each including:

✓ surveys of work accomplished to date
✓ current trends in research and applications
✓ future prospects.

As an open-access journal **ACTA TECHNICA CORVINIENSIS – Bulletin of Engineering** will serve the whole engineering research community, offering a stimulating combination of the following:

✓ Research Papers – concise, high impact original research articles,
✓ Scientific Papers – concise, high impact original theoretical articles,
✓ Perspectives – commissioned commentaries highlighting the impact and wider implications of research appearing in the journal.

ACTA TECHNICA CORVINIENSIS – Bulletin of Engineering encourages the submission of comments on papers published particularly in our journal. The journal publishes articles focused on topics of current interest within the scope of the journal and coordinated by invited guest editors. Interested authors are invited to contact one of the Editors for further details.

BASIC INSTRUCTIONS AND MANUSCRIPT REQUIREMENTS

The basic instructions and manuscript requirements are simple:

✓ Manuscript shall be formatted for an A4 size page.
✓ The all margins of page (top, bottom, left, and right) shall be 20 mm.
✓ The text shall have both the left and right margins justified.
✓ Single-spaced text, tables, and references, written with 11 or 12-point Georgia or Times New Roman typeface.
✓ No Line numbering on any pages and no page numbers.
✓ Manuscript length must not exceed 15 pages (including text and references).
✓ Number of the figures and tables combined must not exceed 20.
✓ Manuscripts that exceed these guidelines will be subject to reductions in length.

The original of the technical paper will be sent through e-mail as attached document (*.doc, Windows 95 or higher). Manuscripts should be submitted to e-mail: redactie@fih.upt.ro, with mention **"for ACTA TECHNICA CORVINIENSIS"**.

STRUCTURE

The manuscript should be organized in the following order: Title of the paper, Authors' names and affiliation, Abstract, Key Words, Introduction, Body of the paper (in sequential

headings), Discussion & Results, Conclusion or Concluding Remarks, Acknowledgements (where applicable), References, and Appendices (where applicable).

THE TITLE

The title is centered on the page and is CAPITALIZED AND SET IN BOLDFACE (font size 14 pt). It should adequately describe the content of the paper. An abbreviated title of less than 60 characters (including spaces) should also be suggested. Maximum length of title: 20 words.

AUTHOR'S NAME AND AFFILIATION

The author's name(s) follows the title and is also centered on the page (font size 11 pt). A blank line is required between the title and the author's name(s). Last names should be spelled out in full and succeeded by author's initials. The author's affiliation (in font size 11 pt) is provided below. Phone and fax numbers do not appear.

ABSTRACT

State the paper's purpose, methods or procedures presentation, new results, and conclusions are presented. A nonmathematical abstract, not exceeding 200 words, is required for all papers. It should be an abbreviated, accurate presentation of the contents of the paper. It should contain sufficient information to enable readers to decide whether they should obtain and read the entire paper. Do not cite references in the abstract.

KEY WORDS

The author should provide a list of three to five key words that clearly describe the subject matter of the paper.

TEXT LAYOUT

The manuscript must be typed single spacing. Use extra line spacing between equations, illustrations, figures and tables. The body of the text should be prepared using Georgia or Times New Roman. The font size used for preparation of the manuscript must be 11 or 12 points. The first paragraph following a heading should not be indented. The following paragraphs must be indented 10 mm. Note that there is no line spacing between paragraphs unless a subheading is used. Symbols for physical quantities in the text should be written in italics. Conclude the text with a summary or conclusion section. Spell out all initials, acronyms, or abbreviations (not units of measure) at first use. Put the initials or abbreviation in parentheses after the spelled-out version. The manuscript must be writing in the third person ("the author concludes… ").

FIGURES AND TABLES

Figures (diagrams and photographs) should be numbered consecutively using Arabic numbers. They should be placed in the text soon after the point where they are referenced. Figures should be centered in a column and should have a figure caption placed underneath. Captions should be centered in the column, in the format "Figure 1" and are in upper and lower case letters.

When referring to a figure in the body of the text, the abbreviation "Figure" is used Illustrations must be submitted in digital format, with a good resolution. Table captions appear centered above the table in upper and lower case letters.

When referring to a table in the text, "Table" with the proper number is used. Captions should be centered in the column, in the format "Table 1" and are in upper and lower case letters. Tables are numbered consecutively and independently of any figures. All figures and tables must be incorporated into the text.

EQUATIONS & MATHEMATICAL EXPRESSIONS

Place equations on separate lines, centered, and numbered in parentheses at the right margin. Equation numbers should appear in parentheses and be numbered consecutively. All equation numbers must appear on the right-hand side of the equation and should be referred to within the text.

CONCLUSIONS

A conclusion section must be included and should indicate clearly the advantages, limitations and possible applications of the paper. Discuss about future work.

Acknowledgements

An acknowledgement section may be presented after the conclusion, if desired. Individuals or units other than authors who were of direct help in the work could be acknowledged by a brief statement following the text. The acknowledgment should give essential credits, but its length should be kept to a minimum; word count should be <100 words.

References

References should be listed together at the end of the paper in alphabetical order by author's surname. List of references indent 10 mm from the second line of each references. Personal communications and unpublished data are not acceptable references.

- ✓ *Journal Papers:* Surname 1, Initials; Surname 2, Initials and Surname 3, Initials: Title, Journal Name, volume (number), pages, year.
- ✓ *Books:* Surname 1, Initials and Surname 2, Initials: Title, Edition (if existent), Place of publication, Publisher, year.
- ✓ *Proceedings Papers:* Surname 1, Initials; Surname 2, Initials and Surname 3, Initials: Paper title, Proceedings title, pages, year.

ACTA TECHNICA CORVINIENSIS – Bulletin of Engineering is an international and interdisciplinary journal which reports on scientific and technical contributions.

The **ACTA TECHNICA CORVINIENSIS – Bulletin of Engineering** advances the understanding of both the fundamentals of engineering science and its application to the solution of challenges and problems in engineering and management, dedicated to the publication of high quality papers on all aspects of the engineering sciences and the management.

You are invited to contribute review or research papers as well as opinion in the fields of science and technology including engineering. We accept contributions (full papers) in the fields of applied sciences and technology including all branches of engineering and management. Submission of a paper implies that the work described has not been published previously (except in the form of an abstract or as part of a published lecture or academic thesis) that it is not under consideration for publication elsewhere. It is not accepted to submit materials which in any way violate copyrights of third persons or law rights. An author is fully responsible ethically and legally for breaking given conditions or misleading the Editor or the Publisher.

The Editor reserves the right to return papers that do not conform to the instructions for paper preparation and template as well as papers that do not fit the scope of the journal, prior to refereeing. The Editor reserves the right not to accept the paper for print in the case of a negative review made by reviewers and also in the case of not paying the required fees if such will be fixed and in the case time of waiting for the publication of the paper would extend the period fixed by the Editor as a result of too big number of papers waiting for print. The decision of the Editor in that matter is irrevocable and their aim is care about the high content-related level of that journal.

The mission of the **ACTA TECHNICA CORVINIENSIS – Bulletin of Engineering** is to disseminate academic knowledge across the scientific realms and to provide applied research knowledge to the appropriate stakeholders. We are keen to receive original contributions from researchers representing any Science related field.
We strongly believe that the open access model will spur research across the world especially as researchers gain unrestricted access to high quality research articles. Being an Open Access Publisher, Academic Journals does not receive payment for subscription as the journals are freely accessible over the internet.

GENERAL TOPICS

ENGINEERING
- ✓ Mechanical Engineering
- ✓ Metallurgical Engineering
- ✓ Agricultural Engineering
- ✓ Control Engineering
- ✓ Electrical Engineering
- ✓ Civil Engineering
- ✓ Biomedical Engineering
- ✓ Transport Engineering
- ✓ Nanoengineering

CHEMISTRY
- ✓ General Chemistry
- ✓ Analytical Chemistry
- ✓ Inorganic Chemistry
- ✓ Materials Science & Metallography
- ✓ Polymer Chemistry
- ✓ Spectroscopy
- ✓ Thermo-chemistry

ECONOMICS
- ✓ Agricultural Economics
- ✓ Development Economics
- ✓ Environmental Economics
- ✓ Industrial Organization
- ✓ Mathematical Economics
- ✓ Monetary Economics
- ✓ Resource Economics
- ✓ Transport Economics
- ✓ General Management
- ✓ Managerial Economics
- ✓ Logistics

INFORMATION SCIENCES
- ✓ Computer Science
- ✓ Information Science

EARTH SCIENCES
- ✓ Geodesy
- ✓ Geology
- ✓ Hydrology
- ✓ Seismology
- ✓ Soil science

ENVIRONMENTAL
- ✓ Environmental Chemistry
- ✓ Environmental Science & Ecology
- ✓ Environmental Soil Science
- ✓ Environmental Health

AGRICULTURE
- ✓ Agricultural & Biological Engineering
- ✓ Food Science & Engineering
- ✓ Horticulture

BIOTECHNOLOGY
- ✓ Biomechanics
- ✓ Biotechnology
- ✓ Biomaterials

MATHEMATICS
- ✓ Applied mathematics
- ✓ Modeling & Optimization
- ✓ Foundations & Methods

ACTA TECHNICA CORVINIENSIS – Bulletin of Engineering has been published since 2008, as an online, free-access, international and multidisciplinary publication of the Faculty of Engineering Hunedoara.

We are very pleased to inform that our international and interdisciplinary journal ACTA TECHNICA CORVINIENSIS – Bulletin of Engineering completed its eleven years of publication successfully [issues of years 2008 –2018, Tome I–XI]. In a very short period it has acquired global presence and scholars from all over the world have taken it with great enthusiasm.

Every year, in four online issues (fascicules 1 – 4), ACTA TECHNICA CORVINIENSIS – Bulletin of Engineering [e-ISSN: 2067-3809] publishes a series of reviews covering the most exciting and developing fields of science and technology. Each issue contains papers reviewed by international researchers who are experts in their fields. The result is a journal that gives the scientists and engineers the opportunity to keep informed of all the current developments in their own, and related, areas of research, ensuring the new ideas across an increasingly the interdisciplinary field.

Now, when we celebrate the tenth years anniversary of ACTA TECHNICA CORVINIENSIS – Bulletin of Engineering, we are extremely grateful and heartily acknowledge the kind of support and encouragement from all contributors and all collaborators!

On behalf of the Editorial Board and Scientific Committees of ACTA TECHNICA CORVINIENSIS – Bulletin of Engineering, we would like to thank the many people who helped make this journal successful. We thank all authors who submitted their work to ACTA TECHNICA CORVINIENSIS – Bulletin of Engineering.

ACTA TECHNICA CORVINIENSIS – Bulletin of Engineering exchange similar publications with similar institutions of our country and from abroad.

INDEXES & DATABASES

We are very pleased to inform that our international scientific journal ACTA TECHNICA CORVINIENSIS – Bulletin of Engineering completed its eleven years of publication successfully [2008–2018, Tome I–XI].

In a very short period the ACTA TECHNICA CORVINIENSIS – Bulletin of Engineering has acquired global presence and scholars from all over the world have taken it with great enthusiasm.

We are extremely grateful and heartily acknowledge the kind of support and encouragement from all contributors and all collaborators!

ACTA TECHNICA CORVINIENSIS – Bulletin of Engineering is accredited and ranked in the "B+" CATEGORY Journal by CNCSIS – The National University Research Council's Classification of Romanian Journals, position no. 940 (http://cncsis.gov.ro/).

ACTA TECHNICA CORVINIENSIS – Bulletin of Engineering is a part of the ROAD, the Directory of Open Access scholarly Resources (http://road.issn.org/).

ACTA TECHNICA CORVINIENSIS – Bulletin of Engineering is also indexed in the digital libraries of the following world's universities and research centers:

WorldCat – the world's largest library catalog
https://www.worldcat.org/
National Lybrary of Australia
http://trove.nla.gov.au/
University Library of Regensburg – GIGA German Institute of Global and Area Studies
http://opac.giga-hamburg.de/ezb/
Simon Fraser University – Electronic Journals Library
http://cufts2.lib.sfu.ca/
University of Wisconsin – Madison Libraries
http://library.wisc.edu/
University of Toronto Libraries
http://search.library.utoronto.ca/
The University of Queensland
https://www.library.uq.edu.au/
The New York Public Library
http://nypl.bibliocommons.com/
State Library of New South Wales
http://library.sl.nsw.gov.au/
University of Alberta Libraries – University of Alberta
http://www.library.ualberta.ca/
The University of Hong Kong Libraries
http://sunzi.lib.hku.hk/
The University Library – The University of California
http://harvest.lib.ucdavis.edu/

ACTA TECHNICA CORVINIENSIS – Bulletin of Engineering is indexed, abstracted and covered in the world–known bibliographical databases and directories including:

INDEX COPERNICUS – JOURNAL MASTER LIST
http://journals.indexcopernicus.com/
GENAMICSJOURNALSEEK Database
http://journalseek.net/
DOAJ – Directory of Open Access Journals
http://www.doaj.org/
EVISA Database
http://www.speciation.net/
CHEMICAL ABSTRACTS SERVICE (CAS)
http://www.cas.org/
EBSCO Publishing
http://www.ebscohost.com/
GOOGLE SCHOLAR
http://scholar.google.com
SCIRUS – Elsevier
http://www.scirus.com/
ULRICHSweb – Global serials directory
http://ulrichsweb.serialssolutions.com
getCITED
http://www.getcited.org
BASE – Bielefeld Academic Search Engine
http://www.base-search.net
Electronic Journals Library
http://rzblx1.uni-regensburg.de
Open J–Gate
http://www.openj-gate.com
ProQUEST Research Library
http://www.proquest.com
Directory of Research Journals Indexing
http://www.drji.org/
Directory Indexing of International Research Journals
http://www.citefactor.org/

ISSN: 2067-3809